SENSIBLE HEAT FLUX ESTIMATION UNDER UNSTABLE CONDITIONS FOR SUGARCANE USING TEMPERATURE VARIANCE AND SURFACE RENEWAL

by

ELTAYEB SULIEMAN NILE

B.Sc. Hons. and M.Sc. (Agronomy), University of Khartoum

Thesis submitted in fulfillment of the requirements for the degree of

DOCTOR OF PHILOSOPHY

in Agrometeorology

Soil-Plant-Atmosphere Continuum Research Unit

School of Environmental Sciences

Faculty of Science and Agriculture

University of KwaZulu-Natal

Pietermaritzburg

South Africa

March, 2010

Preface

The research contained in this dissertation was carried out at the Discipline of Agrometeorology, School of Environmental Sciences, Faculty of Science and Agriculture, University of KwaZulu-Natal, Pietermaritzburg. The research undertaken here was financially supported by University of KwaZulu-Natal.

The duration of this study was from May 2006 to October 2009.

The contents of this work have not been submitted in any form to another university and, except where the work of others is acknowledged in the text, the results are the authors own investigation.

As the candidate's supervisor, regular consultation took place between the candidate and me throughout the investigation. I agree to submit the thesis to the Faculty of Science and Agriculture Higher Degrees Office for examination by the University appointed examiners.

Signed ………………….…………… Date ………..………..

MJ Savage:

Professor of Agrometeorology

DECLARATION 1

I .... declare that

1. The research reported in this dissertation, except where otherwise indicated, is my original work.

2. This dissertation has not been submitted for any degree or examination at any other university.

3. This dissertation does not contain other persons' data, pictures, graphs or other information, unless specifically acknowledged as being sourced from other persons.

4. This dissertation does not contain other persons' writing, unless specifically acknowledged as being sourced from other researchers. Where other written sources have been quoted, then:
   a. their words have been re-written but the general information attributed to them has been referenced;
   b. where their exact words have been used, their writing has been placed inside quotation marks, and referenced.

4. Where I have reproduced a publication of which I am an author, co-author or editor, I have indicated in detail which part of the publication was actually written by myself alone and have fully referenced such publications.

5. This dissertation does not contain text, graphics or tables copied and pasted from the Internet, unless specifically acknowledged, and the source being detailed in the dissertation and in the References sections.

Signed ……………….…………… Date ……….………..

Eltayeb S. Nile

DECLARATION 2 - Publications

1. Nile E.S., Savage M.J., 2009. Temperature variance for estimating evaporation above crop canopies: Theory and practice. In preparation.

2. Nile E.S., Savage M.J., 2009. Evaluation of surface renewal applied to sugarcane for estimating sensible heat flux. In preparation.

3. Nile E.S., Savage M.J., 2009. Sensible heat flux estimation using temperature-variance over sugarcane. In preparation.

4. Nile E.S., Savage M.J., 2009. Sensible heat flux estimation over sparse and dense sugarcane using surface renewal. In preparation.

5. Nile E.S., Savage M.J., 2009. Long-term estimation of sensible heat flux and evaporation for sugarcane using eddy covariance, temperature variance and surface renewal. In preparation.

In all of these papers in preparation, I collected and analyzed the data and prepared the first drafts of the papers.

Signed ……………….
Eltayeb S. Nile

ACKNOWLEDGEMENTS

I would like to express my most sincere appreciation to my supervisor Professor Michael J Savage, Agrometeorology Discipline, at the University of KwaZulu-Natal (UKZN) for his excellent supervision, invaluable help, guidance, patience and encouragement throughout the study period and for very efficient proof reading of this thesis. I have learnt various skills from studying under his supervision which will benefit me in future.

I am grateful to Mrs Jothimala Manickum for her assistance during the field work, Managing Director, M. van Deventer and Farm Manager, G. Stopforth of Baynesfield Estate for the use of the commercial sugarcane field, and Mrs Meryl Savage for providing support and transport and for her hospitality.

I wish to thanks my fellow Agrometeorology postgraduate students, Dr M. Mengistu, Mr N. Moyo, Dr G. Odhiambo and Mr M. Abraha for their technical help during the laboratory and the field work and for facilitating an excellent and enjoyable productive working atmosphere.

Special thanks to the Council for Scientific and Industrial Research (CSIR) staff, Prof. C.S. Everson and Mr A. Clulow, for providing instrumentation.

Funding from UKZN, South Africa, and government of the Sudan to pursue my study is gratefully acknowledged.

Special thanks go to my parents who provided generous support and encouragement, my son Mohamed for his sacrifice and accepting reduce some of his rights while I was away and busy studying and M. Shwanaz and his family for moral support and their visits.

I would like also to express my special thanks to my Sudanese colleagues, UKZN, and my friends in my home country for their assistance and encouragement during my study period.

ABSTRACT

Increased pressure on the available limited water resources for agricultural production has a significant impact on sugarcane production. Routine monitoring of evaporation with reliable accuracy is essential for irrigation scheduling, for more efficient use of the available water resources and for management purposes. An indirect method for estimating evaporation involves measuring the sensible heat flux (H) from which latent energy flux and hence total evaporation can be calculated, as a residual using the shortened energy balance from measurements of net irradiance and soil heat flux. Various methods for measuring H may include Bowen ratio energy balance, eddy covariance (EC), flux variance (FV), optical scintillation, surface renewal (SR) and temperature variance (TV). Each method has its own advantages and disadvantages, in terms of method theoretical assumptions, accuracy, complexity, cost, fetch requirements and power consumption.

The TV and SR methods are inexpensive and reasonably simple with a reduced power requirement compared to other methods since they require high frequency air temperature data which is obtained by using an unshielded naturally-ventilated type-E fine-wire thermocouple at a single point above the canopy surface. The TV method is based on the Monin-Obukhov similarity theory (MOST) and uses the mean and standard deviation of the air temperature for each averaging period. Currently, there are two TV methods used for estimating sensible heat flux (H_{TV}) at sub-hourly time intervals, one includes adjustment for stability, and a second that includes adjustment for air temperature skewness. Another method used to estimate sensible heat flux from the mean and standard deviation of air temperature is based on MOST and uses spatial second-order air temperature structure function. For the TV method adjusted for stability and the method based on MOST that uses a spatial second-order air temperature structure function, the Monin-Obukhov atmospheric stability parameter (ζ) is needed. The parameter ζ can be estimated from EC measurements or alternatively estimated independently using an iteration process using horizontal wind speed measurements. The TV method including adjustment for air temperature skewness requires the mean and standard deviation of the air temperature and air temperature skewness for each averaging time period as the only input.

The SR method is based on the coherent structure concept. Currently, there are various SR models method for estimating sensible heat flux. These include an ideal SR analysis model method based on an air temperature structure function analysis, the SR analysis model with a finite micro-front period, combined SR with K-theory and combined SR model method based on MOST. The ideal SR analysis model based on an air temperature structure function analysis should be calibrated to determine the SR weighting factor (α). The other SR approaches require additional measurements such as crop height and horizontal wind speed measurements. In all of the SR approaches, air temperature time lags are used when calculating the air temperature structure functions.

In this study, the performance of TV and SR methods were evaluated for estimation of sensible heat and latent energy fluxes at different heights for air temperature time lags of 0.4 and 0.8 s for daytime unstable conditions against EC above a sugarcane canopy at the Baynesfield Estate in KwaZulu-Natal, South Africa. For all methods, latent energy flux (LE) and hence evaporation was estimated as a residual from the shortened energy balance equation using H estimates and net irradiance and soil heat flux density measurements.

The ideal SR analysis model method based on an air temperature structure function analysis approach was calibrated and validated against the EC method above the sugarcane canopy using non-overlapping data sets for daytime unstable conditions during 2008. During the calibration period, the SR weighting factor α was determined for each height and air temperature time lag. The magnitude of α ranged from 0.66 to 0.55 for all measurement heights and an air temperature time lag of 0.8 s. The α value increased with a decrease in measurement height and an increase in air temperature time lag. For the validation data set, the SR sensible heat flux (H_{SR}) estimates corresponded well with EC sensible heat flux (H_{EC}) for all heights and both air temperature time lags. The agreement between H_{SR} and H_{EC} improved with a decrease in measurement height for the air temperature time lag of 0.8 s. The best H_{SR} *vs* H_{EC} comparisons were obtained at a height of 0.20 m above the crop canopy using α = 0.66 for an air temperature time lag of 0.8 s. The residual estimates of latent energy flux by SR and EC methods were in good agreement. The LE_{SR} at a height of 0.20 m above the canopy yielded the best comparisons with LE_{EC} estimated as a residual.

The performance of the TV method, including adjustment for stability, and adjustment for air temperature skewness was evaluated against EC estimates of sensible heat flux for daytime unstable conditions. The sensible heat flux estimated using MOST and a spatial second-order air temperature structure function was also compared with EC. The sign of the third-order air temperature structure function was used to identify unstable conditions. The performance of the TV methods compared to EC for estimating sensible heat flux was good for measurements either within the roughness sub-layer or the inertial sub-layer with improvement with increase in measurement height. The sensible heat flux estimated using MOST and the spatial second-order air temperature structure function was good compared to H_{EC} with an improvement in the correspondence for an air temperature time lag of 0.8 s. Best results for the TV methods and sensible heat flux obtained from MOST and the spatial second-order air temperature structure function approach were obtained for heights of 1.50 and 0.75 m above the crop surface respectively. The TV method, including adjustment for air temperature skewness, performed well in estimating sensible heat and latent energy flux compared to the other methods. The free convection limit forms for sensible heat flux estimation for the TV method and the MOST-based method that included the air temperature structure function provided poor estimates with significant bias (with slope less than 0.75).

The performance of SR models method were evaluated for daytime unstable conditions in the roughness and inertial sub-layers when the sugarcane was sparse and for when it was dense. Sensible heat flux estimates using the original and other SR approaches (H_{SR}) were found to be comparable H_{EC}. The α was determined by plotting H_{SR} *vs* H_{EC} for each measurement height and both air temperature time lags. The weighting factor (α') was also calculated using friction velocity and a stability function and varied between 0.31 to 0.95 for the various heights. The value of α increased with decrease in measurement height for an air temperature time lag of 0.8 s. It is observed that α' values were greater compared to α. The sensible heat flux estimated using the original SR approach for which α value was determined by calibration with EC yielded more accurate estimates than when α' was calculated using friction velocity and a stability function. Various other SR estimates applied to the roughness sub-layer obtained by calculation, one using a finite micro-front ramp SR model, another using K-theory and others that combine SR and MOST and their free convection forms produced very good H_{SR} estimates. Improved H_{SR}

estimates were observed using combined SR and K-theory approaches. The combined SR and MOST that uses either the standard deviation of the air temperature or the air temperature structure function performed well in the inertial sub-layer but as expected the respective free convection forms performed poorly. The performance of the original and other SR approaches was improved when the sugarcane was dense and with more complete cover. The H_{SR} estimates obtained by the combined SR model and K-theory was superior compared to those obtained using the other approaches.

The EC, TV including adjustment for air temperature skewness and SR methods were used for long-term estimates of the sensible heat flux H and evaporation for sugarcane. The sign of the third-order air temperature structure function was used to identify unstable conditions. The daily total sensible heat flux for the TV method, adjusted for air temperature skewness, and SR sensible heat flux estimates showed good agreement with H_{EC} for all measurement heights. The best comparisons with H_{EC} were obtained at heights of 1.50 and 0.50 m above the crop surface for the TV, adjusted for air temperature skewness, and SR sensible heat flux estimates respectively. Seasonal variation of the energy balance components and evaporation using EC, TV method including adjustment for air temperature skewness at a height 1.50 m above the crop surface and SR method at a height of 0.50 m above the crop surface (using an air temperature time lag of 0.8 s and calibrated using a weighting factor of 0.62 were investigated for a one-year period. Evaporation and energy balance components varied with time throughout the day, from day to day, and from season to season due to the variation in environmental conditions such as net irradiance due to cloud, and rainfall occurrence. The daily total evaporation varied between a maximum value of about 7.5 mm day^{-1} in summer and a minimum of about 1.2 mm day^{-1} in winter for cloudless conditions. The average daily evaporation for the whole period was 2.06 mm day^{-1}.

The footprint analysis for sensible heat flux was performed to determine the cumulative fraction of measured sensible heat flux to the surface source flux ratio, and the peak location of the footprint during unstable conditions. The analysis indicated that more than 91 % of the measured sensible heat flux was from the experimental site for which the fetch distance was 97 m.

Overall, the TV method, including adjustment for air temperature skewness, and the SR method both showed promise as relatively inexpensive and reasonably simple methods with low-power requirements compared to other methods for obtaining *H*. The datalogger requirements are less onerous than that for EC although the fine-wire thermocouples (TCs) are to damage. Missing data due to damaged TCs can be avoided by using multiple TCs. The TV method, including adjustment for air temperature skewness, does not require calibration or validation compared to the SR method. This study showed that the long-term sensible heat flux estimates using the TV method, including adjustment for air temperature skewness, for measurements taken at 1.5 m above the crop canopy and SR at 0.2 m were reasonably accurate (slope = 0.93 and RMSE = 0.59 MJ m^{-2}). The daily total crop evaporation varied between a maximum value of about 7.5 mm day^{-1} in summer and a minimum of about 1.2 mm day^{-1} in winter. Therefore evaporation can be estimated if the other components of the energy balance are measured accurately.

TABLE OF CONTENTS

LIST OF TABLES

LIST OF FIGURES

Chapter 1: Introduction

1.1 Motivation

Water is a limited resource and increasingly becoming scarce and expensive in different parts of the world including South Africa. The challenge created by increased water scarcity is heightened by the increasing costs of developing new water supplies, degradation of soil in irrigated areas, groundwater depletion, water pollution, evaporative losses, and wasteful use of water (Rosegrant *et al*., 2005). The Republic of South Africa National Water Act (1998) requires that available water resources should be used effectively and efficiently. To this end, an account of the water being used requires information from water users of the economy.

In South Africa, an increasing population requires more food and timber production by expanding irrigated agricultural and forestry lands. Furthermore there is increased water usage by industries, municipalities and others sectors (Savage *et al*., 2004). This results in continuous pressure on available water resources for agricultural production. It is therefore very important to use available water resources (rainfall and/or irrigation water) efficiently and effectively, which is considered one of main water management strategies under these conditions (Bazza, 2005). These strategies would increase the crop yield per unit area, reduce costs and protect water resources. A key to improved water resources management is based on quantifying and understanding the processes involved in evaporation that is a component of both the water balance and the surface energy balance of a cropped surfaces. Therefore, accurate and continuous measurements of evaporation and energy balance components would allow for the management of the water resources. Such measurements would be useful in many fields such as hydrology, meteorology and environmental studies.

In meteorology, evaporation is the process of transforming liquid water into water vapour with little change in temperature, and transferring it from the surface to air. Crop evaporation, which includes crop transpiration, is the most important process that represents the major consumptive use of irrigation water and rainfall in agricultural areas (Gowda *et al*., 2008). Evaporation occurs under the influence of a number of climatic and biological factors (Rosset *et al*., 1997; Wever *et al*., 2002) and represents 60 % of total precipitation reaching land surfaces (Brutsaert, 1982).

Evaporation, also referred to the total crop evaporation, is difficult to measure or estimate accurately although there are different micrometeorological methods for measuring or estimating evaporation. In the energy balance, evaporation appears as the latent energy flux term. Therefore evaporation can be indirectly estimated as latent energy flux through surface energy balance from sensible heat flux estimates and measured net irradiance and soil heat flux.

Various methods for measuring or estimating total crop evaporation include Bowen ratio energy balance, eddy covariance (EC), flux variance (FV), optical scintillation, surface renewal (SR), temperature variance (TV) and weighing lysimeter. The EC method can measure LE directly using two instruments or EC-measured sensible heat flux can be measured directly with one instrument and latent energy (evaporation) calculated from the knowledge of the shortened energy balance terms. The other methods, except the weighing lysimeter method, also combine the latent energy flux which is obtained through surface energy flux density from sensible heat flux estimates, and latent energy of vapourization to determine the water loss due to evaporation. The weighing lysimeter and EC systems allow latent energy flux, and hence evaporation to be calculated directly. The Bowen ratio energy balance system uses air temperature and water vapour pressure gradients for estimating sensible heat and latent energy flux densities. The FV method allows sensible and latent energy flux densities to be estimated from water vapour pressure and air temperature measurements at a single point. The SR and scintillation methods, and also the TV method all allow sensible heat flux to be estimated, from which latent energy flux is calculated as a residual using the shortened energy balance equation.

The weighing lysimeter method is accurate but rarely used outside of experimental research institutes (Castellví, 2004). The EC method is considered the preferable and more accurate point-measurement method for sensible heat and latent energy flux density representing a footprint area. But it is limited by complexity, cost and sensitivity of the instruments to damage (Drexler *et al.*, 2004) and its measurements are interrupted by disturbance of the sonic signal by rainfall, fog, insects and dirt. In addition, a full guidance on system set up and EC raw data processing is still unavailable (Mauder *et al*., 2007;

Castellví *et al*., 2008). The Bowen ratio method is sensitive to the biases of the instrument used for measuring the vertical gradients of air temperature and water vapour pressure (Rosenberg *et al*., 1983), and requires extensive fetch. The scintillometer method is an expensive method, based on the Monin-Obukhov similarity theory (MOST) and requires a fairly high level of expertise to operate. In addition, its measurements are interrupted by optical interception by rainfall, fog, insects, and the method requires vertical air temperature gradient measurements to distinguish between upward and downward direction of the sensible heat flux (Savage, 2009).

Sugarcane (*Saccharum officinarum*) is grown under rainfall or supplementary irrigation in South Africa. The total production area increased from 380.6 million hectares in 1993/94 to 422.8 million hectares in 2007/08 (SASA, 2009a). Most of the sugarcane producing areas are located in the Eastern Cape, KwaZulu-Natal and Mpumalanga provinces. The sugarcane N12 variety is currently most widely grown in the rainfed areas (SASA, 2009b).

In sugarcane fields, evaporation is commonly estimated using grass reference evaporation or tall crop reference evaporation estimation from automatic weather station data measurements (solar irradiance, air temperature, water vapour pressure and wind speed) at a single point, and crop coefficients. Although this evaporation method has recently been improved to allow hourly estimation of reference evaporation by changing the surface resistance values (Allen *et al*., 2006), knowledge of the crop factor is still required for estimating the actual evaporation. Few field studies have been conducted that focus on evaporation estimation over sugarcane using micrometeorological methods such as eddy covariance (Denmead and MacDonald, 2008), Bowen ratio energy balance (Burger, 1999; McGlinchey and Inman-Bamber, 2002; Shinichi *et al*., 2004), and scintillometer methods (Wiles, 2006).

It is the nature of the above-mentioned drawbacks associated with the various methods for estimating evaporation of agricultural crops that motivated the attempts to find alternative simple, accurate and inexpensive methods and with reduced power requirement so as to allow unattended use at distant sites. The TV and SR methods provide advantageous ways that allow sensible heat flux to be estimated using high frequency air temperature measurements and thereafter the latent energy flux is estimated as a residual of the surface energy balance when the net irradiance and soil heat flux are either measured or estimated. These methods have several advantages over the other micrometeorological methods. They are simple, inexpensive and minimize the problems related to leveling, relative instrument-separation and rotations which cause uncertainties in the eddy covariance and other methods based on profile measurements. In addition, they do not require sophisticated and expensive high frequency wind velocity measurements. The datalogger requirements are less onerous than that for EC although the fine-wire thermocouples TCs are sensitive to damage. Missing data due to damaged TCs can be avoided by using multiple TCs.

After Tillman (1972) published his first work on the TV method based on MOST, many studies have evaluated the performance of this method for different vegetated surfaces and stability conditions (e.g., Hsieh and Katul, 1996; Katul *et al*., 1996; Wesson *et al.*, 2001; Sugita and Kawakubo, 2003; Castellví and Martínez-Cob, 2005; Hsieh *et al*., 2008). Currently, there are two TV methods used for estimating sensible heat flux H_{TV} at sub-hourly time intervals: one includes correction for stability, and a second that includes adjustment for air temperature skewness. For comparison purposes, another method based on MOST that was used the air temperature structure function. The SR method is based on coherent structure theory and its performance was evaluated for a variety of canopy surfaces and water under different atmospheric stability conditions (e.g., Snyder *et al*., 1996; Castellví *et al*., 2002, Castellví, 2004; Savage *et al*., 2004; Castellví and Martínez-Cob, 2005; Castellví *et al*., 2006a, b; Mengistu, 2008; Castellví and Snyder, 2009a ,b). Recently, different approaches of the SR method were proposed: an ideal SR analysis model based on structure function analysis; SR analysis model with finite micro-front period (Chen *et al*., 1997b); and a combined SR analysis and similarity theory method (Castellví, 2002; Castellví, 2004; Castellví and Martínez-Cob, 2005; Castellví *et al*., 2006a).

1.2 Objectives

The TV and SR methods for estimating sensible heat flux H have been applied above annual cereal crops but there has been no published work involving biannual crops such as sugarcane. The overall aim of this research was therefore to estimate H over sugarcane using TV and SR methods from which evaporation can be estimated using the shortened energy balance equation. To achieve this aim, there are a number of specific objectives:

- to calibrate and validate the performance of the SR method for estimating sensible heat by using EC measurements above sugarcane;
- to estimate sensible heat over sugarcane using different approaches of the TV method at different measurement heights, and compare with EC measurements;
- to estimate sensible heat using the SR methods at different measurement heights over sugarcane, and compare with EC measurements;
- to quantify the temporal variations in the total crop evaporation, using TV and SR, and energy balance components over sugarcane.

1.3 Thesis structure

The thesis comprises seven chapters: Chapter 1 outlines the motivation and objectives of the study as well as the thesis structure. In Chapter 2, a brief overview of the fundamental structure of the atmosphere is presented and the theoretical background of several micrometeorological methods for estimating sensible heat and latent energy fluxes used in this study with emphasizing on the TV and SR methods are also discussed. In Chapter 3, the SR method for estimating sensible heat flux is calibrated against the EC method and validated at four measurement heights above a sugarcane canopy using two time air temperature lags. Chapter 4 describes the performance of two different TV methods: the TV method including stability correction and the other including adjustment for air temperature skewness, and the method that based on MOST and uses air temperature structure function for estimating H at sub-hourly time intervals, in comparison to the EC method. In Chapter 5, the performance of the SR approaches at four measurement heights for two time lags for estimating sensible heat flux are evaluated. In Chapter 6, the results of energy balance components and evaporation estimates for sugarcane canopy using TV and SR methods as well as their seasonal variation are presented. The last chapter summarizes the results of the study and includes future research plans.

Chapter 2: Literature review

2.1 Fundamental structure of the atmosphere

2.1.1 Atmospheric boundary layer

The atmospheric boundary layer plays an important role in determining evaporation and energy balance components. The planetary boundary layer (PBL) is the lower part of the troposphere that is directly influenced by temporal and spatial changes in the biosphere and coupled to the earth's surface by turbulent exchange processes (Stull, 1988). This layer is mainly characterized by diurnal variations of its atmospheric parameters such as temperature and humidity. These variations are caused by the underlying surface, which forces the changes in the boundary layer *via* transport processes. The depth of this layer is not constant, varying in time and space and ranges from tens of meters when the air near the surface is stably stratified to several kilometers when the air is convectively unstable (Dabberdt *et al.*, 1993). The planetary boundary layer has been described in more detail by Oke (1987), Stull (1988), Garratt (1992) and Arya (2001). The atmospheric boundary layer can be subdivided roughly into an outer region which is known as the Ekman layer and inner region. In the Ekman layer, the Coriolis force due to rotation of the earth is very important and the flow is much less dependent on the surface characteristics. For the inner region, flow is mainly depend on the surface characteristics and is much less affected by Coriolis force (Weiss, 2002). Above the atmospheric boundary layer is the free atmosphere which is characterized as non-turbulent or intermittently turbulent. The structure of the atmospheric boundary layer is illustrated (Fig. 2.1).

2.1.2 Internal boundary layer

The internal boundary layer (*IBL*) is the region of atmosphere adjacent to the surface where the influence of the new surface conditions is detected (Savelyev and Taylor, 2005) and representing about 10 % of planetary boundary layer (Panofsky and Dutton, 1984). Within this layer, the turbulent motions cause interaction between the earth's surface and the atmosphere, the wind direction does not change with height and the strong vertical gradients in air temperature, humidity, carbon dioxide, wind and other scalars exist. These

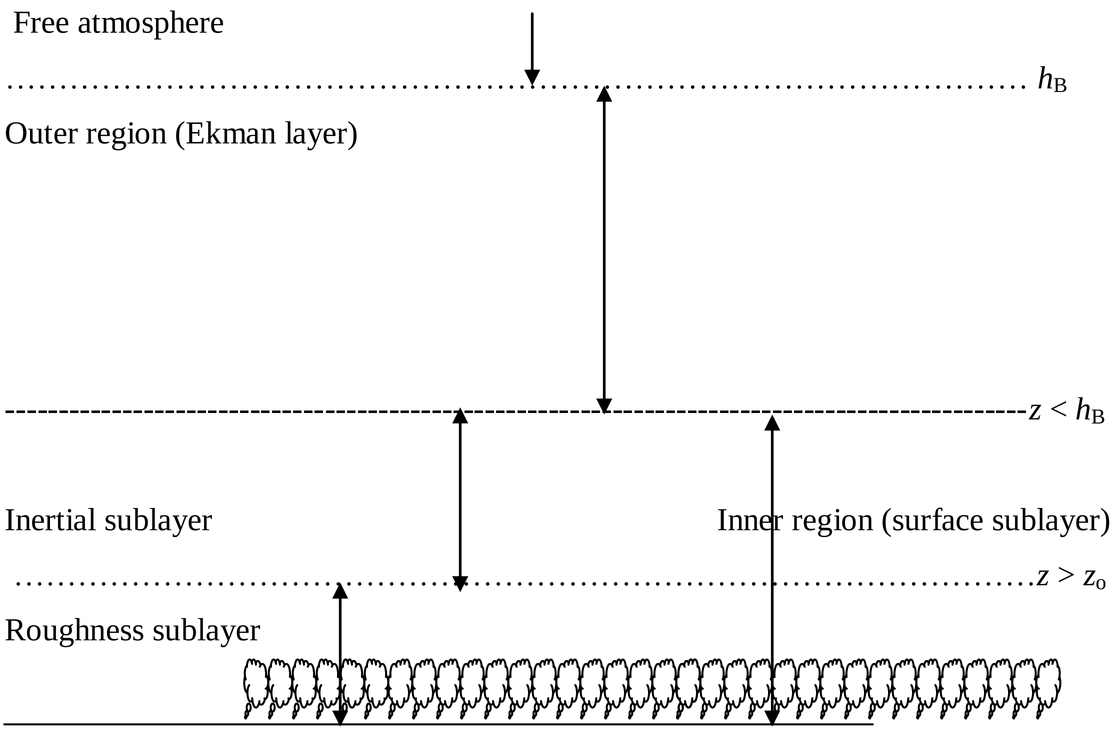

Fig. 2.1 Schematic representation showing the sub-regions of the atmospheric boundary layer; h_B is the boundary layer depth, z the height above ground and z_o the surface roughness length.

strong gradients control the transfer of momentum, mass and heat through this layer (Kaimal and Finnigan, 1994). The depth of the IBL depends on the surface roughness length and upwind fetch, and is estimated using the Munro and Oke (1975) equation for stable conditions (Savage *et al.*, 1997):

$$\delta = x^{0.8} z_o^{0.2} \tag{2.1}$$

where x in the upwind fetch (m) which is defined as the distance upwind from the point of measurements to the edge of the new surface (Evett, 2002), and z_o the roughness length (m) obtained from wind speed profiles, or from the approximation $z_o = 0.13\ h$ where h is the canopy height (m). The magnitude of the *IBL* may extend from 1 m (in extremely stable nocturnal conditions) to 500 m (in convective, unstable conditions) (Savage *et al.*, 2004). This layer is considered the appropriate layer for micrometeorological measurements. The internal boundary layer comprises of the roughness and the inertial sub-layers. The roughness sub-layer is the layer located below the inertial sub-layer in which the local air flow influenced by individual surface roughness elements (Katul *et al*., 1999; Mahrt, 2000). In this layer, Monin-Obukhov similarity theory (MOST) is not valid and the flux measurements are proportional to the measurement height above the soil surface (Chen *et al*., 1997b). The height of the roughness sub-layer depends on plant height and the atmospheric stability conditions (Garratt, 1980; Raupach *et al*., 1996; Graefe, 2004; Harman and Finnigan, 2007) and extends up to 1.5 to 3 times the canopy height *h* (Cellier and Brunet, 1992; Kaimal and Finnigan, 1994). It can be estimated as (Sellers *et al*., 1986):

$$z^* = h + 2(h - d) \approx \frac{5h}{3} \tag{2.2}$$

where *d* is the zero displacement (m). For sparse and tall canopies, the roughness sub-layer is estimated as (Garratt, 1980):

$$z^* = a\,D + d \tag{2.3}$$

where *a* is a coefficient and *D* the interrow spacing. The coefficient *a* approximately ranges between 4 and 6 with higher values for *a* within this range noticed under near neutral conditions (Castellví *et al*., 2006a). Cellier and Brunet (1992) found *a* = 3.1 for a sugarcane and *a* = 4.2 for maize. The inertial sub-layer is the layer in which fluxes are constant with height and its structure depends on the scales such as friction velocity and height (Monteith and Unsworth, 1990). In the first few tens of meters to 500 m, the inertial sub-layer depth is assumed to be obtained as (Brutsaert 1982):

$$\delta' = 0.1\, x^{0.8}\, z_o^{0.2}, \qquad \text{for a smooth-rough transition} \tag{2.4}$$

$$\delta' = 0.05\, x^{0.8}\, z_o^{0.2} \qquad \text{for a rough-smooth transition} \tag{2.5}$$

In this layer, MOST is applicable and the flux measurements are proportional to *z* - *d* (Chen *et al*., 1997b).

2.1.3 Turbulence

Turbulence is the flow characterized by the irregular and random fluctuations in velocity, temperature, and scalar concentrations around their mean values with time and space (Arya, 2001) and plays an important role in changing the air properties and creating disturbance in scalar fluxes in the atmospheric boundary layer (e.g., sensible heat and latent energy fluxes). The main characteristics of turbulence are that the gradients are created by vortices and occur in all directions, the turbulence is nonlinear and rotates strongly with three-dimensional eddies, as well as the flows are diffusive and intermittent (Panofsky and Dutton, 1994). The motions in the atmospheric boundary layer are always turbulent. Turbulence is continuous in the surface layer and disappears or is periodically insignificant in the upper part of the atmospheric boundary layer (Arya, 2001). In micrometeorology, Monin and Obukhov (1954) proposed a method for flux estimation that has received intensive attention in micrometeorology and is referred to as the Monin-Obukhov similarity theory (MOST).

2.1.4 Monin-Obukhov similarity theory

MOST and its associated empirical stability functions have been successfully used for describing fluxes of momentum and other quantities in the turbulence surface layer over homogeneous surface with stationary flow (Nakamura and Mart, 2001) and to date remains one of the most important theories in micrometeorology. MOST combines the mechanical and convective turbulence theories to determine the scalar fluxes. For a constant flux layer, Monin and Obukhov (1954) proposed a few key parameters for determining the turbulence structure: velocity scale (friction velocity), buoyancy parameter, kinematic surface stress, height above the ground, temperature scale and humidity scale (Kaimal and Finnigan, 1994; Arya, 2001). In the atmospheric surface layer, MOST assumes that the flux-gradient relationship can be formulated in terms of the height above the ground and the Obukhov length. The Obukhov length (L_o) is the height where the energy that is produced mechanically equals the amount of energy which is thermally produced or consumed. The term L_o is used as a measure of the atmospheric stratification dynamics, with $L_o > 0$ for stable conditions and $L_o < 0$ for unstable, and can be estimated as (Monin and Obukhov, 1954; Savage *et al*., 1997; Savage *et al*., 2004; Moraes *et al*., 2005):

$$L_o = -u_*^3 \frac{T_a}{k\,g} \frac{\rho_a c_p}{H} \text{ or equivalently } L_o = -u_*^2 \frac{T_a}{k\,g\,T_*} \tag{2.6}$$

where u_* is the friction velocity (m s^{-1}), T_a the absolute temperature (K), k the von Kármán constant (0.4), g the acceleration due to gravity (m s^{-1}), ρ_a the density of air (kg m^{-3}), c_p the specific heat capacity of air at constant pressure (J kg^{-1} K^{-1}) and H the sensible heat flux (W m^{-2}). The friction velocity u_* (m s^{-1}) at the surface is obtained as (Garratt, 1992; Nakamura and Mart, 2001; Moraes *et al.*, 2005)

$$u_* = \left((\overline{u^{'}w^{'}})^2 + (\overline{v^{'}w^{'}})^2 \right)^{1/4} \tag{2.7}$$

where u, v, and w are the three dimensional orthogonal wind speeds, u', v', and w' are the fluctuations from the mean of u, v, and w respectively.

The turbulence flow characteristics can be expressed by the atmospheric stability parameter ζ (dimensionless) proposed by Monin and Obukhov (1954) as:

$$\zeta = (z-d)/L_o. \tag{2.8}$$

The atmospheric conditions can be categorized into five groups according to ζ (Deardorf, 1978; Arya, 2001):

- convective: $\zeta < 0.05$;
- unstable: $-0.05 \leq \zeta < -0.02$;
- neutral: $-0.02 \leq \zeta < 0.02$;
- stable-continuous: $0.02 \leq \zeta < 0.2$;
- stable sporadic: $\zeta > 0.2$.

2.2 Footprint analysis

Meteorological measurements of the turbulent fluxes such as sensible heat and latent energy fluxes, between the underlying surface and the atmosphere often depend on the determination of these fluxes at a point above the surface. The measurements at this point reflect the transport of turbulent eddies carrying heat energy or mass from upwind sources. All micrometeorological methods rely in their theory on the assumption of an ideal homogeneous surface (Drexler *et al*., 2004). In practice, most of the surfaces especially vegetated surfaces, show spatial variability in their exchange activities. Also, the surface is usually surrounded by different agricultural and natural vegetation canopies. Therefore, estimation of footprint for turbulence flux is crucial for proper execution of micrometeorological measurements as the footprint determines the relative influence of the underlying area on these fluxes. The flux measurement footprint is defined as the spatial context of the measurement of surface layer fluxes (Schmid, 2002). The footprint function $F(x, z_m - d)$ for a scalar flux measured at height z_m (m) and at a downwind fetch distance x (m) away, for a surface with a zero displacement height d (m) is mathematically defined as (Horst and Weil, 1992):

$$F(x, z_m - d) = \int_{-\infty}^{x} S(x) f(x, z_m - d)\, dx \tag{2.9}$$

where $S(x)$ is the surface source strength (W m^{-2} for sensible heat flux footprints) and f the footprint at a distance x. Hsieh *et al*. (2000) proposed the following model, mainly analytical, for estimating footprint of the surface flux density

$$f(x, z_m - d) = \frac{1}{k^2 x^2} D z_u^P |L_o|^{1-P} \exp\left(\frac{-1}{k^2 x} D z_u^P |L_o|^{1-P} \right) \tag{2.10}$$

where z_u is the length scale, and D and P the similarity constants obtained by Hsieh *et al*. (2000) and given in Table 2.1. Savage *et al*. (2004) defined z_u to include d and z_o and to apply a correction as follows:

$$z_u = \frac{(z_m - d)^2}{z_m - (z_o + d)} \left(\mathrm{In} \frac{(z_m - d)}{z_o} - 1 + \frac{z_o}{(z_m - d)} \right). \tag{2.11}$$

According to Calder (1952) and Gash (1986), the peak of the footprint x_{peak} (m) can be estimated as a function of L_o and z_u:

Table 2.1 The values of the similarity constants *D* and *P* for different atmospheric stability

Atmospheric stability	*D*	*P*
Unstable	0.28	0.59
Near-neutral and neutral	0.97	1.00
Stable	2.44	1.33

$$x_{peak} = \frac{D\, z_u^P \left|L_o\right|^{1-P}}{2k^2}. \tag{2.12}$$

The cumulative fraction of the flux F to surface source flux S_o ratio, at distance x from the source and at an effective height of $z_m - d$ from the ground surface, can be estimated using (Hsieh *et al.*, 2000):

$$\frac{F(x, z_m - d)}{S_o} = \exp\left(\frac{-2}{x} x_{peak}\right). \tag{2.13}$$

The size and shape of the flux footprint mainly depends on measurement height, surface roughness and atmospheric stability (Gash, 1986; Leclerc and Thurtell, 1990). The footprint size decreases and the peak contribution moves closer to the instruments with a decrease in measurement height, with an increase in surface roughness, and with changes in atmospheric stability from stable to unstable condition. The footprint is used for specifying the relative contribution of each source element of the upwind surface area to the measured concentration or flux, and provides an estimate of the height-fetch ratio which determines the appropriate height of instruments for flux measurements, especially under horizontal inhomogeneities such as changes in the surface roughness or water content (Luhar and Rao, 1994; Hsieh *et al.*, 2000). The footprint is also necessary to link measurements at different scales, such as eddy-covariance flux data with soil chamber measurements, or tower measurements with remote sensing information (Göckede *et al.*, 2005).

2.3 Radiation and energy balance

Most of the environmental processes near the earth's surface get their energy from heat energy or mass exchanges between the earth and the atmosphere (e.g. evaporation). The source of energy is radiant energy initially provided by the absorption of solar irradiance. The radiation balance for a flat and extensive surface is an accounting of the incoming and outgoing components of radiation. These components are balanced over the surface as a whole over time period and can be expressed as:

$$R_n = I_s(1-r) + L_d - L_u \tag{2.14}$$

where R_n is the net irradiance, I_s the incoming shortwave irradiance, r the surface refection coefficient, and L_d and L_u the downward and emitted long wave irradiances respectively. Net irradiance R_n links the surface radiation and energy balance. The conservation of R_n at the surface to heating the air and/or the subsurface, evaporate water and used physical and biological processes without any gain or lost due to the surface can be expressed as (Rosenberg *et al*., 1983):

$$R_n = LE + H + G + M + S + V \tag{2.15}$$

where LE is the latent energy flux, H the sensible heat flux, G the soil heat flux, M the energy flux associated by biochemical processes, S the energy flux into/or out of plant tissues and V the energy flux lost or gained by horizontal advection. All components of the energy balance are in W m^{-2}. Advection and the energy flux associated with photosynthesis and respiration, and energy stored in the canopy are relatively smaller and neglected (Thom, 1975). Then, Eq. (2.15) can be simplified by neglecting the smaller terms. Hence the shortened energy balance equation is given by:

$$R_n = LE + H + G. \tag{2.16}$$

The shortened energy balance is regarded as essential for estimating LE and hence evaporation E, as a residual and for testing the accuracy and reliability of the scalar fluxes measurements (Brotzge and Crawford, 2003) in the absence of the direct measurements of LE. The available energy flux (A) for any surface is the difference between R_n and G and is partitioned into the sensible heat flux and latent energy flux:

$$R_n - G = LE + H \ . \tag{2.17}$$

A sign convention is required for application of the energy balance equation. The sign convention used is that fluxes directed toward the surface are negative and those directed away are positive. During the daytime, energy balance components are usually positive.

2.3.1 Net irradiance

Net irradiance R_n, measured using a net radiometer, is an important aspect in energy balance studies and more so in evaporation studies. Also R_n can be estimated from measured incoming solar irradiance (Allen *et al*., 1998). Various types of net radiometers differing in their accuracy (Savage and Heilman, 2009) and type - e.g., dome or domeless instruments, directly measure R_n above the surface. The net radiometer should be calibrated against a standard reference net radiometer or irradiance source (Savage *et al*., 1997; Savage and Heilman, 2009). The sources of error in R_n are due to calibration and field measurements such as the leveling and placement of the sensor. The net irradiance errors due to dirt or damaged domes or levelling are negligible (Payero *et al*., 2003). Many studies determined the fractional error in R_n. For instance, Angus and Watt (1984) found the fractional error in R_n is about 0.025 R_n and this was confirmed by Savage (2009).

2.3.2 Soil heat flux

Soil heat flux G is the sum of the average soil heat flux at depth 0.08 m and the average soil heat flux above the soil heat flux plates. Soil heat flux plays a significant role in the energy balance and evaporation estimates especially above sparse vegetation in semi-arid regions. The most common method for measuring G is a combination method (Tanner, 1960) which uses the soil heat flux plates, soil temperature and soil water content sensors. Soil heat flux G is estimated as:

$$G = G_{plate} + G_{stored} \tag{2.18}$$

where G_{plate} is the soil heat flux measured with soil heat flux plates and the heat energy flux stored above the soil heat flux plates (G_{stored}) is:

$$G_{stored} = \rho_{soil}\, c_{soil}\, \frac{\Delta z\, \overline{\Delta T}_{soil}}{\Delta t} \tag{2.19}$$

where ρ_{soil} is the bulk density of dry soil (kg m^{-3}), c_{soil} the specific heat capacity of soil (J kg^{-1} ^{o}C^{-1}), ΔT_{soil} the change in the average soil temperature above the soil heat flux plate (^{o}C), from one time period to next, dt the time between temperature averages (s) and Δz the soil depth (m). The specific heat capacity of the soil is calculated using:

$$\rho_{soil}\, c_{soil} = \rho_{soil} c_{dsoil} + \rho_w\, \theta_v\, c_w \tag{2.20}$$

where c_{dsoil} is the specific heat capacity of dry soil (840 J kg^{-1} ^{o}C^{-1}), ρ_w the density of water (1000 kg m^{-3}), θ_v the soil water content (m^3 m^{-3}), c_w the specific heat capacity of water (4200 J kg^{-1} ^{o}C^{-1}), and Δz the soil heat flux plates depth (m). There are many sources of errors in measurements of G. According to Savage (2009), these errors include calibration errors and field measurement errors such as errors associated with changes in soil temperature from one measurement period to another, errors due the positioning of the sensors and errors in the measurement of soil water content. Furthermore, the placement of a soil heat flux plate may alter the movement of energy and water in the area surrounding its position.

2.3.3 Sensible heat flux

Sensible heat flux H is the heat energy flux transferred from or to the soil or vegetation surfaces to the atmosphere by conduction and convection as a result of temperature differences between the underlying surface and the atmosphere. There are different micrometeorological methods for estimating H, including Bowen ratio, eddy covariance, flux variance, scintillometer and surface renewal methods. Aspects of the meteorological methods applied in the current study for estimating H above the canopy surface are discussed and the advantages and disadvantages of these methods are highlighted in later sections.

2.3.4 Latent energy flux

Latent energy LE is the energy removed by the evaporation of water (or gained by the condensation), which results in the change of evaporated (or condensed) water from the liquid to the vapour state (vapour to the liquid state) with little temperature change, and is given by the product of the evaporation rate and the specific latent heat of vaporization of water. LE can be directly measured or indirectly estimated as a residual using the shortened energy balance equation:

$$LE = R_n - H - G. \tag{2.21}$$

Since independent measurements of LE were not available in this study, LE was estimated as a residual using the shortened energy balance equation. The error in R_n, G and H measurements should be determined when LE is estimated as a residual. The fractional errors in R_n, G and H can be estimated by installing several sensors at the same height above the canopy surface (or different soil locations and at the same soil depth) at different points in the study area. The measurement errors for R_n and G can be determined by calibration.

2.4 Temperature variance method

Wyngaard *et al*. (1971) and Tillman (1972) initiated the flux variance method which is based on MOST. According to this theory, for uniform surfaces, the relation between the fluxes and variances of atmospheric scalars is applied (Weaver 1990; de Bruin *et al*., 1993). This method allows turbulent scalar fluxes to be estimated from measurements of the scalar at a height above the canopy surface. The most common scalar is air temperature which is then used to estimate sensible heat flux and this has been referred to as the temperature variance (TV) method. This method is less expensive and reasonably simple with relatively low power requirements. Currently, there are two methods for estimating H_{TV}, one that includes an adjustment using stability (Wyngaard *et al*., 1971), and a second that includes an adjustment using air temperature skewness (Tillman, 1972). There are other methods very similar to the TV method such as the method of de Bruin *et al*. (1993) that is based on MOST and uses a spatial second-order air temperature structure function.

The TV method has been tested and used for different surface types, homogeneous and heterogeneous surfaces, and different atmospheric stability conditions (e.g. Hsieh and Katul, 1996; Aubinet, 1997; Wesson *et al*., 2001; Choi *et al*., 2004; van Dijk *et al*., 2004; Castellví and Martínez-Cob, 2005; Gao *et al*., 2006; Hsieh *et al*., 2008) and has provided reasonable estimates of sensible heat flux during unstable conditions. Most of these studies used the TV method, including adjustment for stability. Castellví and Martínez-Cob (2005), based on their study above olive trees to estimate H_{TV} in the roughness and inertial sub-layers, reported that the accuracy of the H_{TV} estimate in the inertial sub-layer was improved compared to the roughness sub-layer. The TV method has several advantages over other micrometeorological methods: it is simple and does not require sophisticated and expensive high frequency wind speed measurements or calibration against standard methods. Generally, the main drawbacks of the TV method are that the TV similarity constants need to be determined *a priori* (Hsieh *et al*., 2008) and that the thermocouple is sensitive to damage.

2.4.1 Temperature variance including adjustment for stability

The TV method depends on the standard deviation of air temperature (σ_T) and the temperature scale of turbulence (T_*) (K). For estimating sensible heat flux ($H_{TV(S)}$), a relationship between σ_T and T_*, based on MOST, is needed. This relationship can be found using surface-layer similarity. Generally, MOST describes the relationship between T_* and σ_T over a uniform flat surface as a function of atmospheric stability (Tillman, 1972):

$$\frac{\sigma_T}{T_*} = f(-\zeta) = g_1(\zeta) \qquad (2.22)$$

with:

$$T_* = \frac{H}{\rho_a \, c_p \, u_*} \qquad (2.23)$$

where $f(\zeta)$ is the universal stability function and $g_1(\zeta)$ the empirical atmospheric stability similarity function proposed by Tillman (1972). Following Tillman (1972), a commonly used expression for $g_1(\zeta)$ is:

$$g_1(\zeta) = \frac{T_*}{\sigma_T} = \begin{cases} C_1 / (C_2 - \zeta)^{1/3}, & \zeta \le 0 \\ 1/C_3 & \zeta > 0 \end{cases} \tag{2.24}$$

where C_1, C_2 and C_3 are universal similarity constants. Based on the work by Wyngaard *et al*. (1971), Tillman (1972) found 0.9 and 0.05 values for C_1 and C_2 respectively. From the literature, C_3 is not well defined and has been found to vary between 1.85 (Wesely, 1988) to 4.0 (Wesson *et al*., 2001). Albertson *et al*. (1995) reported that $f(-\zeta)$ must satisfy two limits: the neutral case limit where the stability parameter ζ approaches near zero and σ_T/T_* approaches a constant and the free convection limit, ζ approaches infinity and σ_T/T should be independent of friction velocity. For the neutral case, σ_T/T_* converges to a value C_3 (Wyngaard *et al*., 1971):

$$\frac{\sigma_T}{T_*} = C_3 \tag{2.25}$$

and C_2 is related to C_1 and C_3 as (Tillman, 1972):

$$C_2 = \left(C_1 / C_3 \right)^3. \tag{2.26}$$

For the free convection limit where the dominant motions are in the vertical direction due to buoyant forces rather than in the horizontal due to mechanical shearing, Eq. (2.22) can be reduced to (Wyngaard *et al*., 1971):

$$\frac{\sigma_T}{T_*} = \frac{C_1}{(-\zeta)^{1/3}}. \tag{2.27}$$

By combining Eqs (2.22), (2.23), (2.24), and L_o, Wyngaard *et al*. (1971) and Tillman (1972) derived the following expression for sensible heat flux adjusted for stability $H = H_{TV(S)}$ using σ_T and $\overline{T_a}$ measurements at a height z above soil surface as:

$$H_{TV(S)} = \begin{cases} \rho_a c_p \left(\dfrac{\sigma_T}{C_1}\right)^{3/2} \left(\dfrac{k g z}{\overline{T}_a}\right)^{1/2} \left(\dfrac{C_2 - \zeta}{-\zeta}\right)^{1/2}, & \zeta < 0 \\ -\rho_a c_p \left(\dfrac{\sigma_T}{C_2}\right)^{3/2} \left(\dfrac{k g z}{\overline{T}_a}\right)^{1/2}. & \zeta \geq 0 \end{cases} \tag{2.28}$$

Sensible heat flux may be estimated from σ_T, $\overline{T}_a$ and ζ above the roughness sub-layer, using Eq. (2.28). The parameter ζ is needed for this method to identify unstable conditions and is included in the calculations. The free convection limit for Eq. (2.28) is obtained by assuming the limit for $\zeta > C_2$, and has proved to perform adequately under slightly unstable conditions and can be expressed as (Tillman, 1972):

$$H_{TV} = \rho_a c_p \left(\frac{\sigma_T}{C_1}\right)^{3/2} \left(\frac{k g z}{\overline{T}_a}\right)^{1/2}. \qquad \zeta \leq -0.05 \tag{2.29}$$

The free convection limit under slightly unstable conditions can be more easily used for estimating sensible heat flux since it is independent of ζ and requires σ_T and $\overline{T}_a$ measurements as the only input data.

The parameter ζ can be estimated from EC measurements or alternatively estimated independently by an iteration process. The iteration process requires the additional measurements of wind speed as an input. According to Brutsaert (1982) and Kustas *et al*. (1994), u_* can be estimated using MOST, either from standard deviation of the vertical wind speed (σ_w) or mean horizontal wind speed (u) measurements as:

$$u_* = \frac{\sigma_w}{a\left(1 - b\zeta\right)^{1/3}} \tag{2.30}$$

or

$$u_* = \frac{k u}{\ln\left(\left(z_r - d\right)/ z_o\right) - \psi_m} \tag{2.31}$$

where a and b are the universal constants with values of 1.3 and 2.0 respectively, z_r the wind speed measurement height (m), and ψ_m the universal stability correction factor for momentum given as (Dyer, 1974):

$$\psi_m = \begin{cases} 0.5\pi + 2\ln\left[\dfrac{1+x}{2}\right] + \ln\left[\dfrac{1+x^2}{2}\right] - 2\arctan(x), & \zeta \leq 0 \\ -4.7\zeta & \zeta > 0 \end{cases} \tag{2.32}$$

where $x = (1 - 16\ \zeta)^{1/4}$. An iterative process is used to determine H. Initially, to start the iterative procedure, L_o is assumed to be -1 x 10^9 m to get a first approximation for u_*. This provides a first approximation of L_o and H through Eqs (2.6) and (2.28) respectively. The procedure is iterated, also using Eqs (2.30) or (2.31) and Eq. (2.32), until convergence in L_o is achieved. The convergence occurs when the absolute difference between former and latter values of L_o does not change more than a prescribed limit of 0.001 m.

2.4.2 Temperature variance including adjustment for air temperature skewness

According to MOST, Tillman (1972) noted that non-dimensional functions such as the air temperature skewness (S_k) are determined by z/L_o. The air temperature skewness is defined as:

$$S_k = \frac{1}{\sigma_T{}^3}\left[\frac{1}{n}\sum_{i=1}^{n}(T_i - \overline{T})^3\right] \tag{2.33}$$

where n is the number of the observations within the averaging time period, T_i an air temperature sample at time i, and $\overline{T}$ and σ_T the mean and standard deviation of air temperature for the averaging time period. The ζ parameter can be determined as a function of S_k by plotting the data in linear and semi-log form using:

$$\zeta = -A\exp(BS_k) \qquad -3.0 < \zeta \leq -0.01 \tag{2.34}$$

where A and B are positive constants of 0.0137 and 4.39 respectively (Tillman, 1972), obtained by the natural log of Eq. (2.35) and using a linear square fit, assuming that errors occur in both ζ and S_k. If S_k is zero for the neutral case, ζ can be determined as:

$$\zeta = A - A\exp\,(B\,S_k). \tag{2.35}$$

By combining Eqs (2.34) and (2.28), Tillman (1972), applying MOST, derived an expression for sensible heat flux $H = H_{TV(Sk)}$ adjusted for air temperature skewness and T_a at one level above the canopy surface as:

$$H_{TV(Sk)} = \begin{cases} \rho_a\, c_p \left(\dfrac{\sigma_T}{C_1}\right)^{3/2} \left(\dfrac{k\,g\,z\left(C_2 + A\exp(B\,S_k)\right)}{T_a\,A\exp(B\,S_k)}\right)^{1/2}, & \zeta < 0 \\ -\rho_a\, c_p \left(\dfrac{\sigma_T}{C_2}\right)^{3/2} \left(\dfrac{k\,g\,z}{T_a}\right)^{1/2}. & \zeta \geq 0 \end{cases} \tag{2.36}$$

Tillman (1972) also proposed the following expression for estimating u_*:

$$u_* = \left[\frac{\sigma_T}{C_1}\,\frac{kgz}{T_a}\,\frac{\left(C_2 - \zeta\right)^{1/3}}{-\zeta}\right]^{1/2}. \qquad -3.0 < \zeta \leq -0.03 \tag{2.37}$$

Combining Eqs (2.34) and (2.37) yields

$$u_* = \left[\frac{\sigma_T}{C_1}\,\frac{k\,g\,z}{T_a}\,\frac{\left(C_2 + A\exp(B\,S_k)\right)^{1/3}}{A\exp\left(B\,S_k\right)}\right]^{1/2}. \tag{2.38}$$

The application of Eq. (2.36) for estimating $H = H_{TV(Sk)}$ has several advantages; it is independent of EC measurements and requires high-frequency air temperature measurements as the only input data to obtain the sensible heat flux. The sign of the third-order air temperature structure function is used to identify unstable conditions. The iteration process and wind speed measurements are not needed.

2.4.3 Sensible heat flux from MOST and a spatial second-order air temperature structure function

The estimation of sensible heat flux using MOST and a spatial second-order air temperature structure function (C_{TT}) is very similar to the TV method. C_{TT} above the uniform surface for steady-state atmospheric conditions is defined by (Hill, 1992):

$$C_{TT} = \frac{\left(T_{x1} - T_{x2}\right)^2}{x_{12}^{2/3}} \tag{2.39}$$

where T_{x1} and T_{x2} are the air temperatures measured at positions x_1 and x_2, at the same time respectively, and x_{12} is the spatial separation between the two measurements of air temperature. Using MOST, Wyngaard *et al*. (1971) found:

$$\frac{C_{TT}(z-d)}{T_*^2} = g_2(\zeta) \tag{2.40}$$

where $g_2(\zeta)$ is an empirical atmospheric stability similarity function. Wyngaard *et al*. (1971) proposed use of a widely accepted expression for $g_2(\zeta)$ as:

$$g_2(\zeta) = \begin{cases} C_{T1} / (1 - C_{T2}\,\zeta)^{2/3}, & \zeta < 0 \\ C_{T1} / (1 - C_{T3}\,\zeta)^{2/3} & \zeta \geq 0 \end{cases} \tag{2.41}$$

where C_{T1}, C_{T2} and C_{T3} are the universal similarity constants with values 4.9, 7 and 2.75 or 2.4 respectively. Wyngaard (1973) explained the change in C_{T3} from 2.4 to 2.75 as reflecting the change in the von Kármán constant from 0.35 to 0.4.

According to Taylor (1938), the frozen turbulence hypothesis states that the spatial correlation of air temperature measurements at two points at the same time can be converted to the temporal correlation of air temperature measurements at two times at the same point as $x_{12} = u\ r$ where r is the air temperature time lag (s), u the mean horizontal wind speed (m s^{-1}) which can be measured with a sonic anemometer or alternatively a wind speed sensor. The frozen turbulence hypothesis is used to convert a spatial data series to a time series. Hence C_{TT} can also be estimated from the time series from the second-order air temperature structure ($S^n_{(r)}$) (Castellví *et al*., 2006a):

$$C_{TT} = \frac{\left(T_{x_1} - T_{x_1}\right)^2}{(ur)^{2/3}} = \frac{S^2_{(r)}}{(ur)^{2/3}}. \tag{2.42}$$

The $S^n_{(r)}$ can be obtained from high-frequency air temperature measurements as:

$$S^n(r) = \frac{1}{m-j}\sum_{i=1+j}^{m}(T_i - T_{i-j})^n \tag{2.43}$$

where m is the number of data points measured at a frequency f (in Hz) within an averaging period, generally 30 min, n the power of the air temperature structure functions (n = 2), T_i the i^{th} air temperature sample, i the data point number and j the number of the lags between data points corresponds to an air temperature time lag r given by $r = j / f$. The direction of H is determined according to the sign of the third-order air temperature structure function for which n = 3 in Eq. (2.43). Combining Eqs (2.39) and (2.40), and u_* *via* L_o, de Bruin *et al*. (1993) provided an expression to estimate the sensible heat flux $H = H_{MOST}$ using C_{TT} and T_a measurements:

$$H_{(MOST)} = \rho_a\, c_p \left(k\, g\, z/\overline{T_a}\right)^{1/2} \frac{C_{TT}{}^{3/4}}{(-\zeta\, g_2(\zeta)^{3/2})^{1/2}}. \tag{2.44}$$

Sensible heat flux can be estimated using Eq. (2.44) from $\overline{T_a}$, C_{TT} and u measurements in conjunction with the Taylor hypothesis of frozen turbulence using Eq. (2.42). The main drawback of Eq. (2.44) is that it requires *prior* previous knowledge of ζ to identify unstable conditions.The free convection form for Eq. (2.44) holds under slightly unstable conditions and is expressed as (Castellví *et al*., 2006a):

$$H_{(MOST)} = 0.8\rho_a\, c_p z \frac{(k\, g)^{1/2}}{T_a{}^{1/2}} C_{TT}^{3/4}, \qquad \zeta << -0.14 \tag{2.45}$$

Based on Chen *et al*. (1997b), sensible heat flux estimates are proportional to z in the roughness sub-layer while in the inertial sub-layer they are proportional to z - d.

2.5 Surface renewal method

The surface renewal (SR) concept was developed in the chemical engineering field (Higbie, 1935) and is based on the coherent structures concept. Paw U and Brunet (1991) introduced the SR method for estimating sensible heat flux $H = H_{SR}$ over natural surfaces using high frequency air temperature measurements at a single level using unshielded and naturally-ventilated fine-wire thermocouples. This method is attractive because it is simple, uses low-cost thermocouples, operates in either the roughness sub-layer or the inertial sub-layer, and overcomes the difficulties associated with other micrometeorological methods (Drexler *et al*., 2004; Paw U *et al*., 2005; Castellví *et al*., 2008). The SR method can be used at frequencies between 2 and 10 Hz. The former allows the method to be used by using inexpensive loggers compared to EC. A full description of the detailed theoretical aspects of the SR method has been highlighted (Snyder *et al*., 1997; Spano *et al*., 1997a, b; Paw U *et al*., 2005; Mengistu, 2008; Mengistu and Savage, 2010). The disadvantages of the SR method are that it requires calibration against EC and the thermocouple is sensitive to the damage.

The performance of SR was evaluated for a variety of vegetated surfaces and different stability conditions (e.g., Paw *et al*., 1995; Snyder *et al*., 1996; Spano *et al*., 1997, 2000; Castellví *et al*., 2002; Spano *et al*., 2002; Castellví, 2004; Castellví and Martínez-Cob, 2005; Castellví *et al*., 2006a, b; Simmons *et al*., 2007; Mengistu, 2008; Castellví and Snyder, 2009a, b; Jarmain *et al*., 2009). The performance of the SR method over open water was also evaluated by Mengistu (2008) and Jarmain *et al*. (2009). These studies recommended the SR method for estimating H and thereafter determining LE. Recent studies evaluated the performance of SR under the influence of regional advection and have provided reliable estimates of sensible heat and latent energy fluxes. For instance, Castellví and Snyder (2009b), in their work on the performance of the SR method to estimate sensible heat flux over two growing rice fields under the influence of regional advection, found the SR-estimated sensible heat flux gave results that were similar to those measured using EC. Castellví *et al*. (2008) reported that the SR method produced very good and reliable estimates of sensible heat flux and latent energy flux as a residual for measurements in the inertial sub-layer under the influence of regional advection.

Currently, there are various SR model methods for estimating sensible heat flux that include an ideal SR analysis model method based on an air temperature structure function analysis, the SR analysis using a ramp model with finite micro-front period based on Chen *et al*. (1997a), combined SR analysis model method with K-theory (Castellví, 2004) and the combined SR model method based on MOST that uses standard deviation of air temperature or the second-order air temperature structure function (Castellví *et al*., 2006a). Each approach has its own distinct advantages, disadvantages, theoretical assumptions, and spatial and temporal measurement scales. The application of these methods for long-term estimation of evaporation has not received sufficient attention.

2.5.1 Ideal surface renewal analysis model method based on structure function analysis

SR analysis assumes that at some instant an air parcel that suddenly moves down to the surface and remains connected with the sources (sinks) for a period of time, begins to be heated (cooled) because of the sensible heat exchange between the air and canopy elements. The parcel then ejects upwards and is replaced by new parcel sweeps towards the surface (Paw U *et al*., 1995; Katul *et al*., 1996; Snyder *et al*., 1996, 1997; Paw U *et al*., 2005; Castellví *et al*., 2008). Coherent structures are responsible for the majority of vertical transport of momentum, heat and the other scalars (Gao *et al*., 1989; Lohou *et al*., 2000). Ramp events are observed in the air temperature traces as a result of the turbulent coherent structures. These ramps, for stable and unstable conditions are characterized by amplitude and total ramp period parameters (Paw U and Brunet, 1991). It is assumed that the total ramp period consists of a ramp period l and a quiescent ramp period s. Paw U *et al*. (1995) presented a diagram for renewal process and summarized that as an ideal comprehensive scheme for ramp events in the scalar trace (Fig. 2.2). Following Paw U and Brunet (1991) and Paw U *et al*. (1995), the sensible heat flux can be determined as the change of heat content of the air with time ($M_{air}\ c_p\ dT/dt$) per unit area (A) as follows (Savage *et al*., 2004):

$$H_{SR} = c_p \frac{M_{air}}{A} \frac{dT}{dt} \tag{2.46}$$

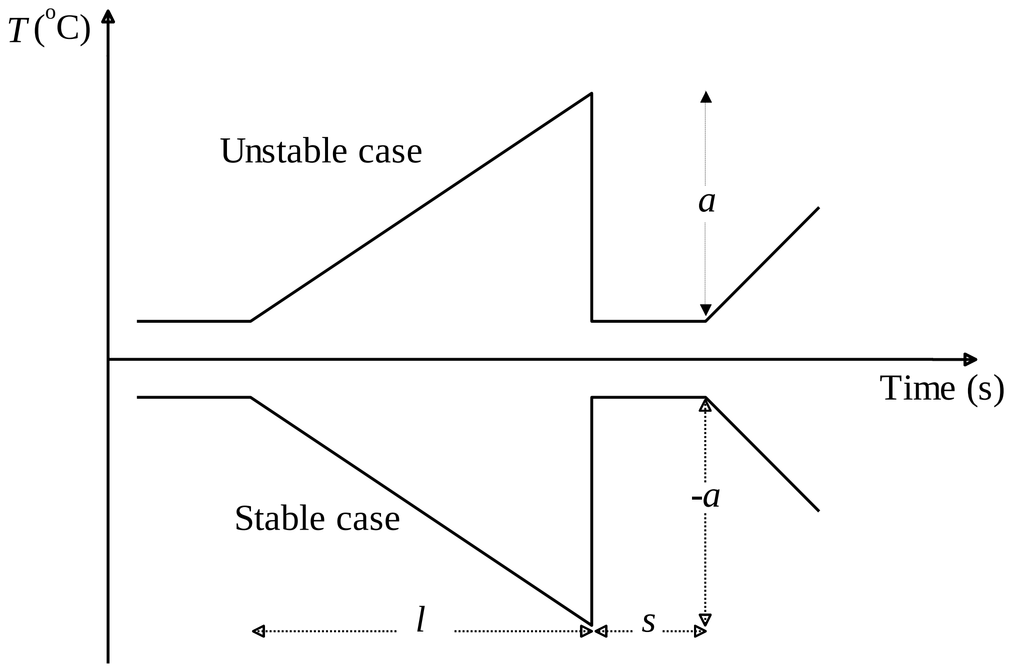

Fig. 2.2 An ideal SR analysis ramp model proposed by Paw U *et al*. (1995), assumes a quiescent period and a sharp instantaneous decrease in air temperature, where l and s are the ramping and quiescent periods respectively

where M_{air} is the mass of air heated (or cooled) by the rate of change in the air temperature difference dT/dt, and c_p the specific heat capacity of air at constant pressure. To simplify Eq. (2.46), M_{air} can be expressed in terms of ρ_a and the volume of air V per horizontal unit area A:

$$H_{SR} = \rho_a c_p \frac{V}{A} \frac{dT}{dt}. \tag{2.47}$$

The measured change in the air temperature with time is the partial derivative of temperature with time $\partial T/\partial t$ rather than dT/dt because air temperature is measured at a fixed point (Snyder *et al*., 1997). The term V/A represents the vertical distance (measurement height above the soil surface). It is assumed that the internal advection is negligible and hence:

$$H_{SR} = \rho_a \, c_p \, z \frac{\partial T}{\partial t} \tag{2.48}$$

where z is the measurement height above the soil surface and $\partial T / \partial t$ can be replaced by the ratio of the ramp amplitude a and the total ramp period $\tau = l + s$ in Eq. (2.49) to determine sensible heat flux. Therefore for the SR method, the sensible heat flux is determined using (Paw U *et al*., 1995):

$$H_{SR} = \alpha \, z \rho_a \, c_p \frac{a}{l + s} \tag{2.49}$$

where α is the SR weighting factor defined as a factor that corrects for the unequal heating or cooling from the measurement height to the ground and should be firstly determined by the comparisons of SR and eddy covariance sensible heat flux estimates. The weighting factor depends on time lag, an air temperature structure function, measurement height and plant canopy height, and the size of the fine-wire thermocouple used to measure air temperature at high frequency (Paw U *et al*., 2005). Paw U *et al.* (1995) reported that the SR weighting factor is 0.5 for maize, Walnut orchard, and mixed deciduous forest for measurement height at the canopy top and 1 for short grass for measurements at a height of 1 m above the grass. Duce *et al*. (1998) found that the weighting factor above bare soil is 0.9, 1.04, and 1.88 when the thermocouple size is 12.7, 25.4 and 76.2 μm respectively. Calibration of parameter α can be avoided by dividing the canopy into different thin sub-layers with assuming that $\alpha = 1$ for each layer, and then the total sensible heat flux is the sum of sensible heat fluxes for these sub-layers of the canopy (Spano *et al*., 2000). The quantity $\alpha \, z$ has a physical meaning, representing the volume of air per unit of ground area exchanged on average for each ramp in the sample period for the measurement height z (Paw U *et al*., 1995). Castellví *et al.* (2002) interpreted $\alpha \, z$ as the mean eddy size responsible for the renewal process. The amplitude and ramp period are estimated following the structure function approach of van Atta (1977): the air temperature structure function $S^n(r)$ is obtained from high frequency air temperature measurements using Eq. (2.43). The average a in the time interval can be determined from the solution of the polynomial equation (Spano *et al*., 1997a, b; Paw U *et al*., 2005):

$$a^3 + \left(10S^2(r) - \frac{S^5(r)}{S^3(r)}\right)a + 10S^3(r) = 0 \qquad (2.50)$$

and the total ramping period $l + s$ is estimated using:

$$l + s = -\frac{a^3 r}{S^3(r)}. \qquad (2.51)$$

The direction of H_{SR} is determined according to the sign of the amplitude a (positive for unstable conditions and negative for stable) (Snyder *et al.*, 1997). Many studies have evaluated the performance of Eq. (2.49) over a variety of canopies surfaces (e.g., Snyder *et al.*, 1996; Spano *et al.*, 1997b; Zapata and Martínez-Cob, 2001, 2002; Savage *et al*., 2004; Mengistu, 2008).

The main advantages of the SR method are that it is relatively low cost and simple because it requires high frequency air temperature measurements using fast response fine-wire thermocouples as an input to obtain the sensible heat flux regardless of stability conditions and without need for air temperature profile and wind speed data. Also the SR overcomes the problems related to fetch requirements, leveling, shadowing, orientation, relative instrument separation, and rotation, which introduce potential uncertainties in the eddy covariance method and other methods based on profiles (Anandakumar, 1999; Castellví *et al*., 2008). The main drawback of the SR analysis is that α must be determined.

2.5.2 Surface renewal ramp model method with finite micro-front period

Chen *et al*. (1997a) proposed a ramp model method that neglects the quiescent period but includes finite micro-front time instead of an instantaneous sharp decrease in air temperature as shown in Fig. (2.3), to overcome numerical complexity. In this model, a and τ can be estimated using a cubic temperature structure function from high frequency air temperature data as follows (Chen *et al*., 1997b):

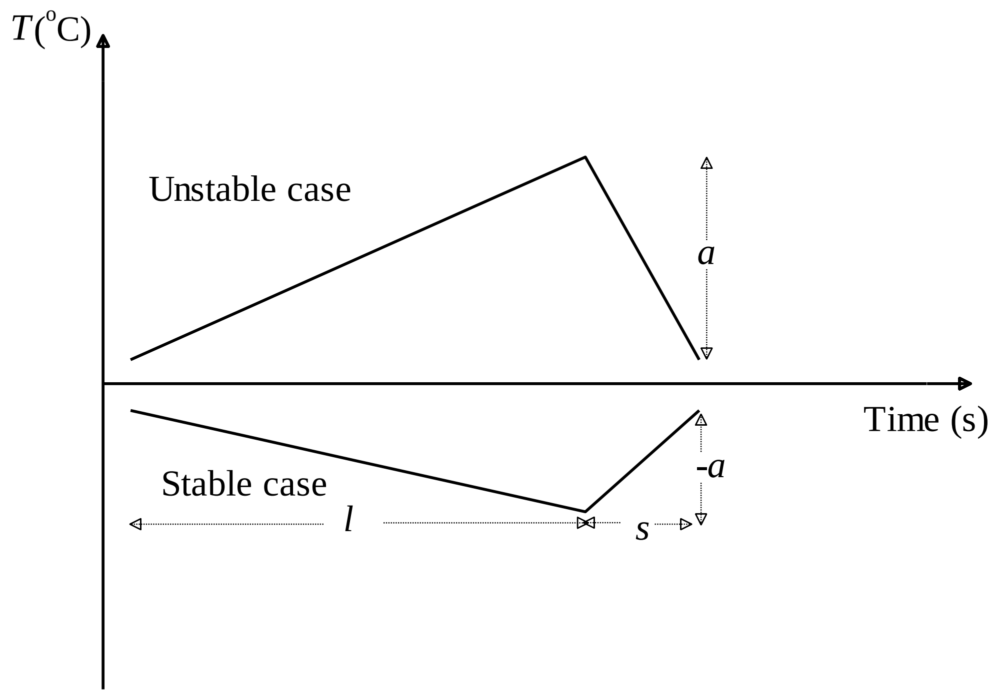

Fig. 2.3 SR analysis ramp model that neglects the quiescent period and assumes a finite micro-front time period: *l* and *s* are the ramp period and finite micro-front period respectively (Chen *et al*., 1997a).

$$\frac{a}{\tau^{1/3}} = -\gamma\left(\frac{S^3_{(r_m)}}{r_m}\right)^{1/3} \tag{2.52}$$

where r_m is the time lag that maximizes $-(S^3_{(r)}/r)^{1/3}$ and γ the correction coefficient for differences between $a/\tau^{1/3}$ and the maximum value $-(S^3_{(r)}/r)^{1/3}$ and ranges from 1 to 1.2 for straw mulch and bare soil (Chen *et al*., 1997b) and from 0.9 to1.1 for Douglas-fir forest (Castellví *et al*., 2006a). Raupach *et al*. (1989) expected that for plant canopies $1/\tau$ should scale with maximum wind shear (du/dz at $z = h$, where u is the mean wind speed and h the canopy height). Transport of momentum and scalar fluxes is dominated by eddies of length scale comparable with h and with $z - d$ in the canopy and the roughness sub-layer, and the inertial sub-layer respectively (Chen *et al*., 1997b). Chen *et al*. (1997b) assumed that $1/\tau$ can be scaled as follows:

$$\frac{1}{\tau}=\begin{cases}\beta\dfrac{u_*}{h}, & 0.2h<z\leq h+2(h-d)\\ \beta\dfrac{u_*}{z-d} & z>h+2(h-d),\ z\leq 0.2h\end{cases} \tag{2.53}$$

where β is the empirical coefficient. Following Sellers *et al*. (1986), the roughness sub-layer is assumed to be between $z = h$ and $z = h + 2(h - d)$. The layer adjacent to the soil within the canopies ($z = 0.2\ h$) is treated as the inertial sub-layer, with appropriate u and d for the soil or canopy understudy (Lee and Black, 1993).

Combining Eqs (2.49), (2.52) and (2.53) produces the following expression for estimating sensible heat flux at any height above ground, z, either within or above a canopy and over an averaging period:

$$H=\begin{cases}-\alpha'\beta^{2/3}\gamma\,\rho_a c_P\left(S^3_{(r_m)}/r_m\right)^{1/3}u_*^{2/3}\dfrac{z}{h^{2/3}}, & 0.2h<z\leq h+2(h-d)\\ -\alpha'\beta^{2/3}\gamma\,\rho_a c_P\left(S^3_{(r_m)}/r_m\right)^{1/3}u_*^{2/3}\dfrac{z}{(z-d)^{2/3}} & z-d>h+2\,(h-d),\ z-d\leq 0.2h\end{cases} \tag{2.54}$$

where $\alpha'\beta^{2/3}\gamma$ is the empirical combined coefficient which is a common for both roughness and inertial sub-layers. The α' value, as distinct from α obtained by regression, is a computed value. The recommended mean values for α', β, γ and the combined coefficient $\alpha'\beta^{2/3}\gamma$, for Douglas-fir forest, straw mulch, and bare soil (Chen *et al*., 1997b) are presented in Table 2.2. Chen *et al*. (1997b) recommended $\alpha'\beta^{2/3}\gamma$ = 0.4 for Douglas-fir forest, bare soil and straw mulch. Novak *et al*. (2000) applied this model within and above a barley-straw mulch in both normal and artificially wetted states to esti-

Table 2.2 Average coefficients α', β, γ and the combined coefficient $\alpha'\beta^{2/3}\gamma$ for Douglas-fir forest, straw mulch and bare soil (Chen *et al*., 1997b).

Canopy	α'	β	γ	$\alpha'\beta^{2/3}\gamma$
Douglas-fir forest	0.527	0.705	1.001	0.418
Straw mulch	0.511	0.538	1.175	0.397
Bare soil	0.691	0.398	1.104	0.413

mate sensible heat flux. For application of Eq. (2.54), $-\gamma\left(S^3_{(r_m)}/r_m\right)^{1/3}$ from high frequency air temperature data, and u_* from horizontal wind speed measurements are needed. The approach does not require calibration and slow dataloggers may be limited in determining the third-order air temperature structure function (Mengistu and Savage, 2010).

2.5.3 Combined surface renewal analysis model method with K-theory

To avoid the problems associated with Eq. (2.49), including calibration against EC or measurements at several layers within the canopy which is costly and physically impossible, Castellví *et al*. (2002) proposed a SR model based on the K-theory to estimate sensible heat flux using high-frequency air temperature. Using K-theory, sensible heat flux is expressed as:

$$H = \rho_a c_P K_h \frac{dT}{dz} \tag{2.55}$$

where T is the average air temperature and K_h the turbulent exchange coefficient for sensible heat flux where K_h is defined as (Arya, 2001):

$$K_h = \frac{ku_*(z-d)}{\phi_h(\zeta)} \tag{2.56}$$

where $\phi_h(\zeta)$ is the stability function for heat flux in the inertial sub-layer. Based on various micrometeorological experiments, the most widely accepted formulation for $\phi_h(\zeta)$ is (Businger *et al*., 1971; Arya, 2001):

$$\phi_h(\zeta) = \begin{cases} 0.74\left(1-9\zeta\right)^{-1/2}, & \zeta < 0 \\ 0.74, & \zeta = 0 \\ 0.74 + 4.7\zeta. & \zeta > 0 \end{cases} \tag{2.57}$$

Since the variable $\alpha' z$ in Eq. (2.49) physically represents the eddy size responsible for the renewal process, Castellví *et al*. (2002) proposed the following relationship:

$$\frac{a}{\alpha' z}\alpha\frac{dT}{dz}=\begin{cases}\beta\dfrac{a}{z}, & h\le z\le h+2(h-d)\\[2ex] \beta\dfrac{a}{z-d}. & z-d>h+2(h-d)\end{cases} \tag{2.58}$$

By combining Eqs (2.55), (2.56) and (2.58), Castellví (2004) found the following expressions to estimate sensible heat flux:

$$H_{SR}=\begin{cases}\rho_a c_p\, k\,\beta\, K_h^*\,\dfrac{a}{z}, & h\le z\le h+2(z-d)\\[2ex] \rho_a c_p\, k\,\beta\, K_h\,\dfrac{a}{z-d}. & z-d>h+2(z-d)\end{cases} \tag{2.59}$$

where β is the scale parameter, expressed as β_1/k and β_2/k for measurements in the roughness and the inertial sub-layer respectively, and K_h^* the turbulent exchange coefficient for sensible heat flux in the roughness sub-layer. Cellier and Brunet (1992) found the following relationship between K_h and K_h^*:

$$\frac{K_h}{K_h^*}=\frac{\phi_h^*}{\phi_h}. \tag{2.60}$$

Integrating Eq. (2.56) in Eq. (2.60), K_h^* can be expressed as:

$$K_h^*=\frac{k\,u_*\,z^*}{\phi_h(\zeta)}. \tag{2.61}$$

Castellví *et al*. (2002) proposed the following relation to estimate sensible heat flux in the roughness and the inertial sub-layers, by combining Eq. (2.59) with corresponding K_h and K_h^* to produce:

$$H_{SR} = \begin{cases} \rho_a c_p \, \beta_1 \, a \dfrac{z^*}{z} \dfrac{u_*}{\phi_h(\zeta)}, & h \le z \le z^* \\ \rho_a c_p \, \beta_2 \, a \dfrac{u_*}{\phi_h(\zeta)}. & z - d > z^* \end{cases} \tag{2.62}$$

where β_1 and β_2 are the scale parameters for the roughness and inertial sub-layers respectively. They found the magnitude of β_1 ranging from 0.23 to 0.33 and the magnitude of β_2 ranging from 0.10 to 0.15 for different crop canopies. For application of Eq. (2.62), wind speed measurements are required for estimating u_* iteratively.

Following Castellví (2004), α' in Eq. (2.49) is estimated as:

$$\alpha' = \begin{cases} \left(\dfrac{k \, z^* \, \tau \, u_*}{\pi \, z^2 \, \phi_h(\zeta)} \right)^{1/2}, & h \le z \le z^* \\ \left(\dfrac{k(z-d)\tau \, u_*}{\pi \, z^2 \, \phi_h(\zeta)} \right)^{1/2}. & z - d > z^* \end{cases} \tag{2.63}$$

Castellví (2004) derived the following expression for estimating β in Eq. (2.59) in the roughness and the inertial sub-layers:

$$\beta = \begin{cases} \left(\dfrac{z^2}{k\pi z^*} \dfrac{\phi_h(\zeta)}{\tau u_*} \right)^{1/2}, & h \le z \le z^* \\ \left(\dfrac{z-d}{k\pi} \dfrac{\phi_h(\zeta)}{\tau u_*} \right)^{1/2}. & z - d > z^* \end{cases} \tag{2.64}$$

The square root in Eq. (2.64) depends on other variables and yields close-calibrated β values when the distance between measurement heights is insignificant (Castellví, 2004). Thus parameter β is weakly dependent on the measurement height. It was found that β was 0.25 and 0.37 in the roughness sub-layer for wheat and grapevine respectively, and 0.25 for grass in the inertial sub-layer (Castellví, 2004). On the basis of ramp frequency scales with wind shear, Chen *et al*. (1997a) scaled $1/\tau \, u_*$ over z or z - d in the roughness and inertial sub-layers respectively.

Combining Eqs (2.49) and (2.63) or Eqs (2.59) and (2.64) produces the following relation for sensible heat flux (Castellví, 2004):

$$H_{SR} = \begin{cases} \rho_a c_p \dfrac{a}{\tau^{1/2}} \left(\dfrac{u_*}{\phi_h(\zeta)} \right)^{1/2} \left(\dfrac{k z^*}{\pi} \right)^{1/2}, & h \le z \le z^* \\ \rho_a c_p \dfrac{a}{\tau^{1/2}} \left(\dfrac{u_*}{\phi_h(\zeta)} \right)^{1/2} \left(\dfrac{k(z-d)}{\pi} \right)^{1/2}. & z-d > z^* \end{cases} \tag{2.65}$$

Equation (2.65) is exempt from calibration regardless of measurement height and stability parameter and valid over homogeneous surfaces. Additional measurements of horizontal wind speed are needed to determine u_* iteratively. Also, a minor error in the ramp amplitude may cause a large error in ramp duration. In addition, error in estimating H may occur for measurements above sparse canopy cover, where fetch is limited.

By substituting Eq. (2.52) and u_* definition *via* L_o in Eq. (2.65) gives the following expression for sensible heat flux (Castellví, 2004):

$$H_{SR} = \begin{cases} \rho_a c_p \left(\dfrac{g}{T} \right)^{1/5} k^{4/5} \left(\dfrac{z^*}{\pi} \right)^{3/5} z^{1/5} \left[-\gamma^3 \left(\dfrac{S^3_{(r_m)}}{r_m} \right) \right]^{3/5} \dfrac{1}{a^{3/5}} \left(\dfrac{1}{-\zeta\, \phi_h^3(\zeta)} \right)^{1/5}, & h \le z \le z^* \\ \rho_a c_p \left(\dfrac{g}{T} \right)^{1/5} \dfrac{\left(k(z-d)\right)^{4/5}}{\pi^{3/5}} \left[-\gamma^3 \left(\dfrac{S^3_{(r_m)}}{r_m} \right) \right]^{3/5} \dfrac{1}{a^{3/5}} \left(\dfrac{1}{-\zeta\, \phi_h^3(\zeta)} \right)^{1/5}. & z-d > z^* \end{cases} \tag{2.66}$$

It is found that application of Eq. (2.66) using $\gamma = 1.1$ provides good performance for different measurement heights above the crop surface (Castellví and Martínez-Cob, 2005). Equation (2.66) requires calibration to determine γ and depends on ζ. For different canopies, the value of γ varies by less than 25 % with respect to unity (Chen *et al.*, 1997b). Additional measurement of horizontal wind speed is needed to determine L_o iteratively.

For the free convection condition ($-3.0 \le \zeta \le -0.03$), the functions $1/(\zeta\, \phi_h^3(\zeta))^{1/5}$ in Eq. (2.66) can be set as a constant value of 2.4 and hence rewritten as (Castellví *et al.*, 2006a):

$$H_{SR} = \begin{cases} 2.4\rho_a c_p \left(\dfrac{g}{T_a}\right)^{1/5} k^{4/5} \left(\dfrac{z^*}{\pi}\right)^{3/5} z^{1/5} \left(-\gamma^3 \dfrac{S^3_{(r_m)}}{r_m}\right)^{3/5} \dfrac{1}{a^{3/5}}, & h \le z \le z^* \\ 2.4\rho_a c_p \left(\dfrac{g}{T_a}\right)^{1/5} \dfrac{\left(k(z-d)\right)^{4/5}}{\pi^{3/5}} \left(-\gamma^3 \dfrac{S^3_{(r_m)}}{r_m}\right)^{3/5} \dfrac{1}{a^{3/5}} & z-d > z^* \end{cases} \tag{2.67}$$

Eq. (2.67) is independent of calibration, u_* and ζ and therefore allows sensible heat flux to be estimated for unstable conditions using high-frequency air temperature measurements, from which a, $r_{(m)}$, and $S^3_{(r_m)}$ are determined, in both roughness and inertial sub-layers with a relative accuracy of less than 8.5 % (Castellví and Martínez-Cob, 2005).

Following Castellví *et al.* (2006a), an expression for determining u_* can be derived by combining Eqs (2.49), (2.52), (2.63) and L_o as:

$$u_* = \begin{cases} \left[\left(\dfrac{g}{T}\right)^2 k^3 z^2 z^* \dfrac{\gamma^3}{\pi a}\left(-\dfrac{S^3_{(r_m)}}{r_m}\right)\right]^{1/5} \left[\dfrac{1}{\zeta^2 \phi_h(\zeta)}\right]^{1/5}, & h \le z < z^* \\ \left[\left(\dfrac{g}{T}\right)^2 (k(z-d))^3 \dfrac{\gamma^3}{\pi a}\left(-\dfrac{S^3_{(r_m)}}{r_m}\right)\right]^{1/5} \left[\dfrac{1}{\zeta^2 \phi_h(\zeta)}\right]^{1/5}. & z-d > z^* \end{cases} \tag{2.68}$$

2.5.4 Combined SR analysis model method with similarity theory that uses air temperature standard deviation

Castellví *et al.* (2006a) proposed an approach for estimating sensible heat flux, using SR and similarity concepts and depends on the standard deviation of the air temperature. According to MOST, standard deviation of air temperature σ_T above the uniform surface in a steady-state atmospheric condition can be expressed as a function of atmospheric stability (Wyngaard *et al.*, 1971):

$$\sigma_T / T_* = g_1(\zeta) = f(-\zeta) \tag{2.69}$$

where $g_1(\zeta)$ is the empirical atmospheric stability similarity based relationship valid in inertial sub-layer and given by Tillman (1971) as:

$$g_1(\zeta) = \begin{cases} 0.95\left(0.05-\zeta\right)^{-1/3}, & \zeta < 0 \\ 2.5, & \zeta = 0 \\ -2. & \zeta > 0 \end{cases} \tag{2.70}$$

Because MOST is not valid in the roughness sub-layer, Castellví *et al*. (2006a) assumed that the ratio $\phi_h(\zeta)/g_1(\zeta)$ also holds true in the roughness sub-layer through the following proportionality relationship:

$$\frac{k\beta a}{\sigma_T} = \frac{\phi_h(\zeta)}{g_1(\zeta)} = \mu\frac{\phi_h^*(\zeta)}{g_1^*(\zeta)} \tag{2.71}$$

where $g_1^*(\zeta)$ is the empirical atmospheric stability similarity based relationship valid in the roughness sub-layer and μ the proportionality parameter. For practical application, Castellví *et al*. (2006a) set μ equal to 1.0. Wesson *et al*. (2001) found that $g_1^*(\zeta)$ is proportional to $g_1(\zeta)$. MOST is true for measurements in the inertial sub-layer and it is known that:

$$\frac{z-d}{T_*}\frac{dT}{dz} = \frac{\phi_h(\zeta)}{k}. \qquad z-d > z^* \tag{2.72}$$

For measurements in the inertial sub-layer, combining Eqs (2.58) and (2.72) yields the following expression that combines SR and MOST (Castellví *et al*., 2006a):

$$\frac{a}{T_*} = \frac{\phi_h\left(\zeta\right)}{k\beta}. \qquad z-d > z^* \tag{2.73}$$

Combining Eqs (2.68), (2.69) and (2.73) for measurements in the roughness sub-layer and Eqs (2.55), (2.58), (2.61), and (2.68), for measurements in the inertial sub-layer, produces the following expressions for estimating sensible heat flux above the canopy surface as:

$$H_{SR} = \begin{cases} \rho_a c_p \left[\dfrac{(\gamma z^*)^3}{z} \dfrac{k\, g}{T_a} \sigma_T \left(-\dfrac{S^3_{(r_m)}}{r_m} \right) \right]^{1/3} \left(\alpha\,(k\,\beta)^2 \right)^{1/3} \left(\dfrac{1}{-\zeta^{1/3}\ \phi_h^{2/3}(\zeta)\ g_1^{1/3}(\zeta)} \right), & h \le z \le z^* \\ \rho_a c_p \left[\gamma^3 (z-d) \dfrac{k\, g\, z}{T_a} \sigma_T \left(-\dfrac{S^3_{(r_m)}}{r_m} \right) \right]^{1/3} \left(\alpha\,(k\,\beta)^2 \right)^{1/3} \left(\dfrac{1}{-\zeta^{1/3}\ \phi_h^{2/3}(\zeta)\ g_1^{1/3}(\zeta)} \right). & z - d > z^* \end{cases} \tag{2.74}$$

Castellví *et al*. (2006a) derived the following relationship for estimating $\left(\alpha\,(k\,\beta)^2 \right)^{1/3}$ as:

$$\left(\alpha\,(k\,\beta)^2 \right)^{1/3} = \begin{cases} \left(\dfrac{k}{\pi} \right)^{1/2} \dfrac{z^{2/3}}{(z^*)^{1/2}} \left(\dfrac{\phi_h(\zeta)}{\tau\, u_*} \right)^{1/6}, & h \le z \le z^* \\ \left(\dfrac{k}{\pi} \right)^{1/2} \left(\dfrac{z-d}{z^{2/3}} \right)^{1/2} \left(\dfrac{\phi_h(\zeta)}{\tau\, u_*} \right)^{1/6}. & z - d > z^* \end{cases} \tag{2.75}$$

On the basis of ramp frequency scales with wind shear, Chen *et al*. (1997b) used z and $z - d$ for the roughness and inertial sub-layers respectively. Castellví *et al*. (2006a) proposed new generalized scales that depend on the stability parameter $\lambda(\zeta) = (z - d)/(\tau\, u_*)$ and $\lambda^*(\zeta) = z \,/\, (\tau\, u_*)$ for the roughness and the inertial sub-layers respectively. Substituting $\lambda(\zeta)$ and $\lambda^*(\zeta)$ expression into Eq. (2.75) yields:

$$\left(\alpha(k\beta)^2 \right)^{1/3} = \begin{cases} \left(\dfrac{k}{\pi} \right)^{1/2} \left(\dfrac{z}{z^*} \right)^{1/2} \left(\lambda^*(\zeta)\phi_h(\zeta) \right)^{1/6}, & h \le z \le z^* \\ \left(\dfrac{k}{\pi} \right)^{1/2} \left(\dfrac{z-d}{z} \right)^{1/3} \left(\lambda(\zeta)\phi_h(\zeta) \right)^{1/6}. & z - d > z^* \end{cases} \tag{2.76}$$

Chen *et al*. (1997b) assumed that $\lambda^*(\zeta)$ is independent of ζ, namely that $\lambda^*(\zeta) = \lambda^*$. Castellví *et al*. (2006a) based on their experimental data collected above various canopies, approximated $(\lambda(\zeta))^{1/3}$ and $(\lambda^*(\zeta))^{1/3}$ to a constant value of 0.75 during unstable conditions regardless of the measurement height above the canopy and canopy type.

Sensible heat flux can be estimated in either the roughness or inertial sub-layers during different atmospheric stability, using Eq. (2.74) from air temperature data. Eq.

(2.74) includes u_* and ζ and hence iteration and wind speed measurements at one level are required as an input.

The free convection case forms for Eq. (2.74) can be expressed as (Castellví *et al.*, 2006a):

$$H_{SR} = \begin{cases} 1.65\rho_a c_p \gamma \dfrac{k^{5/6} g^{1/3}}{\pi^{1/2}} z^{1/6} (z^*)^{1/2} \left(\dfrac{\sigma_T}{T_a} \left(-\dfrac{S^3_{(r_m)}}{r_m} \right) \right)^{1/3}, & h \le z \le z^* \\ 1.65\rho_a c_p \gamma \dfrac{k^{5/6} g^{1/3}}{\pi^{1/2}} (z-d)^{2/3} \left(\dfrac{\sigma_T}{T_a} \left(-\dfrac{S^3_{(r_m)}}{r_m} \right) \right)^{1/3}. & z-d > z^* \end{cases} \tag{2.77}$$

For a variety of canopies, Castellví *et al.* (2006a) found that Eq. (2.74) and its free convection form, Eq. (2.77), performed very well for the measurements above the canopy, in roughness and/or inertial sub-layers, using $\gamma = 1.1$. The free convection form, Eq. (2.77) is useful to estimate sensible heat flux from air temperature measurement as the only input, above the crop surface (either in roughness or inertial sub-layers) under unstable conditions.

2.5.5 Combined SR analysis model method with similarity theory that uses second-order air temperature structure function

According to MOST, the relationship between the air temperature structure function parameter C_{TT} and air temperature scale above the uniform surface in a steady-state atmospheric condition can be expressed as a function of atmospheric stability (Wyngaard *et al.*, 1971):

$$\frac{C_{TT}(z-d)}{T_*^2} = g_2(\zeta) = f_{TT}(-\zeta) \tag{2.78}$$

where $g_2(\zeta)$ is an empirical atmospheric stability similarity based relationship valid in the inertial sub-layer and given by (Wyngaard *et al.*, 1971):

$$g_2(\zeta) = \begin{cases} 4.9(1-7\zeta)^{-2/3}, & \zeta < 0 \\ 4.9, & \zeta = 0 \\ 4.9(1+2.75\zeta). & \zeta > 0 \end{cases} \tag{2.79}$$

From Eqs (2.68), (2.73) and (2.78) for measurements in the inertial sub-layer, the following expression permits sensible heat flux to be estimated as (Castellví *et al.*, 2006a):

$$H_{SR} = \rho_a c_p \left(\frac{\gamma^3 (z-d)^{4/3} k\, g\, z}{T} C_{TT}^{\ 1/2} \left(-\frac{S^3_{(r_m)}}{r_m} \right) \right)^{1/3} \frac{1}{-\zeta^{\,1/3}\ \phi_h^{2/3}(\zeta)\ g_1^{1/3}(\zeta)}. \quad z-d > z^* \tag{2.80}$$

The free convection form ($\zeta \le$ -0.1) of Eq. (2.80) is expressed as (Castellví *et al.*, 2006a):

$$H_{SR} = 1.65\, \rho_a c_p \gamma \frac{k^{5/6} g^{1/3} (z-d)}{\pi^{1/2}}^{7/9} \left(\frac{C_{TT}^{\ 1/2}}{T} \left(-\frac{S^3_{(r_m)}}{r_m} \right) \right)^{1/3}. \quad z-d > z^* \tag{2.81}$$

Castellví *et al.* (2006a), from their experimental data collected above different canopy types in the inertial sub-layer, found that Eq. (2.80) and its free convection form, Eq. (2.81), performed excellently during unstable conditions. Eq. (2.81) provides a practical method to estimate sensible heat flux in the inertial sub-layer but requires wind speed measurements at one level as input to calculate the friction velocity and stability parameter using iteration. The free convection form, Eq. (2.81), revealed a weak dependence on the stability parameter under slightly unstable conditions. Therefore, Eq. (2.81) can be used to estimate sensible heat flux using air temperature measurement as the only input, in the inertial sub-layer under unstable conditions. The main drawback of Eqs (2.80) and (2.81) is that they are not valid when the fetch is limited.

2.6 Eddy covariance method

The EC method was pioneered by Swinbank (1951) and allows scalar fluxes between the turbulent atmosphere and underlying surfaces to be measured directly or indirectly from the other terms of the energy balance at a single point above the surface. The principle of this method is that turbulent motions of moving air transport heat and mass between the surface and atmosphere (Baldocchi, 2003). On the basis of mass flow and Reynolds' rules of averaging, the EC method can be used to determine the mass and energy flux exchange between the underlying surface and atmosphere (Baldocchi, 2003). The EC method is based on simultaneous measurements of vertical wind speed and the turbulent scalar fluctuations and involves determining their covariance over a time interval. For instance, sensible heat flux (*H*) using EC method depends on the covariance between the fluctuations in vertical wind speed (w') and sonic temperature (T_s'):

$$H_{sonic} = \rho_a c_p \overline{w'T_s'} \tag{2.82}$$

where w' and T_s' are the fluctuations from the mean vertical wind speed w and sonic temperature T_s respectively and the overbar indicate the averaging time interval. Following Kaimal and Finnigan (1994) and Oncley *et al*. (2007), coordinate rotations for the three wind velocity components, *u*, *v* and *w*, and correction to remove the effects of the instrument tilt and air-flow irregularities must be performed post-data collection. There are two methods for determining rotational angle: planar method (Kaimal and Finnigan, 1994) and double rotation method (Paw U *et al*., 2000). The H_{sonic} values also require correction for the effects of water vapour pressure and Bowen ratio, using the average values $\bar{e}$ and $\bar{\beta}$ respectively, using the relationship (Odhiambo and Savage, 2009):

$$H_{EC} = H_{sonic}\left(1 + \frac{0.322\,\bar{e}}{\bar{P}} + \frac{10^{-3}\left(0.722\,\bar{P} - 0.399\,\bar{e}\right)}{\bar{\beta}}\right)^{-1} \tag{2.83}$$

in which $\bar{e}$ (kPa) can be obtained using air temperature and relative humidity measurements. The atmospheric pressure $\bar{P}$ (kPa) is estimated following Savage *et al*. (1997) using altitude, average water vapour pressure $\bar{e}$ and an average of the measured air temperature and $\bar{\beta}$ estimated using:

$$\overline{\beta} = \frac{H_{sonic}}{R_n - G - H_{sonic}}. \tag{2.84}$$

Three crucial factors that affect the accuracy of the EC measurements are the averaging period, the measurement height and the content of the scalar cospectrum at periods longer than the averaging period (Finnigan *et al*., 2003). The EC method requires an extensive homogeneous flat site with adequate fetch. A fetch to height ratio of 100:1 is usually considered adequate but a greater fetch is desirable (Kaimal and Finnigan, 1994). The EC system must be installed at a height that allows the small eddies to be completely detected. Savage *et al*. (1995) reported that a height of 1 m above the canopy surface is suitable for EC measurements above a short turf grass surface during unstable conditions. The covariance averaging time must be long enough to include frequencies at the low end, such as of the order of 0.01 Hz or less (Kaimal and Finnigan, 1994; Odhiambo and Savage, 2009). The averaging time for EC measurement being 15 to 30 min is used in most agrometeorological experiments (Finnigan *et al*., 2003). For taller crops, larger averaging time may be required (Sun *et al*., 2006).

The main advantages of the EC method are that it directly measures sensible heat and latent energy fluxes, and provides independent measurements of energy balance terms (Brotzge and Crawford, 2003), no assumptions are made about the land surface properties such as aerodynamic roughness or zero-plane displacement, and no corrections for atmospheric stability are necessary (Ham and Heilman, 2003). The EC method has disadvantages that the instruments are expensive and sensitive to damage; the EC sensor must respond very fast (10 Hz) to sense all eddies contributing to the vertical flux transport. In addition the EC method requires that the temporal cospectra of the vertical wind speed and the scalar fluctuations must extend to very low frequencies (Green, 2001; Drexler *et al*., 2004). Insufficient fetch, horizontal misalignment and rotation cause significant uncertainties in EC measurements.

2.7 Reference evaporation method

The FAO Penman-Monteith method published by the Food and Agriculture Organization in Irrigation and Drainage Paper No. 56 (Allen *et al*., 1998) has been used extremely for estimating grass reference evaporation using automatic weather station measurements (solar irradiance, air temperature, relative humidity and wind speed). The reference crop is generally grass with a fixed crop height (0.12 m), surface reflection coefficient of 0.23, surface resistance of 70 s m^{-1}, and not water limited (Allen *et al*., 1998). The FAO56 Penman-Monteith (PM) equation for measuring daily reference evaporation (mm day^{-1}) can be expressed as (Allen *et al*., 1998, 2006):

$$ET_o = \frac{\Delta . r_a (R_{net} - G) + \rho_a \, c_p \; \delta e}{\left(\Delta \; r_a + \gamma \; (r_s + r_a)\right)\left(\rho_w \; L_v\right)} \tag{2.85}$$

where Δ is the slope of the saturation water vapour pressure at the surface temperature (kPa $^{o}C^{-1}$), δe the water vapour pressure deficit (kPa), r_s and r_a the canopy surface and aerodynamic resistances (s m^{-1}) respectively, ρ_w the density of liquid water (kg m^{-3}) and L_v the latent energy of vapourization. Allen *et al*. (1998) recommended for application of the FAO56 Penman-Monteith (PM) equation for estimating daily grass reference evaporation, a surface resistance of 50 and 200 s m^{-1} for daytime and nighttime respectively and an aerodynamic resistance r_a =208 / U_2, in which U_2 is the horizontal wind speed at 2 m above the soil surface. The FAO56 Penman-Monteith (PM) equation has been developed by Allen *et al*. (2006) for daily to hourly or sub-hourly estimates for both grass reference and tall-crop reference evaporation by changing the surface resistance values to r_s = 30 and 200 s m^{-1} for daytime and nighttime respectively, and aerodynamic resistance r_a =118/U_2. Finally, the crop evaporation (E) in mm day^{-1} for daily time steps and mm h^{-1} for hourly time steps is calculated as:

$$E = K_c \times ET_o \tag{2.86}$$

where K_c is the crop coefficient factor defined as the ratio of the actual crop evaporation E to reference crop evaporation ET_o. The main uncertainty of this method is that the net irradiance and soil heat flux are usually estimated indirectly from the available measured solar irradiance. Furthermore, the crop factor varies considerably with climate, crop variety, crop growth stage and land management practices.

Chapter 3: Evaluation of surface renewal applied to sugarcane for estimating sensible heat flux

Abstract

In South Africa, continuous pressure on available limited water resources in sugarcane areas due to competition with others crops, expansion of irrigated agricultural areas and occasional drought highlights the importance of evaporation data. The surface renewal (SR) method was used to estimate sensible heat flux from which latent energy flux was calculated as a residual of the shortened energy balance, over a sugarcane canopy at the Baynesfield Estate in KwaZulu-Natal. Surface renewal estimates of sensible heat (H_{SR}) were compared with eddy covariance sensible heat (H_{EC}) estimates during daytime hours for unstable conditions. For SR, 10-Hz air temperature data were collected, and using time lags of 0.4 and 0.8 s and measurement heights of 0.20, 0.50, 0.75 and 1.50 m above the crop surface, H_{SR} was calculated. For the calibration data set, from day of year 241 to 297, 2008, the weighting factor α was obtained by plotting H_{EC} against H_{SR} for the time lags and all measurement heights. The magnitude of α ranged from 0.66 to 0.55 for the 0.8-s time lag and all heights. For the validation data set, from day of year 192 to 240 and 298 to 354, 2008, the half-hourly H_{SR} values corresponded well with H_{EC} for both time lags and all heights. Linear regression statistics showed that the agreement between H_{SR} for the 0.8-s time lag and H_{EC} improved as measurement height decreased. The H_{SR}, using $\alpha = 0.66$ for a time lag of 0.8 s, for a height of 0.20 m above the crop surface yielded the best comparison with H_{EC}. The latent energy flux for each method was estimated as a residual using either H_{SR} or H_{EC}, and measured net irradiance and soil heat flux. The half-hourly residual estimates of latent energy flux by SR and by eddy covariance were in good agreement. Based on these results, the SR method provides a simple and relatively inexpensive method for estimating sensible heat and latent energy flux above the sugarcane canopy if α is known.

Keywords: Air temperature, Eddy covariance, Energy balance, High frequency

3.1 Introduction

Water is a limited resource and becoming more expensive and scarcer due to population increases, expansion of irrigated agricultural areas, and increasing usage of water by industry and other sectors. Sugarcane is grown under rain-fed or supplementary irrigation conditions in many parts of South Africa. There is continuous pressure on the available limited water resources under sugarcane due to competition with others crops, expansion of irrigated agricultural areas and occasional drought. Therefore, there is a need for continuous and accurate estimation of crop evaporation to maximize utilization of available irrigation water resources and crop water use efficiency. Traditionally, total evaporation estimates are based on climatic data for estimating grass reference evaporation or tall-crop reference evaporation (Allen *et al.*, 1998, 2006), followed by the application of the crop factor approach. The main uncertainty of this method is that net irradiance and soil heat flux are usually estimated indirectly from the available measured solar irradiance. Furthermore, the crop factor varies considerably with climate, crop variety, crop growth stage and land management practices. Different micrometeorological methods for estimating evaporation, including eddy covariance (EC), Bowen ratio energy balance, scintillometer, surface renewal (SR) and temperature variance methods, involve measuring the sensible heat flux (H) from which latent energy flux and hence total evaporation can be calculated, as a residual using the shortened energy balance from measurements of net irradiance and soil heat flux. The weighing lysimeter and EC methods allow direct estimation of latent energy flux from which evaporation may be estimated. There have been a few studies involving the estimation of evaporation over sugarcane using micrometeorological methods such as EC (Denmead and MacDonald, 2008), Bowen ratio energy balance (Burger, 1999; McGlinchey and Inman-Bamber 2002; Inman-Bamber and McGlinchey, 2003; Shinichi *et al.*, 2004), and scintillometry (Wiles, 2006) methods. Although the EC method is considered the standard meteorological method for measuring or estimating LE (Drexler *et al.*, 2004; Meyer and Baldocchi, 2005; Savage, 2009), application of EC for long-term monitoring of evaporation is limited by its complexity, high power consumption, stringent instrumental requirements, high cost and sensitivity of the instruments to damage (Drexler *et al.*, 2004). The scintillometer method is expensive and requires a fairly high level of expertise to operate and the weighing lysimeter method is accurate but rarely used outside of experimental research institutes. The Bowen ratio method is sensitive to the biases of the instruments used for measuring vertical gradients of air temperature and water vapour pressure (Rosenberg *et al*., 1983; Savage *et al*., 2009), and requires extensive fetch. Due to the above-mentioned difficulties, attempts to find a simple and inexpensive method for estimating evaporation have been a challenge for agricultural research in recent years.

The SR method was first proposed by Paw U and Brunet (1991) and allows the sensible heat flux $H = H_{SR}$ to be estimated using high frequency air temperature measurement at a single point above the crop surface when a weighting factor (α) is known. Theoretical details of the SR method have been reviewed (e.g., Paw U *et al*., 1995; Snyder *et al*., 1996, 1997; Drexler *et al*., 2004; Savage *et al*., 2004; Paw U *et al*., 2005; Mengistu, 2008; Mengistu and Savage, 2010). This method has several advantages over other micrometeorological methods: it is relatively inexpensive, simple with a reduced power requirement, and does not require sophisticated equipment (Snyder *et al*., 1996; Savage *et al*., 2004; Paw U *et al*., 2005). Furthermore, the SR method can be applied either in the roughness or inertial sub-layers (Paw U *et al*., 2005) and used unattended at distant sites. However, the SR method requires calibration because of a weighting factor α obtained by comparing H_{SR} measurements with measurements from a standard such as EC method. The SR also depends on the air temperature time lag used when calculating H_{SR}. Several studies have been conducted over a variety of vegetated surfaces to validate the application of the SR method (e.g., Paw U *et al*., 1995; Duce *et al*., 1997; Spano *et al*., 1997a, b, 2000; Zapata and Martínez-Cob, 2001, 2002; Simmons *et al*., 2007; Hanson *et al*., 2008; Mengistu, 2008; Castellví and Snyder, 2009a, b) and provided very good estimates of H_{SR} during unstable conditions. In South Africa, Savage *et al*. (2004) applied the SR method to estimate H_{SR} above a grassland surface and Mengistu (2008) applied the method to estimate H_{SR} above different vegetated surfaces and a water body and obtained reasonable results for these surfaces. The SR method has not been applied to sugarcane.

The objectives of this study were: to calibrate and validate the SR method for estimating H_{SR} at four measurement heights against EC measurements above sugarcane for air temperature time lags of 0.4 and 0.8 s, and to determine α for sugarcane.

3.2 Theory

3.2.1 Energy balance

The SR method estimates of sensible heat flux and together with the shortened energy balance equation allows the latent energy flux *LE* to be estimated as a residual. The surface energy balance in shortened form is expressed as:

$$R_n = G + H + LE \tag{3.1}$$

where R_n is the net irradiance, *G* the soil heat flux, *H* the sensible heat flux, and *LE* the latent energy flux. The energy flux associated with photosynthesis and respiration, energy stored in the plant canopy and advection are assumed to be negligible.

3.2.2 Surface renewal method

The SR method for estimating the sensible heat flux based on the coherent structures concept and was pioneered by Paw U and Brunet (1991). The coherent structures theory assumes that an air parcel sweeps from above the canopy to the canopy surface. The air parcels begins to be cooled or heated when near or in the canopy because of the sensible heat exchange between the air and canopy elements. Ramps are observed in the air temperature traces as a result of the turbulent coherent structures. These ramps, for stable and unstable conditions, are characterized by air temperature amplitude *a* and total ramp period *l* and *s* parameters (Paw U and Brunet, 1991). It is assumed that the total ramp period consists of a ramp period *l* and a quiescent ramp period *s*. The amplitude *a* is positive for unstable conditions and negative for stable. The ramp amplitude and total ramp period for a fixed averaging time interval are used to estimate sensible heat flux over the given crop canopy surface using the SR method (Paw U and Brunet, 1991; Paw U *et al.*, 1995; Snyder *et al.*, 1996). Following Paw U and Brunet (1991) and Paw U *et al*. (1995), the sensible heat flux can be determined as the change of heat content of the air with time ($M_{air}\, c_p\, dT/dt$) per unit area (*A*) as follows (Savage *et al.*, 2004):

$$H_{SR} = c_p \frac{M_{air}}{A} \frac{dT}{dt} \tag{3.2}$$

where M_{air} is the mass of air heated (or cooled) by the rate of change in the air temperature difference dT/dt, and c_p the specific heat capacity of air at constant pressure. To simplify Eq. (3.2), M_{air} can be expressed in terms of ρ_a and the volume of air V per horizontal unit area A:

$$H_{SR} = \rho_a c_p \frac{V}{A} \frac{dT}{dt}\,. \tag{3.3}$$

The measured change in the air temperature with time is the partial derivative of temperature with time $\partial T/\partial t$ rather than dT/dt because air temperature is measured at a fixed point (Snyder *et al.*, 1997). The term V/A represents the vertical distance (measurement height above the soil surface). It is assumed that the internal advection within the air volume V is negligible and hence:

$$H_{SR} = \rho_a c_p z \frac{\partial T}{\partial t} \tag{3.4}$$

where z is the measurement height above the soil surface and $\partial T/\partial t$ can be replaced by the ratio of the ramp amplitude a and the total ramp period $l + s$ in Eq. (3.4) to determine sensible heat flux . Therefore for the SR method, the sensible heat flux is determined using (Paw U *et al.*, 1995):

$$H_{SR} = \alpha z \rho_a c_p \frac{a}{s+l} \tag{3.5}$$

where α is a weighting factor defined as a factor that corrects for the unequal heating or cooling from the measurement height to the ground. The weighting factor depends on the air temperature time lag, an air temperature structure function, measurement height and plant canopy height, and the size of the fine-wire thermocouple used to measure air temperature at high frequency (Paw U *et al.*, 2005). However, αz has a physical meaning, representing the volume of air per unit of ground area exchanged on average for each ramp in the sample period for the measurement height z (Paw U *et al.*, 1995). Castellví *et al.* (2002) interpreted αz as the mean eddy size responsible for the renewal process. The amplitude and ramp period are estimated following the structure function approach of van Atta (1977). The air temperature structure function $S^n(r)$ is obtained from high frequency air temperature measurements using the following relationship:

$$S^n(r) = \frac{1}{m-j} \sum_{i=1+j}^{m} (T_i - T_{i-j})^n \qquad (3.6)$$

where m is the number of data points measured at frequency f (Hz) in the averaging time interval, n the power of the structure function, j the number of the lags between data points corresponding to an air temperature time lag $r = j/f$, and T_i the i^{th} air temperature sample.

The average ramp amplitude a in the time interval can be determined from the solution of the polynomial equation (Snyder *et al.*, 1996):

$$a^3 + \left(10S^2(r) - \frac{S^5(r)}{S^3(r)} \right) a + 10S^3(r) = 0 \qquad (3.7)$$

and the total ramping period $l + s$ is estimated using:

$$l + s = -\frac{a^3 r}{S^3(r)}. \qquad (3.8)$$

3.3 Materials and methods

A field experiment was carried out over a 3-ha area of commercial sugarcane (variety N14), at the Baynesfield Estate in KwaZulu-Natal, South Africa (29.45 ^{o}S, 30.18 ^{o}E) with an altitude of 910 m above MSL (Fig. 3.1). The Baynesfield climate is classified as sub-humid with dry and cool winters and warm and rainy summers. The mean monthly air temperatures ranges from a maximum of 21.1 ^{o}C in January to a minimum of 13.3 ^{o}C in June with a mean annual precipitation of 844 mm. Precipitation falls as rain, most of it in the humid summer months. The soil is classified as the Hutton form with clay content of

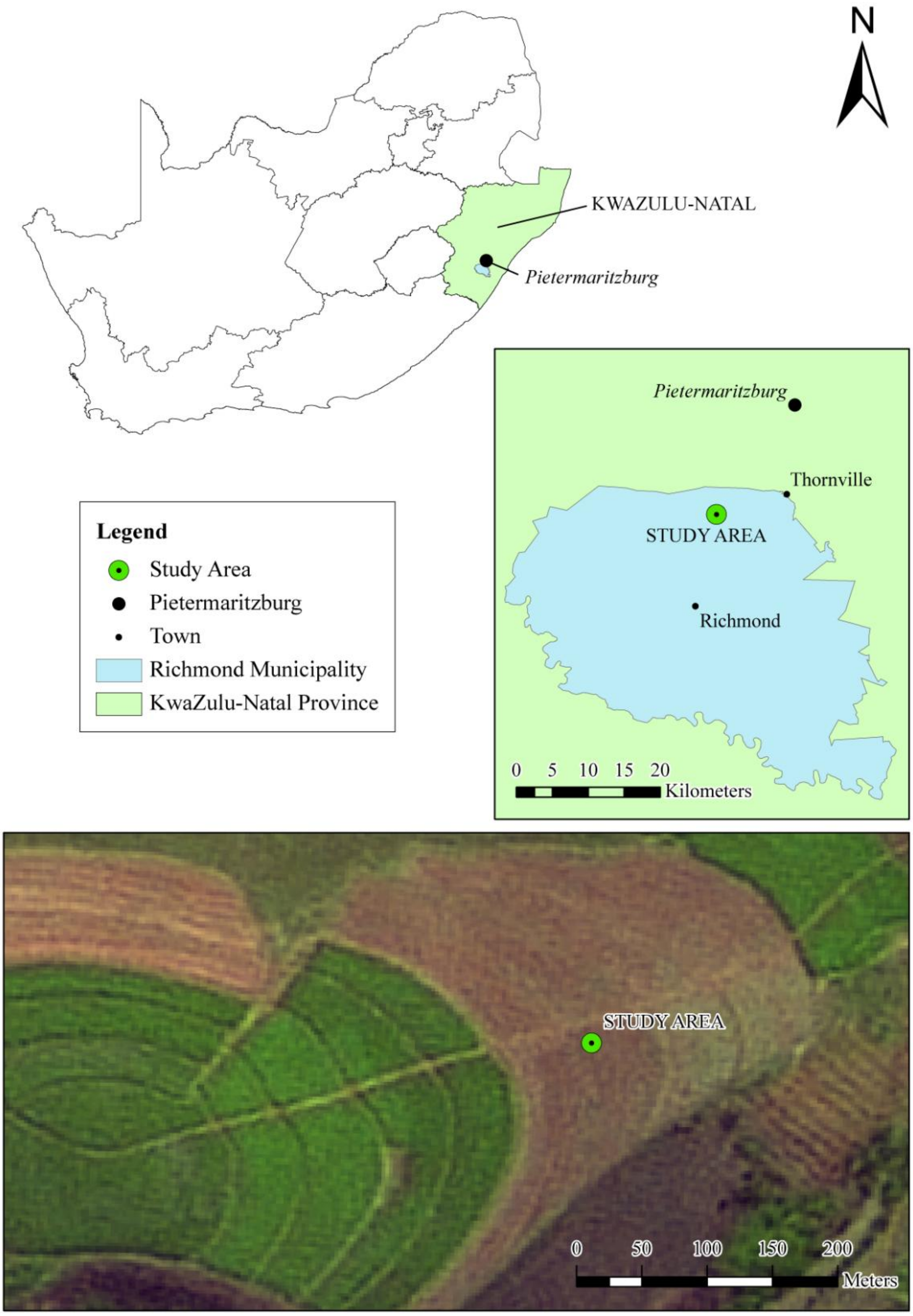

Fig. 3. 1 A map showing the location of the study area.

550 to 650 g kg^{-1} (Haynes *et al*., 2003).

The sugarcane was planted in December 2007, with a row spacing of 1 m and planting spacing of 0.50 m. The crop height was 1.2 m at the beginning of the experiment when the crop was six months old. The experimental area is bordered on the south east by a small water reservoir, and for the other directions by sugarcane. The predominant wind direction is easterly. The upwind fetch available for the measurements was 97 m from the predominant wind direction, which occurred almost all of the time during the daytime unstable conditions.

The data collected and analysed were for the period from 11 to 18 July and 25 July to 20 December 2008 (day of year from 191 to 199 and day of year from 206 to 354 respectively).

Two micrometeorological masts were located at about 15 and 50 m from the west and south edges of the field, respectively. For the SR method, four unshielded and naturally-ventilated type-E fine-wire thermocouples (75-µm diameter) were used to measure high frequency air temperature, placed at heights of 0.20, 0.50, 0.75, and 1.50 m above the crop surface. The measurement heights were adjusted when the crop height increased to maintain the height above the crop surface. All thermocouples were connected to the CR3000 datalogger (Campbell Scientific Inc., Logan, Utah, USA). Air temperature data were sampled at a frequency of 10 Hz. Time lags r = 0.4 and 0.8 s were used when calculating the air temperature structure functions (Eq. (3.6)). The second-, third- and fifth-order air temperature structure functions which are required by the van Atta (1997) approach for the SR method, were determined online after lagging the air temperature data by 0.4 and 0.8 s. The data were then averaged every two minutes and thirty minutes and stored in the datalogger and then used for further analysis. The amplitude a and the total ramping period $l + s$ were determined from the air temperature structure functions using the two time lags and the van Atta (1977) analysis approach. The two-minute SR sensible heat flux H_{SR} was calculated and the data then averaged to half-hourly values. The sign of the ramp amplitude was used to determine atmospheric stability (positive indicates unstable conditions and negative indicates stable). The H_{EC} measurements were used to calibrate the SR method. The half-hourly values of the uncalibrated H_{SR} estimates of were corrected for unequal heating between the ground and the measurement height (Snyder *et al.*, 1996; Spano *et al.*, 1997a, b).

For purposes of surface fluxes comparisons, a three-dimensional ultra-sonic anemometer (model 81000, RM Young, Traverse City, Michigan, USA) which represented the EC system, was connected to the CR3000 datalogger and installed adjacent to the thermocouples to estimate $H = H_{EC}$ at a height of 2.15 m above the soil surface at the start of experiment and 2.37 m above the soil surface at the end of the experiment. The scan rate for the EC measurements was 10 Hz. All EC data were processed online every 2 and 30 minutes in the datalogger and stored for further analysis, including 10-Hz data. The sonic sensible heat flux H_{sonic} was calculated as: $H_{sonic} = \rho_a\, c_p\, \overline{w'T_s'}$ where w' and T_s' are the fluctuations from the mean vertical wind speed w and sonic temperature T_s respectively. Sensible heat flux was recalculated following coordinate rotations for the three wind velocity components, *u*, *v* and *w*, and correction to remove the effects of instrument tilt and air-flow irregularities using the procedures similar to those of Kaimal and Finnigan (1994) and Oncley *et al.* (2007). Similar ρ_a and c_p values were used for calculating EC and SR sensible heat flux for each time period (Savage *et al.*, 1997). The H_{EC} values were corrected for the effects of water vapour pressure and Bowen ratio, using the average values $\bar{e}$ and $\bar{\beta}$ respectively, using the relationship (Odhiambo and Savage, 2009):

$$H_{EC} = H_{sonic}\left(1 + \frac{0.322\,\bar{e}}{\bar{P}} + \frac{10^{-3}\left(0.722\,\bar{P} - 0.399\,\bar{e}\right)}{\bar{\beta}}\right)^{-1} \tag{3.9}$$

in which $\bar{e}$ (kPa) was obtained using air temperature and relative humidity measurements using two Vaisala air temperature and relative humidity instruments (Campbell HMP45C) connected to the CR1000 datalogger with one at each height of 0.50 and 1.50 m above the crop canopy. The atmospheric pressure $\bar{P}$ (kPa) was estimated following Savage *et al.* (1997) using altitude, average water vapour pressure $\bar{e}$ and an average of the measured air temperature from the fine-wire thermocouples and $\bar{\beta}$ estimated using:

$$\overline{\beta} = \frac{H_{sonic}}{R_n - G - H_{sonic}}. \tag{3.10}$$

Additional measurements included the remaining energy balance components with R_n, soil heat flux, soil temperature and soil water content measured every one second, averaged every two-minute and stored using the CR1000 datalogger for further analysis. A NR LITE net radiometer (Kipp & Zonen, Delft, The Netherlands) to measure R_n was mounted at a height of 1.50 m above the crop surface and adjusted according to the changes in crop height. Soil heat flux G_{plate} at 0.08 m below the soil surface was measured using two soil heat flux plates buried horizontally. Spatially-averaged soil temperature was obtained using two pairs of type-E thermocouples in metal tubes buried in the soil at depths of 0.02 and 0.06 m above the soil heat flux plates. Soil water content was measured using a frequency domain reflectometer (ThetaProbe, model ML2x, Delta-T Devices, Cambridge, England) inserted vertically in the soil close to the area where soil heat flux plates and soil thermocouples were buried. The heat flux stored above the soil heat flux plates G_{stored} was calculated from measured average soil temperature and soil water content θ_v (m^3 m^{-3}) as:

$$G_{stored} = \left(\rho_{soil}\, c_{dsoil} + \rho_w\, \theta_v\, c_w\right) \frac{\Delta z\, \overline{\Delta T}_{soil}}{\Delta t} \tag{3.11}$$

where ρ_{soil} is the soil bulk density (kg m^{-3}), c_{dsoil} the dry soil specific heat capacity (840 J kg^{-1} ^{o}C^{-1}), ρ_w the density for water (1000 kg m^{-3}), θ_v the soil water content (m^3 m^{-3}), c_w the specific heat capacity for water (4200 J kg^{-1} ^{o}C^{-1}), Δz the soil heat flux plates depth (m), $\overline{\Delta T}_{soil}$ the average change in soil temperature above the soil heat flux plates (^{o}C), and Δt the time between temperature average measurements (s). The soil heat flux G was then calculated as:

$$G = G_{plate} + G_{stored}. \tag{3.12}$$

The H_{SR} and H_{EC} data for the period from day of year 241 to 297 (2008) were used for calibration purposes to determine α by linear regression for the two air temperature time lags for each height using Eq. (3.5). The data for the period from day of year 192 to 240 and 298 to 354 (2008) were used for validation purposes.

3.4 Results and discussion

3.4.1 Sensible heat flux

The first three SR measurement heights were in the roughness sub-layer and the upper-most SR height in the inertial sub-layer. The transition zone between these layers was assumed to be defined by 5 *h*/3 where *h* is the canopy height (m) (Sellers *et al.*, 1986).

To determine the effect of the measurement height and air temperature time lag on the H_{SR} estimates and the weighting factor α, the half-hourly values of H_{SR} estimates at heights of 0.20, 0.50, 0.75, and 1.50 m above the canopy surface for time lags of 0.4 and 0.8 s were compared with H_{EC} measurements at height varied between 2.15 and 2.37 m above the soil surface, for unstable conditions during daytime hours from 06h00 to 18h00.

The statistical data for the un-calibrated H_{SR} *vs* H_{EC} comparisons, corresponding to $\alpha = 1$, are presented (Table 3.1). Generally, the SR method overestimated the sensible heat flux compared to the EC method for all measurement heights and both time lags. Whatever the measurement height, the best performance of the SR method was observed for a time lag of 0.8 s. Mengistu (2008) attributed the increase in root mean square error (RMSE), between H_{SR} *vs* H_{EC}, when using a shorter time lag to the possibility that the shorter time lag could be too short for the formation of air temperature ramps. The SR method overestimated the sensible heat flux for all measurement heights with a slope greater than 1.33. The difference between un-calibrated H_{SR} and H_{EC} generally increased as the measurement height increased (Table 3.1). At lower measurement heights, H_{SR} corresponded more closely to H_{EC} compared to the other measurement heights.

The H_{SR} estimates require calibration against H_{EC} to correct for the effects of unequal heating or cooling below the height of the sensor. The weighting factor α represented by the slope of the linear fit through the origin, was determined by simple linear regression between H_{SR} estimates (*x*-axis) for heights of 1.50, 1.80, 2.05 and 2.80 m

Table 3.1 Regression statistics for the calibration period for half-hourly H_{EC} (x-axis) at height ranged from 2.15 to 2.37 m above the soil surface *vs* un-calibrated H_{SR} (y-axis) estimates at measurement heights z = 0.20, 0.50, 0.75 and 1.50 m above the crop surface for time lags of 0.4 and 0.8 s for daytime unstable conditions.

z (m)	Time lag (s)	Intercept (W m^{-2})	Slope	RMSE (W m^{-2})	r^2	n
0.20	0.4	23.64	1.50	51.38	0.85	1063
	0.8	18.10	1.33	37.81	0.89	1087
0.50	0.4	25.69	1.58	63.52	0.80	1059
	0.8	20.87	1.39	43.89	0.87	1088
0.75	0.4	29.17	1.56	65.29	0.79	1042
	0.8	22.80	1.42	48.50	0.85	1073
1.50	0.4	38.72	1.63	78.73	0.73	1028
	0.8	29.94	1.51	57.36	0.82	1049

above the soil surface and both air temperature time lags against H_{EC} (y-axis) at a height of 2.25 m above the soil surface (Table 3.2). The α value decreased with increase in measurement height and with decrease in air temperature time lag. The greatest α was obtained at lowest measurement height and for a time lag of 0.8 s and significantly differed compared to the other measurement heights. Duce *et al*. (1997) applied the SR method above three different plant canopies, grass (*Alta fescue*), wheat and sorghum using different time lags, r = 0.25, 0.50, 0.75 and 1 s. They reported that α increased with an increase in the time lag and a decrease in measurement height. Similar results were reported in the previous experiments for different plant canopies (Snyder *et al*., 1996; Mengistu, 2008). Generally, the results indicated that α varies with measurement height and air temperature time lag.

Half-hourly H_{SR} estimates, corrected using the α–value from the regression analysis, for all measurements heights and both air temperature time lags for unstable conditions during daytime hours from 06h00 to 18h00, were plotted against H_{EC} for the validation period as presented in Table 3.3. These comparisons were performed to validate the SR method for estimating the sensible heat and latent energy flux above the sugarcane. Good agreement between SR and EC methods was observed for all measurement heights and both air temperature time lags. The half-hourly H_{SR} estimates for all measurement heights using a time lag of 0.8 s were plotted *vs* H_{EC} for the validation period (Fig. 3.2) to

Table 3.2 The weighting factor α during the calibration period for daytime unstable conditions using time lags *r* of 0.4 and 0.8 s at different measurement heights above the soil surface.

z (m)	Time lag (s)	α	*n*
1.50	0.4	0.57 [a]	1063
	0.8	0.66 [b]	1087
1.80	0.4	0.53 [c]	1059
	0.8	0.62 [d]	1088
2.05	0.4	0.53 [c]	1042
	0.8	0.60 [d]	1073
2.80	0.4	0.48 [e]	1028
	0.8	0.55 [a]	1049

The same letter for different data sets indicates no significance differences at 95 % probability

Table 3.3 Regression statistics during the validation period for half-hourly H_{SR} estimates, using a time lag of 0.8 s and at measurement heights of 0.20, 0.50, 0.75, and 1.50 m above the crop canopy, *vs* H_{EC} at height ranged from 2.15 to 2.37 m above the soil surface.

z (m)	Time lag (s)	Intercept (W m^{-2})	Slope	RMSE (W m^{-2})	r^2	Forced slope	*n*
0.20	0.4	6.88	0.83	21.41	0.85	0.88	1690
	0.8	6.28	0.88	19.29	0.89	0.93	1752
0.50	0.4	7.42	0.83	23.07	0.83	0.88	1658
	0.8	7.83	0.88	21.40	0.87	0.94	1693
0.75	0.4	9.63	0.84	26.74	0.79	0.91	1667
	0.8	8.95	0.90	23.90	0.84	0.96	1710
1.50	0.4	11.50	0.83	30.01	0.74	0.91	1648
	0.8	10.98	0.88	27.09	0.80	0.96	1709

determine the effect of measurement height on the H_{SR} estimates. The agreement between H_{SR} and H_{EC} is good, with a slope value greater than 0.88, coefficient of determination (r^2) close to 0.8 and a RMSE less than 27.09 W m^{-2}. There is a slight a decrease in accuracy with increase in measurement height. The best results were observed for the lowest height, with a slope value of 0.88, r^2 = 0.89 and RMSE value of 19.29 W m^{-2} (Fig. 3.2a). The H_{SR} estimates for the upper-most height were in good agreement with H_{EC} (Fig. 3.2d) but biased with increased RMSE compared to the other heights. Snyder *et al*. (1996) attributed

(**a**) 0.20 m

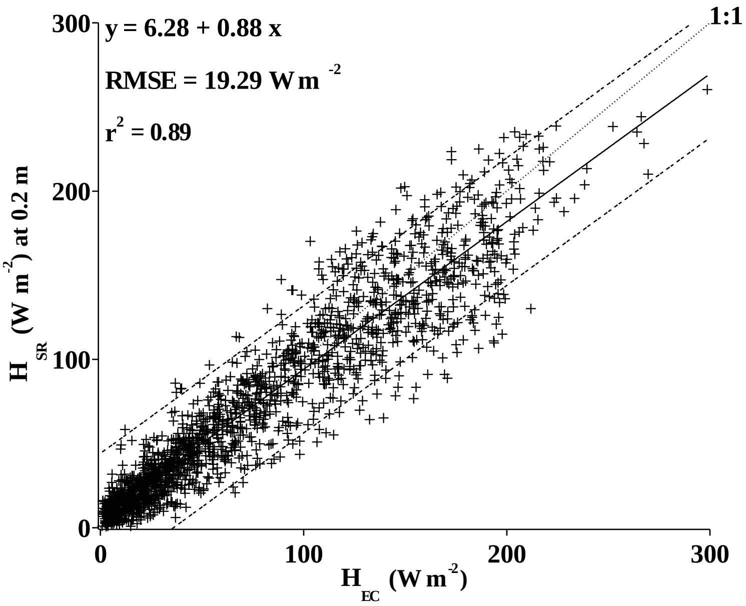
1:1
y = 6.28 + 0.88 x
RMSE = 19.29 W m -2
r2 = 0.89
300
200
100
0
0
100
200
300
HSR (W m-2) at 0.2 m
HEC (W m-2)

(**b**) 0.50 m

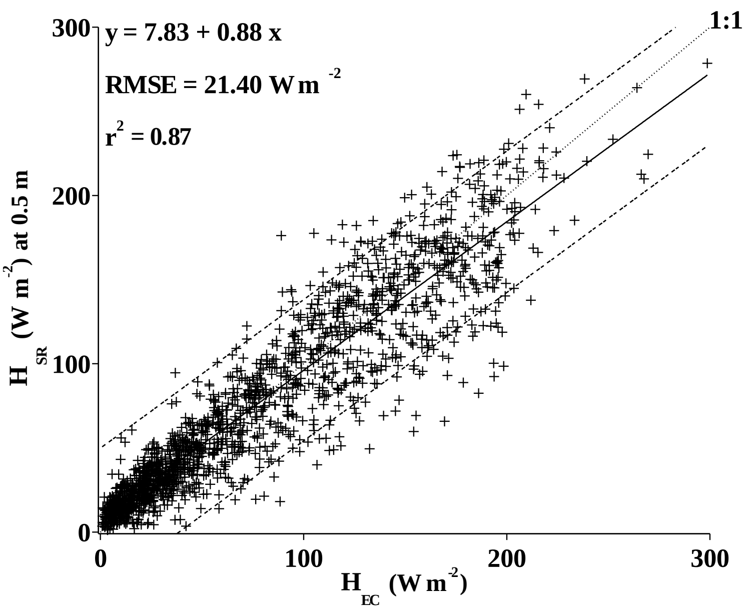
1:1
y = 7.83 + 0.88 x
RMSE = 21.40 W m -2
r2 = 0.87
300
200
100
0
0
100
200
300
HSR (W m-2) at 0.5 m
HEC (W m-2)

(**c**) 0.75 m

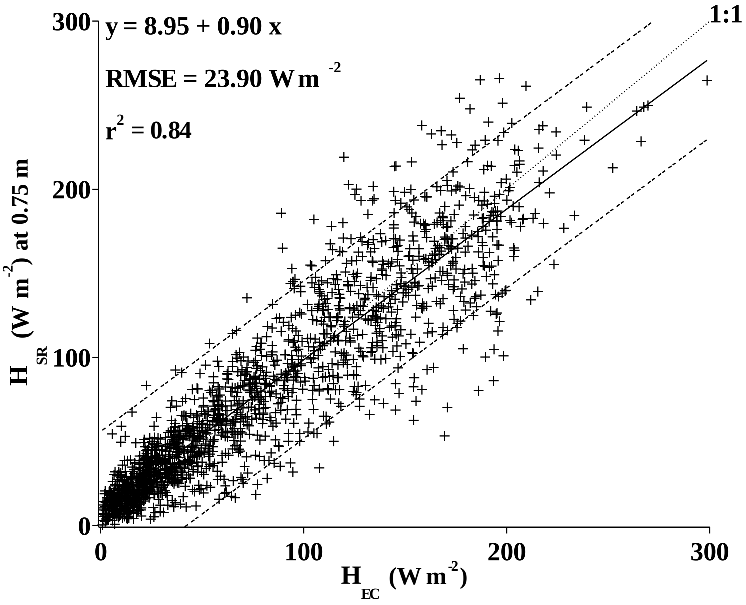

(**d**) 1.50 m

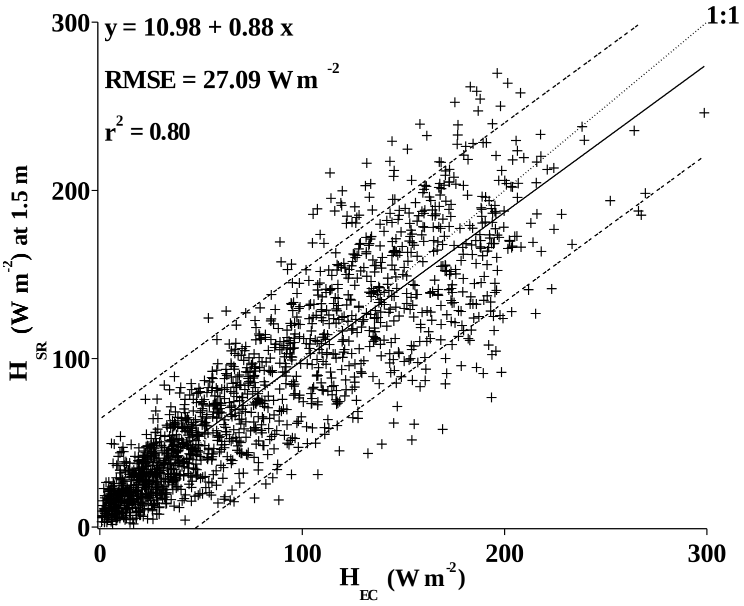

Fig. 3.2 Validation plots of half-hourly H_{SR} estimates, using a time lag of 0.8 s, *vs* H_{EC} over the sugarcane: (a) H_{SR} at 0.20 m above the crop surface *vs* H_{EC}; (b) at 0.50 m; (c) at 0.75 m; (d) at 1.50 m. The wide confidence bands represent the 95 % confidence level for a single-predicted *y*-value.

the lack of accuracy at the greater measurement heights due to the possibility that such heights were above the fully adjusted boundary layer. The greater slope was observed for the measurements at a height of 0.75 m above the crop surface since this height was closest to the EC height. It is noted that there is relatively more scatter for sensible heat flux values greater that 100 W m^{-2}. This was also clearly observed in the diurnal variation plots (data not shown). The slope and r^2 increased and RMSE decreased as the measurement height decreased. The SR method underestimated, compared to H_{EC}, by about 12 % at 0.20, 0.50 and 1.50 m above the crop surface and by about 10 % at a height of 0.75 m. It is observed that when the obtained weighting factor was applied for the validation data, the agreement between H_{SR} estimate and H_{EC} was improved (Tables 3.2 and 3.3).

Diurnal variations in the half-hourly H_{SR} estimates for all measurement heights using a time lag of 0.8 s and H_{EC} and net irradiance (right hand *y*-axis) for a clear day, day of year 226 (2008), and a day with variable cloud, day of year 322 (2008), are shown in Fig. 3.3. The sensible heat flux values, derived using SR, are in agreement with EC, perhaps slightly less around midday. The H_{SR} estimates underestimated H_{EC} and exhibited more variation compared to H_{EC} estimates, especially during days with variable cloud (Fig. 3.3b). The variations in net irradiance during a day with variable cloud are reflected in the sensible heat flux as shown in Fig. 3.3b. Generally, the H_{EC} is better correlated with net irradiance than the H_{SR} estimates.

Detection and understanding of ramp amplitude and total ramp period as well as wind speed are crucial for the SR analysis as they are associated with the exchange of sensible heat between the surface and the atmospheric layer. The diurnal variation of the H_{SR} estimates and the associated a and $1/(l + s)$ at height of 1.50 m above the soil surface for both air temperature time lags are shown (Fig. 3.4). Also shown is the horizontal wind speed for the unstable conditions for this day of year 281, 2008. The variations of the H_{SR} estimate are associated with variation in a and $1/(l + s)$ for both air temperature time lags. The inverse total ramp period agrees reasonably well with H_{SR} estimates compared to a. Anandakumar (1999), in his experiment over a wheat canopy, reported that the H_{SR} estimates were slightly better correlated with $1/(l + s)$ than with a. The ramp amplitude is greater for the 0.8-s air temperature time compared to the 0.4-s air temperature time lag while for $1/(l + s)$ the opposite occurs. These results explain H_{SR} overestimation when the 0.4-s air temperature time lag is used.

(a)

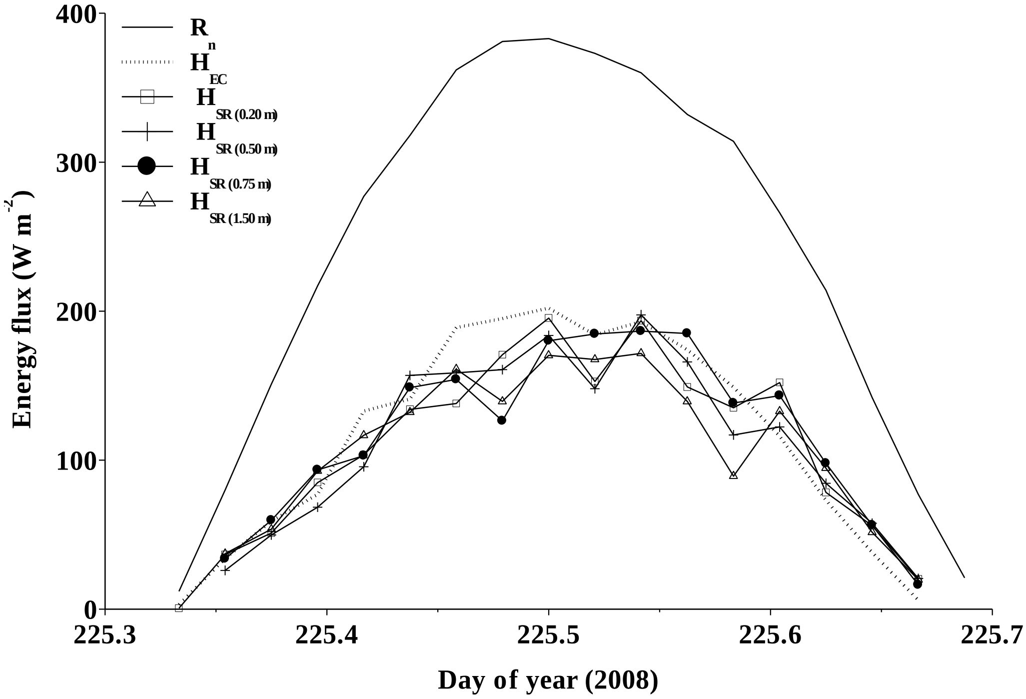

(b)

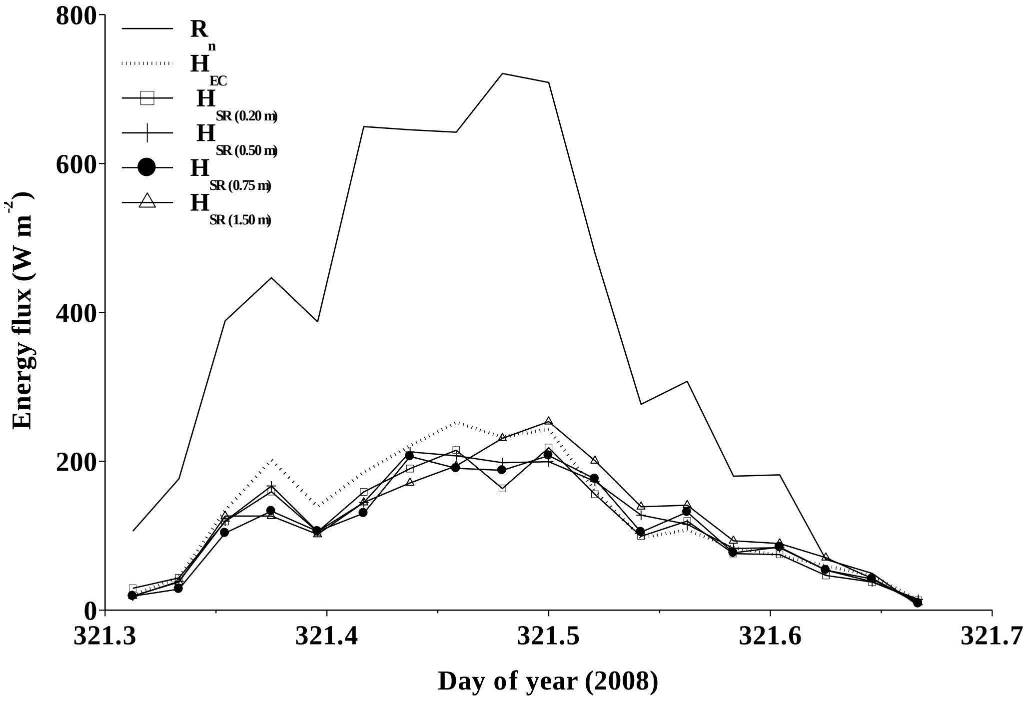

Fig. 3.3 Diurnal variations of half-hourly H_{SR} estimates for all heights and a time lag of 0.8 s and H_{EC} along with net irradiance for daytime unstable conditions over the sugarcane for (a) a clear day (day of year 226, 2008) and (b) a day with variable cloud (day of year 322, 2008).

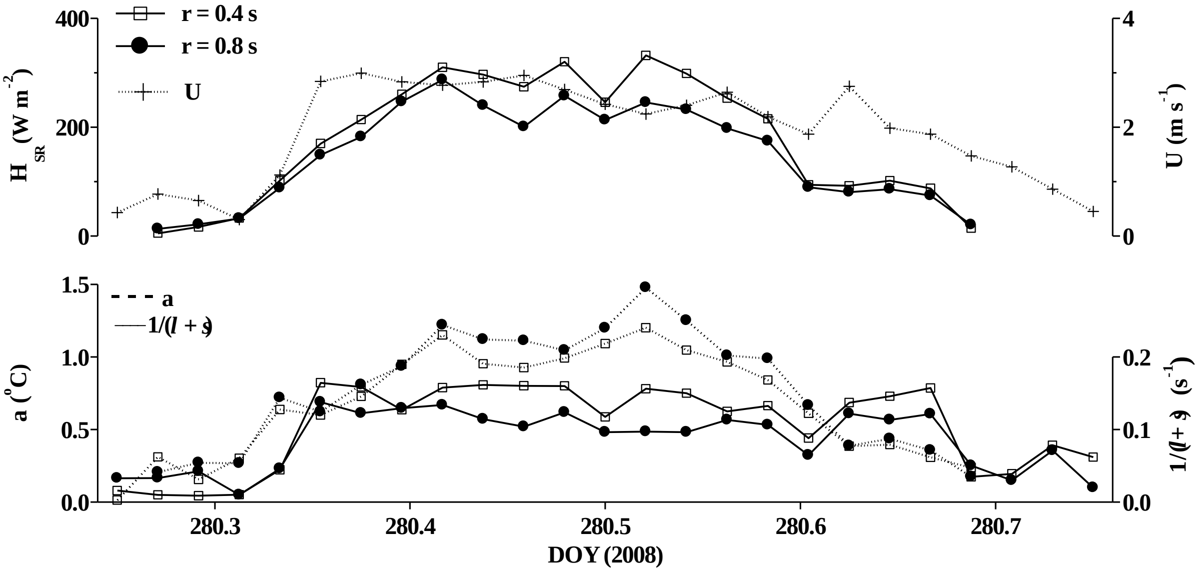

Fig. 3.4 Half-hourly H_{SR}, ramp amplitude *a* (°C) and inverse total ramp period 1/(*l* + *s*) (s^{-1}) estimates using the two time lags for a height of 1.50 m above the soil surface, and EC wind speed *U* (m s^{-1}) for daytime unstable conditions, day of year 281 (2008).

A representative sample of two minutes of 10-Hz air temperature fluctuations at four heights over a 1.3 m-tall sugarcane canopy during unstable conditions is shown (Fig. 3.5). Air temperature fluctuations increase relatively rapidly followed by a sharp decrease because heated air from the crop canopy elements eject upward into the air. This indicates that the air temperature fluctuations show a ramp pattern. Snyder *et al*. (1997) reported that when air temperature traces exhibit gradual warming followed by a sharp decrease, the air is unstable, *a* is positive, and sensible heat flux is upward and positive. Also in Fig. 3.5, the ramps are relatively different for the different measurement heights especially at heights of 1.50 and 1.80 m above the soil surface.

3.4.2 Latent energy flux

The surface renewal LE_{SR}, and eddy covariance LE_{EC} latent energy fluxes were estimated as a residual using the shortened energy balance from measured sensible heat flux, net irradiance and soil heat flux measurements. Only positive latent energy flux data during daytime hours from 06h00 to 18h00 were used in the analysis because the positive latent energy flux corresponds to evaporation and this occurs mainly during the daytime.

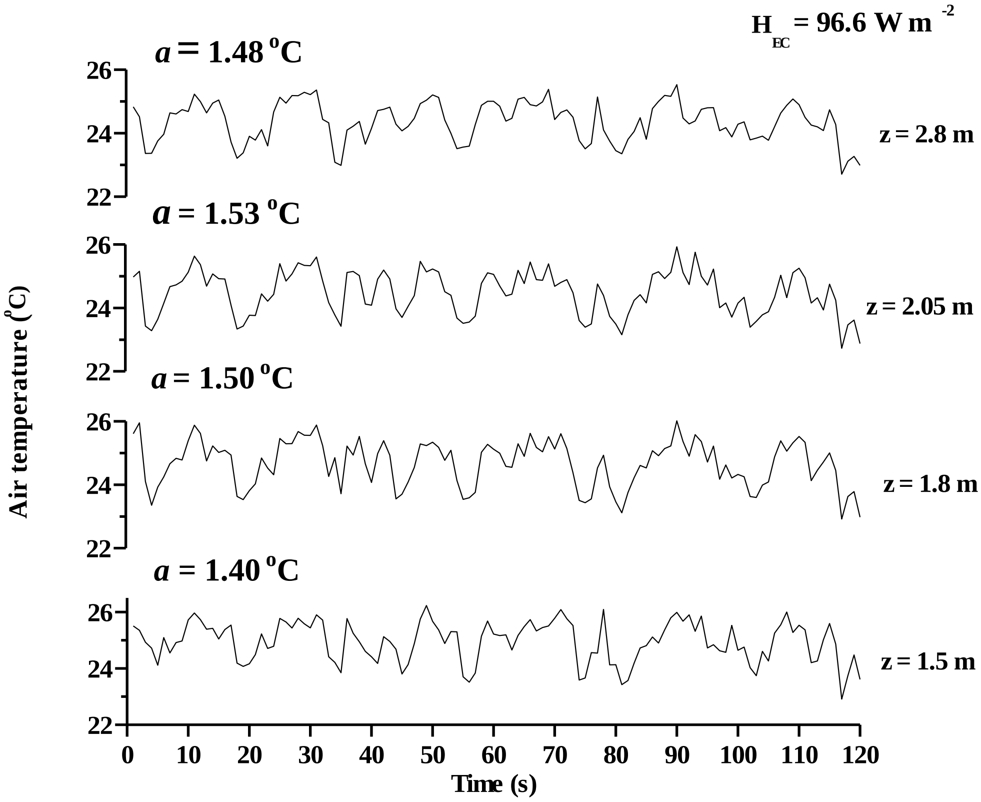

Fig. 3.5 A sample of two minutes of 10-Hz (11h58 to 12h00 on day of year 257, 2008) air temperature measurements exhibiting ramp characteristics for unstable conditions for four measurement heights above the soil surface for the 1.3-m tall sugarcane.

The linear regression statistics of half-hourly residual SR latent energy flux LE_{SR} estimates at measurement heights of 0.20, 0.50, 0.75, and 1.50 m above the crop surface for time lags of 0.4 and 0.8 s *vs* LE_{EC} during the daytime hours from 06h00 to 18h00 for day of year from 191 to 199, from 206 to 240 and from 298 to 354 (2008) are presented in Table 3.4. The SR sensible heat flux gave a very good estimate of latent energy flux for all heights and both air temperature time lags with a slope close to unity and RMSE less than 32.11 W m^{-2}. The SR latent energy flux using a time lag of 0.8 s yielded the best results with a slope close to 0.9 and lower RMSE values for the first three heights compared to the time lag of 0.4 s (Table 3.4). At the highest height, 1.50 m above the crop surface, the LE_{SR} *vs* LE_{EC} yielded greater RMSE values for both air temperature time lags. The LE_{SR} overestimated compared to LE_{EC} for the first three measurement heights (Figs 6a, b and c) and underestimated LE_{EC} at the highest height (Fig. 3.6d). The LE_{SR} accuracy, as indicated by RMSE, was improved as measurement height decreased. This finding is in good

Table 3.4 Regression statistics for the validation period for half-hourly LE_{SR} *vs* LE_{EC} estimates of latent energy flux for both time lags and all measurements heights for daytime unstable conditions

$z - h$ (m)	Time lag (s)	Intercept (W m^{-2})	Slope	RMSE (W m^{-2})	r^2	n
0.20	0.4	0.53	1.05	28.06	0.97	1654
	0.8	-0.45	1.04	25.09	0.98	1699
0.50	0.4	2.95	1.04	29.37	0.97	1630
	0.8	0.87	1.01	26.70	0.97	1645
0.75	0.4	2.18	1.02	33.21	0.96	1626
	0.8	0.53	1.00	29.38	0.97	1659
1.50	0.4	4.35	1.00	36.59	0.95	1607
	0.8	2.54	0.98	32.11	0.96	1640

agreement with results by Mengistu (2008) who conducted several experiments above different vegetated surfaces and open water in South Africa using the SR method. The best LE_{SR} estimate was noticed at a height of 0.20 m above the crop surface with a regression slope close to one and r^2 of 0.90 (Fig. 3.6a). The RMSE values were greater for the LE_{SR} *vs* LE_{EC} comparisons compared to those obtained from H_{SR} and H_{EC} comparisons. This be due to the fact that the errors associated with measurements of net irradiance R_n and soil heat flux G were included in both SR and EC estimates of LE.

Diurnal comparisons between half-hourly LE_{SR} for an air temperature time lag of 0.8 s and all measurement heights for unstable conditions during the daytime hours, for a clear day and a day with variable cloud are presented in Fig. 3.7. The diurnal trend of LE_{SR} and LE_{EC} estimates confirm the agreements between the SR and EC methods. The LE_{SR} estimates was greater than LE_{EC} for LE values greater than 300 W m^{-2}, as shown in Fig. 3.7a and b. In Fig. 3.7b, the magnitude of the latent energy flux was greater than R_n during the late afternoon. This may be due to uncertainties derived from the neglect of other terms of the energy balance - for example, advection from surrounding areas - and measurement errors.

(**a**) 0.20 m

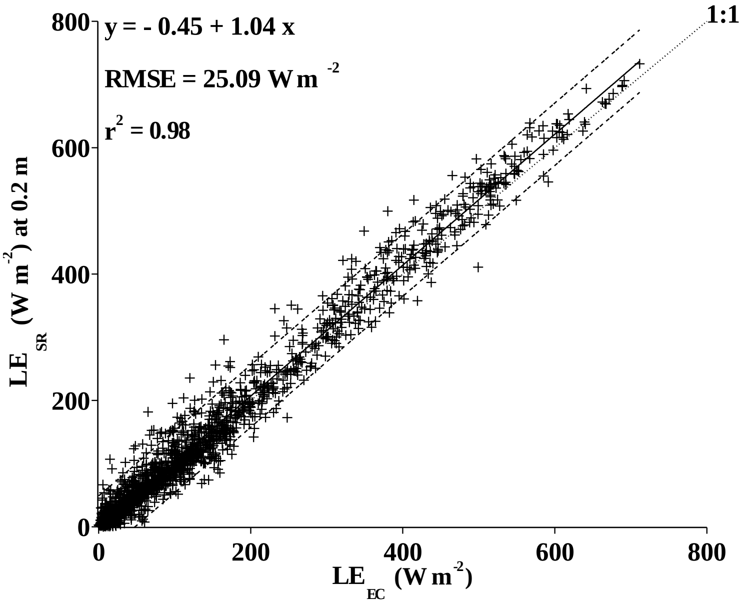
1:1
y = - 0.45 + 1.04 x
RMSE = 25.09 W m -2
r2 = 0.98
LESR (W m-2) at 0.2 m
LEEC (W m-2)
0
200
400
600
800

(**b**) 0.50 m

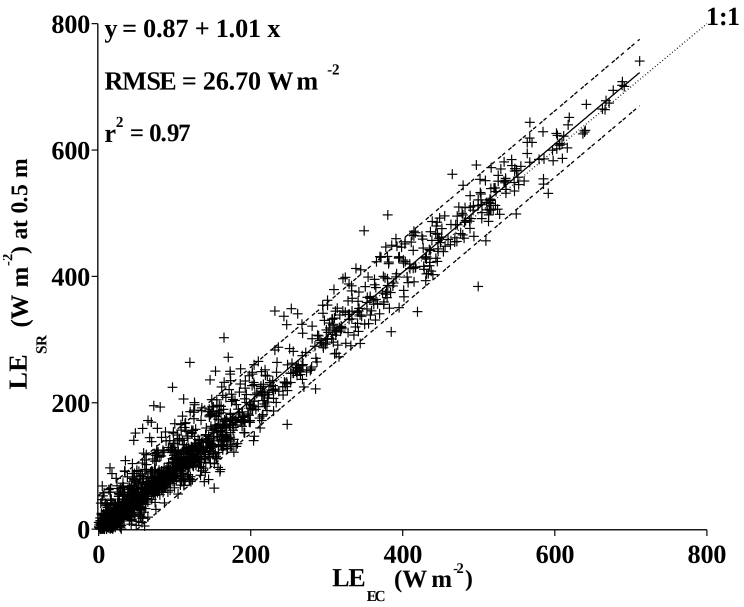
1:1
y = 0.87 + 1.01 x
RMSE = 26.70 W m -2
r2 = 0.97
LESR (W m-2) at 0.5 m
LEEC (W m-2)
0
200
400
600
800

(**c**) 0.75 m

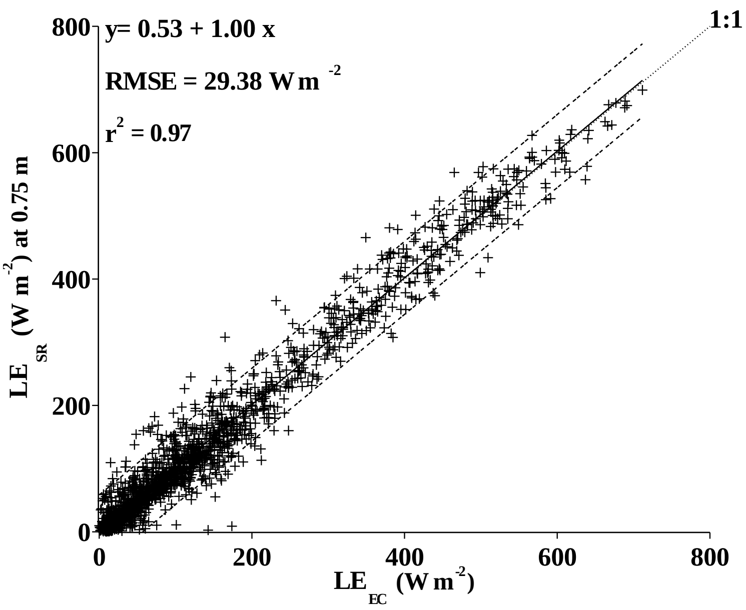

(**d**) 1.50 m

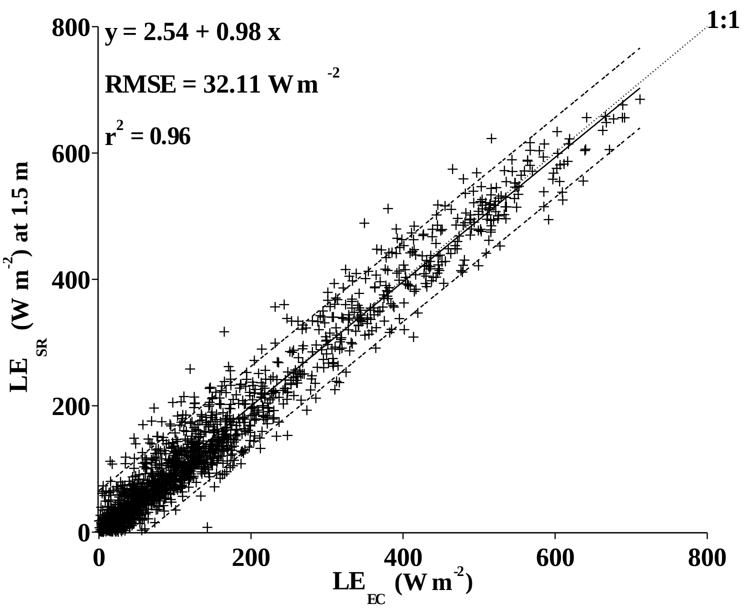

Fig. 3.6 Half-hourly LE_{SR} obtained using H_{SR} estimates for the validation period, using a time lag of 0.8 s, *vs* LE_{EC} estimates over the sugarcane for unstable conditions during daytime 06h00 to 18h00: (a) LE_{SR} at 0.200 m above the crop surface *vs* LE_{EC}; (b) at 0.50 m; (c) at 0.75 m; (d) at 1.50 m.

(**a**)

(**b**)

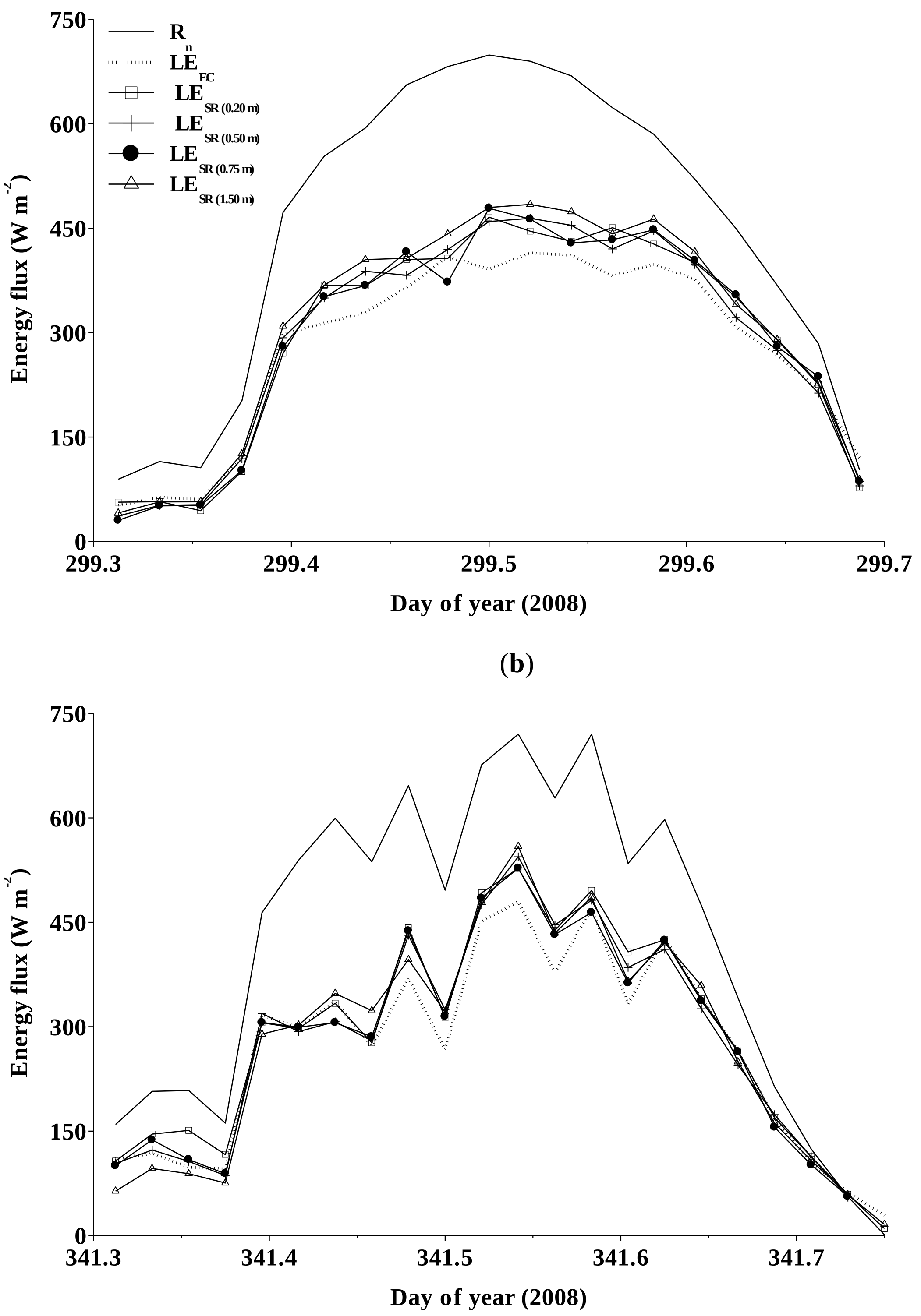

Fig. 3.7 Diurnal variations in half-hourly LE_{SR} estimates using a time lag of 0.8 s for all measurement heights and LE_{EC} along with net irradiance for unstable conditions for a clear day (day of year 300, 2008) and (b) a day with variable cloud (day of year 342, 2008).

3.5 Summary and conclusions

High frequency air temperature data were collected at four heights above a sugarcane crop surface for 0.4- and 0.8-s air temperature time lags and sensible heat flux using the SR method was estimated for unstable conditions during the daytime hours. The SR method was calibrated and validated against the EC method above the sugarcane canopy using non reserved data sets. During the calibration period, the weighting factor α was determined for each height and air temperature time lag. The magnitude of α ranged from 0.66 to 0.55 for all measurement heights and the air temperature time lag of 0.8 s. The α value increased with decrease in measurement height and an increase in the air temperature time lag. For the validation data set, the H_{SR} estimates corresponded well with H_{EC} estimates for all heights and both time lags. The agreement between SR and EC estimates of the sensible heat flux improved with a decrease in measurement height for the air temperature time lag of 0.8 s. The best H_{SR} *vs* H_{EC} comparisons were obtained at a height of 0.20 m above the crop canopy using α = 0.66 for an air temperature time lag of 0.8 s. The latent energy flux estimated as a residual involved using either H_{SR} obtained using a time lag of 0.8 s or H_{EC} estimates and measured R_n and G. The residual estimates of latent energy flux by SR and EC methods were in good agreement. The LE_{SR} at a height of 0.20 m above the canopy yielded the best comparisons with LE_{EC}. Based on these results, the SR method provides a simple and relatively inexpensive method for estimating sensible heat and latent energy flux (evaporation) above the sugarcane canopy if α is known.

Chapter 4: Evaluation of temperature variance method applied above sugarcane for estimating sensible heat flux during unstable conditions

Abstract

Reasonably accurate estimates of the sensible heat flux (*H*) from which the latent energy flux can be calculated as a residual of the shortened energy balance, is required in the agricultural and hydrological sciences. This allows an accurate estimate of crop evaporation for irrigation scheduling and water resources management. The temperature variance (TV) method was used to estimate *H* over a commercial sugarcane (*Saccharum officinarum*) canopy, in KwaZulu-Natal, South Africa. The performance of the TV method, including stability correction, and correction for air temperature skewness was evaluated against eddy covariance (EC) estimates of sensible heat flux during unstable conditions. The sensible heat flux estimated using the Monin-Obukhov similarity theory (MOST) and a spatial second-order air temperature structure function was also compared with EC measurements. High frequency air temperature measurements were collected at four heights: 0.20, 0.50, 0.75 and 1.50 m above the sugarcane canopy surface. The sign of the third-order air temperature structure function was used to identify unstable conditions. The performance of the TV methods compared to EC for estimating sensible heat flux was good for measurements either within the roughness sub-layer or within the inertial sub-layer with improvement with increase in measurement height. The sensible heat flux estimated using MOST and the spatial second-order air temperature structure function was reasonable with an improvement in the correspondence for an air temperature time lag of 0.8 s. Best results for the TV methods and sensible heat obtained from MOST and use the spatial second-order air temperature structure function approach were obtained for heights of 1.50 and 0.75 m above the crop surface respectively. The TV method, including correction for air temperature skewness, performed well in estimating sensible heat and latent energy flux compared to the other methods. The free convection limit forms for sensible heat flux estimation for the TV method and the MOST-based method that included the air temperature structure function provided poor estimates with significant bias. Based on these results, the TV method, adjusted for air temperature skewness, is an

attractive one for estimating *H* and evaporation as it is simple, relatively inexpensive, independent of EC measurements and only uses high frequency air temperature measurements as an input.

Keywords: Air temperature, Energy balance, Evaporation, High frequency, Standard deviation.

4.1 Introduction

Water is a limited resource and increasingly becoming more expensive and scarce in different countries. In South Africa, there is continuous pressure on available limited water resources in sugarcane areas due to competition with others crops, expansion of irrigated agricultural areas and variable rainfall. Methods for estimating crop evaporation therefore are needed. Generally, the weighing lysimeter method allows for direct estimate of evaporation. The EC method can measure LE directly using two instruments or EC-measured sensible heat flux can be measured directly with one instrument and latent energy (evaporation) calculated from the knowledge of the shortened energy balance terms. Application of EC method for long-term monitoring of evaporation is limited by its complexity, power consumption, stringent instrumental requirements, expensive and sensitivity of the instruments to damage whereas the weighing lysimeters are not affordable outside experimental research institutes and represents a small area (Drexler *et al.*, 2004). Therefore, indirect methods have been developed to estimate evaporation. Generally, the traditional method used to estimate evaporation in sugarcane areas is based on climatic data to estimate grass reference evaporation or tall-crop reference evaporation (Allen *et al.*, 1998, 2006), followed by the application of the crop factor approach. The main disadvantages of this method are that the net irradiance and soil heat flux are usually indirectly estimated from the available measured solar irradiance. Furthermore, the crop factor varies considerably with climate, crop variety, crop growth stage and land management practices. Hence indirect micrometeorological methods for estimating evaporation are attractive since they are more accurate compared to traditional method, and simple and inexpensive compared to direct measurement methods. A relatively inexpensive method for estimating evaporation involves measuring the sensible heat flux (*H*) from which the latent energy flux and hence total evaporation can be calculated, as a residual using the shortened energy balance from the measurements of net irradiance and soil heat flux. The reliability of evaporation estimates is continually improving with the use of new methods and improved instruments. Among these methods, the temperature variance (TV) method is inexpensive, reasonably simple and with relatively low-power requirements. Furthermore, the TV method may be used unattended at distant sites. The TV method especially uses exclusively air temperature measurements compared to the flux variance method for which latent energy and carbon fluxes may be estimated from the standard deviation of water vapour pressure and carbon dioxide concentration respectively.

The TV method, based on Monin-Obukhov similarity theory (MOST), was first proposed by Tillman (1972) and allows the sensible heat flux $H = H_{TV}$ (W m^{-2}) to be estimated at a height above the surface from the air temperature data measured using an unshielded and naturally-ventilated fine-wire thermocouple. The TV method has been tested and used for different surface types, both homogeneous and heterogeneous surfaces, and different atmospheric stability conditions (e.g., Tillman, 1972; de Bruin *et al*., 1993; Padro, 1993; Katul *et al*., 1995; Hsieh and Katul, 1996; Katul *et al*., 1996; Aubinet, 1997; Wesson *et al*., 2001; Choi *et al*., 2004; Van Dijk *et al*., 2004; Castellví and Martínez-Cob 2005; de Bruin and Hartogensis, 2005; Gao *et al*., 2006; Hiesh *et al*., 2008) and provided reasonable estimates of the H_{TV} during unstable conditions. Castellví and Martínez-Cob (2005), based on their study above olive trees to estimate H_{TV} in the surface-layer and mixed-layer, reported that the accuracy of the H_{TV} estimates in the surface-layer was relatively better compared to the mixed-layer. Currently, there are two TV methods for estimating H_{TV}, the first one corrected for stability (Wyngaard *et al*., 1971), and the second adjusted for air temperature skewness (Tillman, 1972). There is another estimation method, very similar to the TV method, such as the method of de Bruin *et al*. (1993) that is based on MOST and includes the spatial second-order air temperature structure function. The Monin-Obukhov atmospheric stability parameter ζ is included in the calculations for the TV method and to identify unstable conditions. ζ can be estimated from EC measurements or alternatively estimated independently by an iteration process. The iteration process requires the additional measurements of wind speed as an input.

The aim of this study was to evaluate the performance of the TV method, with and without adjustment for air temperature skewness, as a practical method for estimating sensible heat flux and hence latent energy flux, the latter as a residual of the shortened energy balance equation, above a sugarcane canopy in the roughness and the inertial sub-layers.

4.2 Theory

4.2.1 Energy balance

The shortened surface energy balance is used to estimate evaporation using micrometeorological methods, including the TV method. The shortened energy balance form neglects advection and the energy associated with photosynthesis and respiration, and energy stored in the canopy (Thom, 1975). For a flat extensive surface it is expressed as:

$$R_n = LE + H + G \tag{4.1}$$

where R_n is the net irradiance and G the soil heat flux. All terms are in W m^{-2}. Fluxes directed toward the surface are regarded as negative and those directed away from the surface are positive.

4.2.2 Temperature variance method

The flux variance method is based on MOST. According to this theory, for uniform surfaces, the relation between the fluxes and variances of atmospheric scalars is applied (Weaver 1990; de Bruin *et al*., 1993). The most common scalar is air temperature which is then used to estimate sensible heat flux and this has been referred to as temperature variance (TV) method. This method allows the sensible heat flux $H = H_{TV}$ to be estimated from high frequency air temperature measurements at a single-level. There are two different TV methods: the TV method corrected for stability and the TV method adjusted for air temperature skewness. There is anther method, very similar to TV method, the method of de Bruin *et al*. (1993), that is based on MOST and uses the spatial second-order air temperature structure function.

4.2.2.1 Temperature variance method including adjustment for stability (Method 1)

Wyngaard *et al*. (1971) and Tillman (1972) derived the following expression for estimating sensible heat flux $H = H_{TV(S)}$, corrected for stability, using the air temperature standard deviation σ_T and the absolute air temperature T_a (K) measurements at height z above soil surface as:

$$H_{TV(S)} = \begin{cases} \rho_a c_p \left(\dfrac{\sigma_T}{C_1}\right)^{3/2} \left(\dfrac{k g z}{T_a}\right)^{1/2} \left(\dfrac{C_2 - \zeta}{-\zeta}\right)^{1/2}, & \zeta < 0 \\ -\rho_a c_p \left(\dfrac{\sigma_T}{C_2}\right)^{3/2} \left(\dfrac{k g z}{T_a}\right)^{1/2}, & \zeta \geq 0 \end{cases} \tag{4.2}$$

where ρ_a is the density of air (kg m^{-3}), c_p the specific heat capacity of air at constant pressure (J kg^{-1} ^{o}C^{-1}), k von Kármán constant (0.4), g the acceleration due to gravity (m s^{-2}), z the measurement height (m), ζ the atmospheric stability function parameter obtained following Businger *et al*. (1971) as $\zeta = (z - d)/L_o$ where L_o is the Obukhov length (m) and d the zero displacement height (m), and C_1 and C_2 the universal similarity constants with values of 0.95 and 0.0549 respectively (Tillman, 1972). The free convection limit for Eq. (4.2) is obtained by assuming the limit for $\zeta > C_2$ and has proved to perform adequately under slightly stable conditions and can be expressed as (Tillman, 1972):

$$H_{TV} = \rho_a c_p \left(\frac{\sigma_T}{C_1}\right)^{3/2} \left(\frac{k g z}{T_a}\right)^{1/2}. \qquad \zeta \leq -0.05 \tag{4.3}$$

4.2.2.2 Temperature variance including adjustment for air temperature skewness (Method 2)

Tillman (1972), based on MOST, derived an expression for estimating sensible heat flux $H = H_{TV(Sk)}$ adjusted for the air temperature skewness S_k, and T_a at one level above the crop canopy surface as:

$$H_{TV(Sk)} = \begin{cases} \rho_a\, c_p \left(\dfrac{\sigma_T}{C_1}\right)^{1.5} \left(\dfrac{k\,g\,z\left(C_2 + A\exp(B\,S_T)\right)}{T_a\, A\exp(B\,S_T)}\right)^{1/2}, & \zeta < 0 \\ -\rho_a\, c_p \left(\dfrac{\sigma_T}{C_2}\right)^{3/2} \left(\dfrac{k\,g\,z}{T_a}\right)^{1/2} & \zeta \geq 0 \end{cases} \tag{4.4}$$

where A and B are 0.0137 and 4.39 respectively (Tillman, 1972). The air temperature skewness S_k is defined as:

$$S_k = \frac{1}{\sigma_T^{\ 3}} \left[\frac{1}{n} \sum_{i=1}^{n} (T_i - \overline{T})^3 \right] \tag{4.5}$$

where n is the number of the observations within the averaging time period, T_i an air temperature at time i, $\overline{T}$ the mean air temperature and σ_T the air temperature standard deviation.

4.2.3 Sensible heat flux from MOST and air temperature structure function (*Method 3*)

The sensible heat flux from MOST and spatial second-order air temperature structure function (method 3) is very similar to the TV method. According to MOST, method 3 allows sensible heat flux $H = H_{MOST}$ to be estimated without TV using a spatial second-order air temperature structure function (C_{TT}) and T_a measurements (de Bruin *et al*., 1993):

$$H_{MOST} = \rho_a\, c_p \left(k\, g\, z / T_a\right)^{1/2} \frac{C_{TT}^{\ 3/4}}{(-\zeta\, g_2(\zeta)^{3/2})^{1/2}} \tag{4.6}$$

where $g_2(\zeta)$ is an empirical atmospheric stability similarity function. Wyngaard *et al*. (1971) proposed a widely-accepted expression for $g_2(\zeta)$ as:

$$g_2(\zeta) = \begin{cases} C_{T1} / (1 - C_{T2}\,\zeta)^{2/3}, & \zeta < 0 \\ C_{T1} / (1 - C_{T3}\,\zeta)^{2/3} & \zeta \geq 0 \end{cases} \tag{4.7}$$

where C_{T1}, C_{T2} and C_{T3} are the universal similarity constants with values 4.9, 7 and 2.75 or 2.4 respectively. Hill (1992) defined C_{TT} as:

$$C_{TT} = \frac{\left(T_{x1} - T_{x2}\right)^2}{x_{12}^{2/3}} \tag{4.8}$$

where T_{x1} and T_{x2} are the air temperature measured at positions x_1 and x_2, at the same time, respectively, and x_{12} is spatial separation between the two measurements of air temperature. According to Taylor (1938), the frozen turbulence hypothesis states that the spatial correction of air temperature measurements at two points at the same time can be converted to the temporal correlation of air temperature measurements at two times at the same point as $x_{12} = u\ r$ where r is the air temperature time lag (s) and u the mean horizontal wind speed (m s^{-1}) which can be measured with a sonic anemometer or alternatively wind speed and direction sentry sensor. The hypothesis is used to convert spatial data series to time series. Hence C_{TT} can also be estimated from the time series from a second-order air temperature structure (Castellví *et al.*, 2006a):

$$C_{TT} = \frac{\left(T_{x1} - T_{x2}\right)^2}{(ur)^{2/3}} = \frac{S^2_{(r)}}{(ur)^{2/3}} \tag{4.9}$$

where $S^2_{(r)}$ is a second-order air temperature structure function, which can be obtained from high frequency air temperature measurements using (van Atta, 1977) using:

$$S^n(r) = \frac{1}{m-j}\sum_{i=1+j}^{m}(T_i - T_{i-j})^n \tag{4.10}$$

where n is the power of air temperature structure functions (n =1), m the number of data points measured at a frequency f (in Hz) within an averaging period typically 2 minutes, T_i the i^{th} air temperature sample, i the data point number and j the number of the lags between data points corresponds to an air temperature time lag r given by $r = j / f$. The direction of H is determined according to the sign of the third-order air temperature structure function for which n = 3 in Eq. (4.10).

The free convection limit form for Eq. (4.6) holds under slightly unstable conditions and is expressed as (Castellví *et al.*, 2006a):

$$H = 0.8\rho_a c_p z \frac{(k\,g)^{1/2}}{T_a^{1/2}} C_{TT}^{3/4}, \qquad \zeta << -0.14 \tag{4.11}$$

Based on Chen *et al*. (1997b), the sensible heat flux estimates are proportional to z in the roughness sub-layer while in the inertial sub-layer they are proportional to z - d.

4.3 Materials and methods

A field experiment was conducted within a 3-ha area of commercial sugarcane (variety N14), at the Baynesfield Estate in KwaZulu-Natal, South Africa (29.45 ^{o}S, 30.18 ^{o}E) with an altitude of 910 m above MSL. Baynesfield climate is classified as sub-humid with dry and cool winters and warm and rainy summers. The mean monthly air temperature ranges from a maximum of 21.1 ^{o}C in January to a minimum of 13.3 ^{o}C in June with mean annual precipitation of 844 mm. Precipitation falls as rain, most of it in the humid summer months. The soil is classified as the Hutton form with clay content of 550 to 650 g kg^{-1} (Haynes *et al*., 2003). The predominant wind direction is easterly. The upwind fetch available for the measurements was 97 m from the predominant wind direction. The experiment plot was bordered on the south east by a small water reservoir, and for the other directions by sugarcane differing in their heights and stages.

The sugarcane was planted as a rainfed crop during December 2007, with a row spacing of 1 m and plant spacing of 0.50 m.

The data collected for the period from 8 September to 10 October 2008 (day of year 212 to 283, 2008) were analysed and used. The crop height h (m) was measured every two weeks and ranged between 1.32 to 1.98 m during the measurements period. The roughness sub-layer height z^* was estimated as (Garratt, 1980):

$$z^* = a\,D + d \tag{4.12}$$

where a is a coefficient and D the inter-row spacing (= 1 m). A recommended value of a = 3.1 was used. When the crop was dense, the height of the roughness sub-layer z^* was also estimated as $z^* = 5\ h\ /\ 3$. The inertial sub-layer was estimated through the upwind fetch x and roughness length parameters z_o as (Brutsaert, 1982):

$$\delta' = 0.1 x^{0.8} z_o^{\ 0.2}\ . \qquad (4.13)$$

Two micrometeorological masts supporting different sensors were located at about 15 and 50 m from north and south edges of the field respectively.

For the TV methods and method 3, four unshielded and naturally-ventilated 75-µm type-E fine-wire thermocouples, placed at heights of 0.20, 0.50, 0.75 and 1.50 m above the crop surface, were used to measure high frequency air temperature. At each height, a parallel combination fine-wire thermocouple was used. The thermocouples were pointed toward the predominant wind direction which occurred during daytime hours. The measurement heights were adjusted when crop height increased. At each site visit, the thermocouples were checked for damage, cleanliness, insects and cobwebs. All thermocouples were connected to the CR3000 datalogger (Campbell Scientific Inc., Logan, Utah, USA). All air temperature data were sampled at a scan rate of 10 Hz. The air temperature standard deviation and second- and third-order air temperature structure functions were calculated from high frequency air temperature measurements. The averaging periods were two and 30 min intervals. These averages were stored in the datalogger for further analysis. The air temperature skewness S_k values were computed from high frequency air temperature data using Eq. (4.5). The time series second-order air temperature structure function $S^2(r)$ was converted to the spatial series air temperature structure function C_{TT} using Eq. (4.9) and horizontal wind speed u measured using a wind sentry wind speed and direction (model 03001, RM Young, Traverse City, Michigan, USA) at a height of 3.5 m above the soil surface. The following set of the sensible heat flux estimates were determined for each height: the TV method including stability correction ($H_{TV(S)}$) using Eq. (4.2); TV method adjusted for air temperature skewness ($H_{TV(Sk)}$) using Eq. (4.4); the sensible heat flux obtained from MOST based on the method that includes air temperature structure function (H_{MOST}) using Eq. (4.8). The sensible heat flux using free convection limit forms were also obtained using Eqs (4.3) and (4.11).

A three-dimensional ultra-sonic anemometer (model 81000, RM Young) which represents the EC system used for obtaining sensible heat flux $H = H_{EC}$, was connected to the CR3000 datalogger and installed adjacent to the thermocouples at a height that varied between 2.1 to 3.0 m above the soil surface depending on the crop height. The sonic anemometer was pointed towards north. The scan rate of the EC data measurements was 10 Hz. All EC data were processed online every 2-minute and half-hourly and stored for further analysis. Sensible heat flux was calculated following coordinate rotations for the three wind velocity components, *u*, *v* and *w*, and correction to remove the effects of instrument tilt and air-flow irregularities using the procedures similar to those of Kaimal and Finnigan (1994) and Oncley *et al*. (2007). The sonic sensible heat flux H_{sonic} was calculated as: $H_{sonic} = \rho c_p \overline{w'T_s'}$, where w' and T_s' are the fluctuations from the mean vertical wind speed w and sonic temperature T_s respectively. To obtain H_{EC}, the H_{sonic} values were also corrected for the effects of water vapour pressure and Bowen ratio using (Odhiambo and Savage, 2009):

$$H_{EC} = H_{sonic}\left(1 + \frac{0.322\bar{e}}{\bar{P}} + \frac{10^{-3}\left(0.722\bar{P} - 0.399\bar{e}\right)}{\bar{\beta}}\right)^{-1} \tag{4.14}$$

where $\bar{e}$ is the average water vapour pressure (kPa) obtained using air temperature and relative humidity measurements using two Vaisala air temperature and relative humidity instruments (Campbell HMP45C) connected to the CR1000 datalogger with one at each height of 0.50 and 1.50 m above the crop canopy, $\bar{P}$ (kPa) the average atmospheric pressure (kPa) estimated following Savage *et al*. (1997) using altitude, average water vapour pressure $\bar{e}$ and an average of the measured air temperature from the fine-wire thermocouples and $\bar{\beta}$ the average Bowen ratio estimated using:

$$\bar{\beta} = \frac{H_{sonic}}{R_n - G - H_{sonic}}. \tag{4.15}$$

The friction velocity u_* was calculated from the dimensional orthogonal wind speed measured with a three-dimensional sonic anemometer as: $[(\overline{u'w'})^2 + (\overline{v'w'})^2]^{1/4}$ (Garratt, 1992) where u, v, and w are the three dimensional orthogonal wind speeds, u', v', and

w' are the fluctuations from the mean of the u, v, and w respectively. The L_o was estimated from computed H_{sonic}, u_* and measured air temperature as:

$$L_o = -u_*^3 \frac{T_a}{kg} \frac{\rho c_p}{H} \text{ or equivalently } L_o = u_*^2 \frac{T_a}{kgT_*} \tag{4.16}$$

where T_* is the temperature scale of turbulence (K). The sign of ζ was used to identify atmospheric stability conditions (negative sign indicates unstable conditions and positive sign indicates stable conditions). The sign of the third-order air temperature structure function was also used to identify unstable conditions for the TV method adjusted for air temperature skewness, and for the method based on MOST and uses the air temperature structure function.

Additional measurements included the remaining energy balance components, R_n and soil heat flux, soil temperature and soil water content measured every one second, averaged every two-minute and stored in the CR1000 datalogger for further analysis. A NR LITE net radiometer (Kipp & Zonen, Delft, The Netherlands) to measure R_n was mounted at a height of 1.50 m above the crop surface and adjusted according to the changes in crop height. Soil heat flux G_{plate} at the 0.08 m below the soil surface was measured using two soil heat flux plates buried horizontally. Spatially-averaged soil temperature was obtained using two pairs of type-E thermocouples in metal tubes buried in the soil at depths of 0.02 and 0.06 m above the soil heat flux plates. Soil water content was measured using a frequency domain reflectometer (ThetaProbe, model ML2x, Delta-T devices, Cambridge, England) inserted vertically in the soil close to the area where soil heat flux plates and soil thermocouples were buried. The heat flux stored above the soil heat flux plates G_{stored} was calculated as:

$$G_{stored} = \left(\rho_{soil}\, c_{dsoil} + \rho_w\, \theta_v\, c_w\right) \frac{\Delta z\, \overline{\Delta T}_{soil}}{\Delta t} \tag{4.17}$$

where ρ_{soil} is the soil bulk density (kg m^{-3}), c_{dsoil} the dry soil specific heat capacity (840 J kg^{-1} ^{o}C^{-1}), ρ_w the density for water (1000 kg m^{-3}), θ_v the soil water content (m^3 m^{-3}), c_w the specific heat capacity for water (4200 J kg^{-1} ^{o}C^{-1}), Δz the soil depth (m), $\overline{\Delta T}_{soil}$ the average change in soil temperature above the soil heat flux plates (^{o}C), and Δt the time between temperature average measurements (s). The soil heat flux G was then calculated as:

$$G = G_{plate} + G_{stored} \,. \tag{4.18}$$

4.4 Results and discussion

4.4.1 Sensible heat flux

Sensible heat estimates were obtained using various methods for measurement heights of 0.20, 0.50, 0.75 and 1.50 m above the sugarcane canopy surface for the period from day of year 212 to 283, 2008. The top of the roughness sub-layer above the canopy surface was determined to be at 0.88 m above the crop surface and so the first three measurement heights were in the roughness sub-layer and the upper-most one was in the inertial sub-layer. The following set of sensible heat flux estimates were determined for each height and evaluated against EC measurements: the TV method including adjustment for stability ($H_{TV(S)}$) (method 1) using Eq. (4.2); the TV method including adjustment for air temperature skewness ($H_{TV(Sk)}$) (method 2) using Eq. (4.4); the method was based on MOST and uses a second-order air temperature structure function (H_{MOST}) (method 3) using Eq. (4.11). The free convection sensible heat flux was also obtained using Eqs (4.3) and (4.9).

4.4.1.1 Method 1-H_{TV} with stability adjustment

Half-hourly $H_{TV(S)}$ estimates for each height were plotted against H_{EC} measurements at a height that varied between 2.1 to 3.0 m above the soil surface depending on the crop height, for unstable conditions during the daytime hours from 06h00 to 18h00 (Fig. 4.1). For measurements within the roughness sub-layer, the half-hourly $H_{TV(S)}$ estimates were in reasonable agreement with H_{EC} (Figs 4.1a, b and c), with a more-improved result observed at a height of 0.20 m above the crop surface with a slope of 1.13, coefficient of determination (r^2) of 0.94 and relative mean square error (RMSE) of 19.61 W m^{-2} (Fig. 4.1a). As shown in Fig. 4.1d, a very good agreement between half-hourly $H_{TV(S)}$ estimates and H_{EC} is observed with a slope of 1.06, r^2 = 0.93 and RMSE of 21.94 W m^{-2} for

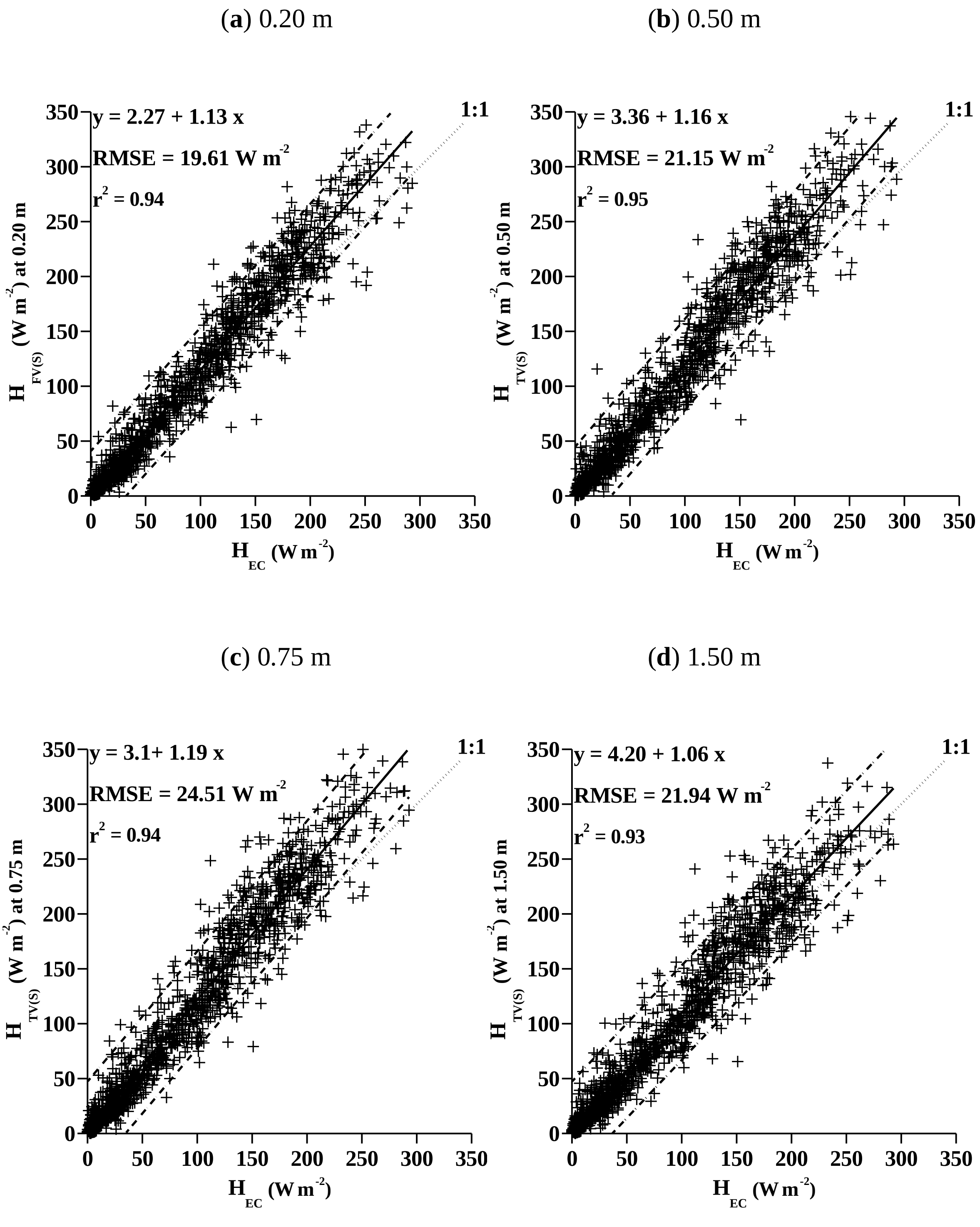

Fig. 4.1 Plots of half-hourly $H_{TV(S)}$ estimates (Method 1) at the four measurement heights, *vs* H_{EC} estimates over the sugarcane for daytime unstable conditions: (a) $H_{TV(S)}$ at 0.20 m above the canopy surface *vs* H_{EC}; (b) at 0.50 m; (c) at 0.75 m; (d) 1.50 m. The wide confidence bands represent the 95 % confidence level for a single-predicted *y*-value.

measurements within the inertial sub-layer. It is noticeable that RMSE values increased with increase in measurement height. The maximum RMSE value obtained was 24.51 W m^{-2} at a height of 0.75 m above the crop surface. Castellví and Martínez-Cob (2005) reported that lower RMSE values at the canopy top cannot be attributed to an improved performance of the TV method at this level but rather as a consequence that the TV method was uncertain near neutral conditions. The $H_{TV(S)}$ estimates were slightly biased, overestimating within the roughness sub-layer by more than 13 % as shown in Figs 4.1a, b, and c, and within the inertial sub-layer by 6 % as shown in Fig. 4.1d. Generally, the TV method including stability correction performed better within the inertial sub-layer compared to the roughness sub-layer due to fact that MOST is valid in the inertial sub-layer (Brutsaert, 1982; Kaimal and Finnigan, 1994).

4.4.1.2 Method 2-H_{TV} with air temperature skewness adjustment

The performance of the TV method adjusted for air temperature skewness in obtaining $H_{FV(Sk)}$ estimates for daytime unstable conditions within the roughness and the inertial sub-layers was also evaluated against EC and is shown in Fig. 4.2. The TV method corrected for air temperature skewness showed very good agreement with the H_{EC} for measurements within either the roughness sub-layer or the inertial sub-layer with a slope very close to unity and r^2 increasing with increase in measurement height. The RMSE values for the TV method adjusted for air temperature skewness were lower compared to the TV method including stability correction, and decreased with increase in measurement height. The improved $H_{TV(Sk)}$ estimates were observed at a height of 1.50 m above the crop canopy, with a slope of 0.97, r^2 = 0.88 and RMSE of 26.21 W m^{-2} (Fig. 4.2d) compared to the roughness sub-layer. The $H_{TV(Sk)}$ estimates slightly biased, and overestimated H_{EC} by less than 9 % in the roughness sub-layer (Figs 4.2a, b, and c) and underestimated H_{EC} by 3 % in the inertial sub-layer (Fig. 4.2d).

4.4.1.3 Method 3-H_{MOST} using $S^2(r)$

The regression statistics of half-hourly sensible heat flux H_{MOST} using MOST and the spatial series second-order air temperature structure function using air temperature time lags of 0.4 and 0.8 s at all measurement heights *vs* H_{EC} are presented (Table 4.1). Whatever

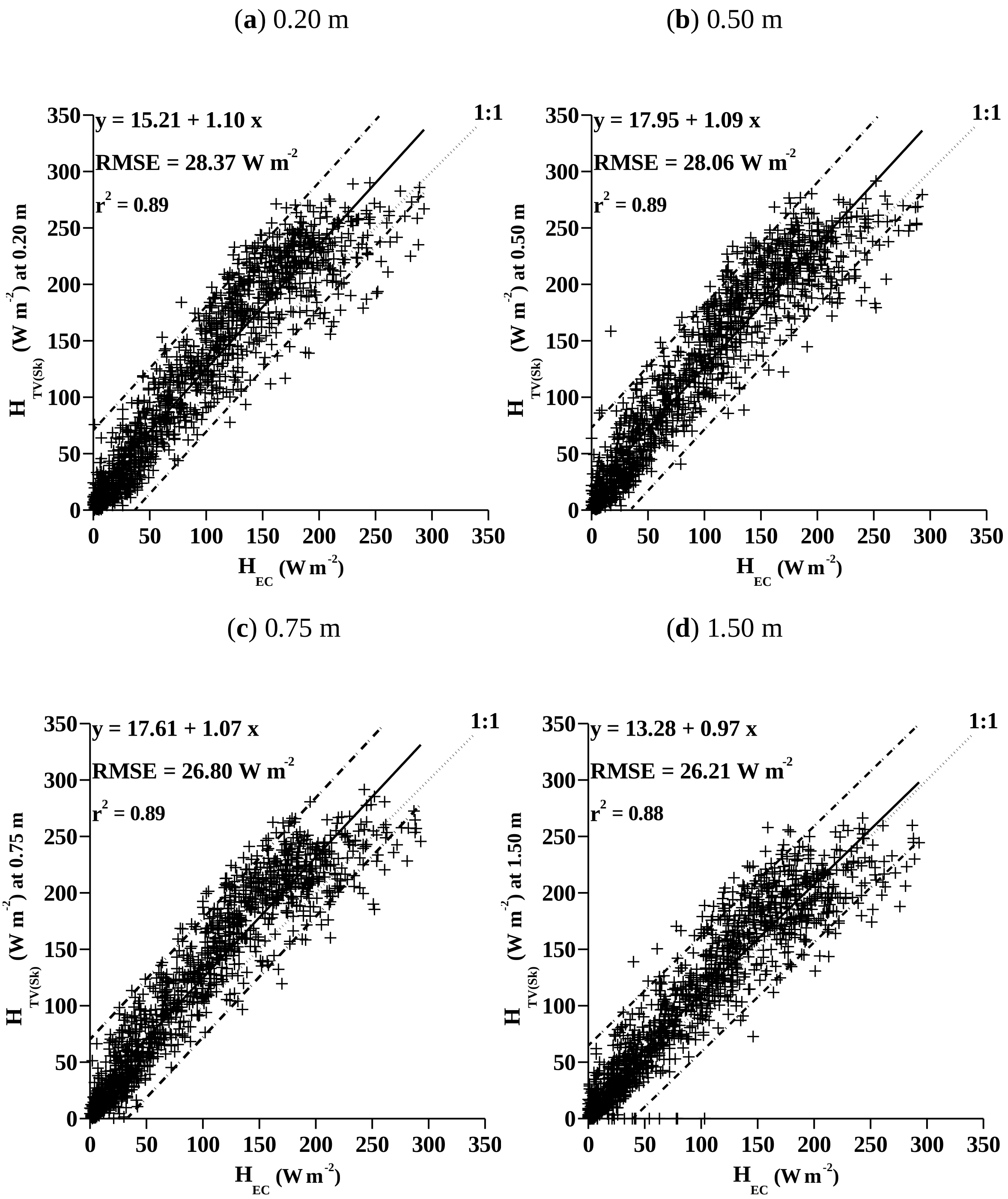

Fig. 4.2 Plots of half-hourly $H_{TV(Sk)}$ estimates (Method 2) at four different measurement heights, *vs* H_{EC} estimates over the sugarcane: (a) $H_{TV(Sk)}$ at 0.20 m above the canopy surface *vs* H_{EC}; (b) at 0.50 m; (c) at 0.75 m; (d) 1.50 m.

Table 4.1 Regression statistics of half-hourly H_{MOST} estimates (Method 3) at all measurement heights, using air temperature time lags of 0.4 and 0.8 s, *vs* H_{EC} measurements over the sugarcane.

z - *h* (m)	Time lag (s)	Intercept (W m^{-2})	Slope	r^2	RMSE (W m^{-2})	*n*
0.20	0.4	2.09	0.68	0.90	14.96	1144
	0.8	1.99	0.78	0.90	16.61	1143
0.50	0.4	2.39	0.77	0.90	16.49	1141
	0.8	1.96	0.85	0.91	17.24	1140
0.75	0.4	2.86	0.76	0.89	17.59	1141
	0.8	2.23	0.86	0.90	18.55	1141
1.50	0.4	4.06	0.63	0.87	15.72	1142
	0.8	3.26	0.71	0.89	16.33	1140

the measurement height within the roughness sub-layer or the inertial sub-layer, comparison between H_{MOST} and H_{EC} was good for both air temperature time lags with a slope significantly biased from unity and lower RMSE values. The H_{MOST} estimates using an air temperature time lag of 0.8 s showed a more-improved comparison with H_{EC} compared to an air temperature time lag of 0.4 s since the shorter air temperature time lag affects the air temperature structure function value. Fig. 4.3 shows the comparison between H_{MOST} estimated using an air temperature time lag of 0.8 s and H_{EC}. For measurements within the roughness sub-layer, the r^2 values indicated very good agreement for these data sets, with the best comparisons between H_{MOST}, at a height of 0.75 m above the crop, and H_{EC} with a slope of 0.86 and RMSE = 18.55 W m $^{-2}$ (Fig. 4.3c). Although the upper measurement height was within the inertial sub-layer for which MOST is valid, the performance of this method was poor with a slope of 0.71, r^2 = 0.89 and RMSE = 16.33 W m^{-2} (Fig. 4.3d). Generally, whatever the measurement height, H_{MOST} was biased, underestimating compared to H_{EC} for both roughness and inertial sub-layers.

Overall, the sensible heat flux comparisons with HEC using the TV method adjusted for air temperature skewness (method 2) was more-improved for both the roughness and inertial sub-layers compared to that estimated using TV method corrected for stability and the method based on MOST and structure function. The TV method corrected for stability and the method based on MOST and structure function involve □ in their calculations and therefore depend on EC measurements via u*. Thus, the TV method

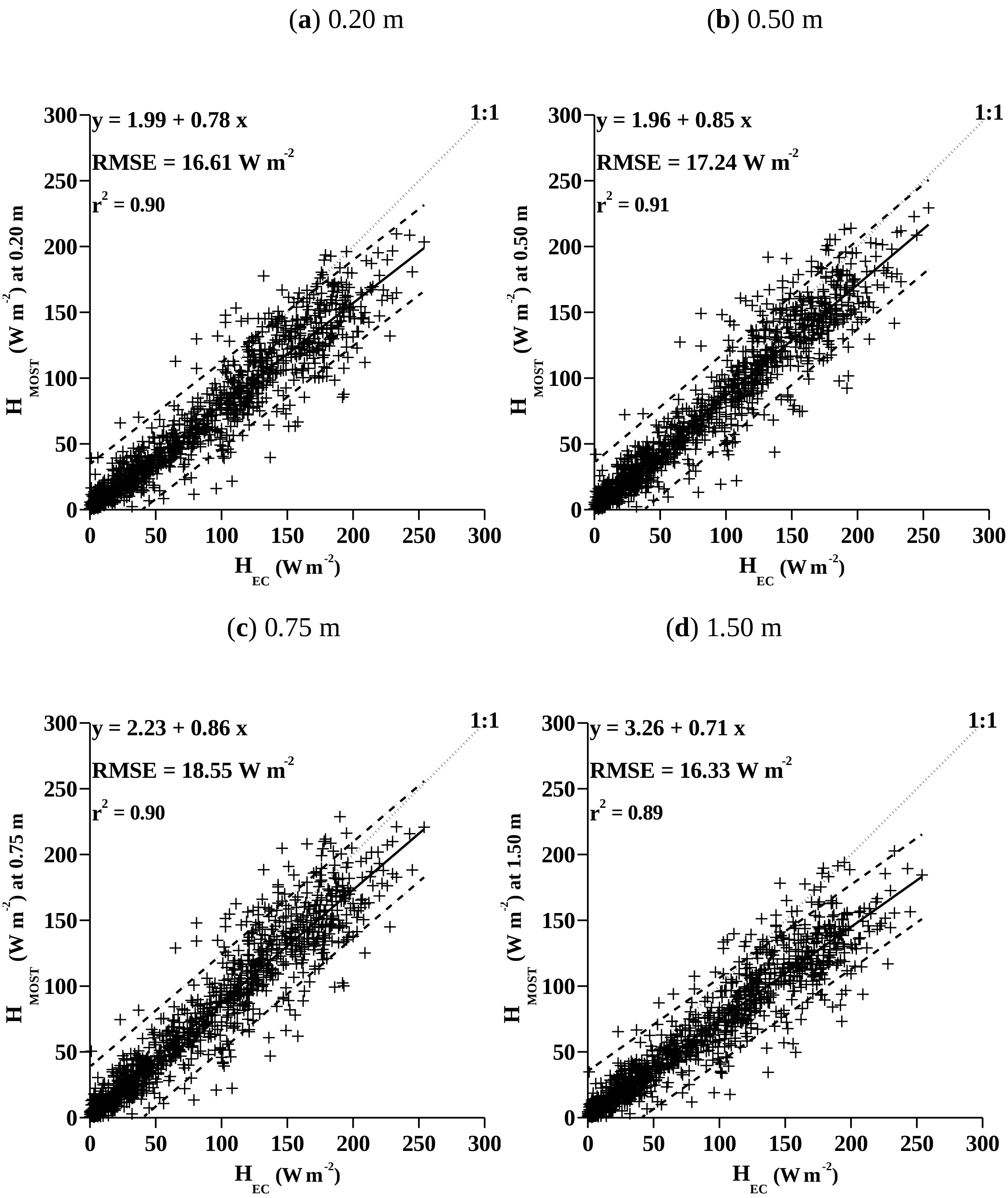

Fig. 4.3 Plots of half-hourly H_{MOST} estimates at four different measurement heights, *vs* H_{EC} estimates over the sugarcane: (a) H_{MOST} at 0.20 m above the canopy surface *vs* H_{EC}; (b) at 0.50 m; (c) at 0.75 m; (d) 1.50 m.

including adjustment for air temperature skewness is attractive since it is independent of the EC measurements and requires the high frequency air temperature measurements and measurement height as the only input data to obtain the sensible heat flux.

The free convection limit forms of the TV methods, including stability correction and that adjusted for air temperature skewness, are the same and expressed by Eq. (4.3). The free convection limits holds for $\zeta \leq -0.05$. The free convection limit form for the method based on MOST that uses the spatial second-order air temperature function expressed Eq. (4.11) and is true for $\zeta \leq -0.14$. The simple linear regression statistics of half-hourly $H_{TV\ (\mathrm{Eq.(4.3)})}$ and H_{MOST} (Eq. (4.11)) estimates using Eqs (4.3) and (4.11) respectively at all measurement heights *vs* H_{EC} are presented (Table 4.2). For measurements within the roughness sub-layer, H_{TV} (Eq. (4.3)) and H_{MOST} (Eq. (4.11)) estimates corresponded well with H_{EC} with a slope less than 0.75. The best results were obtained at the highest measurement height within this layer for both equations. For the inertial sub-layer, Eqs (4.3) and (4.11) showed reasonable performance with slopes of 0.75 and 0.65, and r^2 = 0.68 and 0.64 respectively. The RMSE values were greater for measurements within the inertial sub-layer compared to the roughness sub-layer. Eq. (4.3) performed better compared to Eq. (4.11). Generally, the TV method produced better results

Table 4.2 Regression statistics of half-hourly H for the convection limit forms sensible heat flux estimates (Eqs (4.3) and (4.11)) at all measurement heights *vs* H_{EC}.

Regression statistics	H_{TV} vs H_{EC}	$z - h$ (m)			
		0.20	0.50	0.75	1.50
Intercept (W m^{-2})	H_{TV}(Eq.(4.3)) vs H_{EC}	9.93	11.11	11.38	13.23
	H_{TV}(Eq.(4.11)) vs H_{EC}	15.42	15.16	14.18	12.74
Slope	H_{TV}(Eq.(4.3)) vs H_{EC}	0.55	0.62	0.66	0.75
	H_{TV}(Eq.(4.11)) vs H_{EC}	0.65	0.61	0.61	0.65
RMSE (W m^{-2})	H_{TV}(Eq.(4.3)) vs H_{EC}	19.88	33.23	26.90	25.55
	H_{TV}(Eq.(4.11)) vs H_{EC}	23.38	26.25	38.25	26.83
r^2	H_{TV}(Eq.(4.3)) vs H_{EC}	0.81	0.80	0.77	0.68
	H_{TV}(Eq.(4.11)) vs H_{EC}	0.68	0.68	0.68	0.64
n	H_{TV}(Eq.(4.3)) vs H_{EC}	676	876	876	932
	H_{TV}(Eq.(4.11)) vs H_{EC}	578	586	586	586

within the inertial sub-layer compared to the roughness sub-layer. As mentioned previously, the poorer performance in the roughness sub-layer is due to the fact that MOST is not valid in this layer.

Diurnal variations of the half-hourly $H_{TV(S)}$, $H_{TV(Sk)}$ and H_{MOST} estimates at a height of 1.50 m above the crop surface, H_{EC} estimates at a height of 0.85 m above the crop surface and net irradiance, for a clear day (day of year 252, 2008) and a day with variable cloud (day of year 268, 2008) are presented in Fig. 4.4. On both days, H_{MOST} was relatively lower compared to $H_{TV(S)}$, $H_{TV(Sk)}$ and H_{EC}, in spite of the good correspondence between $H_{TV(S)}$ *vs* H_{EC} and $H_{TV(Sk)}$ *vs* H_{EC} as shown in Fig. 4.4. The sensible heat flux fluctuated with changes in net irradiance according to cloud cover, as shown in Fig. 4.4b.

4.4.2 Latent energy flux

The TV $LE_{TV(S)}$, $LE_{TV(Sk)}$, MOST–based method LE_{MOST} (using an air temperature time lag of 0.8 s), and LE_{EC} estimates were calculated as residuals of the shortened energy balance (Eq. 4.1) for half-hourly data. Only positive latent energy flux estimates for unstable conditions during the daytime hours from 06h00 to 18h00 corresponding to evaporation were used. Diurnal variations of half-hourly $LE_{TV(S)}$, $LE_{TV(Sk)}$ and LE_{MOST} estimates at a height of 1.50 m above the crop surface in the inertial sub-layer, and LE_{EC} estimates, along with R_n are presented (Fig. 4.5). On clear days, $LE_{TV(S)}$ overestimated LE_{EC} during early morning and otherwise underestimated LE_{EC} for LE values greater than 150 W m^{-2}, and $LE_{TV(Sk)}$ and LE_{MOST} overestimated LE_{EC} as shown in Fig. 4.5a. For days with variable cloud, all methods overestimated LE_{EC} as shown in Fig. 4.5b. The latent energy flux tracked the diurnal pattern in net irradiance R_n.

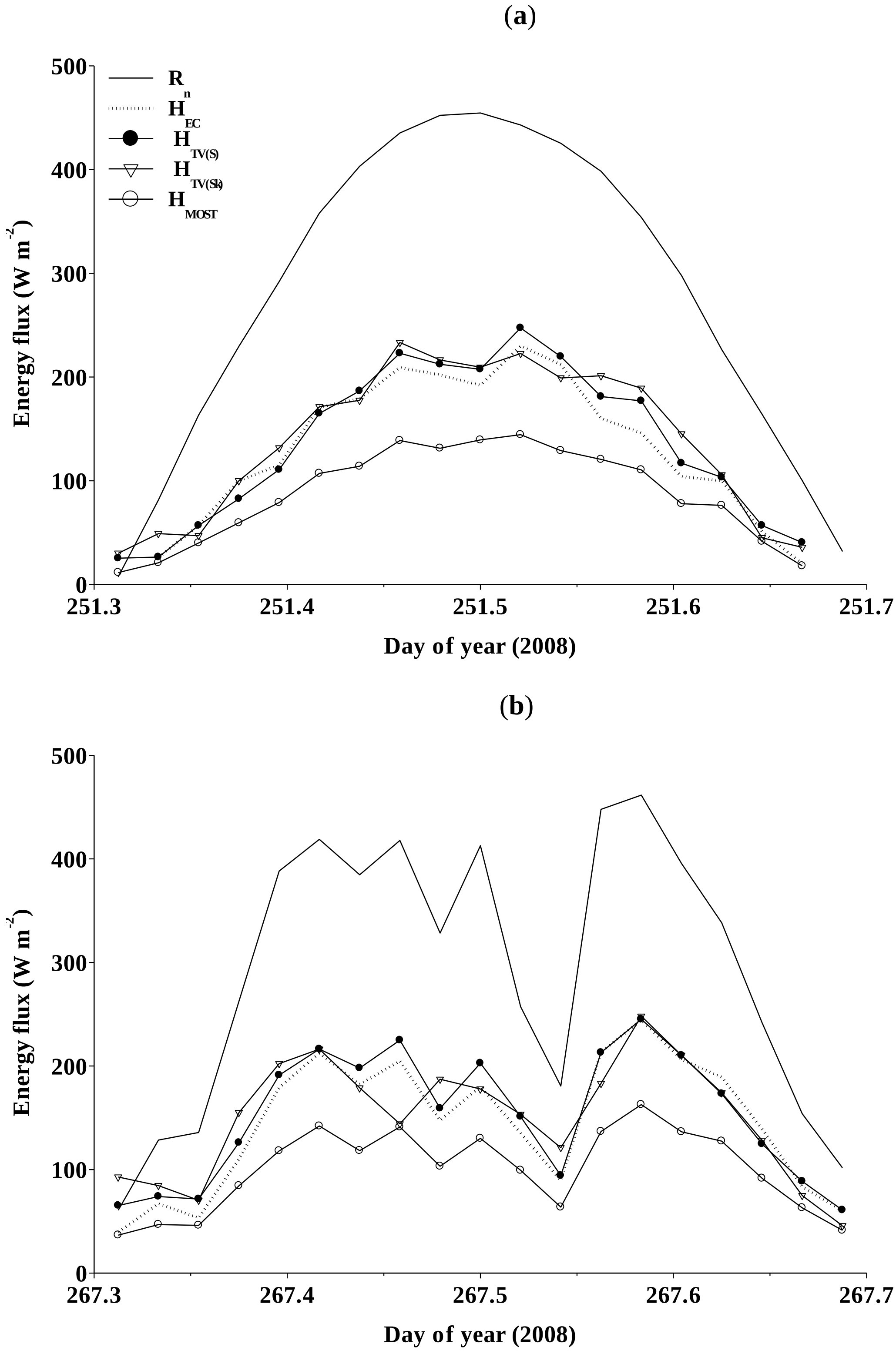

Fig. 4.4 Diurnal variations of half-hourly $H_{TV(S)}$, $H_{TV(Sk)}$ and H_{MOST} estimates at a height of 1.50 m above the crop surface, H_{EC} along with R_n above the sugarcane for (a) clear day (day of year 252, 2008) and (b) day with variable cloud (day of year 268, 2008).

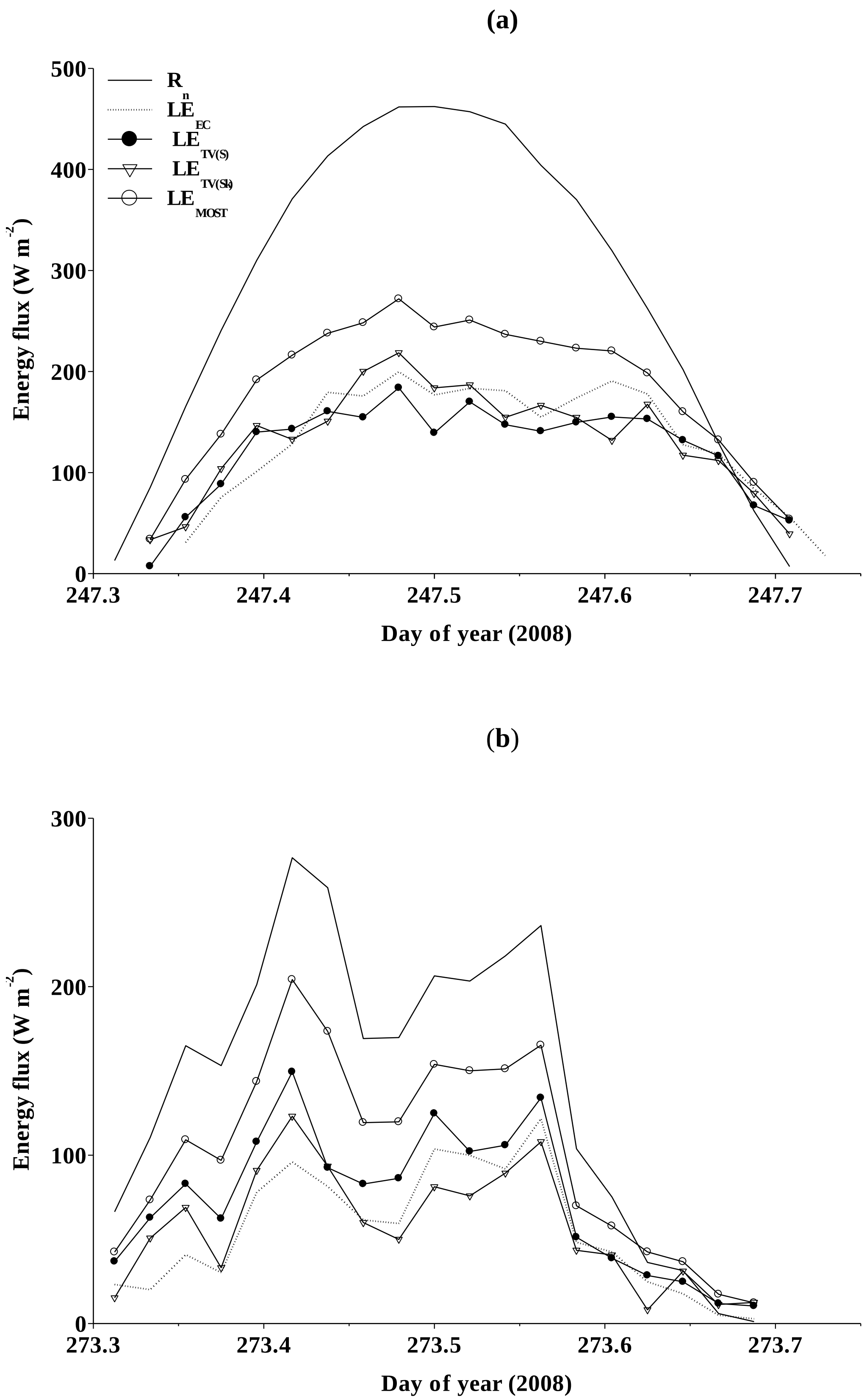

Fig. 4.5 Diurnal variations of half-hourly $LE_{TV(S)}$, $LE_{TV(Sk)}$, LE_{MOST} and LE_{EC} at a height of 1.50 m above the canopy surface along with R_n above the sugarcane for (a) clear day (day of year 248, 2008) and (b) day with variable cloud (day of year 274, 2008).

4.5 Summary and conclusions

The performance of the TV method in estimating sensible heat flux, including adjustment for stability (method 1) and adjusted for air temperature skewness (method 2), and the sensible heat flux from MOST and using the spatial second-order air temperature structure function (method 3) and their free convection limits forms were evaluated above sugarcane for unstable conditions within the roughness and the inertial sub-layers by comparison with EC measurements. The performance of the TV method was good for measurements either within the roughness sub-layer or within the inertial sub-layer and more improved with increase in measurement height. The sensible heat flux using method 3 was reasonable but biased with the comparison improved for an air temperature time lag of 0.8 s. Improved comparisons were obtained at a height of 1.50 and 0.75 m above the crop surface for the TV methods and method 3 respectively.

Overall, the TV method adjusted for skewness was superior in estimating sensible heat and latent energy flux compared to the other temperature–based methods. The free convection limit forms of the TV method and method 3 provided poor estimates of sensible heat flux with significant bias compared to H_{EC}. Based on these results, the TV method, adjusted for air temperature skewness, is an attractive method for estimating H and evaporation as it is a simple, inexpensive, independent of EC measurements, and only uses high-frequency air temperature measurements and measurement height as inputs. The measurements should be taken within the inertial sub-layer (at a height of 1.50 m above the crop surface)

Chapter 5: Sensible heat flux estimation over sparse and dense sugarcane using surface renewal analysis

Abstract

Sensible heat and latent energy fluxes over sparse and dense sugarcane canopies conditions were estimated using surface renewal (SR) and eddy covariance (EC) methods. The performance of SR models were evaluated during daytime unstable conditions at measurement heights of 0.20, 0.50, 0.75 and 1.50 m above the crop canopy surface and using air temperature time lags of 0.4 and 0.8 s. Sensible heat flux estimates using the original and other SR approaches (H_{SR}) are comparable with EC sensible heat flux (H_{EC}). The SR weighting factor (α) was determined by plotting H_{SR} *vs* H_{EC} for each measurement height and both air temperature time lags. A weighting factor α' was also calculated using friction velocity and a stability function. The α increased with a decrease in measurement height for the 0.8-s air temperature time lag. It is observed that α' values were greater compared to α. The sensible heat flux estimated using the original SR approach for which α value is determined by calibration with EC yielded more accurate estimates than when α' was calculated using friction velocity and a stability function. Various other SR estimates applied to the roughness sub-layer obtained by calculation, one using a finite micro-front ramp SR model, another using K-theory and others that combine SR and Monin-Obukhov similarity theory (MOST) and their free convection forms produced very good H_{SR} estimates. Improved H_{SR} estimates were observed using a combined SR and K-theory approach. The combined SR and MOST approach that uses either an air temperature standard deviation or an air temperature structure function performed well in the inertial sub-layer but its respective free convection forms performed poorly. The performance of the original and other SR approaches was improved when the crop was dense and hence more homogeneous. The H_{SR} estimates obtained by the SR analysis based on a finite micro-front ramp SR model was superior compared to those obtained using the other approaches.

5.1 Introduction

Evaporation is recognized as the most important process that represents the major consumptive use of irrigation water and rainfall on agricultural areas (Gowda *et al.*, 2008). Accurate and continuous measurement of evaporation is an important aspect for available water resources management in water-scarce countries including South Africa.

Different micrometeorological methods have been used to estimate evaporation, such as the Bowen ratio energy balance (BR), eddy covariance (EC), scintillometer, surface renewal (SR) and temperature variance (TV) methods. There have been few studies of evaporation estimation over sugarcane using micrometeorological methods. Examples of such include the BR (Burger, 1999; McGlinchey and Inman-Bamber 2002; Inman-Bamber and McGlinchey, 2003; Shinichi *et al.*, 2004), EC (Denmead and MacDonald, 2008), and scintillometer (Wiles, 2006) methods. These methods are expensive and their instruments are sensitive to damage. They also require extensive fetch and site homogeneity (Drexler *et al.*, 2004). In the case of scintillometer method, the Monin-Obukhov similarity theory (MOST) is required.

The SR method for estimating sensible heat flux was pioneered by Paw U and Brunet (1991). Theoretical details of the SR method have been reviewed (e.g., Paw U *et al.*, 1995; Snyder *et al.*, 1996, 1997; Drexler *et al.*, 2004; Savage *et al.*, 2004; Paw U *et al.*, 2005; Mengistu, 2008). The SR method for the estimation of sensible heat flux uses high frequency air temperature measurements at a single point above the canopy surface (typically 10 Hz). The latent energy flux may then be estimated as a residual from the shortened energy balance form from surface renewal sensible heat flux (H_{SR}), the measured net irradiance R_n and the soil heat flux G. The SR method for estimating sensible heat flux over natural surfaces is an attractive one compared to other micrometeorological methods because it is simple, low-cost, and it overcomes many of the problems associated with application of the similarity principle. In addition, the SR method may be applied close to the canopy surface which in turn makes easier for access of instrumentation above tall canopies and it is applicable when the wind fetch is limited (Castellví *et al.*, 2006a).

The objective of this study is to evaluate the performance of five SR approaches for estimating sensible heat and latent energy fluxes above sparse and dense sugarcane canopies conditions in comparison with EC measurements and to determine the effect of measurement height, air temperature time lag and crop height on the weighting factor.

5.2 Theory

5.2.1 Energy balance

From the SR analysis method for estimating sensible heat flux, the shortened energy balance may be used to estimate the latent energy flux *LE* as a residual. The shortened surface energy balance is expressed as:

$$R_n = G + H + LE \tag{5.1}$$

where R_n is the net irradiance, *G* the soil heat flux, *H* the sensible heat flux, and *LE* the latent energy flux. The energy flux associated with photosynthesis and respiration, and energy stored in the plant canopy and advection are assumed to be negligible.

5.2.2 Surface renewal method

The SR method for estimating the sensible heat flux was pioneered by Paw U and Brunet (1991) and is based on the coherent structures concept**.** The coherent structure theory assumes that an air parcel sweeps from above the canopy to the canopy surface. The air parcels begin to be cooled or heated when near or in the canopy because of the sensible heat exchanges between the air and canopy elements. Ramps are observed in the air temperature traces as a result of the turbulent coherent structures. These ramps for stable and unstable conditions, are characterized by an air temperature amplitude and total ramp period parameters where *l* is the ramping period (s) and *s* the quiescent period (s) (Paw U and Brunet, 1991).

5.2.2.1 Ideal SR analysis model method based on an air temperature structure function analysis

In this approach, the following expression is used for estimating $H = H_{SR}$ (Paw U *et al.*, 19 95):

$$H_{SR} = \alpha\, z\, \rho_a\, c_P\, \frac{a}{l+s} \tag{5.2}$$

where α is a weighting factor defined as a factor that corrects for the unequal amount of the scalar from the measurement height z to the ground, which in this case is air temperature but it also applies to other scalars such as water vapour density. In Eq. (5.2), ρ_a is the density of air (kg m^{-3}), c_p the specific heat capacity of air at constant pressure (J kg^{-1} ^{o}C^{-1}), a the amplitude and total ramp period τ is equal to $l+s$. The quantity $\alpha\, z$ has a physical significance, representing the volume of air per unit of ground area exchanged on average for each ramp in the sample period for the measurement height (Paw U *et al.*, 2005). The amplitude and ramp period are estimated following the structure function approach of van Atta (1977): the air temperature structure function $S^n(r)$ is obtained from high frequency air temperature measurements using the following relationship:

$$S^n(r) = \frac{1}{m-j} \sum_{i=1+j}^{m} (T_i - T_{i-j})^n \tag{5.3}$$

where m is the number of data points measured at frequency f (Hz) in the averaging time interval, n the power of the structure function, j the number of the lags between data points corresponding to an air temperature time lag $r = j/f$, and T_i the i^{th} air temperature sample. The average a in the time interval can be determined from the solution of the polynomial equation (Spano *et al.*, 1997a, b; Paw U *et al.*, 2005):

$$a^3 + \left(10S^2(r) - \frac{S^5(r)}{S^3(r)}\right) a + 10\, S^3(r) = 0 \tag{5.4}$$

and the total ramping period $l + s$ is estimated using:

$$l + s = -\frac{a^3 r}{S^3(r)}. \tag{5.5}$$

The SR weighting factor α can be determined by plotting SR sensible heat flux (H_{SR}) *vs* EC sensible heat flux (H_{EC}) measurements. Following Castellví (2004), the parameter hereinafter referred to as α', can be also estimated as:

$$\alpha' = \begin{cases} \left(\dfrac{k\ z^{*}\ \tau\ u_{*}}{\pi\ z^2\ \phi_h(\zeta)} \right)^{1/2}, & h \le z \le z^{*} \\ \left(\dfrac{k(z-d)\tau\ u_{*}}{\pi\ z^2\ \phi_h(\zeta)} \right)^{1/2}. & z - d > z^{*} \end{cases} \tag{5.6}$$

where k is the von Kármán constant (0.4), z* the roughness sub-layer depth, which may be estimated as $z^* = h + 2\ (h - d)$ (Sellers *et al.*, 1986) where h is the crop height (m), d the zero displacement height estimated as 2 h /3, u_* the friction velocity (m s^{-1}) and $\phi_h(\zeta)$ the stability function for heat transfer given by (Businger *et al.*, 1971; Arya, 2001):

$$\phi_h(\zeta) \ = \begin{cases} 0.74(1-9\zeta)^{-1/2}, & \zeta < 0 \\ 0.74, & \zeta = 0 \\ 0.74 + 4.7\zeta & \zeta > 0 \end{cases} \tag{5.7}$$

where ζ is an atmospheric stability parameter defined as $\zeta = (z - d)/L_o$ where L_o is the Obukhov length (m) defined as:

$$L_o = -u_*^3 \frac{T_a}{k\,g} \frac{\rho_a\, c_p}{H} \text{ or equivalently } L_o = -u_*^2 \frac{T_a}{k\,g\,T_*} \tag{5.8}$$

where T_a is the air temperature(^{o}C) and g the acceleration gravity (m s^{-2}).

5.2.2.2 SR ramp model method with finite micro-front period

Chen *et al*. (1997a) proposed a ramp model method that neglects the quiescent period but includes a finite micro-front time, and allows H_{SR} to be estimated, from high frequency air temperature measurements and u_*, as:

$$H = \begin{cases} -\alpha' \beta^{2/3} \gamma \rho_a c_P \left(S^3_{(r_m)} / r_m \right)^{1/3} u_*^{2/3} \dfrac{z}{h^{2/3}}, & 0.2h < z \le h + 2(h-d) \\ -\alpha' \beta^{2/3} \gamma \rho_a c_P \left(S^3_{(r_m)} / r_m \right)^{1/3} u_*^{2/3} \dfrac{z}{(z-d)^{2/3}} & z-d > h+2\,(h-d),\ z-d \le 0.2h \end{cases} \tag{5.9}$$

where $\alpha' \beta^{2/3} \gamma$ is the empirical combined coefficient which is common for both roughness and inertial sub-layers with a recommended value of 0.4 (Chen *et al*., 1997b), $S^3_{(r_m)}$ the third-order of air temperature structure function, r_m an air temperature time lag that maximizes $-(S^3_{(r)}/r)^{1/3}$ and γ the correction coefficient for differences between $a/\tau^{1/3}$ and $-(S^3_{(r)}/r)^{1/3}$ maximum value and ranges between 1 and 1.2 for straw mulch and bare soil (Chen *et al*., 1997b) and between 0.9 and 1.1 for Douglas-fir forest (Castellví *et al*., 2006a).

5.2.2.3 Combined SR analysis model method with K-theory

Using K-theory, Castellví *et al*. (2002) proposed the following expressions for sensible heat flux estimated either in the roughness or inertial sub-layers as:

$$H_{SR} = \begin{cases} \rho_a c_p \beta_1 a \dfrac{z^*}{z} \dfrac{u_*}{\phi_h(\zeta)}, & h \le z \le z^* \\ \rho_a c_p \beta_2 a \dfrac{u_*}{\phi_h(\zeta)} & z-d > z^* \end{cases} \tag{5.10}$$

where β_1 and β_2 are the scale parameters for the roughness and inertial sub-layers respectively. They found the magnitude of β_1 ranging from 0.23 to 0.33 and the magnitude of β_2 ranging from 0.10 to 0.15 for different crop canopies.

Castellví (2004) proposed an expression for estimating sensible heat flux by combining Eqs (5.2) and (5.6):

$$H_{SR} = \begin{cases} \rho_a c_p \dfrac{a}{\tau^{1/2}} \left(\dfrac{u_*}{\phi_h(\zeta)} \right)^{1/2} \left(\dfrac{k\, z^*}{\pi} \right)^{1/2}, & h \le z \le z^* \\ \rho_a c_p \dfrac{a}{\tau^{1/2}} \left(\dfrac{u_*}{\phi_h(\zeta)} \right)^{1/2} \left(\dfrac{k\,(z-d)}{\pi} \right)^{1/2}. & z-d > z^* \end{cases} \tag{5.11}$$

Substituting u_* from the definition of L_o in Eq. (5.11) yields the following expression for sensible heat flux (Castellví, 2004):

$$H_{SR} = \begin{cases} \rho_a c_p \left(\dfrac{g}{T} \right)^{1/5} k^{4/5} \left(\dfrac{z^*}{\pi} \right)^{3/5} z^{1/5} \left[-\gamma^3 \left(\dfrac{S^3_{(r_m)}}{r_m} \right) \right]^{3/5} \dfrac{1}{a^{3/5}} \left(\dfrac{1}{-\zeta\, \phi_h^3(\zeta)} \right)^{1/5}, & h \le z \le z^* \\ \rho_a c_p \left(\dfrac{g}{T} \right)^{1/5} \dfrac{\left(k(z-d) \right)^{4/5}}{\pi^{3/5}} \left[-\gamma^3 \left(\dfrac{S^3_{(r_m)}}{r_m} \right) \right]^{3/5} \dfrac{1}{a^{3/5}} \left(\dfrac{1}{-\zeta\, \phi_h^3(\zeta)} \right)^{1/5}. & z-d > z^* \end{cases} \tag{5.12}$$

For the free convection condition, for which $-3 \le \zeta \le 0.03$, the function $1/(\zeta\, \phi_h^3(\zeta))^{1/5}$ in Eq. (6.12) can be set as a constant value of 2.4 and hence rewritten as (Castellví, 2004; Castellví *et al.*, 2006a):

$$H_{SR} = \begin{cases} 2.4\, \rho_a c_p \left(\dfrac{g}{T_a} \right)^{1/5} k^{4/5} \left(\dfrac{z^*}{\pi} \right)^{3/5} z^{1/5} \left(-\gamma^3 \dfrac{S^3_{(r_m)}}{r_m} \right)^{3/5} \dfrac{1}{a^{3/5}}, & h \le z \le z^* \\ 2.4\, \rho_a c_p \left(\dfrac{g}{T_a} \right)^{1/5} \dfrac{\left(k(z-d) \right)^{4/5}}{\pi^{3/5}} \left(-\gamma^3 \dfrac{S^3_{(r_m)}}{r_m} \right)^{3/5} \dfrac{1}{a^{3/5}}. & z-d > z^* \end{cases} \tag{5.13}$$

5.2.2.4 Combined SR analysis model method with similarity theory that uses air temperature standard deviation

Castellví *et al*. (2006a), by combining SR analysis method and similarity theory, proposed an approach for estimating sensible heat flux above the canopy surface from the air temperature standard deviation σ_T as follows:

$$H_{SR} = \begin{cases} \rho_a c_p \left[\frac{(\gamma z^*)^3}{z} \frac{k\, g}{T_a} \sigma_T \left(-\frac{S^3_{(r_m)}}{r_m} \right) \right]^{1/3} \left(\alpha\, (k\beta)^2 \right)^{1/3} \left(\frac{1}{-\zeta^{1/3}\ \phi_h^{2/3}(\zeta)\ g_1^{1/3}(\zeta)} \right), & h \le z \le z^* \\ \rho_a c_p \left[\gamma^3 (z-d) \frac{k\, g\, z}{T_a} \sigma_T \left(-\frac{S^3_{(r_m)}}{r_m} \right) \right]^{1/3} \left(\alpha\, (k\beta)^2 \right)^{1/3} \left(\frac{1}{-\zeta^{1/3}\ \phi_h^{2/3}(\zeta)\ g_1^{1/3}(\zeta)} \right) & z-d > z^* \end{cases} \tag{5.14}$$

where $g_1(\zeta)$ is an empirical atmospheric stability similarity function based on a relationship proposed by Tillman (1972) and valid for the inertial sub-layer.

The free convection case forms of Eq. (5.14) holds under slightly unstable conditions for ζ< -0.14 and can be expressed as (Castellví *et al*., 2006a):

$$H_{SR} = \begin{cases} 1.65 \rho_a c_p \gamma \frac{k^{5/6} g^{1/3}}{\pi^{1/2}} z^{1/6} (z^*)^{1/2} \left(\frac{\sigma_T}{T_a} \left(-\frac{S^3_{(r_m)}}{r_m} \right) \right)^{1/3}, & h \le z \le z^* \\ 1.65 \rho_a c_p \gamma \frac{k^{5/6} g^{1/3}}{\pi^{1/2}} (z-d)^{2/3} \left(\frac{\sigma_T}{T_a} \left(-\frac{S^3_{(r_m)}}{r_m} \right) \right)^{1/3}. & z-d > z^* \end{cases} \tag{5.15}$$

For a variety of canopies, Castellví *et al*. (2006a) found that Eq. (5.14) and its free convection form, Eq. (5.15), performed very well for measurements above the canopy, in the roughness and/or the inertial sub-layers, using $\gamma = 1.1$.

5.2.2.5 Combined SR analysis model method with similarity theory that uses a second-order air temperature structure function

Applying MOST, Castellví *et al.* (2006a) proposed the following expression that permits sensible heat flux to be estimated for the inertial sub-layer from a third-order air temperature structure function:

$$H_{SR} = \rho_a c_p \left(\frac{\gamma^3 (z-d)^{4/3} k\, g\, z}{T} C_{TT}^{1/2} \left(-\frac{S^3_{(r_m)}}{r_m} \right) \right)^{1/3} \frac{1}{-\zeta^{1/3}\ \phi_h^{2/3}(\zeta)\ g_1^{1/3}(\zeta)} \quad z-d > z^* \tag{5.16}$$

where C_{TT} is the spatial second-order air temperature structure function and $g_2(\zeta)$ an empirical atmospheric stability similarity function based relationship valid for the inertial sub-layer and given by Wyngaard *et al*. (1971).

The free convection form of Eq. (5.16) holds for $\zeta \leq$ -0.1 and is expressed as (Castellví *et al*., 2006a):

$$H_{SR} = 1.65\rho_a c_p \gamma \frac{k^{5/6} g^{1/3} (z-d)}{\pi^{1/2}}^{7/9} \left(\frac{C_{TT}^{\ 1/2}}{T} \left(-\frac{S^3_{(r_m)}}{r_m} \right) \right)^{1/3}. \qquad z-d > z^* \qquad (5.17)$$

Castellví *et al*. (2006a), from their experimental data collected above different canopy types in the inertial sub-layer, found that Eq. (5.16) and its a free convection form, Eq. (5.17), performed excellently during unstable conditions.

5.3 Materials and methods

A field experiment was carried out over a 3-ha area of a commercial sugarcane canopy (variety N14), in the Baynesfield Estate, KwaZulu-Natal, South Africa (29.45^{o} S, 30.18^{o} E) with an altitude of 910 m above MSL. The Baynesfield climate is classified as sub-humid with a dry and cool winter and warm and rainy summer. The mean monthly air temperature ranges from a maximum of 21.1 ^{o}C in January to a minimum of 13.3 ^{o}C in June with a mean annual precipitation of 844 mm. Most precipitation falls as rain in the summer months. The soil is classified as the Hutton form with a clay content of 550 to 650 g kg^{-1} (Haynes *et al.*, 2003). The predominant wind direction is easterly. The upwind fetch available for the measurements was 97 m from the predominant wind direction. The experimental plot was bordered on the south east by a small water reservoir, and for the other directions by sugarcane differing in their heights and stages.

The sugarcane was planted in December 2007, with a row spacing of 1 m and planting spacing of 0.50 m. The crop was six months old with a height of 1.25 m above the soil surface at the beginning of the experiment.

The data collected for the period from 8 August to 10 September 2008 (day of year from 212 to 242, 2008) when the crop was sparse, and from 11 November 2008 to 20 January 2009 (day of year from 297, 2008 to 20, 2009) when the crop was dense, were used.

The crop height h and leaf area index (LAI) were measured every two weeks and monthly respectively. The average h was measured from three randomly selected plants. The LAI was measured when the sky was cloudy or during early morning or late afternoon using an LAI-2000 plant canopy analyzer (Li-Cor. Inc., Lincoln, Nebraska, USA), with a 45^{o} view cap and replicated three times. Then the data was downloaded to a computer using Li-Cor software.

The height of the roughness sub-layer (z^{*}) was estimated as (Garratt, 1980):

$$z^{*} = a\,D + d \qquad (5.18)$$

where a is a coefficient and D the inter row spacing (= 1 m). A recommended value of a = 3.1 was used (Cellier and Brunet, 1992). When the crop was dense, the roughness sub-layer depth was also estimated as z^{*} = 5h/3. The inertial sub-layer depth δ' was estimated through the upwind fetch x and roughness length parameters z_o as (Brutsaert, 1982):

$$\delta' = 0.1 x^{0.8} z_o^{\ 0.2}\,. \qquad (5.19)$$

Two micrometeorological masts were set up at about 15 and 50 m from west and south edges of the field, respectively. For purposes of surface flux comparisons, a three-dimensional ultra-sonic anemometer (model 81000, RM Young, Traverse City, Michigan, USA) which represents the EC system, was connected to the CR3000 datalogger (Campbell Scientific Inc., Logan, Utah, USA) and installed adjacent to the thermocouples to estimate $H = H_{EC}$ at a height of 2.15 m above the soil surface at the start of experiment and 2.75 m above the soil surface last of the experiment months. The sonic anemometer was pointed towards north. The scan rate for the EC measurements was 10 Hz. All EC data were processed online every 2 and 30 minutes in the datalogger and stored for further analysis, including the 10-Hz data. The sonic sensible heat flux H_{sonic} was calculated as: $H_{sonic} = \rho_a\, c_p\, \overline{w' T_s{}'}$ where w' and $T_s{}'$ are the fluctuations from the mean vertical wind speed w and sonic temperature T_s respectively. Sensible heat flux was calculated following coordinate rotations for the three wind velocity components, u, v and w, and correction to remove the effects of the instrument tilt and air-flow irregularities using the procedures similar to those of Kaimal and Finnigan (1994) and Oncley *et al*. (2007). Similar "constants" were used for calculating EC and SR sensible heat flux for each time period (Savage *et al*., 1997). The H_{EC} values were corrected for the effects of water vapour pressure and Bowen ratio, using the average values $\bar{e}$ and $\bar{\beta}$ respectively, using the relationship (Odhiambo and Savage, 2009):

$$H_{EC} = H_{sonic}\left(1+\frac{0.322\,\bar{e}}{\bar{P}}+\frac{10^{-3}\left(0.722\,\bar{P}-0.399\,\bar{e}\right)}{\bar{\beta}}\right)^{-1} \tag{5.20}$$

in which $\bar{e}$ (kPa) was obtained using air temperature and relative humidity measurements using two Vaisala instruments (Campbell HMP45C) connected to the CR1000 datalogger with one at each height of 0.50 and 1.5 m above the crop canopy. The atmospheric pressure $\bar{P}$ (kPa) was estimated following Savage *et al*. (1997) using altitude, average water vapour pressure $\bar{e}$ and an average of the measured air temperature from the fine-wire thermocouples and $\bar{\beta}$ estimated using:

$$\bar{\beta} = \frac{H_{sonic}}{R_n - G - H_{sonic}}. \tag{5.21}$$

The friction velocity u_* was calculated from the dimensional orthogonal wind speed components from the sonic anemometer as: $[(\overline{u'w'})^2 + (\overline{v'w'})^2]^{1/4}$ (Garratt, 1992) where u, v, and w are the three-dimensional orthogonal wind speeds, u', v', and w' are the fluctuations from the mean of u, v, and w respectively.

Additional horizontal wind speed $U_{three\text{-}cup}$ (m s^{-1}) measurements were made using a three-cup anemometer (RM Young, model 03001) at a height of 3.5 m above the soil surface and connected to a Campbell CR10X datalogger. The $U_{three\text{-}cup}$ measurements were scanned every 10 s and averaged every two minutes. The $U_{three\text{-}cup}$ measurements were adjusted to the sonic height z_{sonic} using the neutral wind profile law as:

$$U_{corrected} = U_{three-cup} \frac{\ln\left(\frac{z_{sonic} - d}{z_o}\right)}{\ln\left(\frac{z_{three-cup} - d}{z_o}\right)} \tag{5.22}$$

where $z_{three-cup}$ is the three-cup anemometer height (m) and $U_{correct}$ is the horizontal wind speed adjusted to the height z_{sonic}. Following Weber (1999), the friction velocity u_* was also estimated from the $U_{three-cup}$ and $U_{correct}$ respectively as:

$$u_* = 0.14U\ . \tag{5.23}$$

For the SR methods, four unshielded and naturally-ventilated 75-µm type-E fine-wire thermocouples, placed at heights of 0.20, 0.50, 0.75 and 1.50 m above the crop surface and connected to the CR3000 datalogger, were used to measure high frequency air temperature. At each height, a parallel combination of fine-wire thermocouples was used. The thermocouples were pointed toward the predominant wind direction which occurred during daytime hours. The measurement heights were adjusted when crop height increased. At each height, a parallel combination of fine-wire thermocouples were used. The thermocouples were pointed toward the predominant wind direction which occurred during daytime hours. At each site visit, the thermocouples was checked for damage, cleanliness, insects and cobwebs, and the measurement heights were adjusted according to the crop height increases. Air temperature time lags of 0.4 and 0.8 s were used to calculate the air temperature structure functions. The second-, third- and fifth-order air temperature structure functions which are required by the van Atta approach for SR analysis, were calculated after lagging the air temperature data by 0.4 and 0.8 s. The SR data were sampled at a frequency of 10 Hz and consequently averaged every two min and 30 min and stored for further analysis. The amplitude a and the total ramp period $l + s$ were determined from the air temperature structure functions using the two time lags and the van Atta (1977) analysis approach. The sign of the ramp amplitude was used to determine atmospheric stability (positive indicates unstable condition and negative indicates stable conditions). The two-min SR sensible heat flux H_{SR} was calculated using Eq. (5.2). For other SR approaches, the empirical combined coefficient $\alpha\beta^{2/3}\gamma$, and a correction coefficient γ were set to 0.4 and 1.0 respectively. The α' was calculated using Eq. (5.3).

Based on the Taylor hypothesis of frozen turbulence, the spatial second-order air temperature structure function C_{TT}, in Eqs (5.16) and (5.17), was estimated by converting the second-order air temperature structure function measurements for the time lags as (Castellví *et al.*, 2006a):

$$C_{TT} = \frac{S_{(r)}^{2}}{(U_{correct}\, r)^{2/3}} . \tag{5.24}$$

The empirical atmospheric stability similarity functions, $g_1(\zeta)$ and $g_2(\zeta)$ in Eq. (5.14) were respectively determined as (Wyngaard *et al.*, 1971):

$$g_1(\zeta) = \begin{cases} 0.95(0.05-\zeta)^{-1/3}, & \zeta < 0 \\ 2.5, & \zeta = 0 \\ -2, & \zeta > 0 \end{cases} \tag{5.25}$$

and

$$g_2(\zeta) = \begin{cases} 4.9(1-7\zeta)^{-2/3}, & \zeta < 0 \\ 4.9, & \zeta = 0 \\ 4.9(1+2.75\zeta). & \zeta > 0. \end{cases} \tag{5.26}$$

The sign of the third-order air temperature structure function was also used to identify unstable conditions. Finally, a set of SR sensible heat flux were calculated using the above-mentioned equations.

Additional measurements included the remaining energy balance components, R_n and soil heat flux, soil temperature and soil water content measured every one second, averaged every two min and stored in a Campbell CR1000 datalogger for further analysis. A NR LITE net radiometer (Kipp & Zonen, Delft, The Netherlands), to measure R_n, was mounted at a height of 1.5 m above the crop surface and adjusted according to the changes in crop height. Soil heat flux G_{plate} at the 0.08 m below the soil surface was measured using two soil heat flux plates buried horizontally. Spatially-averaged soil temperature was obtained using two pairs of type-E thermocouples in metal tubes buried in the soil at depths of 0.02 and 0.06 m above the soil heat flux plates. Soil water content was measured using a frequency domain reflectometer (ThetaProbe, model ML2x, Delta-T Devices, Cambridge, England) inserted vertically in the soil close to the area where soil heat flux plates and soil thermocouples were buried. The heat flux stored above the soil heat flux plates G_{stored} was calculated as:

$$G_{stored} = \left(\rho_{soil}\, c_{dsoil} + \rho_w\, \theta_v\, c_w\right) \frac{\Delta z\, \overline{\Delta T}_{soil}}{\Delta t} \tag{5.27}$$

where ρ_{soil} is the soil bulk density (kg m^{-3}), c_{dsoil} the dry soil specific heat capacity (840 J kg^{-1} ^{o}C^{-1}), ρ_w the density of water (1000 kg m^{-3}), θ_v the soil water content (m^3 m^{-3}), c_w the specific heat capacity of water (4200 J kg^{-1} ^{o}C^{-1}), Δz the soil depth (m), $\overline{\Delta T}_{soil}$ the average change in soil temperature above the soil heat flux plates (^{o}C), and Δt the time between temperature average measurements (s). The soil heat flux G was then calculated as:

$$G = G_{plate} + G_{stored}\,. \tag{5.28}$$

5.4 Results and discussion

5.4.1 Friction velocity

For many of the SR approaches, friction velocity u_* plays a key role in estimating sensible heat flux through the stability parameter. Instead of calculating u_* directly from observed fast-response wind measurements it may estimated from wind speed measurements using a three-cup anemometer. Half-hourly u_* estimates (Eq. (5.23)) from $U_{three\text{-}cup}$ and U_{corect} are plotted *vs* u_{*EC} measurements during daytime from 06h00 to 18h00 for day of year 212 to 242 (2008) and 297 (2008) to 20 (2009) and presented (Fig. 5.1). These comparisons were done to evaluate the three cup anemometer wind speed measurements used for estimating u_*. There was good agreement between $u_{*three\text{-}cup}$ estimates and u_{*EC} measurements with a slope of 1.16, coefficient of determination (r^2) of 0.67 and root mean square error (RMSE) value to 0.09 m s^{-1} as shown in Fig. 5.1a. When applying $U_{correct}$ to calculate u_*, the regression slope was slightly improved but u_* was overestimated compared to u_{*EC} (Fig. 5.1b). It is observed that there is more scatter in $U_{three\text{-}cup}$ around 0.20 m s^{-1} due to the

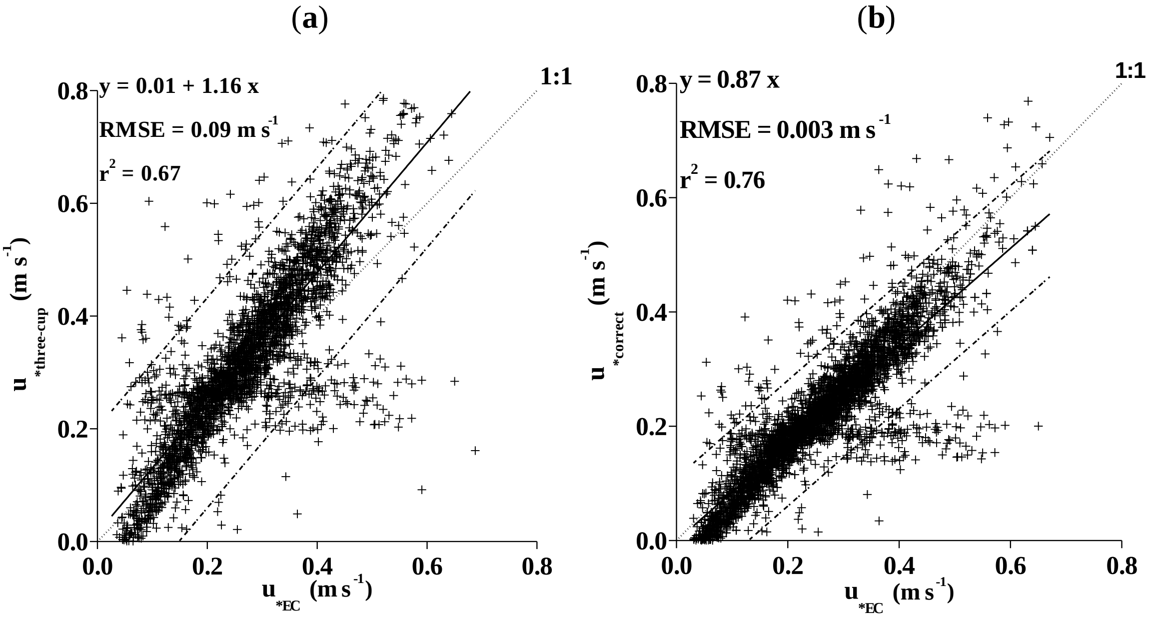

Fig. 5.1 Plot of half-hourly (a) uncorrected $u_{*three\text{-}cup}$ estimates against u_{*EC} measurements and (b) $u_{*correct}$ estimates against u_{*EC} measurements.

threshold of the 3-cup anemometer of approximately around 0.2 m s^{-1}. As an example, Fig. 5.2 shows a time series comparison between half-hourly wind speed measured by the three dimensional sonic (U_{sonic}) and three-cup anemometers. The use of Eq. (5.27) involving the use of three cup anemometer measurements for estimating friction velocity was reasonably accurate. Therefore, the three-cup anemometer measurements are used to estimate the friction velocity in all analyses of the SR methods.

5.4.2 Sensible heat flux under unstable conditions

In this section, the original and new proposed equations of the SR method and their convection limit forms for estimating sensible heat flux were evaluated for daytime unstable conditions at measurement heights of 0.20, 0.50, 0.75 and 1.50 m above the sugarcane canopy and using air temperature time lags of 0.4 and 0.8 s for the period when the sugarcane was sparse and dense for day of year from 297 (2008) to 20 (2009).

To estimate the sensible heat flux using the original SR method, the SR weighting factor α needs to be determined. The α value was determined by plotting half-hourly H_{EC} measurements (y-axis) *vs* H_{SR} estimates (Eq. (5.2)) (x-axis) for each height and the air temperature time lags (Table 5.1). The weighting factor α represents the slope of the linear

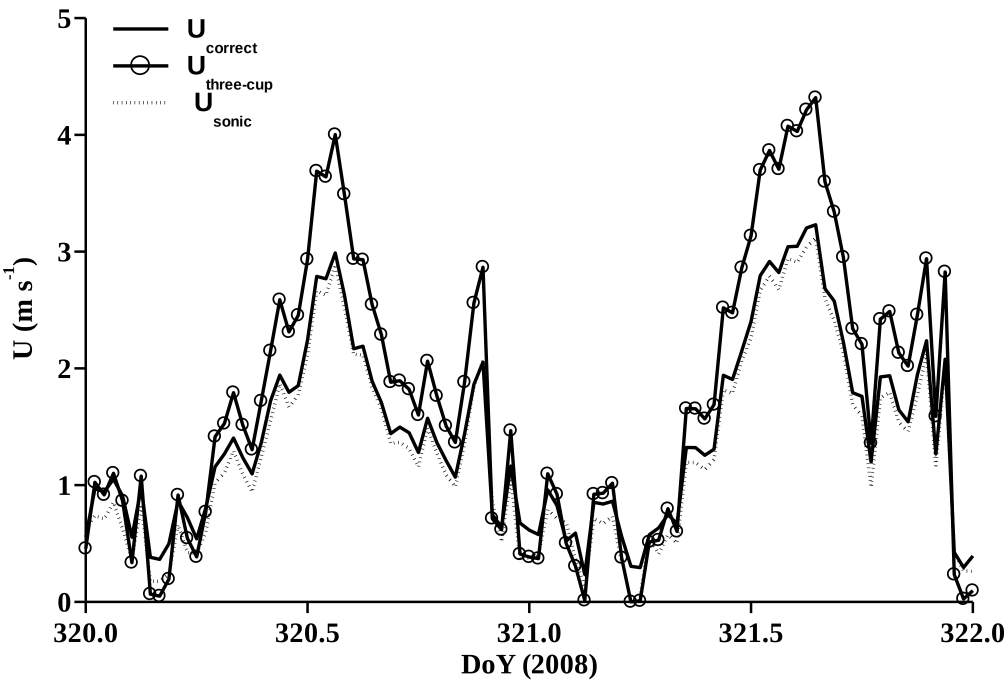

Fig. 5.2 Comparisons between half-hourly $U_{correct}$, $U_{three-cup}$ and U_{EC} for day of year 321 and 322 (2008).

regression forced through the origin. The α' was also determined using Eq. (5.6) (Table 5.1).

Above the sparse sugarcane canopy, the α' was generally greater than α for measurements within the roughness sub-layer, and lower for measurements in the inertial sub-layer (1.50 m above the crop surface) (Table 5.1). Also shown is that α' was greater than α for a dense crop canopy for measurements in the roughness and the inertial sub-layers. For both sparse and dense crop canopies conditions, α values increased for longer air temperature time lag and decreased with increased measurement height. The greatest α values were observed at a height of 0.20 m above the crop surface and for a time lag of 0.8 s. These results are generally consistent with previous studies for different surfaces (Snyder *et al*., 1996; Spano *et al*., 1997b; Zapata and Martínez-Cob, 2001; Mengistu, 2009)

In this study, an α value greater than that reported by Paw U *et al*. (1995) for their measurements above a 2.2-m tall maize canopy was found. It is noticeable that α values were greater above the dense canopy compared to the sparse canopy because the dens

Table 5.1 The α and α' estimates at heights of 0.20, 0.50, 0.75 and 1.50 m above the sugarcane canopy surface for time lags of 0.4 and 0.8 s for daytime unstable conditions for day of year 212 to 247 (2008) and from 297 (2008) to 20 (2009).

Year	DoY	h (m)	LAI (m^2 m^{-2})	r (s)	α (H_{SR} (x-axis) vs H_{EC} (y-axis)) $z-h$ (m)				α' (Eq. (5.6)) $z-h$ (m)			
Sparse canopy					0.20	0.50	0.75	1.50	0.20	0.50	0.75	1.50
2008	212 - 220	1.25	-	0.4	0.56	0.50	0.49	0.44	0.65	0.56	0.51	0.37
				0.8	0.64	0.57	0.54	0.48	0.73	0.62	0.58	0.41
2008	221 - 226	1.29	-	0.4	0.52	0.49	0.45	0.40	0.77	0.66	0.60	0.45
				0.8	0.60	0.58	0.53	0.47	0.84	0.75	0.66	0.48
2008	227 - 242	1.32	-	0.4	0.54	0.51	0.51	0.47	0.84	0.71	0.68	0.49
				0.8	0.63	0.59	0.6	0.55	0.92	0.79	0.74	0.51
Dense canopy												
2008	297 - 311	1.35	-	0.4	0.73	0.65	0.64	0.66	0.84	0.74	0.68	0.50
				0.8	0.81	0.73	0.71	0.72	0.93	0.79	0.73	0.53
2008	312 - 325	1.37	1.95	0.4	0.64	0.55	0.56	0.44	0.82	0.68	0.63	0.46
				0.8	0.70	0.62	0.61	0.49	0.91	0.74	0.67	0.45
2008	326 - 340	1.4	-	0.4	0.63	0.57	0.55	0.45	0.81	0.70	0.67	0.47
				0.8	0.70	0.61	0.59	0.49	0.89	0.74	0.68	0.49
2008	341 - 354	1.44	2.53	0.4	0.62	0.55	0.5	0.44	0.85	0.71	0.66	0.50
				0.8	0.64	0.57	0.52	0.46	0.9	0.76	0.68	0.50
2008/09	355 - 4	1.78	3.06	0.4	0.55	0.50	0.48	0.42	0.83	0.70	0.69	0.48
				0.8	0.56	0.51	0.5	0.44	0.87	0.74	0.74	0.55
2009	5 - 20	1.9	3.19	0.4	0.64	0.48	0.43	0.39	0.79	0.69	0.65	0.45
				0.8	0.54	0.47	0.46	0.41	0.80	0.7	0.66	0.46

crop surface was much more uniform. Half-hourly SR sensible heat flux H_{SR} estimates for each measurement height and the air temperature time lags were compared with H_{EC} for when sugarcane was sparse and when it was dense (Table 5.2). For both sparse and dense canopies conditions, H_{SR} overestimated and was in a poor agreement with H_{EC} with slope values that departed considerably from unity for all heights and the two air temperature time lags (Table 5.2). Slightly-improved results were observed above the dense canopy due to fact that the dense crop is more homogeneous compared to the sparse canopy. These results indicated that H_{SR} need to be calibrated against EC measurements.

Half-hourly H_{SR} estimates using α and α' were also plotted *vs* H_{EC} above these canopies (Table 5.2). Comparisons between H_{SR} using α and α' and H_{EC} were more improved with lower RMSE values compared to H_{SR} using $\alpha = 1$. The performance of SR using a time lag of 0.8 s was also superior using α and α' compared to a time lag of 0.4 s. This result is attributed to the fact that the time lag of 0.4 s is too short for ramp amplitude formation.

For the sparse sugarcane, the comparisons between H_{SR} using α and H_{EC} were reasonably good for all measurement heights and both air temperature time lags. The improved results of H_{SR} using α were observed at 0.50 m above the crop surface for an air temperature time lag of 0.8 s with a slope of 0.83, r^2 = 0.71 and RMSE = 32.62 W m^{-2} (Table 5.2). The agreement between H_{SR} using α' and H_{EC} was very good with a slope close to unity, r^2 values ranging between 0.72 and 0.75 and higher RMSE ranged between 35.05 and 38.33 W m^{-2} for measurements in the roughness sub-layer. The best estimate for H_{SR} using α' within this layer was observed at a height of 0.50 m above the crop surface for an air temperature time lag of 0.8 s with a slope of 0.99, r^2 = 0.74, and RMSE = 35.92 W m^{-2} (Table 5.2). For measurements at 1.50 m above the crop surface, H_{SR} using α' was underestimated with a slope that departed considerably from unity with a reduced RMSE between 30.50 and 29.19 W m^{-2} for air temperature time lags of 0.4 and 0.8 s respectively (Table 5.2).

For the dense sugarcane canopy, half-hourly H_{SR} using α provides very good estimates of H_{EC} with a slope close to 0.89, r^2 greater than 0.85 and small RMSE values at all measurement heights for both air temperature time lags (Table 5.2). The best results

Table 5.2 Linear regression of half-hourly H_{SR} estimates using α and α' at four measurement heights for air temperature time lags of 0.4 and 0.8 s *vs* H_{EC} above the sugarcane for daytime unstable conditions for day of year 212 to 247 (2008) and 297 (2008) to 20 (2009).

$z - h$ (m)	Time lag (s)	Slope	Intercept (W m^{-2})	r^2	RMSE (W m^{-2})	n	Slope	Intercept (W m^{-2})	r^2	RMSE (W m^{-2})	n	Slope	Intercept (W m^{-2})	r^2	RMSE (W m^{-2})	n
Sparse canopy		H_{SR} using α (= 1) *vs* H_{EC}					H_{SR} using α *vs* H_{EC}					H_{SR} using α' *vs* H_{EC}				
0.20	0.4	1.51	27.56	0.69	60.63	410	0.81	15.36	0.69	32.36	410	1.04	14.23	0.73	38.33	407
	0.8	1.31	24.42	0.72	49.21	414	0.82	15.57	0.72	30.82	414	1.04	14.57	0.75	36.86	412
0.50	0.4	1.64	24.86	0.69	66.65	411	0.82	12.70	0.69	33.37	411	1.00	12.38	0.73	36.87	408
	0.8	1.43	23.20	0.71	56.43	417	0.83	13.49	0.71	32.62	417	0.99	10.82	0.74	35.92	415
0.75	0.4	1.64	28.31	0.63	75.87	408	0.79	14.73	0.63	36.16	408	0.93	11.15	0.72	35.05	406
	0.8	1.51	22.48	0.70	59.80	416	0.83	13.04	0.70	32.41	416	0.98	10.46	0.74	35.32	415
1.50	0.4	1.71	40.80	0.59	86.01	396	0.74	18.99	0.60	36.87	396	0.73	13.55	0.67	30.50	394
	0.8	1.56	34.93	0.66	68.25	403	0.78	18.25	0.67	33.39	403	0.72	11.70	0.71	29.19	401
Dense canopy																
0.20	0.4	1.28	22.14	0.89	29.34	1758	0.89	10.23	0.93	16.63	1734	1.07	10.81	0.92	21.06	1740
	0.8	1.20	21.20	0.87	30.46	1822	0.89	9.46	0.93	16.52	1797	1.11	9.67	0.90	23.82	1804
0.50	0.4	1.45	23.99	0.89	34.46	1795	0.88	9.70	0.92	17.43	1739	1.02	10.61	0.92	20.02	1777
	0.8	1.35	23.81	0.87	34.11	1827	0.89	9.22	0.93	16.32	1770	1.04	10.25	0.91	22.38	1807
0.75	0.4	1.46	28.67	0.85	40.37	1816	0.87	10.45	0.89	19.81	1736	0.90	12.62	0.89	20.62	1794
	0.8	1.38	26.76	0.85	37.99	1854	0.88	9.83	0.92	17.36	1772	0.94	11.13	0.89	22.05	1835
1.50	0.4	1.55	36.71	0.76	58.89	1506	0.83	11.16	0.85	24.22	1483	0.72	9.07	0.90	16.63	1493
	0.8	1.49	32.94	0.80	50.60	1563	0.87	10.71	0.90	20.02	1535	0.75	7.76	0.92	15.51	1548

was observed at the lowest measurement height for an air temperature time lag of 0.8 s with a slope of 0.89, r^2 = 0.93 and RMSE =16.52 W m^{-2} (Table 5.2). The comparisons between H_{SR} using α and H_{EC} above the dense canopy was improved compared to that above the sparse canopy. The agreement between H_{SR} using α' and H_{EC} was very good in the roughness sub-layer with improved results observed at a height of 0.50 m above the crop surface for a time lag of 0.4 s with a slope 1.02, r^2 = 0.92 and RMSE of 20.02 W m^{-2} as shown in Table 5.2. In the inertial sub-layer, H_{SR} using α' underestimated H_{EC} by less than 28 % and 25 % for air temperature time lags of 0.4 and 0.8 s respectively. The comparisons between H_{SR} using α' and H_{EC} above the sparse canopy was slightly improved compared to that above the dense canopy.

Overall, the performance of the original SR method (Eq. (5.2)) using α or α' was improved in the roughness sub-layer compared to the inertial sub-layer either the crop was sparse or dense. H_{SR} using α was more comparable to H_{EC} than that obtained using α' for both the roughness and the inertial sub-layers.

The performance of the SR methods (Eqs (5.9), (5.10), (5.11), (5.12), (5.14), and (5.16)) were evaluated *vs* EC measurements above the sparse sugarcane canopy (Table 5.3). The statistical regression parameters for the comparison of H_{SR} using α *vs* H_{EC} are repeated in Table 5.2 and Tables (5.3), (5.4), (5.5) and (5.6) for convenience. The agreement between $H_{SR\ (Eq.\ (5.9))}$ and H_{EC} was improved at all measurement heights using an air temperature time lag of 0.4 s compared to 0.8 s (Table 5.3). The slope, r^2 and RMSE values increased with increase measurement height within the roughness sub-layer. The best performance for Eq. (5.9) was observed at a height 0.75 m above the crop surface for an air temperature time lag of 0.8 s with a slope of 0.96, r^2 = 0.71 and RMSE = 37.99 W m^{-2} (Table 5.3). Generally Eq. (5.9) produced the best results compared to H_{EC} using a time lag of 0.4 s but underestimated H_{EC} especially at the lowest height. The performance of Eq. (5.10) was very good with slope close to unity and lower r^2 values at measurement heights within the roughness sub-layer and reasonably well for measurements within theinertial sub-layer for both air temperature time lags (Table 5.3). At the highest height (1.50 m above the crop canopy surface), the performance of Eq. (5.10) was slightly inferior compared to Eq. (5.2) using α and Eq. (5.9). Improved performance for Eq. (5.10) was noticed at a height of 0.50 m above the crop surface for a time lag of 0.8 s with a slope of

Table 5.3 Linear regression of half-hourly H_{SR} estimates for all measurement heights above the sparse sugarcane canopy surface and both air temperature time lags *vs* H_{EC} for daytime unstable conditions for day of year 212 to 247 (2008).

$z - h$ (m)	Time lag (s)	Slope	Intercept (W m^{-2})	r^2	RMSE (W m^{-2})	n	Slope	Intercept (W m^{-2})	r^2	RMSE (W m^{-2})	n	Slope	Intercept (W m^{-2})	r^2	RMSE (W m^{-2})	n
		H_{SR} using α *vs* H_{EC}					$H_{SR\ (\mathrm{Eq.\ (5.9)})}$ *vs* H_{EC}					$H_{SR\ (\mathrm{Eq.\ (5.10)})}$ *vs* H_{EC}				
0.20	0.4	0.81	15.36	0.69	32.36	410	0.76	2.48	0.72	29.55	391	0.97	10.99	0.70	38.09	356
	0.8	0.82	15.57	0.72	30.82	414	0.74	2.56	0.74	27.03	392	1.08	10.31	0.72	40.35	361
0.50	0.4	0.82	12.70	0.69	33.37	411	0.88	2.15	0.72	33.97	388	0.93	13.39	0.70	37.07	357
	0.8	0.83	13.49	0.71	32.62	417	0.86	2.65	0.74	31.14	387	1.01	12.45	0.71	39.12	365
0.75	0.4	0.79	14.73	0.63	36.16	408	0.97	1.25	0.68	40.95	390	0.89	10.92	0.69	36.08	355
	0.8	0.83	13.04	0.70	32.41	416	0.96	1.88	0.71	37.99	389	0.97	11.13	0.69	39.20	364
1.50	0.4	0.74	18.99	0.60	36.87	396	0.88	2.77	0.68	37.78	390	0.69	9.24	0.84	18.12	343
	0.8	0.78	18.25	0.67	33.39	403	0.88	2.76	0.71	35.13	390	0.78	7.78	0.84	20.49	350
		$H_{SR\ (\mathrm{Eq.\ (5.11)})}$ *vs* H_{EC}					$H_{SR\ (\mathrm{Eq.\ (5.12)})}$ *vs* H_{EC}					$H_{SR\ (\mathrm{Eq.\ (5.14)})}$ *vs* H_{EC}				
0.20	0.4	1.09	12.54	0.80	33.14	418	1.11	14.39	0.84	29.64	371	1.54	7.53	0.90	32.17	398
	0.8	1.09	10.46	0.83	29.94	422	1.11	14.39	0.84	29.64	371	1.57	7.26	0.91	30.98	397
0.50	0.4	1.04	10.51	0.80	31.99	416	1.11	11.24	0.85	28.54	369	1.39	4.44	0.88	30.75	395
	0.8	1.04	8.52	0.82	29.87	423	1.10	9.62	0.87	26.07	377	1.40	4.17	0.90	28.74	397
0.75	0.4	0.93	10.21	0.76	31.82	415	1.01	12.29	0.83	28.38	347	1.17	4.05	0.86	28.42	396
	0.8	0.96	7.86	0.81	28.73	424	1.03	9.61	0.87	24.69	356	1.21	4.03	0.89	25.97	395
1.50	0.4	0.76	13.06	0.73	28.20	403	0.77	15.75	0.77	26.16	337	0.91	3.90	0.84	24.35	403
	0.8	0.78	10.86	0.78	25.59	410	0.80	12.66	0.83	22.37	350	0.95	3.59	0.86	23.30	404
		$H_{SR\ (\mathrm{Eq.\ (5.16)})}$ *vs* H_{EC}														
1.50	0.4	0.88	11.66	0.81	26.71	376										
	0.8	0.95	10.31	0.84	25.60	378										

1.01, r^2 = 0.71, and RMSE = 39.12 W m^{-2} (Table 5.3). The r^2 and RMSE values, for *H* obtained using Eq. (5.10) *vs* H_{EC}, were slightly improved in the inertial sub-layer compared to that obtained in the roughness sub-layer (Table 5.3). Half-hourly H_{SR} (Eq. (5.11)) was in very good agreement with H_{EC} for all heights in the roughness sub-layer and both air temperature time lags. For measurements at 1.50 m above the crop surface, Eq. (5.11) yielded inferior results compared to the roughness sub-layer. H_{SR} (Eq. (5.11)) overestimated H_{EC} at the first two measurement heights and underestimated H_{EC} at 0.75 and 1.50 m above the crop surface (Table 5.3). an improved performance for Eq. (5.11) was observed at a height of 0.75 m above the crop surface for a time lag of 0.8 s with a slope of 0.96, r^2 = 0.81, and RMSE = 28.73 W m^{-2} (Table 5.3). The performance of Eq. (5.12) was very good for both air temperature time lags and measurement within the roughness sub-layer. The improved H_{SR} (Eq. (5.12)) estimates observed at a height of 0.75 m above the crop surface for 0.8-s air temperature time lag with a slope of 1.03, r^2 = 9.61 and RMSE = 24.69 W m^{-2} (Table 5.3). In the inertial sub-layer, Eq. (5.12) provided reasonable estimates of H_{SR} using a time lag of 0.8 s with slope of 0.80, r^2 = 0.83, and RMSE of 22.37 W m^{-2} (Table 5.3). The performance of Eq. (5.14) for estimating SR sensible heat flux was poor for the roughness sub-layer and very good in the inertial sub-layer compared to the above-mentioned equations mainly because Eq. (5.14) is dependant on similarity theory which is only valid within the inertial sub-layer (Bruseart, 1982; Kaimal and Finnigan, 1994). The best H_{SR} (Eq. (5.14)) estimates within the roughness sub-layer were observed at a height of 0.75 m above the crop canopy for 0.4-s air temperature time lag with a slope of 1.17, r^2 = 0.86, and RMSE of 28.42 W m^{-2} (Table 5.3). This result may be due to fact that the measurement height of 0.75 m above the canopy surface was within the transition zone. Eq. (5.16) was only applied within the inertial sub-layer (Castellví *et al.*, 2006a). Eq. (5.16) provided very good estimates of H_{SR} at a height of 1.5 m above the crop canopy for both time lags. Improved H_{SR} (Eq. (5.16)) estimates were observed for the 0.8-s air temperature time lag with a slope of 0.95, r^2 = 0.84, and RMSE of 25.60 W m^{-2} (Table 5.3).

Overall, Eqs (5.9), (5.10), (5.11) and (5.12) performed better in the roughness sub-layer compared to the inertial sub-layer as these equations are less similarity dependant. The use of Eq. (5.10) resulted in improved estimates compared to the other equations for the roughness sub-layer. On the other hand, Eqs (5.14) and (5.16) provided best estimates of H_{SR} within the inertial sub-layer since these equations are based on the similarity theory which is applicable in this sub-layer.

The performance of the SR methods (Eqs (5.9), (5.10), (5.11), (5.12), (5.14), and (5.16)) for estimating H_{SR} were also evaluated by comparison against H_{EC} over the dense sugarcane canopy for all measurement heights and the two time lags (Table 5.4). Compared to H_{EC}, the H_{SR} estimates using Eq. (5.9) were reduced for all heights and both air temperature time lags (Table 5.4). Poor performance of Eq. (5.9) was noticed at a lower height (0.20 m above the crop surface) and the best performance was observed at a height of 0.75 m above the crop canopy for a time lag of 0.8 s within the roughness sub-layer with a slope of 0.81, r^2 = 0.84, and RMSE value of 21.46 Wm^{-2}. In general, $H_{SR\ (\mathrm{Eq.\ (5.9)})}$ yielded the best estimate of H_{EC} using a time lag of 0.8 s compared to 0.4 s either in the roughness or the inertial sub-layers. The r^2 and RMSE for Eq. (5.9) were reduced and greater respectively compared to that for Eq. (5.2). Eq. (5.10) yielded more accurate estimates of H_{SR} in the roughness sub-layer for both air temperature time lags with a slope close to unity and r^2 greater than 0.82 but with greater RMSE value compared to that using Eqs (5.2) and (5.9). The superior performance of Eq. (5.10) was observed at 0.50 m above the crop canopy for a 0.8-s air temperature time lag with a slope equal to unity, r^2 = 0.86, and RMSE value of 25.23 W m^{-2} (Table 5.4). For measurements in the inertial sub-layer (1.5 m above the crop canopy), Eq. (5.10) underestimated H_{EC} by 25 % and 16 % for time lags of 0.4 and 0.8 s respectively. For measurements within the roughness sub-layer, Eq. (5.11) gave very good H_{SR} estimates with a slope close to one, r^2 greater than 0.89 and RMSE less than 22.65 W m^{-2} for both air temperature time lags. It is observed that $H_{SR\ (\mathrm{Eq.\ (5.11)})}$ overestimated H_{EC} at the 0.20- and 0.50-m heights above the crop canopy and underestimated at a height of 0.75 m above the crop canopy. In the inertial sub-layer, Eq. (5.11) performed more poorly compared to that of Eqs (5.2), (5.9) and (5.10) and underestimated H_{EC}. The best performance of Eq. (5.11) was noticed at a height of 0.75 m above the crop canopy for a time lag of 0.8 s with a slope of 0.97, r^2 = 0.89, and RMSE of 21.26 W m^{-2} (Table 5.4). The performance of Eq. (5.12) corresponded well for all heights in the roughness sub-layer and both air temperature time lags. $H_{SR\ (\mathrm{Eq.\ (5.12)})}$ overestimated H_{EC} in the roughness sub-layer, and underestimated H_{EC} within the inertial sub-layer. Good results of $H_{SR\ (\mathrm{Eq.\ (5.12)})}$ estimates were noticed at a height of 0.75 above the crop surface for a time lag of 0.8 s with a slope of 1.10, r^2 = 0.89, and RMSE of 24.86 W m^{-2}. The agreement between $H_{SR\ (\mathrm{Eq.\ (5.14)})}$ and H_{EC} was poor for all measurement heights within the roughness sub-layer and both air temperature time lags (Table 5.4). The $H_{SR\ (\mathrm{Eq.\ (5.14)})}$ estimates are overestimated compared to H_{EC} in the roughness sub-layer. The superior results for Eq. (5.14) were observed within the inertial sub-layer for a 0.4-s air temperature

Table 5.4 Linear regression of half-hourly H_{SR} estimates for four measurement heights above the dense sugarcane canopy surface and both time lags *vs* H_{EC} for daytime unstable conditions for day of year 297 (2008) to 20 (2009).

$z - h$ (m)	Time lag (s)	Slope	Intercept (W m^{-2})	r^2	RMSE (W m^{-2})	n	Slope	Intercept (W m^{-2})	r^2	RMSE (W m^{-2})	n	Slope	Intercept (W m^{-2})	r^2	RMSE (W m^{-2})	n
		H_{SR} using α *vs* H_{EC}					$H_{SR\,\text{(Eq. (5.9))}}$ *vs* H_{EC}					$H_{SR\,\text{(Eq. (5.10))}}$ *vs* H_{EC}				
0.20	0.4	0.89	10.23	0.93	16.63	1734	0.68	1.97	0.85	17.91	1835	0.93	9.61	0.84	25.10	1683
	0.8	0.89	9.46	0.93	16.52	1797	0.70	1.83	0.87	16.58	1829	1.06	7.42	0.86	25.92	1751
0.50	0.4	0.88	9.70	0.92	17.43	1739	0.76	2.70	0.84	20.85	1819	0.90	9.49	0.85	23.78	1724
	0.8	0.89	9.22	0.93	16.32	1770	0.78	2.55	0.86	19.26	1816	1.00	8.01	0.86	25.23	1753
0.75	0.4	0.87	10.45	0.89	19.81	1736	0.78	3.78	0.81	22.92	1897	0.81	11.71	0.82	23.87	1734
	0.8	0.88	9.83	0.92	17.36	1772	0.81	3.11	0.84	21.46	1895	0.92	9.46	0.84	25.03	1780
1.50	0.4	0.83	11.16	0.85	24.22	1483	0.76	3.58	0.78	25.74	1597	0.75	8.41	0.88	17.44	1450
	0.8	0.87	10.71	0.90	20.02	1535	0.79	3.20	0.82	23.47	1593	0.84	6.57	0.90	17.94	1505
		$H_{SR\,\text{(Eq. (5.11))}}$ *vs* H_{EC}					$H_{SR\,\text{(Eq. (5.12))}}$ *vs* H_{EC}					$H_{SR\,\text{(Eq. (5.14))}}$ *vs* H_{EC}				
0.20	0.4	1.10	10.92	0.92	20.93	1734	1.20	17.04	0.93	22.06	1628	1.82	15.55	0.90	33.13	1639
	0.8	1.14	9.65	0.91	22.64	1798	1.25	15.30	0.91	24.96	1693	1.90	15.50	0.89	37.23	1631
0.50	0.4	1.05	10.37	0.92	19.96	1775	1.18	17.03	0.92	22.04	1642	1.61	15.84	0.89	31.30	1621
	0.8	1.07	9.68	0.91	21.24	1806	1.21	16.21	0.91	24.32	1665	1.68	15.63	0.88	34.35	1620
0.75	0.4	0.93	12.35	0.89	20.41	1789	1.05	20.21	0.89	23.58	1592	1.38	16.80	0.84	32.57	1704
	0.8	0.97	10.72	0.89	21.26	1834	1.10	17.83	0.89	24.86	1652	1.45	15.24	0.85	33.36	1699
1.50	0.4	0.75	9.55	0.88	17.85	1490	0.82	13.97	0.91	16.57	1275	0.93	9.33	0.89	19.01	1413
	0.8	0.78	7.96	0.91	16.39	1544	0.84	11.95	0.93	15.63	1342	0.92	10.00	0.83	23.35	1413
		$H_{SR\,\text{(Eq. (5.16))}}$ *vs* H_{EC}														
1.50	0.4	1.11	2.60	0.91	20.10	296										
	0.8	1.20	0.19	0.91	21.66	246										

time lag with a slope of 0.93, r^2 = 0.89, and RMSE = 19.01 W m^{-2} because this equation is more dependent on similarity theory. Eq. (5.16) provided good estimates of H_{SR} in the inertial sub-layer for both air temperature time lags. The superior results of $H_{SR\ (Eq.\ (5.16))}$ were obtained using a time lag of 0.4 s with a slope of 1.11, r^2 = 0.91, and RMSE of 20.10 W m^{-2} (Table 5.4). The $H_{SR\ (Eq.\ (5.13))}$ overestimated H_{EC} by 11 % and 20 % for time lags of 0.4 and 0.8 s respectively.

Diurnal variation of the half-hourly H_{SR} estimates using the original and the other SR approaches at heights of 0.20, 0.50, 0.75 and 1.50 m above the sugarcane canopy for a 0.8-s air temperature time lag, H_{EC}, and R_n for daytime unstable conditions for a clear day (day of year 222 (2008)) are presented in Fig. 5.3. The H_{SR} estimated fluctuated more compared to EC measurements.

Overall, the performance of most SR equations were superior in the roughness sub-layer compared to the inertial sub-layer with improved results observed above the dense sugarcane canopy because the dense canopy was more homogeneous compared to the sparse canopy. The best performance was observed for Eqs (5.10) and (5.11) with Eqs (5.14) and (5.16) performing poorly compared to the other equations.

5.4.3 Sensible heat flux under free convection conditions

The SR free convection limits (Eqs (5.13), (5.15) and (5.17)) hold under slightly unstable conditions. Eq. (5.13) could be applied for the stability interval -3 < ζ < 0.03 with relative errors less than 8.5 % (Castellví *et al.*, 2005). Eqs (5.15) and (5.17) hold for ζ approaches 0.01 (Castellví *et al.*, 2006a). Simple linear regression analysis of SR free convection forms estimates of $H_{SR\ (Eqs\ (5.13))}$, $H_{SR\ (Eq.\ (5.15))}$ and $H_{SR\ (Eq.\ (5.17))}$ *vs* H_{EC} were made to evaluate the performance of these equations over the sparse and dense sugarcane canopies and are presented in Tables 5.5 and 5.6 respectively. The number of observation samples corresponding to the free convection limit interval above the sparse and dense sugarcane were about 70 % and 55 % of the total number of observation samples of daytime unstable conditions respectively. These results indicate that the atmospheric conditions were mostly free convective (Tables 5.5 and 5.6). For measurements above the sparse sugarcane and within the roughness sub-layer, Eq. (5.13) yielded good estimates of H_{SR} compared to H_{EC} with a slope and r^2 close to unity and relative errors less than 18 % for both air temperature

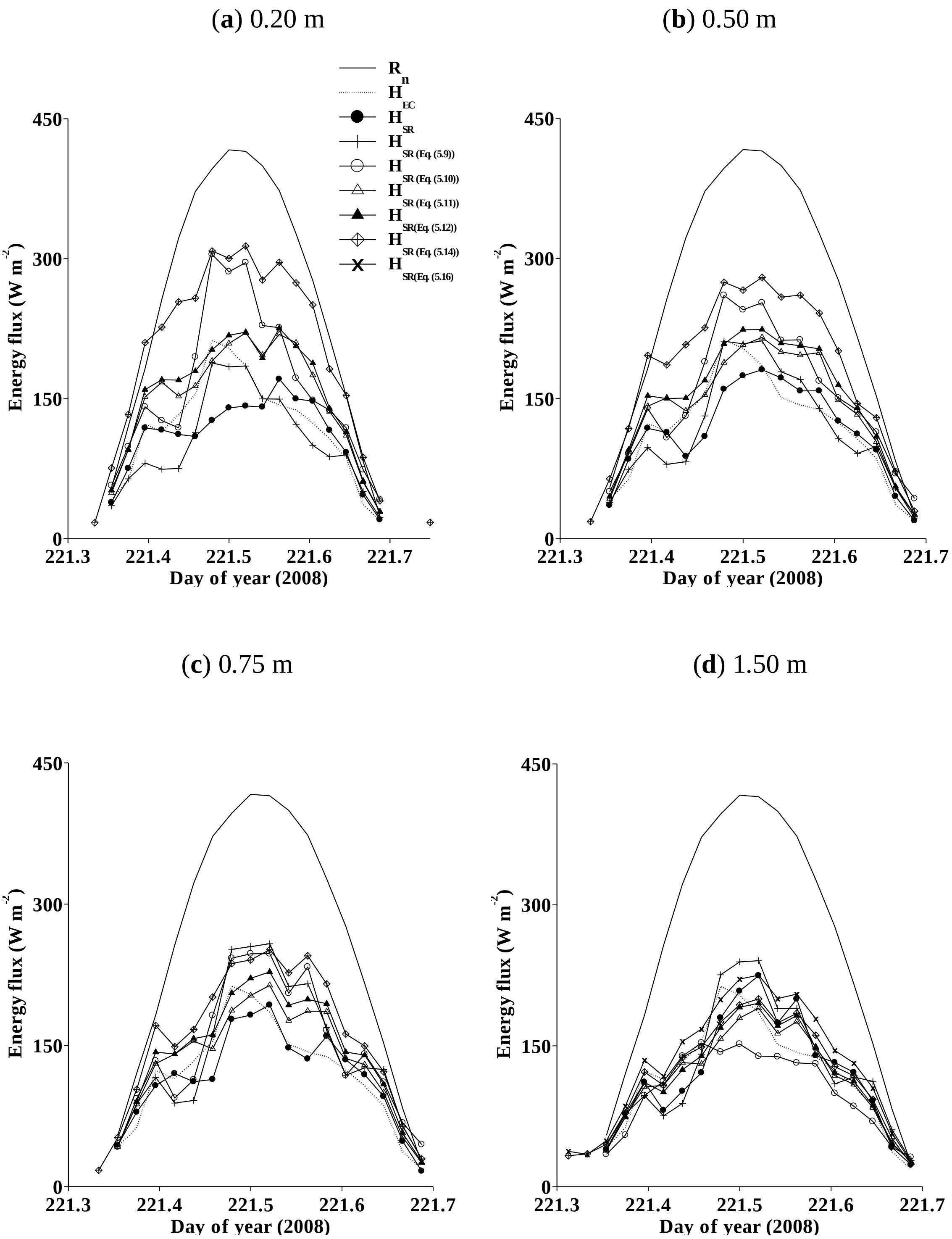

Fig. 5.3 Diurnal variation in half-hourly H_{SR} estimates at 0.20, 0.50, 0.75 and 1.50 m above the sparse sugarcane canopy and using a 0.8-s air temperature time lag, H_{EC} above the sparse sugarcane canopy, and R_n for unstable conditions for day of year 222 (2008)

Table 5.5 Linear regression of half-hourly free convection H_{SR} estimates for four measurement heights above the sparse sugarcane canopy surface and both air temperature time lags *vs* H_{EC} for daytime unstable conditions for day of year 212 to 247 (2008)

z - *h* (m)	Time lag (s)	Slope	Intercept (W m^{-2})	r^2	RMSE (W m^{-2})	*n*	Slope	Intercept (W m^{-2})	r^2	RMSE (W m^{-2})	*n*	Slope	Intercept (W m^{-2})	r^2	RMSE (W m^{-2})	*n*
		H_{SR} (Eq. (5.13)) *vs* H_{EC}					H_{SR} (Eq. (5.15)) *vs* H_{EC}					H_{SR} (Eq. (5.17)) *vs* H_{EC}				
0.20	0.4	1.09	16.07	0.83	29.29	295	0.77	6.50	0.80	22.78	213					
	0.8	1.09	17.62	0.85	27.68	292	0.81	9.31	0.80	24.46	212					
0.500	0.4	1.09	11.58	0.84	28.21	293	0.58	10.63	0.46	37.53	214					
	0.8	1.09	12.36	0.85	27.60	294	0.78	6.16	0.75	26.60	214					
0.75	0.4	0.98	11.91	0.82	27.28	267	0.67	2.79	0.78	21.32	213					
	0.8	1.00	12.42	0.84	26.30	279	0.69	7.28	0.74	24.95	212					
1.50	0.4	0.74	16.44	0.75	25.36	261	0.55	1.46	0.76	18.52	212	0.43	6.01	0.70	16.68	199
	0.8	0.75	15.95	0.79	21.83	249	0.59	2.67	0.76	20.08	213	0.46	7.61	0.69	18.37	199

Table 5.6 Linear regression of half-hourly free convection H_{SR} estimates for four measurement heights above the dense sugarcane canopy surface and both time lags *vs* H_{EC} for daytime unstable conditions for day of year 297 (2008) to 20 (2009).

$z - h$ (m)	Time lag (s)	Slope	Intercept (W m^{-2})	r^2	RMSE (W m^{-2})	n	Slope	Intercept (W m^{-2})	r^2	RMSE (W m^{-2})	n	Slope	Intercept (W m^{-2})	r^2	RMSE (W m^{-2})	n
		$H_{SR\,(\text{Eq. (5.13)})}$ *vs* H_{EC}					$H_{SR\,(\text{Eq. (5.15)})}$ *vs* H_{EC}					$H_{SR\,(\text{Eq. (5.17)})}$ *vs* H_{EC}				
0.20	0.4	1.21	18.89	0.91	25.70	1300	1.01	7.28	0.87	27.30	667					
	0.8	1.26	19.05	0.89	28.39	1334	1.11	9.13	0.87	31.23	523					
0.500	0.4	1.18	18.37	0.90	26.28	1296	0.98	9.05	0.85	31.43	417					
	0.8	1.22	19.14	0.89	28.45	1322	0.98	14.25	0.72	45.62	351					
0.75	0.4	1.05	22.05	0.87	26.87	1274	0.92	7.32	0.83	29.13	335					
	0.8	1.14	21.09	0.87	27.71	1230	0.98	8.46	0.80	33.58	300					
1.50	0.4	0.82	15.07	0.89	18.64	918	0.68	1.79	0.90	16.71	117	0.61	2.00	16.48	0.88	53
	0.8	0.86	13.60	0.91	25.70	963	0.74	2.84	0.91	27.30	87	0.64	1.22	15.50	0.92	40

time lags (Table 5.5). Improved performance of Eq. (5.13) was noticed at 0.75 m above the crop surface for a 0.8-s air temperature time lag with a slope of 1.00, r^2 = 0.84, and RMSE value of 26.30 W m^{-2} (Table 5.5). In the inertial sub-layer, Eq. (5.13) corresponded well with H_{EC} for both time lags with a slope of 0.75 and RMSE was small compared to the measurements within the roughness sub-layer. Generally Eq. (5.13) yielded superior H_{SR} estimates compared to Eq. (5.2) and slightly better compared to Eq. (5.12) because Eq. (5.13) requires air temperature measurements as the only input and is independent of atmospheric stability (Table 5.3 and 5.5). Table 5.5 showed that Eq. (5.15) exhibited good performance within the roughness sub-layer and poor performance within the inertial sub-layer with a RMSE value less than about 38 W m^{-2}. Eq. (5.15) poorly estimated H_{SR} compared to Eqs (5.2) and (5.14). Eq. (5.17) performed poorly with a slope that departed considerably from unity, a RMSE less than 18.5 W m^{-2}, and underestimated H_{SR} by about 50 % (Table 5.5). These results indicated that Eq. (5.13) was superior compared to the free convection limits for the other equations and can be used to estimate H_{SR} over the sparse crop canopy with a random error less than 17 %.

Above the dense canopy, Eq. (5.13) had a similar performance compared to Eq. (5.12) in the roughness sub-layer. The best estimates of $H_{SR \text{ (Eq. (5.13))}}$ was noticed at a height of 0.75 m above the crop canopy for a time lag of 0.4 s with a slope of 1.05 and a random error of 13 % (Table 6). Mengistu (2008), in his experiment over a *Chromolaena* canopy, reported that this equation can be used to estimate H_{SR} with a random error less 7 %. As shown in Table 5.6, for measurements within the roughness sub-layer, Eq. (5.15) performed better compared to Eqs (5.2) and (5.14) for both time lags with a slope closer to unity and r^2 greater than 0.80 and RMSE less than 45.63 W m^{-2}. The superior results for Eq. (5.15) in the roughness sub-layer was observed at a height of 0.75 m above the crop canopy for the 0.8-s air temperature time lag with a slope of 0.98, r^2 = 0.80 and RMSE of 33.58 W m^{-2}. In the inertial sub-layer, $H_{SR \text{ (Eq. (5.15))}}$ produced good estimates of H_{EC} with a random error of 10 %. In Table 5.6, for measurements in the inertial sub-layer, the performance of Eq. (5.17) in estimating sensible heat flux was poor compared to that of Eqs (5.2) and (5.16) for both air temperature time lags.

Overall, for measurements over the dense sugarcane canopy, all free convection limits forms compared well with those for the sparse canopy. Improved performance was observed using Eq. (5.15) compared to the other forms of the free convection equations.

5.4.4 Latent energy flux

Since independent measurements of latent energy flux were not available in this study, the latent energy flux was estimated as a residual from the shortened energy balance equation.

Comparisons of the half-hourly SR latent energy flux (LE_{SR}) estimates obtained using H_{SR} (estimated using the original and the other SR approaches) for all measurement heights for a 0.8-s air temperature time lag, and LE_{EC} along with net irradiance above the sugarcane canopy for selected day of year 351 (2008) are presented in Fig 5.4. All SR approaches, except that using a finite micro-front ramp SR model, underestimated LE_{SR} in the roughness sub-layer. The original SR and that using a finite micro-front ramp SR model corresponded well with EC latent energy flux in the roughness sub-layer compared to the other approaches (Fig. 5.4).

(**a**) 0.20 m

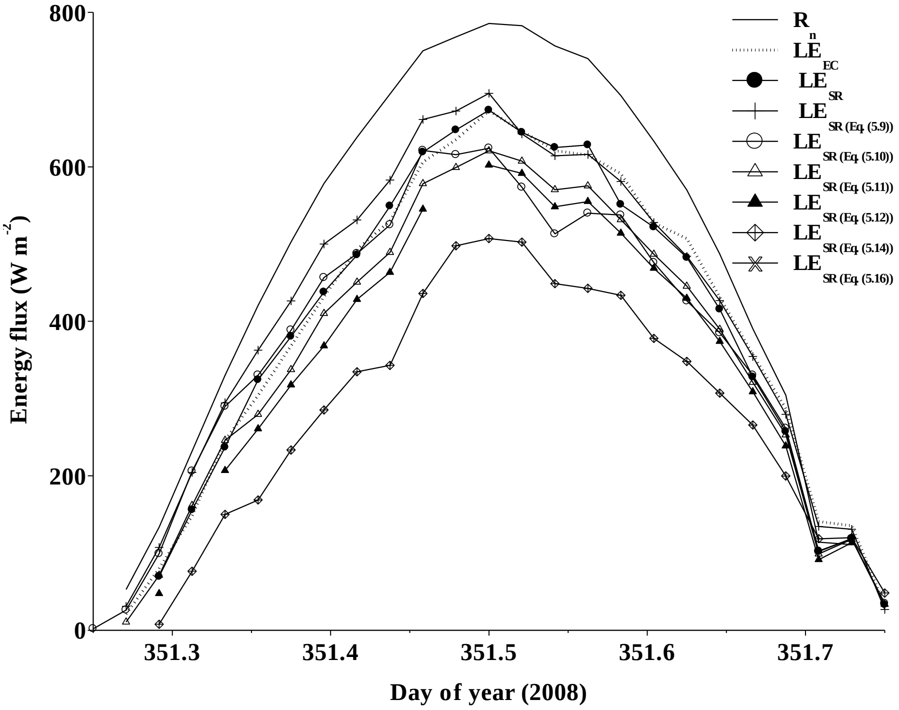
R n
LE EC
LE SR
LE SR (Eq. (5.9))
LE SR (Eq. (5.10))
LE SR (Eq. (5.11))
LE SR (Eq. (5.12))
LE SR (Eq. (5.14))
LE SR (Eq. (5.16))
Energy flux (W m-2)
800
600
400
200
0
351.3
351.4
351.5
351.6
351.7
Day of year (2008)

(**b**) 0.50 m

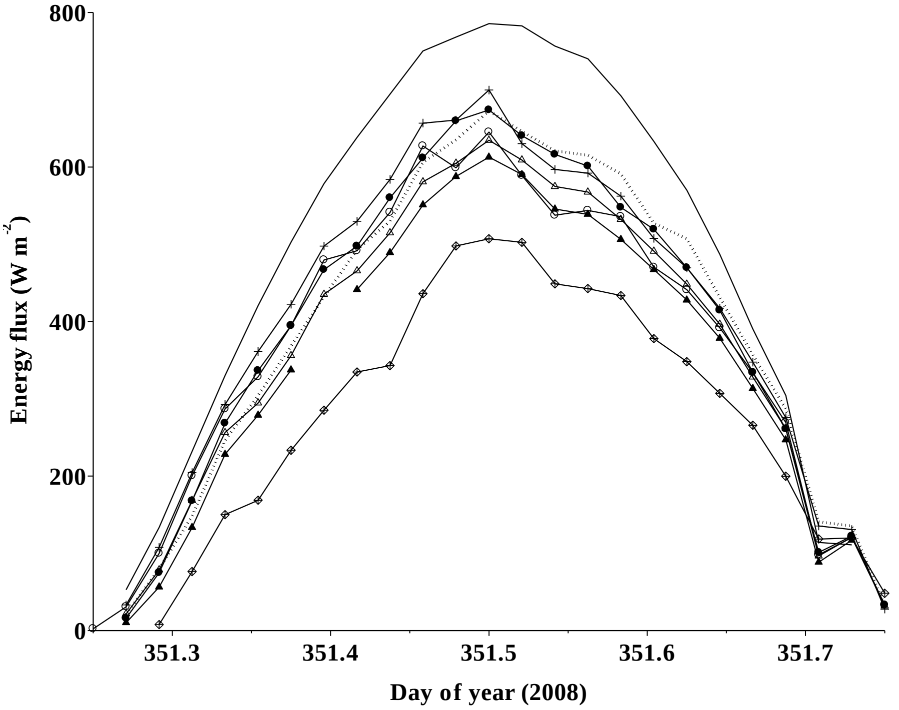
Energy flux (W m-2)
800
600
400
200
0
351.3
351.4
351.5
351.6
351.7
Day of year (2008)

(**c**) 0.75 m

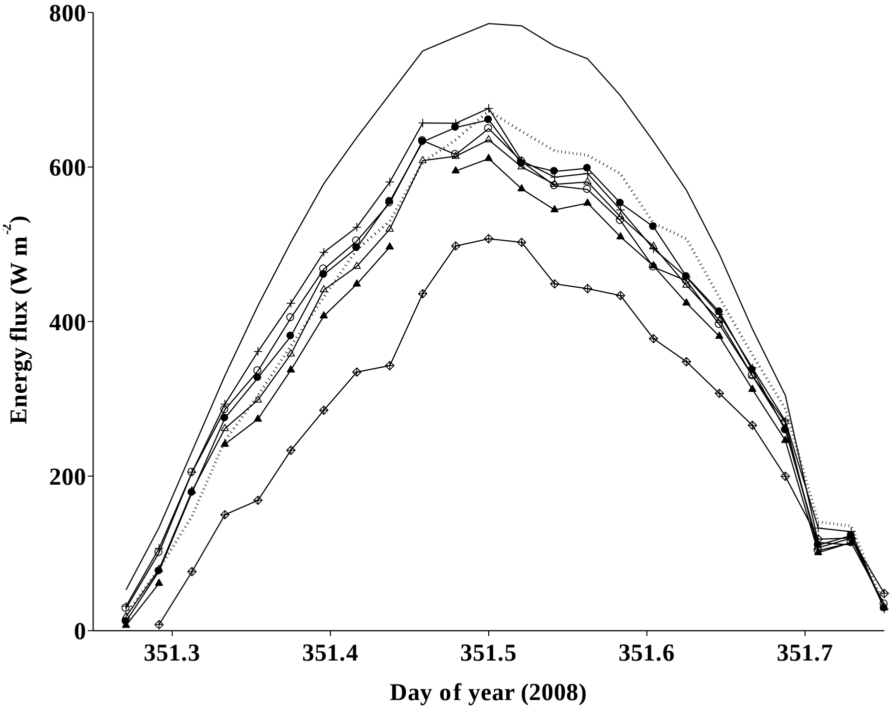

(**d**) 1.50 m

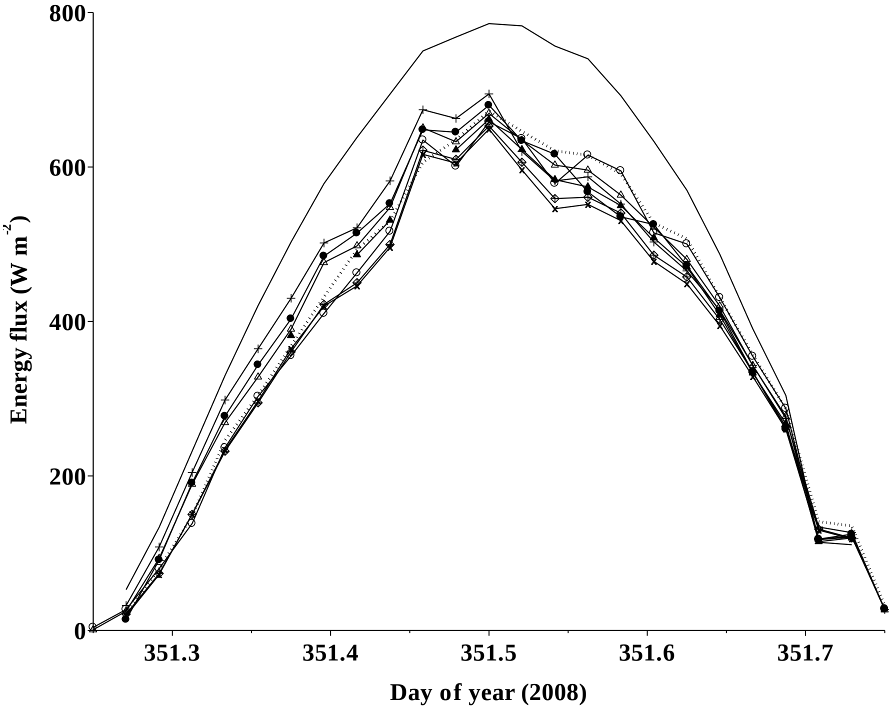

Fig. 5.4 Diurnal variation in half-hourly latent energy flux *LE* estimated using H_{EC} and H_{SR} estimates for all heights above the dense sugarcane canopy and using a 0.8-s air temperature time lag, and R_n for unstable conditions for day of year 351 (2008).

5.5 Summary and conclusions

Sensible heat flux over the sparse and dense sugarcane canopies conditions was estimated using SR and EC methods in the roughness and inertial sub-layers. The H_{SR} values were used to estimate latent energy flux LE as a residual of the shortened energy balance equation using measured net irradiance R_n and soil heat flux G. The performance of the original and new SR models and their free convection limits forms were evaluated for daytime unstable conditions. The effect of measurement height, time lag and crop height on α was also evaluated.

The value of α increased with a decrease in measurement height for increased air temperature time lag. It was observed that α' values were greater compared to α. The H estimated using the original SR approach, for which the α value was determined, yielded more accurate estimates compared to α'. Various other SR estimates applied to the roughness sub-layer obtained by calculation, one using a finite micro-front ramp SR model, another using K-theory and others that combine SR and Monin-Obukhov similarity theory (MOST) and their free convection forms produced good H_{SR} estimates. Improved H_{SR} estimates were observed using a combined SR and K-theory approach. The combined SR and MOST approaches performed well in the inertial sub-layer and their respective free convection forms, performed poorly. The performance of the original and other SR approaches was improved when the crop was dense and hence more homogeneous. The H_{SR} estimates obtained by the SR analysis based on a finite micro-front ramp SR model was superior compared to those obtained using the other approaches. The SR method at heights of 0.50 and 0.75 m above the crop canopy using an air temperature time lag of 0.8 s gave the best estimate of H_{SR}.

Chapter 6: Long-term estimation of sensible heat flux and evaporation for sugarcane using eddy covariance, temperature variance and surface renewal

Abstract

Sugarcane areas in South Africa face continuous pressure on the available limited water resources due to competition with others crops, expansion of irrigated agricultural areas and drought which reflects the importance of estimating evaporation. The eddy covariance (EC), temperature variance (TV) including adjustment for air temperature skewness and surface renewal SR methods were used to estimate the sensible heat flux H from which latent energy flux was calculated as a residual of the shortened energy balance and so evaporation, over a sugarcane canopy at the Baynesfield Estate in KwaZulu-Natal for a one-year period. High-frequency (10 Hz) air temperature data were collected for different measurement heights above the crop surface using unshielded and naturally-unventilated fine-wire thermocouples. The sign of the third-order air temperature structure function was used to identify unstable atmospheric conditions. For SR, two air temperature time lags of 0.4 and 0.8 s, were used. The SR sensible heat (H_{SR}) was estimated and then multiplied by the weighting factor $\alpha = 0.62$ previously determined from simultaneous SR and EC measurements of H for daytime unstable conditions. For the TV method, the skewness of air temperature S_k was used to estimate sensible heat flux ($H_{TV(Sk)}$). Daytime estimates of the daily total $H_{TV(Sk)}$ and H_{SR} using air temperature time lag of 0.8 s were compared with H_{EC} estimates. The $H_{TV(Sk)}$ and H_{SR} using an air temperature time lag of 0.8 s showed quite good agreement with H_{EC} estimates for all measurement heights. The superior results were observed at heights of 0.50 and 1.50 m above the crop surface for SR and TV sensible heat flux estimates respectively. The latter also adjusted for the air temperature skewness. Evaporation and energy balance components varied with time throughout the day, from day to day, and from season to season. The daily total evaporation maximum value was about 7.5 mm in summer and was 1.2 mm for cloudless winter days. The average daily evaporation for the whole period was 2.06 mm. The footprint analysis for sensible heat flux indicated that greater than 91 % of measured sensible heat flux was coming from underlying surface for a fetch distance x of 97 m of the experiment site. The TV method adjusted for the air temperature skewness and the SR method showed promise as being

inexpensive and reasonably simple with low power requirements compared to other methods. The TV method which includes adjustment for the air temperature skewness does not require calibration or validation compared to the SR method.

Keywords*:* Air temperature, Sensible heat, High frequency, Skewness

6.1 Introduction

Evaporation is recognized as the most important process that represents the major consumptive use of irrigation water and rainfall of agricultural areas (Gowda *et al*., 2008). In nature, evaporation is influenced by a number of climatic and biological factors (Rosset *et al*., 1997; Wever *et al*., 2002), with a large variability at various spatial and temporal scales. Evaporation can affect agricultural production and has direct impact on soil water content and the water balance (Wever *et al*., 2002; Watanabe *et al*., 2004). Evaporation links the surface water and energy balances (Czikowsky and Fitziarrald, 2004) and appears as a term of the energy balance as the latent energy flux. The available energy represents the sum of sensible heat and latent energy fluxes. Recently, several micrometeorological studies monitored the evaporation and sensible heat flux for different agricultural ecosystems (e.g. Savage *et al*., 1997; Grelle *et al*., 1999; Wilson and Baldocchi, 2000; Blanken, *et al*., 2001; Wever, *et al*., 2002; Humphreys *et al*., 2003; Savage *et al*., 2004; Watanabe *et al*., 2004; Burba and Verma, 2005; Odhiambo, 2007; Mengistu, 2008). There is a large variation in evaporation and surface energy flux between seasons and between years. Evaluating and understanding these variations is crucial for water resource management and to predict the actual and potential crop production especially in areas where there are scarce water resources.

Sugarcane is grown under both rainfall and supplementary irrigation in South Africa. Most of the sugarcane producing areas are located in the Eastern Cape, KwaZulu-Natal and Mpumalanga provinces. In theses areas, there is continuous pressure on available limited water resources as a result of the erratic rainfall occurrence, expansion of assigned areas and competition with other crops. These aspects have a significant impact on the sugarcane production (Olivier *et al*., 2009). Therefore, accurate and reliable evaporation data are important for irrigation scheduling and the optimum use of the available water resources so that maximum sugarcane yields can be obtained. Few field studies have been conducted that focus on total evaporation estimates over sugarcane using micrometeorological methods such as Bowen ratio-energy balance (Burger, 1999; McGlinchey and Inman-Bamber, 2002; Shinichi *et al*., 2004; Watanabe *et al*., 2004), eddy covariance (Denmead and MacDonald, 2008), and scintillometry methods (Wiles, 2006). The eddy covariance (EC) method is considered the preferable and accurate method for point measurements of sensible heat and latent energy flux. It is however limited by complexity, cost and sensitivity of the instruments to damage (Drexler *et al*., 2004). In addition, a full guidance on system set up and EC raw data processing is still unavailable (Mauder *et al*., 2007; Castellví *et al*., 2008). The Bowen ratio method is sensitive to the biases of the instrument used for measuring vertical gradients of air temperature and water vapour pressure (Rosenberg *et al*., 1983), and requires extensive fetch. The scintillometer method is an expensive method, based on the Monin-Obukhov similarity theory (MOST) and requires a fairly high level of expertise to operate. In addition, as is the case for EC, its measurements are interrupted by optical interception by rainfall, fog, insects, etc. The scintillometer method also requires vertical air temperature gradient measurement to distinguish between upward and downward direction of the sensible heat flux (Savage, 2009). Because of these limitations, a relatively inexpensive method for estimating evaporation involves measuring the sensible heat flux (H) from which latent energy flux and hence total evaporation can be calculated, as a residual using the shortened energy balance from measurements of net irradiance and soil heat flux. Included in these methods are the temperature variance (TV) and surface renewal (SR) methods which are reasonably simple with a reduced power requirement compared to other methods. The TV and SR methods may therefore be used unattended at distant sites.

The objectives of this study were to evaluate the performance of the TV and SR methods in collecting accurate long-term sensible heat flux and estimates of evaporation from sugarcane and to study the effect of the variation of principle factors (weather, plant and soil) on sugarcane evaporation and energy balance terms.

6.2 Theory

6.2.1 Energy balance

The shortened surface energy balance is used to estimate evaporation using micrometeorological methods, including the TV and SR methods. The shortened energy balance form neglects advection and the energy flux associated with photosynthesis and respiration, and energy stored in the canopy (Thom, 1975). For a flat and extensive surface it is expressed as:

$$R_n = LE + H + G \tag{6.1}$$

where R_n is the net irradiance and G the soil heat flux. All terms are in W m^{-2}. Fluxes directed toward the surface are regarded as negative and those directed away from the surface are positive.

6.2.2 Temperature variance method

The TV method, based on MOST was pioneered by Wyngaard *et al*. (1971) and Tillman (1972). According to MOST, for uniform surfaces, the relation between the fluxes and variances of atmospheric scalars has been applied (Weaver 1990; de Bruin *et al*., 1993). The method allows the sensible heat flux $H = H_{TV}$ to be estimated from air temperature measurement at a single-level above the canopy.

The TV method is attractive because it is simple, inexpensive, and allows the sensible heat flux to be estimated from only air temperature measurements at one point using an unshielded and naturally-ventilated fine-wire thermocouple. The main drawbacks of this method are due to the requirements imposed by MOST, namely that the surface layer is over an extensive flat and homogeneous terrain. In practice, this ideal is never attainable. There are two different TV methods: the TV method including an adjustment for stability (Wyngaard *et al*., 1971) and the TV method including an adjustment for air temperature skewness (Tillman, 1972). Each method has their own advantages and disadvantages, in terms of simplicity, accuracy and equipment cost. The TV method including adjustment for skewness air temperature has several advantages over the TV method that adjusts for stability. The former method is independent of EC measurements and requires high-frequency air temperature measurements as the only input data to obtain the sensible heat flux. An iteration process and wind speed measurements are required for the latter method.

According to MOST, Tillman (1972) noted that non-dimensional functions such as the air temperature skewness (S_k) are determined by z/L_o. The air temperature skewness is defined as:

$$S_k = \frac{1}{\sigma_T{}^3}\left[\frac{1}{n}\sum_{i=1}^{n}(T_i - \overline{T})^3\right] \tag{6.2}$$

where n is the number of the observations within the averaging time period, T_i an air temperature sample at time i and over the averaging period, $\overline{T}$ the mean air temperature $\overline{T}$ and σ_T the air temperature standard deviation. The stability parameter ζ can be determined as a function of S_k by plotting ζ and S_k in linear and semi-log form using:

$$\zeta = -A\exp(B\,S_k) \qquad -3 < \zeta \leq -0.01 \tag{6.3}$$

where A and B are positive constants of 0.0137 and 4.39 respectively (Tillman, 1972), obtained by the natural log of Eq. (6.3) and using a linear square fit, assuming that errors occur in both ζ and S_k. If S_k is zero for the neutral case, ζ can be determined as:

$$\zeta = A - A\exp(B\,S_k). \tag{6.4}$$

Tillman (1972), applying MOST, derived an expression for estimating sensible heat flux $H = H_{TV(Sk)}$ adjusted for the air temperature skewness and T_a at one level above the canopy surface as:

$$H_{TV(Sk)} = \begin{cases} \rho_a\, c_p \left(\dfrac{\sigma_T}{C_1}\right)^{3/2} \left(\dfrac{k\, g\, z\left(C_2 + A\exp(B\, S_k)\right)}{T_a\, A\exp(B\, S_k)}\right)^{1/2}, & \zeta < 0 \\ -\rho_a\, c_p \left(\dfrac{\sigma_T}{C_2}\right)^{3/2} \left(\dfrac{k\, g\, z}{T_a}\right)^{1/2}. & \zeta \geq 0 \end{cases} \qquad (6.5)$$

where ρ_a is the density of air (kg m^{-3}), c_p the specific heat capacity of air at constant pressure (J kg^{-1} ^{o}C^{-1}), k von Kármán constant (0.4), g the acceleration due to gravity (m s^{-2}), z the measurement height (m) and C_1, C_2 and C_3 the universal similarity constants with values of 0.95, 0.05, and -2 respectively (Tillman, 1972). The free convection limit for Eq. (6.5) is obtained by assuming the limit for $\zeta > C_2$ and has proved to perform adequately under slightly stable conditions and can be expressed as (Tillman, 1972):

$$H_{TV} = \rho_a\, c_p \left(\frac{\sigma_T}{C_1}\right)^{3/2} \left(\frac{k\, g\, z}{T_a}\right)^{1/2}. \qquad \zeta \leq -0.05 \qquad (6.6)$$

Based on Chen *et al*. (1997b), the TV sensible heat flux estimates are proportional to z in the roughness sub-layer while in inertial sub-layer they are proportional to z - d. where d is the zero displacement (m).

6.2.3 Surface renewal method

The SR method for estimating the sensible heat flux based on the coherent structures concept was pioneered by Paw U and Brunet (1991). The coherent structures theory assumes that an air parcel sweeps from above the canopy to the canopy surface. The air parcels begins to be cooled or heated when near or in the canopy because of the sensible heat exchange between the air and canopy elements. Ramps are observed in the air temperature traces as a result of the turbulent coherent structures. These ramps, for stable and unstable conditions are characterized by amplitude and total ramp period parameters (Paw U and Brunet, 1991). It is assumed that the total ramp period consists of a ramp period l and a quiescent ramp period s. The amplitude a is positive for unstable conditions and negative for stable. The ramp amplitude and total ramp period for a fixed time interval are used to estimate sensible heat flux over the given crop canopy surface using the SR method (Paw U and Brunet, 1991; Paw U *et al*., 1995; Snyder *et al*., 1996). Following Paw

U and Brunet (1991) and Paw U *et al*. (1995), the sensible heat flux can be determined as the change of heat content of the air with time ($M_{air}\ c_p\ dT/dt$) per unit area (A) as follows (Savage *et al*., 2004):

$$H_{SR} = c_p \frac{M_{air}}{A} \frac{dT}{dt} \tag{6.7}$$

where M_{air} is the mass of air heated (or cooled) by the rate of change in the air temperature difference dT/dt. To simplify Eq. (6.7), M_{air} can be expressed in terms of ρ_a and the volume of air V per horizontal unit area A:

$$H_{SR} = \rho_a\, c_p \frac{V}{A} \frac{dT}{dt}\,. \tag{6.8}$$

The measured change in the air temperature with time is the partial derivative of temperature with time $\partial T/\partial t$ rather than dT/dt because air temperature is measured at a fixed point (Snyder *et al*., 1997). The term V/A represents the vertical distance (measurement height above the soil surface). It is assumed that the internal advection is negligible:

$$H_{SR} = \rho_a\, c_p\, z \frac{\partial T}{\partial t} \tag{6.9}$$

where z is the measurement height above the soil surface and $\partial T/\partial t$ can be replaced by the ratio a / (l + s) in Eq. (6.4) to determine sensible heat flux. Therefore for the SR method, the sensible heat flux is determined using (Paw U *et al*., 1995):

$$H_{SR} = \alpha\, z \rho_a\, c_p \frac{a}{l+s} \tag{6.10}$$

where α is a SR weighting factor defined as a factor that corrects for the unequal heating or cooling from the measurement height to the ground. The weighting factor depends on air temperature time lag, an air temperature structure function, measurement height and plant canopy height, and the size of the fine-wire thermocouple used to measure air temperature at high frequency (Paw U *et al*., 2005). However, αz has a physical meaning, representing the volume of air per unit of ground area exchanged on average for each ramp in the sample period for the measurement height z (Paw U *et al*., 1995). Castellví *et al*. (2002) interpreted αz as the mean eddy size responsible for the renewal process. The amplitude and ramp period are estimated following the structure function approach of van Atta (1977): the structure function $S^n(r)$ is obtained from high frequency air temperature measurements using the following relationship:

$$S^n(r) = \frac{1}{m-j}\sum_{i=1+j}^{m}(T_i - T_{i-j})^n \tag{6.11}$$

where m is the number of data points measured at frequency f (Hz) in the averaging time interval, n the power of the structure function, j the number of the lags between data points corresponding to an air temperature time lag $r = j/f$ and T_i the i^{th} air temperature sample. The average a in the time interval can be determined from the solution of the polynomial equation (Spano *et al*., 1997a, b; Paw U *et al*., 2005):

$$a^3 + \left(10S^2(r) - \frac{S^5(r)}{S^3(r)})\right)a + 10S^3(r) = 0 \tag{6.12}$$

and $l + s$ is estimated using:

$$l + s = -\frac{a^3 r}{S^3(r)}. \tag{6.13}$$

6.2.4 Footprint analysis

Estimation of the footprint for sensible heat and latent energy flux measurements is crucial for agricultural and environmental studies as the footprint determines the relative influence of underlying area on these fluxes. The footprint is defined as the spatial context of the measurement of surface layer fluxes (Schmid, 2002), and its size and shape depend on measurement height, surface roughness and atmospheric stability (Gash, 1986; Leclerc and Thurtell, 1990). The footprint function $F(x, z_m - d)$ for a scalar flux measured at height of

z_m (m) and at a downwind fetch distance x (m) away, for a surface with a zero displacement height d (m) is mathematically defined as (Horst and Weil, 1992):

$$F(x, z_m - d) = \int_{-\infty}^{x} S(x) f(x, z_m - d)\, dx \tag{6.14}$$

where S is the surface source flux (W m^{-3}) for sensible heat flux footprint and f the footprint at a distance x. Hsieh *et al*. (2000) proposed the following model, mainly analytical model, for estimating the footprint of the sensible heat flux:

$$f(x, z_m - d) = \frac{1}{k^2 x^2} D z_u^P |L_o|^{1-P} \exp\left(\frac{-1}{k^2 x} D z_u^P |L_o|^{1-P} \right) \tag{6.15}$$

where z_u is the length scale, D and P the similarity constants obtained by Hsieh *et al*. (2000), and L_o defined as:

$$L_o = -u_*^3 \frac{T_a}{k\, g} \frac{\rho_a c_p}{H} \text{ or equivalently } L_o = -u_*^2 \frac{T_a}{k\, g\, T_*} \tag{6.16}$$

where u_* is the friction velocity (m s^{-1}). The values of the similarity constants D and P are 0.28 and 0.59 for unstable, 0.97 and 1 for near neutral and neutral conditions, and 2.44 and 1.33 for stable conditions respectively. Savage *et al*. (2004) defined the length scale to include zero displacement d and surface roughness length z_o and to apply a correction as follows:

$$z_u = \frac{(z_m - d)^2}{z_m - (z_o + d)} \left(\ln \frac{(z_m - d)}{z_o} - 1 + \frac{z_o}{(z_m - d)} \right). \tag{6.17}$$

According to Calder (1952) and Gash (1986), the peak of the footprint x_{peak} (m) can be estimated as a function of L_o and z_u:

$$x_{peak} = \frac{D\, z_u^p |L_o|^{1-p}}{2k^2}. \tag{6.18}$$

The cumulative fraction of the flux F to surface source flux S_o ratio, at distance x from the source and at an effective height of $z_m - d$ from the ground surface, can be estimated using (Hsieh *et al*., 2000):

$$\frac{F(x, z_m - d)}{S_o} = \exp\left(\frac{-2}{x} x_{peak}\right). \qquad (6.19)$$

6.3 Materials and methods

A field experiment was carried out over a 3-ha area of commercial sugarcane (variety N14), at the Baynesfield Estate in KwaZulu-Natal, South Africa (29.45 ^{o}S, 30.18 ^{o}E) with an altitude of 910 m above MSL. The Baynesfield climate is classified as sub-humid with dry and cool winters and warm and rainy summers. The mean monthly air temperature ranges from a maximum of 21.1 ^{o}C in January to a minimum of 13.3 ^{o}C in June with a mean annual precipitation of 844 mm. Precipitation falls as rain, most of it in the humid summer months. The soil is classified as the Hutton form with a clay content of 550 to 650 g kg^{-1} (Haynes *et al*., 2003).

The sugarcane was planted in December 2007, with a row spacing of 1 m and planting spacing of 0.50 m. The experimental plot is bordered on the south east by a small water reservoir, and for the other directions by sugarcane differing in their heights and growth stages. The predominant wind direction is easterly. The upwind fetch available for the measurements was 97 m from the predominant wind direction.

The crop was six months old with a height of 1.22 m above the soil surface at the beginning of the experiment. The data collected and analysed were for a one-year period, from 11 July 2008 to 11 July 2009 (from day of year 192, 2008 to 192, 2009).

Plant physiological growth parameters including crop height h and leaf area index (LAI) were measured every two weeks and monthly respectively. The average h was measured from three randomly selected plants. The LAI was measured when the sky was cloudy or during early morning or late afternoon using an LAI-2000 plant canopy analyzer (Li-Cor. Inc., Lincoln, Nebraska, USA), with a 45^o view cap and replicated three times.

Then the data was downloaded to a computer using Li-Cor software. Canopy surface temperature was measured using two infrared thermometers (Model IRTS-P, Apogee Instruments Inc., Logan, Utah, USA) placed at 0.75 m above the crop canopy surface. Measurements were done every one second and the data averaged every two min and thirty min using the CR3000 datalogger (Campbell Scientific Inc., Logan, Utah, USA).

Two micrometeorological masts for supporting different sensors were located at about 15 and 50 m from west and south edges of the field, respectively. For the TV method adjusted for air temperature skewness and SR estimates of sensible heat flux, four unshielded and naturally-ventilated 75-μm type-E fine-wire thermocouples, placed at heights of 0.20, 0.50, 0.75 and 1.50 m above the crop surface, were used to measure high frequency air temperature. At each height, a parallel combination of fine-wire thermocouples was used. The thermocouples were pointed toward the predominant wind direction which occurred during daytime hours. All thermocouples were connected to the CR3000 datalogger. Air temperature data were sampled at a frequency of 10 Hz. Two air temperature time lags of 0.4 and 0.8 s were used to calculate the air temperature structure functions. The second-, third- and fifth-order air temperature structure functions were determined after lagging the air temperature data by 0.4 and 0.8 s using Eq. 6.11 from high frequency air temperature data. The data were then averaged every two minutes and thirty minutes and stored in the datalogger, for further analysis, including the 10-Hz data.

For the TV method, the air temperature skewness S_k values were computed from high frequency air temperature data using Eq. (6.2) using Fortran software and averages every two minutes. The sign of the third-order air temperature structure function was also used to identify unstable conditions. Then, the TV sensible heat flux corrected for air temperature skewness $H_{TV(\mathrm{Sk})}$ (W m^{-2}) was estimated using Eq. (6.5) for each averaging period from the standard deviation and skewness of air temperature. The constant parameters A and B in Eq. (6.5) were set to 0.0137 and 4.39 respectively.

For SR, the amplitude a and the total ramp period $l + s$ were determined from the air temperature structure functions using the two air temperature time lags and the Van Atta (1977) analysis approach. The sign of a was used to determine atmospheric stability (positive indicates unstable conditions and negative indicates stable). The two-minute SR sensible heat flux H_{SR} was calculated and the data then averaged to half-hourly values. The half-hourly uncalibrated H_{SR} estimates were corrected for unequal heating between the ground and the measurement height (Snyder *et al*., 1996; Spano, *et al*., 1997a, b) using a SR weighting factor α = 0.62 previously obtained by the comparison of simultaneous SR and EC measurements of *H* for daytime unstable conditions.

For purposes of sensible heat flux comparisons, a three-dimensional sonic anemometer (model 81000, RM Young, Traverse City, Michigan, USA) which represents the EC system, was connected to the CR3000 datalogger and installed adjacent to the thermocouples to estimate $H = H_{EC}$ at a height of 2.15 m above the soil surface at the start of experiment and 3.70 m above the soil surface at the end of the experiment. The sonic anemometer was pointed towards north. The scan rate for the EC measurements was 10 Hz. All EC data were processed online every 2 and 30 minutes in the datalogger and stored for further analysis, including 10-Hz data. The sonic sensible heat flux H_{sonic} was calculated as: $H_{sonic} = \rho_a c_p \overline{w'T_s'}$ where w' and T_s' are the fluctuations from the mean vertical wind speed w and sonic temperature T_s respectively. Sensible heat flux was calculated following coordinate rotations for the three wind velocity components, *u*, *v* and *w*, and correction to remove the effects of the instrument tilt and air-flow irregularities using the procedures similar to those of Kaimal and Finnigan (1994) and Oncley *et al*. (2007). Similar "constants" were used for calculating EC and SR sensible heat flux for each time period (Savage *et al*., 1997). The H_{EC} values were corrected for the effects of water vapour pressure and Bowen ratio, using the average values $\bar{e}$ and $\bar{\beta}$ respectively, using the relationship (Odhiambo and Savage, 2009):

$$H_{EC} = H_{sonic}\left(1 + \frac{0.322\,\bar{e}}{\bar{P}} + \frac{10^{-3}\left(0.722\,\bar{P} - 0.399\,\bar{e}\right)}{\bar{\beta}}\right)^{-1} \tag{6.20}$$

in which $\bar{e}$ (kPa) was obtained using air temperature and relative humidity measurements using two Vaisala instruments (Campbell HMP45C) connected to the CR1000 datalogger with one at each height of 0.50 and 1.50 m above the crop canopy. The atmospheric pressure $\bar{P}$ (kPa) was estimated following Savage *et al*. (1997) using altitude, average water vapour pressure $\bar{e}$ and an average of the measured air temperature from the fine-wire thermocouples and $\bar{\beta}$ estimated using:

$$\bar{\beta} = \frac{H_{sonic}}{R_n - G - H_{sonic}}. \tag{6.21}$$

The friction velocity u_* was calculated from the dimensional orthogonal wind speed components from sonic anemometer as: $[(\overline{u'w'})^2 + (\overline{v'w'})^2]^{1/4}$ (Garratt, 1992) where u, v, and w are the three dimensional orthogonal wind speeds and u', v', and w' are the fluctuations from the mean of u, v, and w respectively.

Additional measurements included the remaining energy balance components with R_n, soil heat flux, soil temperature and soil water content measured every one second, averaged every two min and stored using a Campbell CR1000 datalogger for further analysis. A NR LITE net radiometer (Kipp & Zonen, Delft, The Netherlands) to measure R_n was mounted at a height of 1.50 m above the crop surface and adjusted according to the changes in crop height. Soil heat flux G_{plate} at 0.08 m below the soil surface was measured using two soil heat flux plates buried horizontally. Spatially-averaged soil temperature was obtained using two pairs of type-E thermocouples in metal tubes buried in the soil at depths of 0.02 and 0.06 m above the soil heat flux plates. Soil water content was measured using a frequency domain reflectometer (ThetaProbe, model ML2x, Delta-T Devices, Cambridge, England) inserted vertically in the soil close to the area where soil heat flux plates and soil thermocouples were buried. The heat flux stored above the soil heat flux plates G_{stored} was calculated from the measured average soil temperature and soil water content θ_v (m^3 m^{-3}) as:

$$G_{stored} = \left(\rho_{soil}\, c_{dsoil} + \rho_w\, \theta_v\, c_w\right) \frac{\Delta z\, \overline{\Delta T}_{soil}}{\Delta t} \tag{6.22}$$

where ρ_{soil} is the soil bulk density (kg m^{-3}), c_{dsoil} the dry soil specific heat capacity (840 J kg^{-1} ^{o}C^{-1}), ρ_w the density of water (1000 kg m^{-3}), θ_v the soil water content (m^3 m^{-3}), c_w the specific heat capacity of water (4200 J kg^{-1} ^{o}C^{-1}), Δz the soil heat flux plates depth (m), $\overline{\Delta T}_{soil}$ the change in the average soil temperature above the soil heat flux plate (^{o}C), from onetime period to next, and Δt (s) the time between temperature average measurements (s). The soil heat flux G was then calculated as:

$$G = G_{plate} + G_{stored} \,. \tag{6.23}$$

Since direct measurements of the latent energy flux LE was not available during this study, LE from each method was estimated as a residual from the energy balance equation (Eq. (6.1)) from half-hourly H, R_n and G measurements for unstable conditions during daytime hours from 06h00 to 18h00. The disadvantages of the residual method are that: (a) the advection and the canopy stored energy fluxes are assumed to be negligible; (b) the errors in obtaining R_n, H and G are accumulated into LE. Therefore LE could be underestimated or overestimated.

An automatic weather station was set up at the same mast that contained EC, TV and SR systems for monitoring environmental conditions. A pyranometer (CM3, Kipp and Zonen, Delft, Holland) installed at 2.5 m above the crop surface was used to measure solar irradiance. Air temperature and relative humidity, from which water vapour pressure was calculated, were measured using air temperature and relative humidity probe (Campbell CS500). Wind speed was measured using a three-cup anemometer (model 03001, RM Young). Total rainfall was measured using the tipping bucket rain gauge. A scan rate of 10 s was used and the data were logged every two-min and hourly using a Campbell CR10X datalogger. Half-hourly short-grass and tall-crop reference evaporation was calculated hourly using the FAO Penman-Monteith equation and then summed to daily values.

Generally, the measurement heights for all systems were adjusted when the crop height increased to maintain the heights above the crop surface.

The relative contributions to the sensible heat flux from areas at different upwind distance were estimated using the modified footprint model (Hsieh *et al.*, 2000) for a surface with a displacement d and surface roughness length z_o. The magnitude and the peak location of the footprint were determined at midday for four selected days at 2.10 m above the soil surface (DOY 194, 2008), 2.15 m (DOY 251, 2008), 2.25 m (DOY 351, 2008) and 3.66 m (DOY 84, 2009). The days covered different seasons. A footprint function for scale length z_u was estimated using Eq. (6.14). The peak location of footprint x_{peak} and the cumulative fraction of the flux F to surface source flux S_o ratio were estimated using Eqs (6.18) and (6.19) respectively. Constant values of 0.28 and 0.59 were used for the similarity constants D and P respectively in Eq. (6.14). According to Savage *et al*. (2004), the value of the length scale z_u was computed using Eq. (6.17). The L_o in Eq. (6.15) was calculated using Eq. (6.16) from EC-estimated sensible heat flux and friction velocity. The gap in the data set resulted from the power outage, broken sensors, other technical problems and unfavourable weather conditions.

6.4 Results and discussion

6.4.1 Plant growth parameters

The sugarcane growth parameters in terms of plant height h and leaf area index LAI over time are presented in Fig. 6.1. The crop height h at the beginning of experiment was 1.2 m when the crop was six months old. During winter, the crop height increased slowly because of low solar irradiance, and few rain events (Fig. 6.2). The crop height substantially increased at the onset of spring, reached a maximum height during summer due to higher solar irradiance, air temperature and rainfall, decreased slowly during winter and became stable at the end of experiment when the crop matured. The LAI Measurements commenced during November, 2008. The LAI substantially increased to a maximum value of 4.73 in autumn (May) and then decreased as the crop matured and the leaves started to shed.

6.4.2 Environmental conditions

Environmental parameters including solar irradiance (I_s), air temperature (T_{air}), water vapour pressure deficit (VPD), horizontal wind speed (U) and precipitation play an important role in determining the turbulent exchange of mass and energy between the canopy and the atmosphere. Therefore knowledge of the temporal variations of these parameters is necessary for a good understanding of how these fluxes respond to these variations. Fig. 6.2 shows the meteorological conditions and average soil water content (SWC) for the upper 0.15 m of the soil during the study period. The mean daily T_{canopy} for this period is also presented in Fig. 6.2. Various right-hand y-axes and one left-hand y-axis

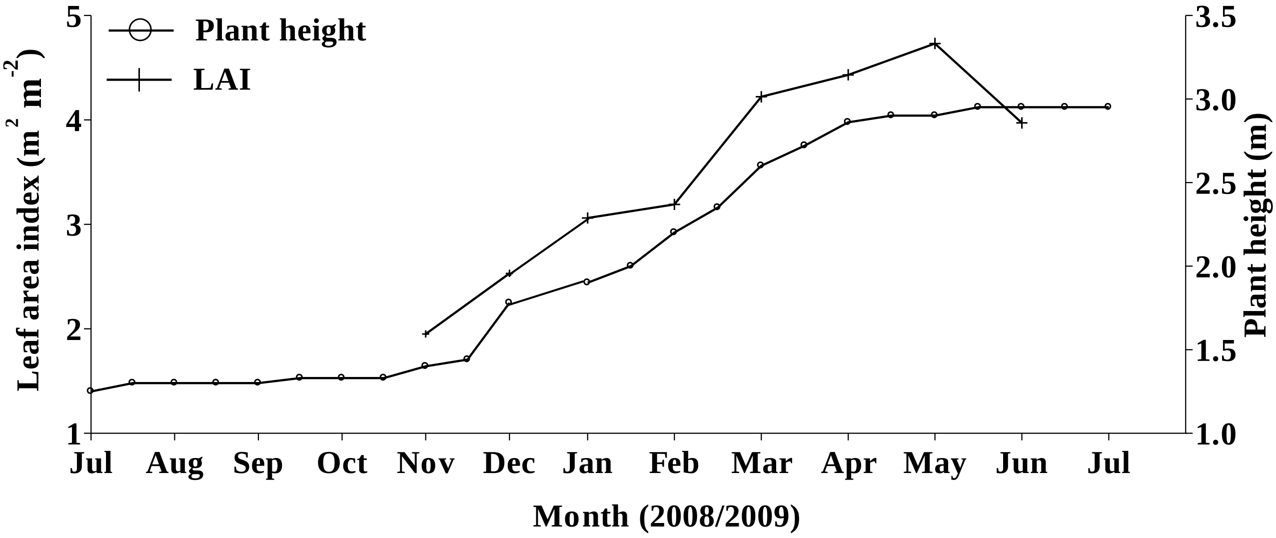

Fig. 6.1 Variation in *LAI* (m^2 m^{-2}) and *h* (m) of sugarcane for the study period.

for *SWC* (m^3 m^{-3}) were used in Fig. 6.2. The magnitude of daily total I_s ranged between 1.50 to 36 MJ m^{-2} with average daily value of 16.89 MJ m^{-2}. The daily total I_s was low and more stable in winter and much greater and fluctuated more in summer as shown in Fig 6.2, because most of the days in summer were cloudy. Mean daily T_{air} and T_{canopy} increased from 10 and 4.5 ^oC in winter to 19.5 and 20.8 ^oC in summer respectively. Mean T_{air} values were low (cool) during most of the days in winter and greater (warm) in the summer compared to the mean daily T_{canopy}. Generally, T_{air} and T_{canopy} fluctuated and responded rapidly to the changing solar irradiance. The *VPD* values were low during wet seasons and increased during dry seasons and showed similar trends to the air temperature as the *VPD* is air temperature dependent (Fig. 6.2). The *U* fluctuated more compared to the other climatic parameters as presented in Fig. 6.2. It was higher during the dry seasons (winter and spring) and then gradually decreased during the wet seasons (summer and autumn) to its minimum value which coincided with rain events. Generally wind speed was not relatively high at this site. The winter and a part of spring were dry (no rain events) with the summer and autumn were rainy. The majority of the rain events were in the summer with significant variation from day to day (Fig. 6.2). The magnitude of mean daily *SWC* ranged from 0.12 m^3 m^{-3} in winter to 0.50 m^3 m^{-3} in summer with an average for the whole period of 0.33 m^3 m^{-3}. The seasonal fluctuations in *SWC* values were mainly related to the distribution and amount of precipitation and evaporation. *SWC* was low during winter and high during summer but varied from day to day.

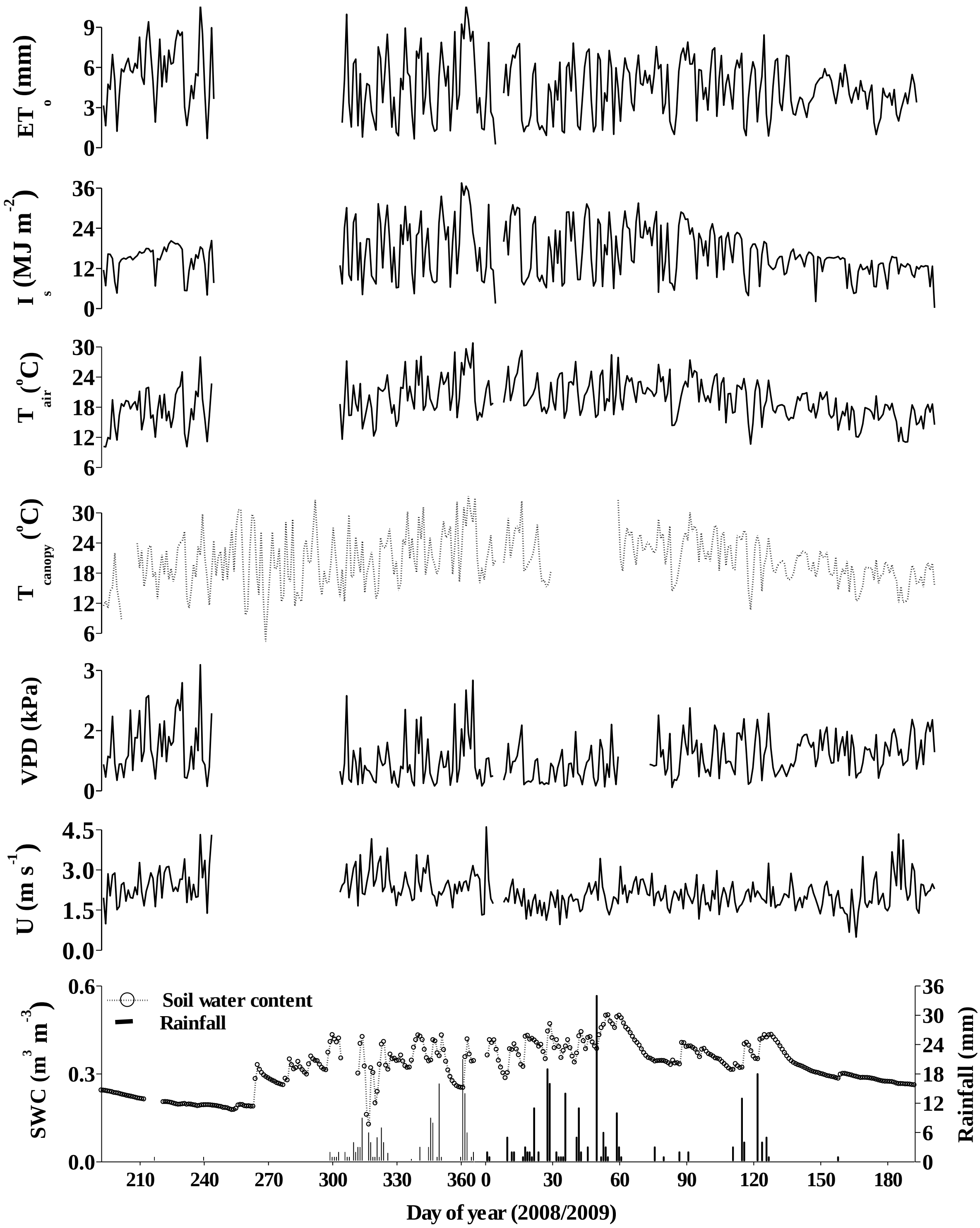

Fig. 6.2 Variation in daily reference tall-crop evaporation (ET_o), solar irradiance I_s (MJ m^{-2}), average air T_{air} (^oC), and canopy temperature T_{canopy} (^oC), water vapour pressure deficit *VPD* (kPa), horizontal wind speed *U* (m s^{-1}), average soil water content (m^3 m^{-3}), and daily total rainfall (mm) for the study period.

6.4.3 Sensible heat flux

Daily total $H_{TV(Sk)}$ estimated using Eq. (6.5) based on the air temperature skewness and H_{SR} estimated using Eq. (6.9), for different measurement heights of 0.20, 0.50, 0.75 and 1.50 m above the canopy were plotted against H_{EC} for unstable conditions during daytime hours from 06h00 to 18h00 for the study period(Figs 6.3 and 6.4 respectively). In each plot, the solid-line represents the linear regression line, and the dotted-line is one to one line relationship, and the dashed-lines are the confidence bands representing the 95 % confidence level for a single predicted y-value. The SR weighting factors α used were 0.66, 0.62, 0.60 and 0.55 for the heights of 0.20, 0.50, 0.75 and 1.50 m above the crop surface respectively. These were previously determined from simultaneous SR and EC measurements of H for various SR heights for daytime unstable conditions. Whatever the measurement height, either in the roughness or the inertial sub-layers, very good agreement between the daily total $H_{TV(Sk)}$ and H_{EC} was observed (Fig. 6.3). The TV method, including adjustment for air temperature skewness, gave a superior result at a height of 1.50 m above the crop surface with a slope of 0.95, coefficient of determination (r^2) of 0.88 and relative mean square error (RMSE) of 0.50 MJ m^{-2} (Fig. 6.3d) because this height was in the inertial sub-layer where MOST is valid (Brutsaert, 1982; Kaimal and Finnigan, 1994). Generally, the daily total of H_{SR} was more scattered around the 1:1 line, and overestimated H_{EC} in the roughness sub-layer and underestimated H_{EC} in the inertial sub-layer. Whatever the measurement height, either in the roughness sub-layer or in the inertial sub-layer, there is very good agreement between the daily total H_{SR} and H_{EC} but with underestimation (Fig. 6.4). Improved results for the SR were obtained at a height of 0.50 m above the crop surface with a slope of 0.96, r^2 = 0.86 and RMSE of 0.46 MJ m^{-2} (Fig. 6.4b). The slope values for the first three-heights were not significantly different from each other except for the upper-most height (data not shown). The slope values for the lowest height were significantly different compared to the other measurement heights (data not shown). Generally, the performance of the TV method adjusted for skewness in estimating sensible heat flux at a height of 1.50 m above the crop canopy was more accurate (r^2 = 0.88) compared to the SR method at a height of 0.50 m (r^2 = 0.86), as presented in Figs 6.3d and6.5c. However, for the 1.50-m height, the TV method resulted in a 5 % underestimation in the sensible heat flux compared to EC measurements (Fig. 6.3d).

(**a**) 0.20 m (**b**) 0.50 m

(**c**) 0.75 m (**d**) 1.50 m

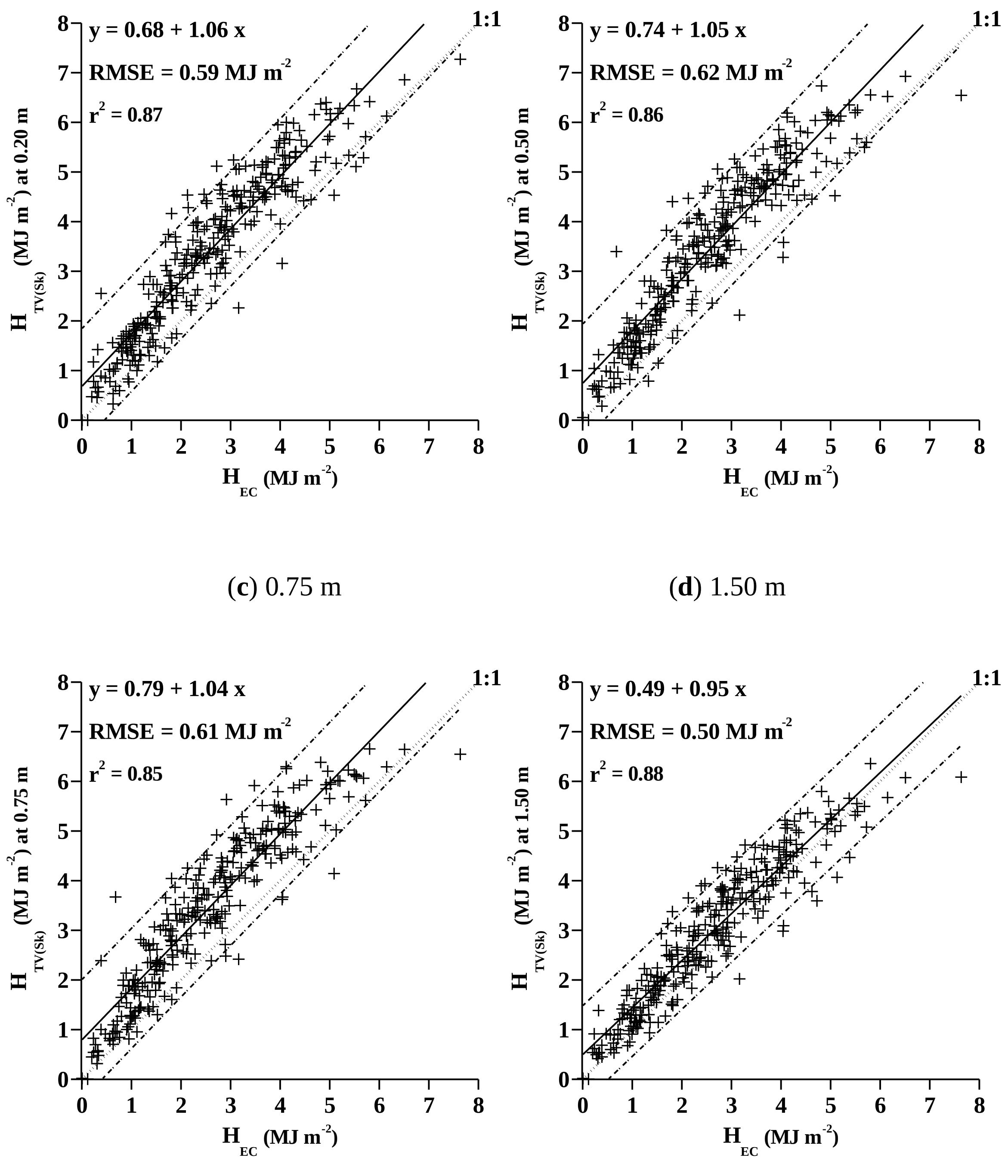

Fig. 6.3 Daily total $H_{TV(Sk)}$ *vs* H_{EC} estimates for the sugarcane canopy for daytime unstable conditions for the study period: (a) $H_{TV(Sk)}$ at a height of 0.20 m above the crop canopy; (b) at 0.50 m; (c) at 0.75 m; (d) at 1.50 m.

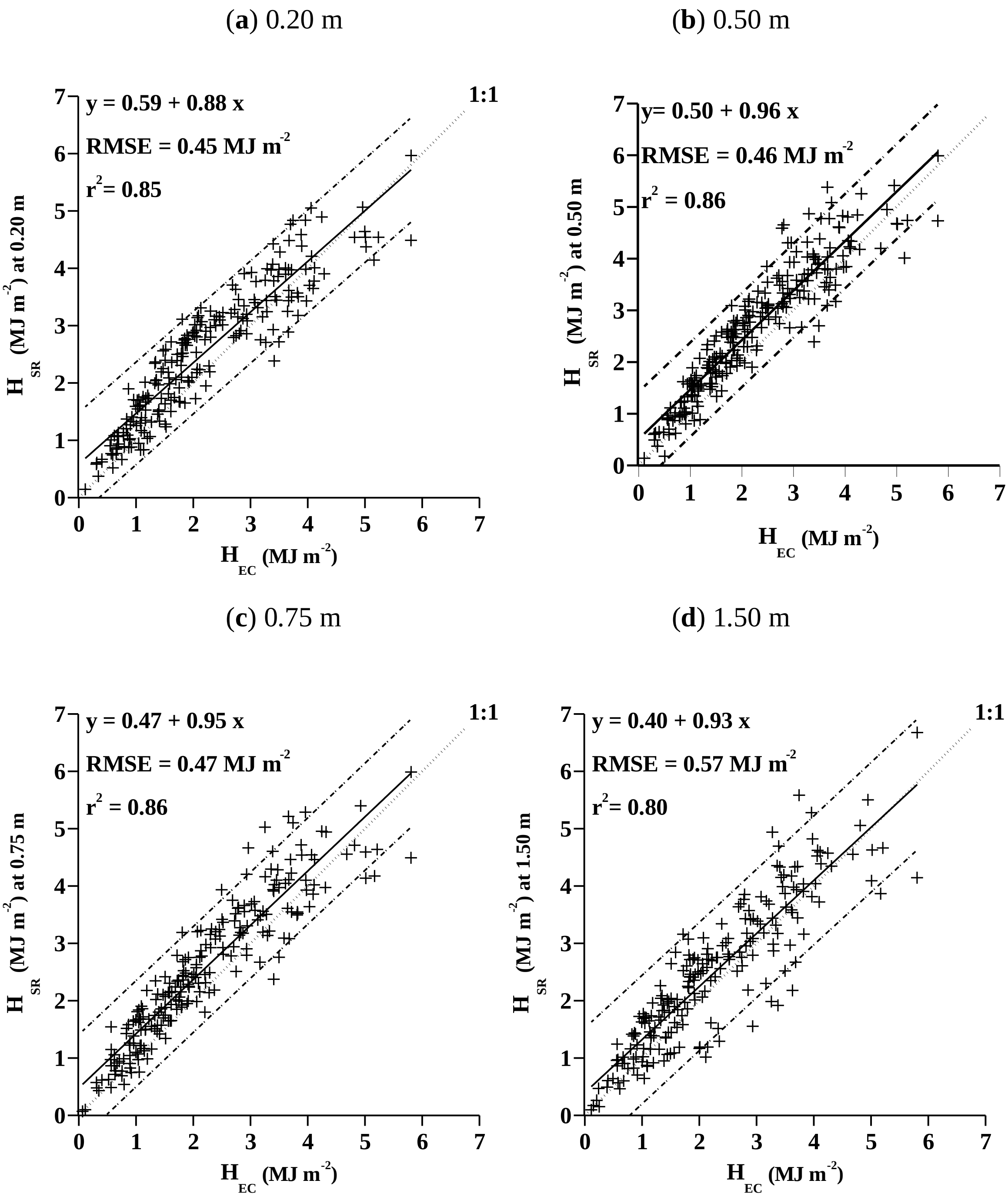

Fig. 6.4 Daily total H_{SR} estimates using a air temperature time lag of 0.8 s *vs* H_{EC} estimates for daytime unstable conditions for the study period: (a) H_{SR} at 0.20 m above the crop canopy; (b) at 0.50 m; (c) at 0.75 m; (d) at 1.50 m.

Diurnal variations of half hourly estimates of H_{EC}, $H_{TV(Sk)}$ at a height of 1.50 m above the crop canopy and H_{SR} (using α = 0.62) at a height of 0.50 m above the crop canopy for an air temperature time lag of 0.8 s along with the R_n for selected clear days covering different seasons (winter, spring and summer in 2008, and autumn 2009), are shown in Fig. 6.5. Since the residual method is used for calculating *LE* the calculated β values are net irradiance dependent *via* the sensible heat flux and latent energy flux. Hence the daily Bowen ratio ($\beta_{weighted}$) calculated from cumulative *H* and *LE* were weighted by half-hourly R_n (Fig. 6.5). Half-hourly $H_{TV(Sk)}$ overestimated H_{EC} most of the time during summer, autumn and winter (Figs 6.5b, c, and d), and underestimated H_{EC} during spring (Fig. 6.5a). The H_{SR} corresponded well with H_{EC} during summer and autumn as shown in Figs 6.5b and c, and overestimated H_{EC} during winter and spring as shown in Figs 6.5a and d. Whatever the season, it is noticed that the H_{SR} estimates were better correlated with H_{EC} most of the time compared to the $H_{TV(Sk)}$ estimates. This is mainly due to the SR method being calibrated against EC measurements whereas the $H_{TV(Sk)}$ estimates were independently determined. The weighted β values were very low in summer (0.12) and autumn (0.43), and very high in winter (0.72) and spring (0.77) since most of R_n is consumed as latent energy flux during wet periods compared to during drier periods (Fig. 6.5). The magnitude of R_n and *H* showed a seasonal variation. The net irradiance was very low during winter months, increased reaching a maximum value in summer and then decreased during autumn (Fig 6.5). In winter, the days were characterized by cold and dry weather with low net irradiance (Fig. 6.5a).

6.4.4 Seasonal estimates of energy balance components and total evaporation

Daily total energy balance components including net irradiance R_n, soil heat flux *G*, sensible heat *H* computed using the TV method, including adjustment for air temperature skewness, and the SR method and latent energy *LE* estimated as a residual of the shortened energy balance (Eq. (6.1)) for sugarcane for the study period are presented in Figs 6.6 and 6.7 respectively. The daily terms for each component were smoothed by calculating 10-dayrunning means for each daily data. The right-hand *y*-axis is used for converting energy balance components from MJ m^{-2} to mm. Daily total estimates of energy balance components for the sugarcane were obtained by summing the half-hourly data during daytime hours from 06h00 to 1800 for each day. The daily total net irradiance was more

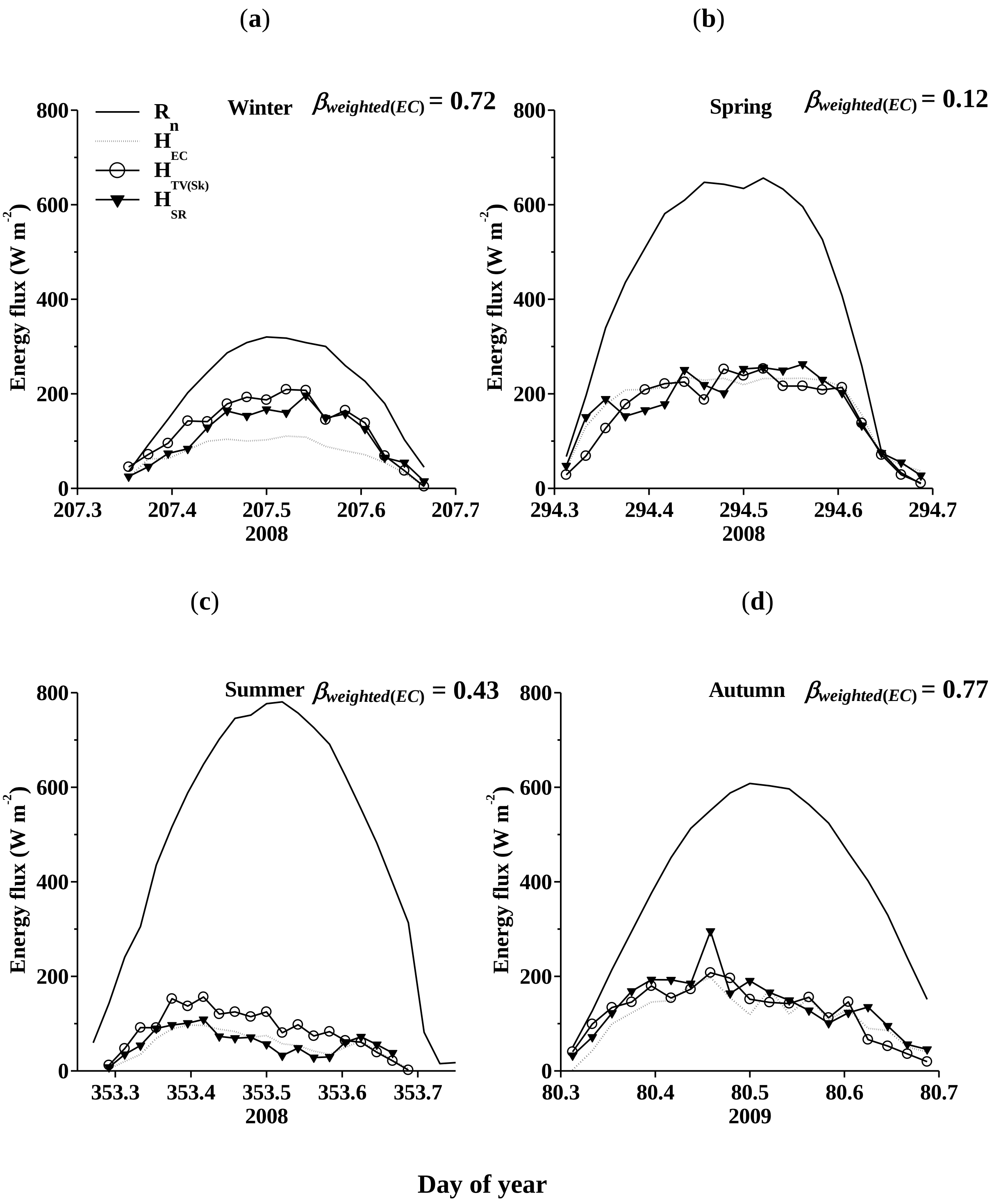

Fig. 6.5 Diurnal variations of the half-hourly estimates of H_{EC}, $H_{TV(Sk)}$ at a height of 1.50 m above the crop canopy, and H_{SR} (using α = 0.62) at a height of 0.50 m above the crop surface.

constant during winter and gradually increased reaching its maximum value during summer and then decreasing to a minimum value at the beginning of winter as shown in Figs 6.6 and 6.7. In winter, daily net irradiance was very low with a peak value ranging between 4 and 7 MJ m^{-2} for most days. In summer, it was greater but fluctuated more peaking about 20 MJ m^{-2}. Most of R_n was consumed as H during the drier periods and as LE after rains. Variability in net irradiance, due to clouds affecting solar irradiance, impacts on the available energy. The daily total H and LE were greater but more consistent and lower respectively during the drier periods (winter and spring). By contrast, H and LE were lower and greater respectively during the wet periods (summer and autumn), as presented in Figs 6.6 and 6.7**.** Variability of H and LE from day to day and from season to season were mainly attributed to the rain events and net irradiance impacting on the available energy. The magnitude of the LE substantially increased after the end of the spring, peaked in midsummer and then decreased to a minimum in winter. In winter, the daily LE estimates were less than 4 MJ m^{-2} mainly due to SWC reduction and reduced R_n. Therefore, a larger portion of available energy A was consumed as sensible heat flux H (Figs 6.6 and 6.7). In summer, the LE peaked at 15 MJ m^{-2}, representing the dominant component of the energy balance as a result of increase in R_n and SWC. The magnitude of the soil heat flux G changed with the change in R_n, soil shading, and SWC which depends on rainfall. Daily G had the smallest magnitude of the energy balance components, ranging between 0.1 and 0.3 MJ m^{-2}. Daily G decreased at the beginning of the experiment because of the increase in crop growth and leaf cover (LAI) reducing the solar irradiance reaching the soil surface. The decrease in G accessed more energy for partitioning between LE and H.

Generally, the TV method including adjustment for air temperature skewness and the SR methods are relatively similar in the estimating of sensible heat and latent energy fluxes on a daily basis, as shown in Figs 6.6 and 6.7.

The daily estimate of evaporation E (mm) using EC, the TV method, including adjustment for air temperature skewness, and the SR method, the available energy flux A (mm), daily total rainfall (mm) and daily average soil water content (mm) are illustrated in Fig 6.8. The daily total rainfall (mm) and daily average soil water content (mm) is repeated (Fig. 6.8) for convenience. In summer, daily total evaporation was high with a maximum value of about 7.5 mm day^{-1} because of the high solar irradiance, soil water content and

(**a**)

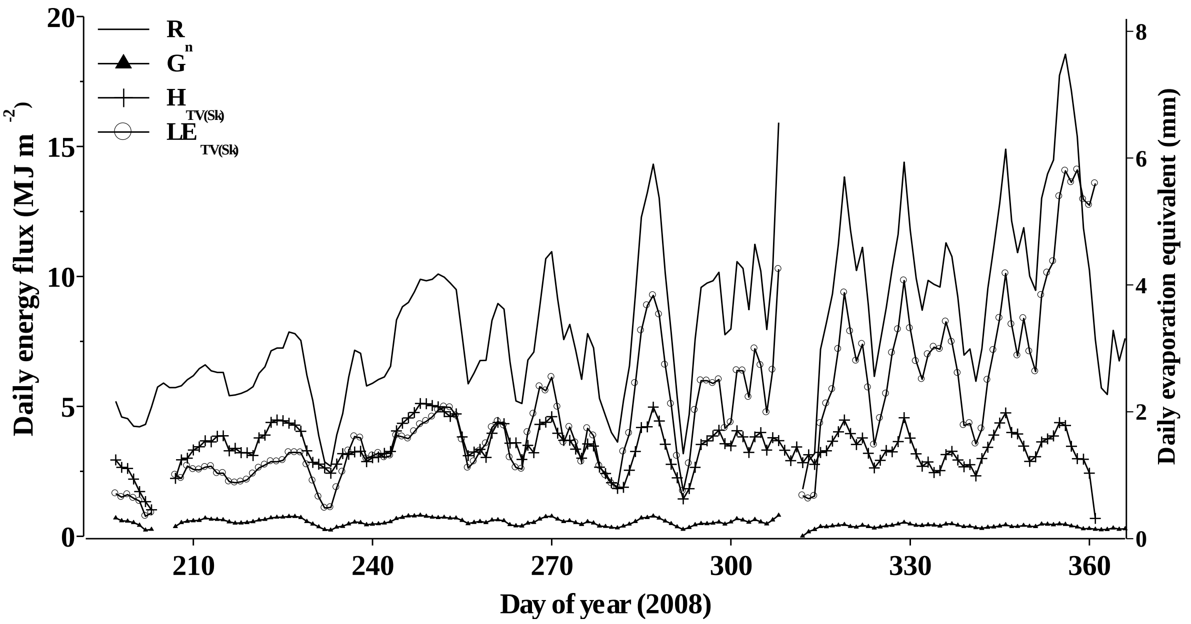

(**b**)

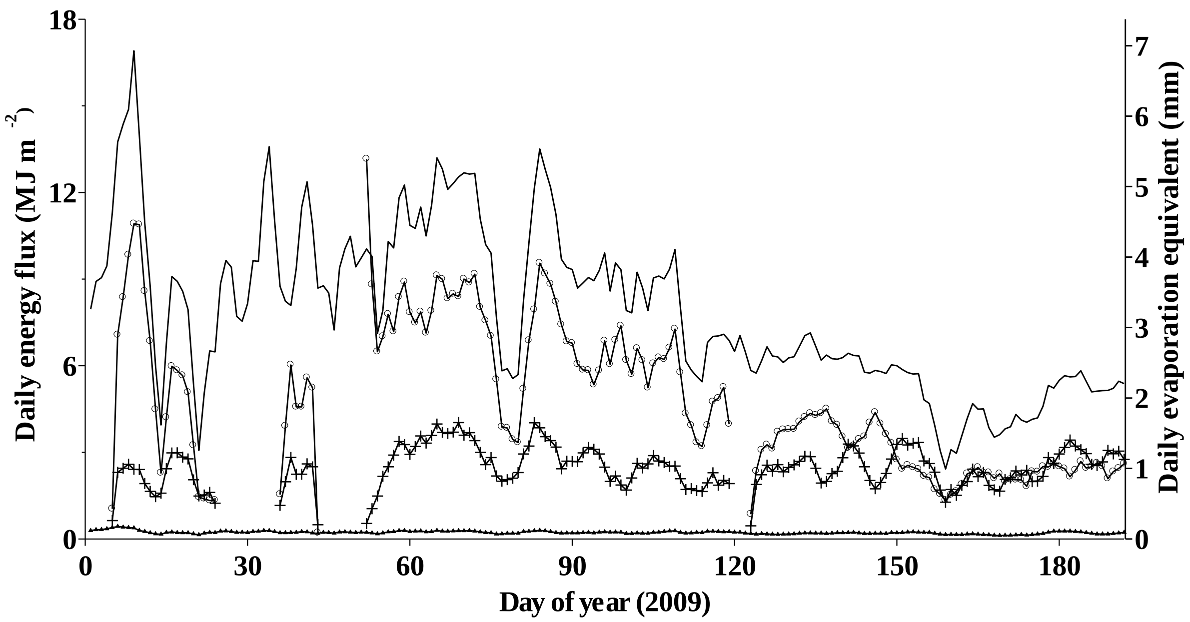

Fig. 6.6 Daily total energy balance components including R_n, G, $H_{TV(Sk)}$ and $LE_{TV(Sk)}$ sugarcane canopy for unstable conditions for a one-year period: (a) day of year 192 to 366 (2008); (b) day of year 1 to 192 (2009).

(**a**)

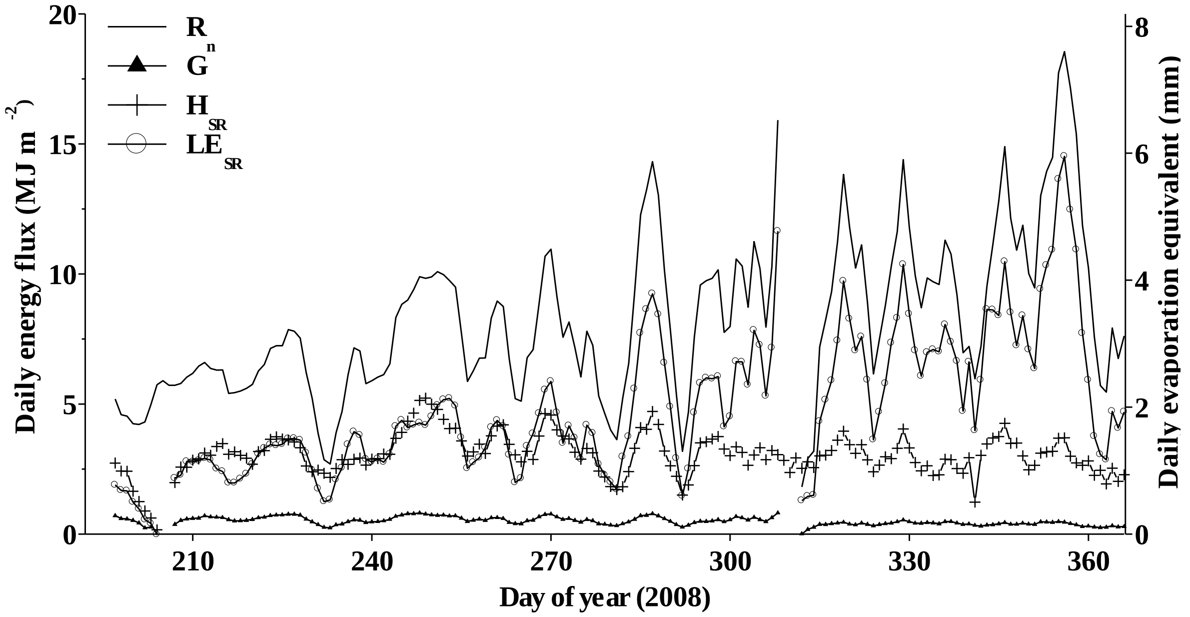

(**b**)

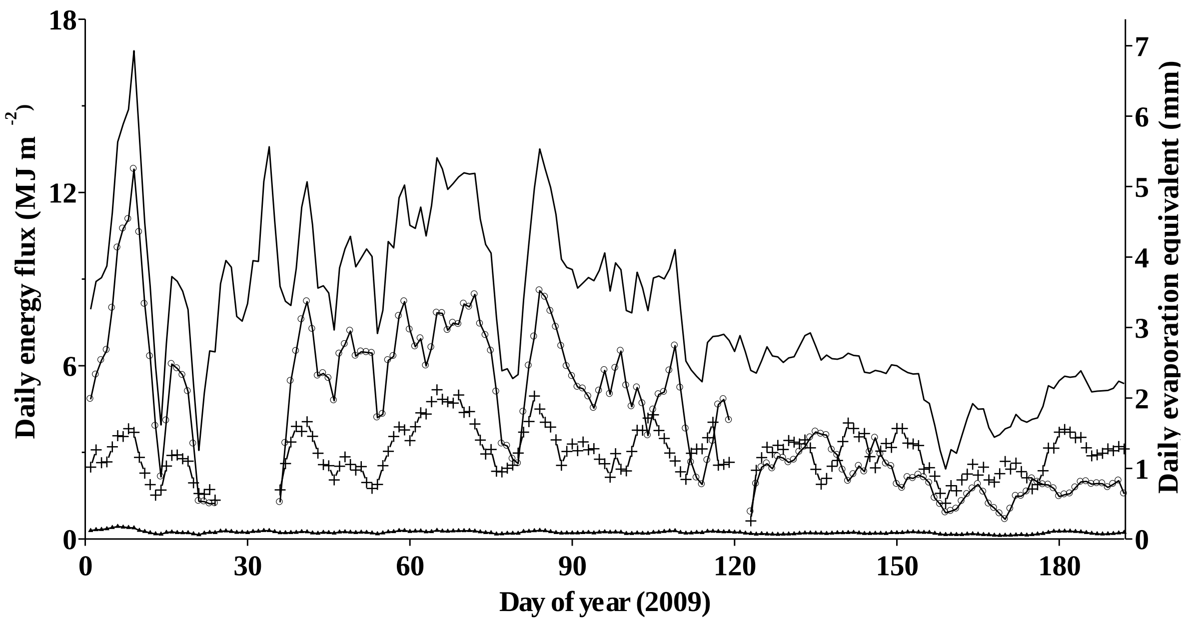

Fig. 6.7 Daily total energy balance components including R_n, G and H_{SR} and LE_{SR}, estimates at a height of 1.50 m above the sugarcane canopy and using an air temperature time lag of 0.8 s, for unstable conditions for a one year period: (a) day of year 192 to 366 (2008); (b) day of year 1 to 192 (2009).

increased leaf area index. Therefore, a large portion of available energy was consumed by evaporation. In winter, the daily total evaporation was relatively low with a maximum value of about 1.2 mm day^{-1}. Previously reported values of the daily total evaporation from sugarcane in the KwaZulu-Natal midlands was around 5 mm day^{-1} in summer and was about 2 mm day^{-1} in winter (Burger, 1999; Wiles, 2006). The daily average sugarcane evaporation for the entire measurement period was 2.06 mm day^{-1}. Watanabe *et al*. (2004) who carried out an experiment above different surfaces to study changes in evaporation, soil water and crop coefficients in sugarcane, cassava and maize fields, reported that the average daily sugarcane evaporation varied between 2 to 6 mm day^{-1} during the wet periods but remained around 1 mm day^{-1} during the drier periods. It is noticeable that the daily total evaporation estimates followed the changes in the available energy flux (Fig. 6.8). It would appear that the system was energy limited rather than soil water content limited because of the high clay content in the soil. On a daily basis for evaporation estimation, the correspondence between the measurements using the TV and EC methods is very good. The SR measurement trend followed that of the EC method but underestimated evaporation from day of year 60 (2009) to the end of the experiment. This may be attributed to the fact that the weighting factor changed with increase of the crop height. The sum of the potential evaporation relative to sum of the actual evaporation was approximately 0.5 for the study period.

The issue of whether sugarcane production is a stream flow reduction activity (SFRA) or not is beyond the scope of the current investigation, although SFRA is defined in the 1998 South Africa water act in Section 36, this definition may be difficult to interpret and apply in this particular case . The collected data may however be useful in this regard.

6.4.5 Footprint

The estimation of the footprint for H and LE is necessary for agricultural and environmental studies since the footprint determines the relative influence of the underlying surface area on the measurement fluxes.

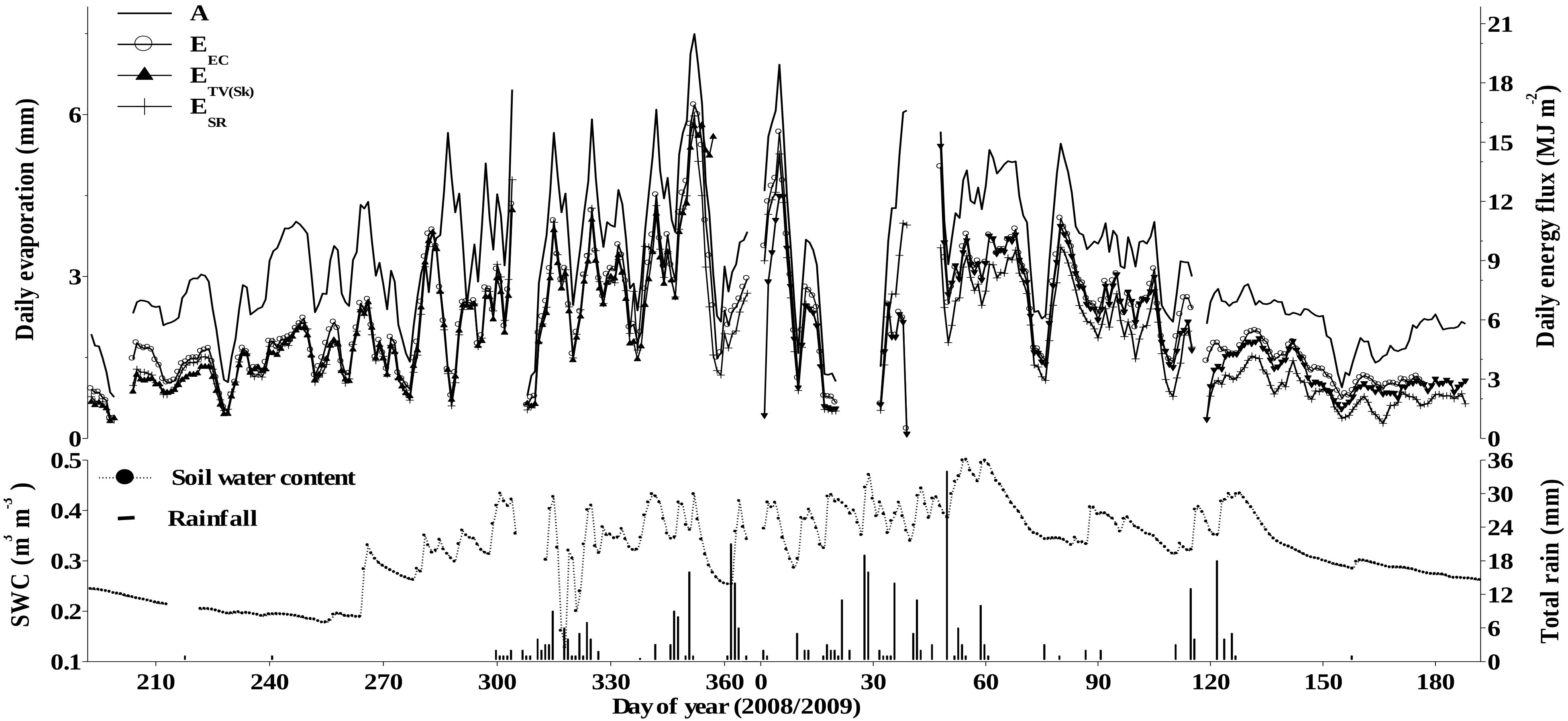

Fig. 6.8 Variation in daily total evaporation estimates (mm) using EC, TV and SR methods, the available energy flux (MJ m^{-2}), daily total rainfall (mm) and daily average *SWC* (m^3 m^{-3}).

The magnitude of the estimated footprint and the cumulative fraction of measured sensible flux to the surface source flux ratio for four selected days for unstable conditions are presented in Fig. 6.9a and b respectively. The days chosen were cloudless and covered different seasons involving winter (day of year 194, 2008), spring (251, 2008), summer (351, 2008), and autumn (83, 2009). The peak location of footprint for each day is also shown in Fig. 6.9a. Since the main aim is to estimate evaporation, all calculations of footprint were done for unstable conditions using Obukhov length L_o values (m), EC-estimated friction velocity u_* and sensible heat flux H_{EC} at midday (the peak of the measured fluxes). The peak location of the footprint differed from day to day as shown in Fig. 6.9a. This is mainly attributed to the change in Obukhov length L_o, plant height and measurement height. Previous studies found the peak location of footprint varies with atmospheric stability (Kljun *et al.*, 2004; Savage *et al.*, 2004; Mengistu, 2008). The cumulative fraction of the measured H to the surface source flux S_o ratio is greater than 0.93 during spring and summer and around 0.91 during winter and autumn for a fetch distance x of 97 m of the experiment site.

The cumulative fraction of the measured flux F to surface source flux S_o ratio at15 m above the soil surface for a windy day (day of year 235, 2008) and at 2.78 m for calm day (day of year 360, 2008) was calculated and presented along with wind speed U (m s^{-1}), Lo and H_{EC} in Tables 6.1 and 6.2. These comparisons were done to demonstrate the impact of wind speed on the footprint. The cumulative fraction of the measured flux F to surface source flux S_o ratio increased with decrease wind speed and decreased with increase wind speed (Tables 6.1 and 6.2). The cumulative fraction of the measured flux F to surface source flux S_o ratio was 0.86 for a windy day (Table 6.1) and 0.89 for a calm day (Table 6.2). This analysis indicated that 86 % of the measured flux came from the upwind fetch of 97 m for a windy day and 89 % for a calm day. These results indicated that the large fetch is needed during windy seasons and greater measurement heights.

(**a**)

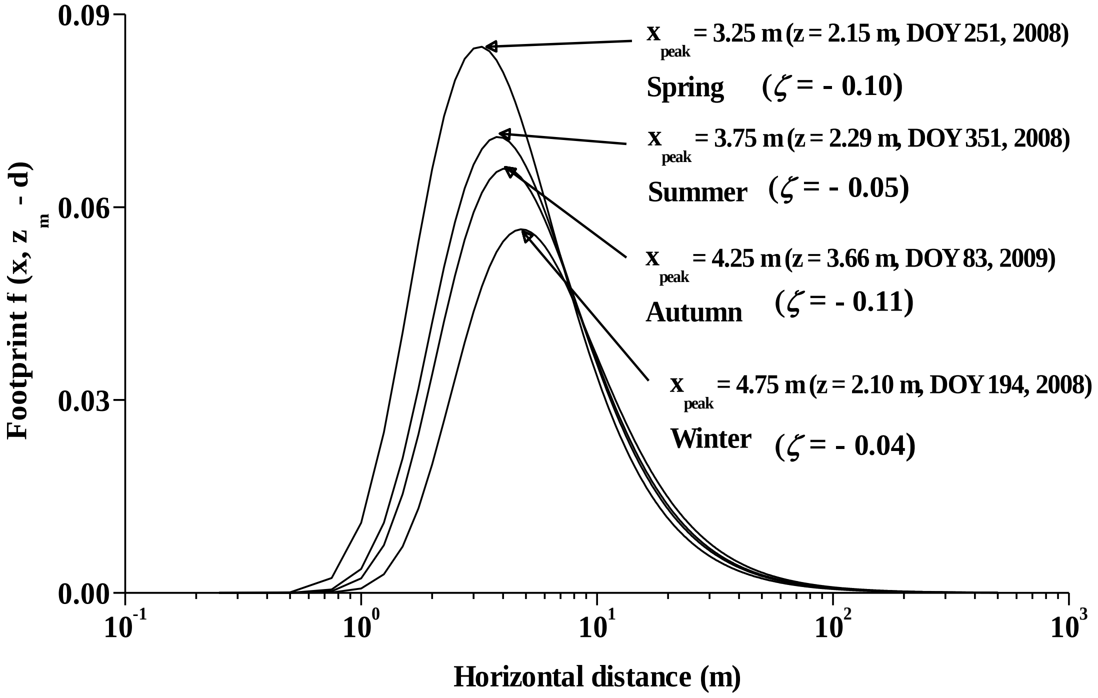

(**b**)

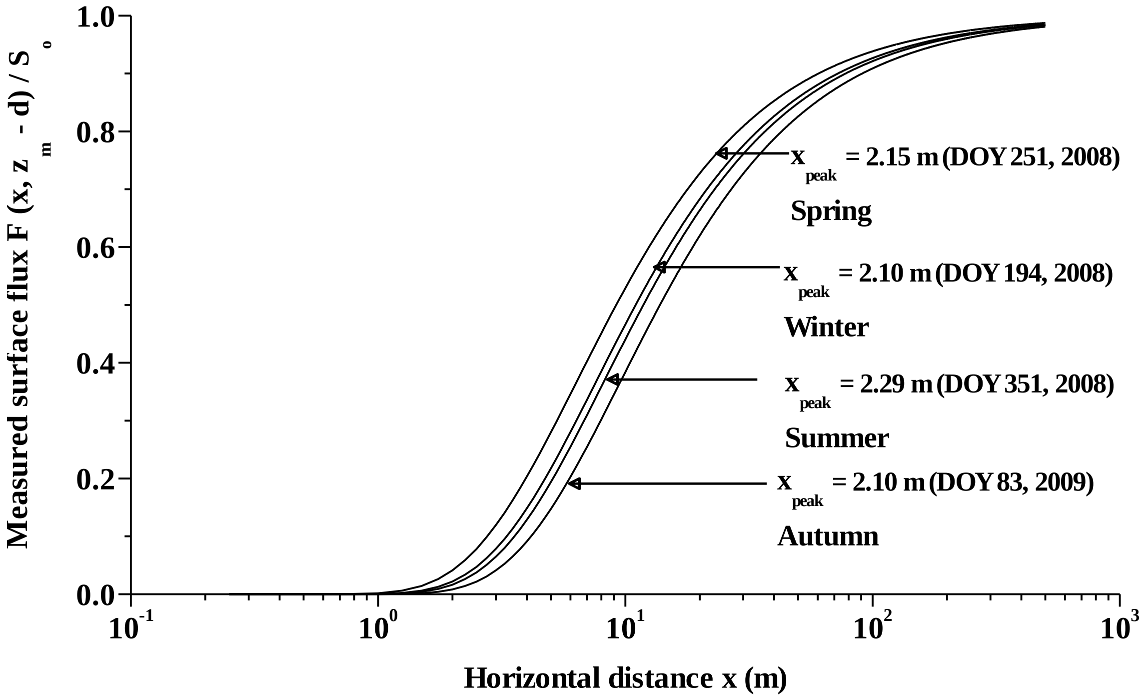

Fig. 6.9 (a) The estimated footprint and (b) the cumulative fraction of the measured flux F to surface source flux S_o ratio at midday for four selected days covering different seasons in 2008 and 2009, based on the Obukhov length estimated from EC measurements.

Table 6.1 The cumulative fraction of the measured flux F to surface source flux S_o ratio, wind speed U (m s^{-1}), L_o (m), ζ and H_{EC} at 2.15 m above the soil surface from 6h00 to 18h00 for a windy day (day of year 235, 2008).

Time	U (m s^{-1})	L_o (m)	ζ	H (W m^{-2})	F / S_o
600	3.12	103.96	-0.01	-60.14	0.84
700	1.94	115.94	-0.01	-10.64	0.83
800	1.26	-40.32	-0.03	32.15	0.89
900	1.66	-23.33	-0.06	76.06	0.91
1000	3.22	-52.46	-0.03	131.59	0.88
1100	3.33	-46.04	-0.03	154.58	0.88
1200	3.86	-76.47	-0.02	123.65	0.86
1300	4.89	-145.05	-0.01	107.03	0.82
1400	4.40	-249.32	-0.01	46.83	0.78
1500	3.58	123.09	0.01	-68.69	0.83
1600	3.37	100.59	0.01	-48.67	0.84
1700	3.01	68.70	0.02	-50.17	0.86
1800	1.58	14.66	0.08	-28.28	0.93
					0.86

Table 6.2 The cumulative fraction of the measured flux F to surface source flux S_o ratio, wind speed U (m s^{-1}), L_o (m), ζ and H_{EC} at 2.63 m above the soil surface from 6h00 to 18h00 for a calm day (day of year 360, 2008).

Time	U (m s^{-1})	L_o (m)	ζ	H (W m^{-2})	F / S_o
600	0.41	-1.12	-1.29	3.05	0.96
700	0.40	-3.81	-0.38	6.02	0.95
800	0.53	-4.66	-0.31	9.91	0.96
900	0.56	-2.62	-0.55	28.30	0.96
1000	0.78	-3.41	-0.42	36.35	0.95
1100	0.78	-4.57	-0.32	66.59	0.94
1200	1.10	-8.77	-0.17	57.89	0.92
1300	1.15	-15.61	-0.09	49.10	0.90
1400	1.31	-32.35	-0.05	26.24	0.86
1500	1.52	-79.09	-0.02	18.67	0.83
1600	1.83	-119.20	-0.01	18.91	0.82
1700	1.69	-134.74	-0.01	14.68	0.73
1800	2.07	-464.45	-0.003	7.38	0.79
					0.89

6.5 Summary and conclusions

The EC, TV, and SR methods were used to estimate H from which latent energy flux was calculated, as a residual of the shortened energy balance, over sugarcane canopy at the Ba ynesfield Estate in KwaZulu-Natal for a one-year period. The input data for the TV method, including adjustment for air temperature skewness and the SR method are high frequency air temperature data obtained by using unshielded and naturally-ventilated type-E fine-wire thermocouples. The third-order air temperature structure function allows unstable conditions to be identified. In this study, the energy balance components and evaporation for commercial sugarcane were highlighted using EC, TV method 2 and the SR method. The daily total $H_{TV(Sk)}$, and H_{SR} estimates using an air temperature time lag of 0.8 s showed quite good agreement with H_{EC} for all measurement heights. The best results were obtained at heights of 0.50 and 1.50 m above the crop surface for H_{SR} and $H_{TV(Sk)}$ estimates respectively. Evaporation and energy balance components varied with time throughout the day, from day to day, and from season to season due to the variation in environmental conditions such as R_n due to cloud, and rainfall occurrence. The daily total evaporation was high in summer and represents a significant component of the energy balance, and was low in winter. The average daily evaporation for the whole period was 2.06 mm day^{-1}. The footprint analysis for sensible heat flux indicated more than 91 % of the measured sensible heat flux was from the experimental site for which the fetch distance was 97 m. The TV method 2 and the SR method both showed promise as reasonably simple and does not require calibration or validation compared to the SR method. This study proved that the long-term sensible heat flux estimates using both methods TV, adjusted for air temperature skewness, and SR methods are accurate at 0.15 m and 0.2 m above the crop surface respectively. Therefore evaporation can be estimated if the other components of the energy balance are measured accurately.

Chapter 7: General summary, conclusions and recommendations for future research

7.1 Summary and conclusions

Demands for water in sugarcane areas have a significant impact on sugarcane production. Therefore, accurate evaporation data is needed for irrigation scheduling, for more efficient use of the available water resources and for management purposes. Sensible heat flux *H* measurements and measurements of net irradiance and soil heat flux have an important role in providing real-time estimates of evaporation by using the shortened energy balance. Searching for an accurate and low-cost method for estimating *H* was the main aim of this study. Included in the methods investigated are the temperature variance (TV) and surface renewal (SR) method, the latter requiring a calibration against eddy covariance (EC) method, which are more simple in terms of post-processing data corrections applied with a reduced power requirement compared to other methods. The TV and SR methods require high-frequency air temperature data which is obtained by using an unshielded and naturally-ventilated type-E fine-wire thermocouple. The TV and SR methods for estimating *H* have been applied above annual cereal crops but there has been no published work involving biannual crops such as sugarcane. The overall aim of this research was therefore to estimate *H* over sugarcane using TV and SR methods and hence evaporation over sugarcane. The study therefore deals with the comparison of TV and SR measurements of *H* against that using the standard EC method.

High frequency air temperature data were collected using unshielded and naturally-ventilated type-E fine-wire thermocouples at the Baynesfield Estate in KwaZulu-Natal, South Africa, to estimate sensible heat flux for daytime unstable conditions using the TV and SR methods at heights of 0.20, 0.50, 0.75 and 1.50 m above a sugarcane canopy for air temperature time lags of 0.4 and 0.8 s. The latent energy flux for each height and air temperature time lag was then estimated as a residual of the shortened energy balance equation. The performance of the different approaches of TV and SR methods for sensible heat flux estimation were evaluated against EC over sugarcane in order to test their reliability for long-term estimation of evaporation.

The ideal SR analysis model method based on an air temperature structure function analysis approach was calibrated and validated against the EC method above the sugarcane canopy using non-overlapping data sets for daytime unstable conditions during 2008. During the calibration period, the SR weighting factor (α), defined as a factor that corrects for the unequal amount of the heating from the measurement height z to the ground, was determined for each height and air temperature time lag from simultaneous SR and EC measurements. The magnitude of α ranged from 0.66 to 0.55 for all measurement heights for an air temperature time lag of 0.8 s. The α value increased with a decrease in measurement height and an increase in air temperature time lag. For the validation data set, the SR sensible heat flux (H_{SR}) estimates corresponded well with EC sensible heat flux (H_{EC}) for all heights and both air temperature time lags. The agreement between H_{SR} and H_{EC} improved with a decrease in measurement height for the air temperature time lag of 0.8 s. The best H_{SR} *vs* H_{EC} comparisons were obtained for a height of 0.20 m above the crop canopy using $\alpha = 0.66$ for an air temperature time lag of 0.8 s. The residual estimates of latent energy flux by SR and EC methods were in good agreement. The LE_{SR} at a height of 0.20 m above the canopy yielded the best comparisons with LE_{EC} estimated as a residual.

The performance of the TV methods in estimating sensible heat flux, including adjustment for stability (method 1) and adjusted for air temperature skewness (method 2), and the sensible heat flux from MOST and using a spatial second-order air temperature structure function (method 3) and their free convection limits forms were evaluated above sugarcane for daytime unstable conditions within the roughness and the inertial sub-layers by comparison with EC measurements. The performance of the TV methods was good for measurements either within the roughness sub-layer or within the inertial sub-layer and more improved with increase in measurement height. The sensible heat flux using method 3 was reasonable but biased with the comparison improved for an air temperature time lag of 0.8 s. Improved comparisons were obtained at a height of 1.50 and 0.75 m above the crop surface for the TV methods and method 3 respectively. Overall, the TV method, adjusted for air temperature skewness, was superior in estimating sensible heat and latent energy flux, the latter compared to the other temperature–based methods when compared to EC method. The free convection limit forms of the TV methods and method 3 provided poor estimates of sensible heat flux with significant bias when compared to H_{EC}.

The performance of SR models methods was evaluated for daytime unstable conditions in the roughness and inertial sub-layers when the sugarcane was sparse and dense. Sensible heat flux estimates using the original SR and other SR approaches are comparable with H_{EC}. The α was determined by plotting H_{SR} *vs* H_{EC} for each measurement height and both air temperature time lags. The SR weighting factor (α') was also calculated using friction velocity and a stability function. The value of α' increased with decrease in measurement height for the 0.8-s air temperature time lag. It is observed that α' values were greater compared to α. The sensible heat flux estimated using the original SR approach for which α value is determined by calibration with EC yielded more-accurate estimates than when α' was calculated using friction velocity and a stability function. Various other SR estimates applied to the roughness sub-layer, one using a finite micro-front ramp SR model, another using K-theory and others that combine SR and MOST and their free convection forms produced very good H_{SR} estimates. Improved H_{SR} estimates were observed using a combined SR method and K-theory approach. The combined SR method and MOST approach that either uses an air temperature standard deviation or an air temperature structure function performed well in the inertial sub-layer. Their respective free convection forms poorly performed. The performance of the original and other SR approaches was improved when the crop was dense because it was more homogeneous. The H_{SR} estimates obtained by the combined SR model and K-theory were superior compared to those obtained using the other approaches.

Long-term estimates of *H* and evaporation as a residual were obtained using EC, TV method 2 and SR methods. The sign of the third-order air temperature structure function was used to identify unstable conditions. The daily total $H_{TV(Sk)}$, and H_{SR} estimates for all measurement heights using an air temperature time lag of 0.8 s showed quite good agreement with H_{EC}. The best results were obtained at heights of 0.50 and 1.50 m above the crop surface for H_{SR} with slope = 0.96 and RMSE = 0.46 MJ m^{-2}, and $H_{TV(Sk)}$ with slope = 0.95 and RMSE = 0.50 MJ m^{-2}, respectively. Seasonal variation of the energy balance components and evaporation using EC, TV method 2 at a height 1.50 m above the crop surface and SR method at heights of 0.5 m above the sugarcane (using air temperature time lag of 0.8 s and calibrated using α = 0.62) were investigated for a one-year period. Evaporation and energy balance components varied with time throughout the day, from day to day, and from season to season due to the variation in environmental conditions such as net irradiance due to cloud, and rainfall occurrence. The daily total evaporation was high in summer and represents a significant component of the energy balance, and is relatively low in winter. The average daily evaporation for the whole period was 2.06 mm day^{-1}. The footprint analysis for sensible heat flux was performed to determine the cumulative fraction of measured sensible flux to the surface source flux ratio, and the peak location of the footprint during unstable conditions. The analysis indicated that more than 91 % of the measured sensible heat flux was from the experimental site for which the fetch distance was 97 m.

Overall, the average daily evaporation for the whole period was 2.06 mm day^{-1} with a maximum value of 7.5 mm day^{-1} in summer and a lower value of 1.2 mm day^{-1} in winter. The TV method 2 at 1.50 m above the crop surface and the SR method (using $\alpha. = 0.66$) at 0.5 m using time lag of 0.8 s showed promise as reasonably inexpensive and simple methods with low-power requirements compared to other methods. The TV method 2 does not require calibration or validation compared to the SR method. This study proved that the long-term sensible heat estimates using both methods are accurate. Therefore evaporation can be estimated as a residual if the other components of the energy balance are measured accurately.

7.2 Recommendations for future research

As a result of this study, the following suggestions, which could contribute to successful management of the available water resources, are recommended for future research. Such research should cover a large sugarcane area or other agriculture plantation areas. Generally, the large aperture scintillometer (LAS) is better suited to remote sensing studies. However it is more expensive. The validation of the remote sensing data would need different measurement points which would require a number of LAS instruments. The TV or SR instruments can possibly be repeated many times within the study area with low cost compared to LAS. Therefore combined land-based sensible heat flux and evaporation estimates using TV and/or SR method with those obtained from remote sensing would result in a greater understanding of the energy balance components and evaporation, and for more efficient use of available water resources.

Future SR research could involve methods that do not require calibration against EC sensible heat flux measurements. Some initial research on this aspect, by Spano *et al.* (2000), indicated that SR measurements at different heights may allow estimates of sensible heat flux for different layers independent of EC measurements. Since the thermocouple is sensitive to damage, one-dimensional sonic anemometers could be used to measure air temperature for each layer. Therefore a number of the one-dimensional sonic anemometers would be needed which would make it as expensive as a three-dimensional sonic anemometer. The advantages of this method are that it can be applied when the fetch is limited, the data does not need coordinate rotation analysis and correction for water vapour and β compared to EC and does not require calibration.

The emphasis of this study is on unstable conditions between 06h00 and 18h00 even though it is recognized that for very low wind speed corresponding to weak turbulence, coherent structures may not be presented. Therefore the performance SR method could be tested for different atmospheric stability conditions.

The other area of research for the future could involve inexpensive methods, such as TV and SR methods, using the mean, standard deviation and structure function of various scalars measurements – specific humidity and mole fraction of carbon dioxide, for example. These investigations could allow direct estimates of *LE*, without resorting to residual estimation of *LE*, and the carbon dioxide flux. Since water use efficiency (WUE) = CO_2 flux / *LE*, measurements of both would yield a direct estimation of water use efficiency. The data of this study could be useful to determine whether or not sugarcane production could be regarded stream flow reduction activity.

References

Albertson, J.D., Parlange, M.B., Katul, G.G., Chu, C.-R., Stricker, H., Tyler, S., 1995. Sensible heat flux from arid regions: a simple flux variance method. Water Resour. Res. 31, 969–973.

Allen, R.G., Pereira, L.S., Raes, D., Smith, M., 1998. Crop Evapotranspiration - Guidelines for computing crop requirements - FAO Irrigation and drainage paper 56. FAO – Food and Agriculture Organization of the United Nations, Rome, Italy. 315 pp.

Allen, R.G., Pruitt, W.O., Wright, J.L., Howell, T.A., Ventura, F., Snyder, S., Itenfisu, D., Steduto, P., Berengena, J., Yrisarry, J.B., Smith, M., Pereira, L.S., Raes, D., Pereira, L., Alves, I., Walter, V., Elliott, R., 2006. A recommendation on standardized surface resistance for hourly calculation of reference ETo by the FAO56 Penman-Monteith method. Agric. Water Manage. 81, 1−20.

Anandakumar, K., 1999. Sensible heat flux over a wheat canopy: optical scintillometer measurements and surface renewal analysis estimations. Agric. For. Meteorol. 96, 145−156.

Angus, D.E., Watts, P.J., 1984. Evapotranspiration - how good is the Bowen ratio method? Agic. Water Manage. 8, 133–150.

Arya, S.P., 2001. Introduction to Micrometeorology. 2nd edition. Academic Press. London, UK. 420 pp.

Aubinet, M., 1997. Comparison between different methods of measurement of momentum and sensible heat fluxes over canopies. Biotechnol. Agron. Environ. 1, 17−25.

Baldocchi, D.D., 2003. Assessing the eddy covariance technique for evaluating carbon dioxide exchange rates of ecosystem: past, present and future. Global Change Biol. 9, 1–14.

Bazza, M., 2005. Policies for water management and food security under water-scarcity conditions: The case of GCC countries. In: 7th Gulf Water Conf. 19-23 November, Kuwait, Kuwait.

Blanken, P. D., Black, T.A, Neumann, H.H., Den Hartog, G., Yang, P.C., Nesic, Z., Lee, X., 2000. The seasonal water and energy exchange above and within a boreal aspen forest. J. Hydrol. 245, 118−136.

Brotzge, J.A., Crawford, K., 2003. Examination of the surface energy budget: a comparison of eddy correlation and Bowen ratio measurement systems. J. Hydrometeorol. 4, 160–178.

Brutsaert, W., 1982. Evaporation into the Atmosphere, D. Riedel Publishing Company, Dordrecht, Holland. 299 pp.

Burba, G.G., Verma, S.B., 2005. Seasonal and interannual variability in evapotranspiration of native tallgrass praire and cultivated wheat ecosystems. Agric. For. Meteorol. 135, 190−201.

Burger, C., 1999. Comparative evaporation measurements above commercial forestry and sugarcane canopies in the KwaZulu-Natal. M.Sc. Agric. thesis, University of Natal, Pietermaritzburg, South Africa. 125 pp.

Businger, J.A., Wyngaard, J.C., Izumi, I., Bradley, E.F., 1971. Flux profile relationships in the atmospheric surface layer. J. Atmos. Sci. 28, 181−189.

Calder, K.L., 1952. Some recent British work on the problem of diffusion in the lower atmosphere. In: Proc. of the US Tech. Conf. on Air Poll. McGraw-Hill, New York, USA. 787-792.

Castellví, F., 2004. Combining surface renewal analysis similarity theory: A new approach for estimating sensible heat flux. Water Resour. Res. 40, W05201, doi:10.1029\2003WR002677.

Castellví, F., Martínez-Cob, A., 2005. Estimating sensible heat flux using surface renewal analysis and flux variance method: A case study over olive trees at Sastago (NE of Spain). Water Resour. Res. 41, W09422, 1−10.

Castellví, F., Martínez-Cob, A., Perez-Coveta, O., 2006a. A comparison of a new existing equations for estimating sensible flux using surface renewal and similarity concepts. Water Resour. Res., 42, W08406, doi:10.1029\2005WR004642, 2006.

Castellví, F., Martinez-Cob, A., Perez-Coveta, O., 2006b. Estimation of sensible and latent heat fluxes over rice using surface renewal. Agric. For. Meteorol. 139, 164–169.

Castellví, F., Perez, P.J., Ibanez, M., 2002. A method based on high-frequency temperature measurements to estimate the sensible heat flux density avoiding the height dependence. Water Resour. Res. 35, W01048, doi:10.1029\2001WR000486.

Castellví, F., Snyder, R.L., 2009a. On the performance of surface renewal analysis to estimate sensible heat flux over two growing rice fields under the influence of regional advection. J. Hydrol. 375, 546−553.

Castellví, F., Snyder, R.L., 2009b. Sensible heat flux using surface renewal analysis. A study case over a peach orchard. Agric. For. Meteorol. 149, 1397–1402.

Castellví, F., Snyder, R.L., Baldocchi, D.D., 2008. Surface energy-balance closure over rangeland grass using the eddy covariance method and surface renewal. Agric. For. Meteorol. 148, 1147−1160.

Cellier, P., Brunet, Y., 1992. Flux-gradient relationships above tall plant canopies. Agric. For. Meteorol. 58, 93–117.

Chen, W., Novak, M.D., Black, T.A., Lee, X., 1997a. Coherent eddies and temperature structure functions for three contrasting surfaces. Part I: Ramp model with finite micro front time. Boundary-Layer Meteorol. 84, 99−123.

Chen, W., Novak, M.D., Black, T.A., Lee, X., 1997b. Coherent eddies and temperature structure functions for three contrasting surfaces. Part II: Renewal model for sensible heat flux. Boundary-Layer Meteorol. 84, 125−147.

Choi, T., Hong, J., Kim, J., Lee, H., Asanuma, J., Ishikawa, H., Tsukamoto, O., Zhiqiu, G., Ma, Y., Ueno, K., Wang, J., Koike, T., Yasunari, T., 2004. Turbulent exchange of heat, water vapour, and momentum over a Tibetan prairie by eddy covariance and flux variance measurements. Geophys. Res. 109, D21106, doi:10.1029/2004JD004767, 2004.

Czikowsky, M.J., Fitziarrald, D.R., 2004. Evidence of seasonal changes in evapotranspiration in eastern U. S. hydrological records. J. Hydrometeorol. 5, 974−988.

Dabberdt, W.F., Lenschow, D. H., Horst, T.W., Zimmerman, P.R., Oncley, S.P., Delany, A.C., 1983. Atmosphere-surface exchange measurements. Sci. 260, 1472 –1481.

de Bruin, H.A.R., Hartogensis, O.K., 2005. Variance method to determine turbulent fluxes of momentum and sensible heat in the stable atmospheric surface layer. Boundary-Layer Meteorol. 166, 385−392.

de Bruin, H.A.R., Kohsiek, W., Van Den Hurk, B.J.J.M., 1993. A verification of some methods to determine the fluxes of momentum, sensible heat and water vapour using standard deviation and structure parameter of scalar meteorological quantities. Boundary-Layer Meteorol. 63, 231−257.

Deardorf, J.W., 1983. Observed characteristics of the outer layer. AMS course on the planetary boundary layer. Boulder, Colorado (unpublished manscript).

Denmead, O.T., MacDonald, B.C.T., 2008. Whole-of-season evaporation and CO2 exchange by sugarcane crops. Geoph. Res. Abs. 10, EGU2008-A-05904.

Drexler, J.Z., Snyder, R.L., Spano, D., Paw U, K.T., 2004. A review of models and micrometeorological methods used to estimate wetland evapotranspiration. Hydrol. Process. 18, 2071−2101.

Duce, P., Spano D., Snyder, R.L., 1998. Effect of different fine-wire thermocouple design on high frequency temperature measuremnt. In: AMS 23th Conf. On Agricultural and Forest Meteorology. Albuquerque, NM, Nov. 2−6, 146-147.

Duce, P., Spano D., Snyder, R.L., Paw U, K.T., 1997. Surface renewal estimates of evapotranspiration; short canopies. Acta Hort. 449, 57−62.

Dyer, A.J., 1974. A review of flux-profile relationships. Boundary-Layer Meteorol. 7, 363–372.

Evett, S.R, 2002. Water and energy balances at soil-plant-atmosphere interfaces. In: Warrick, A.W. (Ed), Soil Physics Companion. CRC Press. Boca Raton, USA. 127–189.

Finnigan, J.J., Clements,R., Malhi, Y., leuning, R., Cleugh, H.A., 2003. A re-evaluation of long term flux measurement techniques:1. Averaging and coordinat rotation. Boundary-Layer Meteorol. 107, 1–48.

Gao, W., Shaw, R.H., Paw U, K.T., 1989. Observation of organized structure in turbulent flow within and above a forest canopy. Boundary-Layer Meteorol. 47, 349–377.

Gao, Z., Bian, L., Chen, Z., Sparrowl, M., Zhang, J., 2006. Turbulent variance characteristics of temperature and humidity over a non-uniform land surface for an agricultural ecosystem in China. Adv. Atmos. Sci. 23, 365−374.

Garratt, J.R., 1980. Surface influence upon vertical profiles in the atmospheric near-surface layer. Q. J. Roy. Meteorol. Soc. 106, 803–819.

Garratt, J.R., 1992. The Atmospheric Boundary Layer. Cambridge University Press, Cambridge, UK. 316 pp.

Gash, J.H.C., 1986. A note on estimating the effect of a limited fetch on micrometeorological evaporation measurements. Boundary-Layer Meteorol. 35, 409−413.

Göckede, M., Markkanen, T., Mauder, M., Arnold, K., Leps, J.P., Foken, T., 2005. Validation footprint models using natural tracer. Agric. For. Meteorol. 135, 314−325.

Graefe, J., 2004. Roughness layer corrections with emphasis on SVAT model applications. Agric. For. Meteorol. 124, 237–251.

Green, A.E., 2001. The practical application of scintillometers in determining the surface fluxes of heat, moisture and momentum. PhD thesis, Wageningen University, The Netherlands. 175 pp.

Grelle, A., Lindroth, A., Molder, M., 1999. Seasonal variation of boreal forest surface conductance and evaporation. Agric. For. Meteorol. 98−99, 563−578.

Gwoda, P.H., Chavez, J.L., Colaizzi, P.D., Evett, S.R., Howell, T.A., Tolk, J.A., 2008. ET mapping for agricultural water management: present status and challenges. Irrig. Sci. 26, 223−237.

Ham, J.M., Heilman, J.L., 2003. Experimental test of density and energy-balance corrections on carbon dioxide flux as measured using open-path eddy covariance. Agron. J. 195, 1393–1403.

Hanson, B., Bali, K., Orloff, S., Putnam, D., 2008. Estimating evapotranspiration of fully- and deficit-irrigated alfalfa in commercial fields with the eddy covariance and surface renewal methods. Paper presentation to the ASABE Annual International Meeting, 29 June to 2 July, Rhode Island, USA.

Harman, I.N., Finnigan, J.J., 2007. A simple unified theory for flow in the canopy and roughness sub-layer. Boundary-Layer Meteorol. 123, 339–363.

Haynes, R.J., Dominy, C.S., Graham, M.H., 2003. Effect of agricultural land use on soil organic matter status and the composition of the earthworm communities in KwaZulu-Natal, South Africa. Agric. Ecosy. Env. 95, 453−464.

Higbie, R., 1935. The rate of absorption of a pure gas into a still liquid during short periods of exposure. Trans. Amer. Inst. Chem. Eng. 31, 365–388.

Hill, R.J., 1992. Review of optical scintillation methods of measuring the refractive-index spectrum, inner scale and surface fluxes. Waves Random Media 2, 179−201.

Horst, T.W., Weil, J.C., 1992. Footprint estimation for scalar flux measurements in the atmospheric surface-layer. Boundary-Layer Meteorol. 59, 279−296.

Hsieh, C., Katul, G., 1996. Estimation of momentum and heat fluxes using dissipation and flux variance methods in the unstable surface layer. Water Resour. Res. 32, 2453−2462.

Hsieh, C., Katul, G., Chi, T., 2000. An approximate analytical model for footprint estimation of scalar fluxes in thermally stratified atmospheric flows. Adv. Water Resour. 23, 765−772.

Hsieh, C., Lai, M., Hsia, Y., Chang, Y., 2008. Estimation of sensible heat, water vapour, and CO_2 fluxes using the flux-variance method. Int. J. Biometeorol. 52, 521−533.

Humphreys, E.R., Black, T.A., Ethier, G.J., Drewitt, G.B., Spittlehouse, D.L., Jork, E.-M., Nesic, Z., Livingston, N.J., 2003. Annual and seasonal variability of sensible and latent heat fluxes above a coastal Douglas-fir forest, British Colombia, Canada. Agric. For. Meteorol. 115, 109−125.

Inman-Bamber, N.G., McGlinchey, M.G., 2003. Crop coefficients and water-use estimates for sugarcane based on long-term Bowen ratio energy balance measurements. Field Crops Res. 83, 125−138.

Jarmain, C., C.S. Everson, M.J. Savage, M.G. Mengistu, A.D. Clulow and M.B. Gush, 2009. Refining tools for evaporation monitoring in support of water resources management. Water Research Commission Report No. 1567, ISBN 978-1-77005-798-2. Pretoria, South Africa. 137 pp.

Kaimal, J.C., Finnigan, J.J., 1994. Atmospheric Boundary Layer Flows, Their Structure and Measurement. Oxford University Press, New York, USA. 289 pp.

Katul, G., Hsieh, C., Bowling, D., Clark, K., Shurpali, N., Turnipseed, A., Albertsons, J., Tu,K., Hollinger, D., Evans, B., Offerle, B., Anderson, D., Ellsworth, D., Vogel, C., Oren, R., 1999. Spatial variability of turbulent fluxes in the roughness sublayer of a new-aged pine forest. Boundary-Layer Meteorol. 93, 1–28.

Katul, G.G., Golz, S.M., Hsieh, C.I., Cheng, Y., Mowry, F., Sigmon, J., 1995. Estimation of surface heat and momentum fluxes using the flux-variance method above uniform and non-uniform terrain. Boundary-Layer Meteorol. 74, 237−260.

Katul, G.G., Hsieh, C., Oren, R., Ellsworth, D., Philips, N., 1996. Latent and sensible heat flux predictions from a uniform pine forest using surface renewal and flux variance methods. Boundary-Layer Meteorol. 80, 249−282.

Kljun, N., Calanca, P., Rotach, M.W., Schmid, H.P., 2004. A simple parameterization for flux footprint predictions. Boundary-Layer Meteorol. 112, 503−523.

Kustas, W.P., Blanford, J.H., Stannard, D.I., Daughtry, C.S.T., Nichols, W.D., Weltz, M.A., 1994. Local energy flux estimates for unstable conditions using variance data in semi-arid rangelands. Water Resour. Res. 30, 1351–1361.

Leclerc, M.Y., Thurtell, G.W., 1990. Footprint prediction of scalar fluxes using a Markovian analysis. Boundary-Layer Meteorol. 25, 247–258.

Lee, X., Black, T.A., 1993. Atmospheric turbulence within and above Douglas-fir stand. Part I: Statistical properties of the velocity field. Boundary-Layer Meteorol. 105, 119–127.

Lohou, F., Druilhet, A., Campistron, B., Redelsperger, J.L., Said, F., 2000. Numerical study of the impact of coherent structures on vertical transfers in the atmospheric boundary layer. Boundary-Layer Meteorol. 97, 361–383.

Luhar, A.K., Rao, K.S., 1994. Lagrangian stochastic dispersion model simulations of tracer data in nocturnal flows over complex terrain. Atmos. Env. 28, 3417−3431.

Mahrt, L., 2000. Surface heterogeneity and vertical structure of the boundary layer. Boundary-Layer Meteorol. 96, 33–62.

Mauder, M., Oncley, S.P., Vogt, R., Weidinger, T., Ribeiro, L., Bernhofer, C., Foken, T., Kosiek, W., De Bruin, H.A.R., Liu, H., 2007. The energy balance experiment EBEX-2000. Part II: Intercomparison of eddy-covariance sensors and post-field data processing methods. Boundary-Layer Meteorol. 123, 29–54.

McGlinchey, M.G., Inman-Bamber, N.G., 2002. Robust estimates of evapotranspiration for sugarcane. Paper presentation to the 76th Congress, South African Sugar Technologists, Association, 30 July to 2 August 2002, Durban, South Africa.

Mengistu, M.G., 2008. Heat and energy exchange above different surfaces using surface renewal. PhD thesis, University of KwaZulu-Natal, Pietermaritzburg, South Africa. 151 pp.

Mengistu, M.G., Savage, M.J. 2010. Surface renewal method for estimating sensible heat flux. Water SA. 36, 9–18.

Meyers, T.P., Baldocchi, D.D., 2005. Current micrometeorological flux methodologies with application in agriculture. In: Hatfield, J.L., Baker, J.M., (Eds), Micrometeorology in Agricultural Systems. Agronomy Monograph No. 47. Amer. Soc. Agron., Madison. pp. 381−396.

Monin, A.S., Obukhov, A.M., 1954. Basic laws of turbulent mixing in the atmosphere near the ground. Trudy. Akad. Nauk. 24, 163−187.

Monteith, J.L., Unsworth, M.H., 1990. Principles of Environmental Physics. 2nd ed. Edward Arnold, London, 291pp.

Moraes, O.L.L., Acevedo, O.C., Degrazi, G.A., Anfossi, D., da Silva, R., Anabor, V., 2005. Surface layer turbulence parameters over a complex terrain. Atmos. Environ. 39, 3103–3112.

Munro, D.S., Oke, T.R., 1975. Aerodynamic boundary-layer adjustment over a crop in neutral stability, Boundary-Layer Meteorol. 9, 53–61.

Nakamura, R., Mahrt, L., 2001. Similarity theory for local and spatially averaged momentum fluxes. Agric. For. Meteorol. 108, 265–279.

Novak, M.D., Chen, W., Orchansky, A.L., Ketler, R., 2000. Turbulent exchange processes within and above a straw mulch. Part II: Thermal and moisture regimes. Agric. For. Meteorol. 102,155–171.

Odhiambo, G.O., 2007. Long-tem measurements of spatially-averaged sensible heat flux for a mixed grassland community, using surface layer scintillometry. PhD thesis, University of KwaZulu-Natal, Pietermaritzburg, South Africa.151 pp.

Odhiambo, G.O., Savage, M.J., 2009. Sensible heat flux by surface layer scintillometry and eddy covariance over a mixed grassland community as affected by Bowen ratio and MOST formulations for unstable conditions. J. Hydrometeorol. 10, 479−492.

Oke, T.R., 1987. Boundary Layer Climates. Metheun, New York.

Olivier, F., Lecler, N., Singels, A., 2009. Increasing water use efficiency of irrigated sugarcane by means of specific agronomic practices. Water Research Commission Report No. 1577/1/09, ISBN 978-1-77005-883-5. Pretoria, South Africa. 127 pp.

Oncley, S.P., Foken, T., Vogt, R., Kohsiek, W., de Bruin, H.A.R., Bernhofer, C., Christen, A., van Gorsel, E., Grantz, D., Feigenwinter, C., Lehner, I., Liebethal, C., Liu, H., Mauder, M., Pitacco, A., Ribeiro, L., Weidinger, T., 2007. The energy balance experiment EBEX-2000. Part I: overview and energy balance. Boundary-Layer Meteorol. 123, 1−28.

Padro, J., 1993. An investigation of flux variance methods and universal functions applied to three land-use types in unstable conditions. Boundary-Layer Meteorol. 66, 413−425.

Panofsky, H.A., Dutton, J.A. 1994. Atmospheric Turbulence: Models and Methods for Engineering Applications. John Wiley and Sons, New York, USA. Pp. 397

Paw U, K.T., Baldocchi, D., Meyers, T.P., Wilson, K.B., 2000. Correction of eddy-covariance measurements incorporating both advective effects and density fluxes. Boundary-Layer Meteorol. 97, 487–511.

Paw U, K.T., Brunet, Y., 1991. A surface renewal measure of sensible heat flux density. In: Preprints, 20th Conference on Agricultural and Forest Meteorology, 10-13 September, Salt Lake City, Utah, American Meteorological Society, Boston, MA, pp. 52−53.

Paw U, K.T., Qui, J., Su, H.B., Watanabe, T., Brunet, Y., 1995. Surface renewal analysis: a new method to obtain scalar fluxes. Agric. For. Meteorol. 74, 119−137.

Paw U, K.T., Snyder, R.L., Spano, D., Su, H.B., 2005. Surface renewal estimates of scalar exchange. In: Hatfield, J.L., Baker, J.M. (Eds), Micrometeorology in Agricultural Systems. Agronomy Monograph no. 47. Amer. Soc. Agron., Madison. pp. 455−483.

Payero, J.O., Neale, C.M.U., Wright, J.L., Allen, R.G., 2003. Guidelines for validating Bowen ratio data. Trans. ASAE. 46, 1051–1060.

Raupach, M.R., Finnigan, J.J., Brunet, Y., 1989. Coherent eddies in vegetation canopies. In: Proc. 4th Australasian Conf. on Heat and Mass Transfer, Christchurch, New Zealand, May 9–12. Bergell House, New York. pp 75–90.

Raupach, M.R., Finnigan, J.J., Brunet, Y., 1996. Coherent eddies in vegetation canopies. In: The Mixing-layer analogy. Boundary-Layer Meteorol. 78, 351–382.

Rosegrant, M.W., Valmonte-Santos, R.A., Cline, S.A., Ringler, C., Li, W., 2005. Water resources, agriculture and pasture: Implications of growing demand and increasing scarcity. p. 227–249. In D.A. McGilloway (Ed) Grassland: A global resource. Proc. 2005 Int. Grassland Congr., Wageningen Academic Publ., The Netherlands.

Rosenberg, N.J., Blad, B.L., Verma, S.B., 1983. Microclimate: The Biological Environment. 2th edition. John Wiley and Sons, New York, USA. 495 pp.

Rosset, M., Riedo, M., Grub, A., Geissmann, M., Fuhrer, J., 1997. Seasonal variation in radiation and energy balances of permanent pastures at different altitudes. Agric. For. Meteorol. 86, 245−258.

SASA, 2009a. Crop data. Available at (http://www.sasa.org.za/Uploads/a73de3a7-bc60−4d53−9111e2b80e4537f3/Crop%20Data.pdf). Accessed, March 18, 2010.

SASA, 2009b. Variety information. Available at (http://www.sasa.org.za/Uploads/sasri/infosheet/VarietyN12.pdf). Accessed, March 18, 2010.

Savage, M.J., 2009. Estimation of evaporation using a dual-beam surface layer scintillometer and component energy balance measurements. Agric. For. Meteorol. 149, 501−517.

Savage, M.J., Everson, C.S., Metelerkamp, B.R., 1997. Evaporation measurement above vegetated surfaces using micrometeorological techniques. Water Research Commission Report No. 349/1/97, ISBN 1−86845−363−4. Pretoria, South Africa. 248 pp.

Savage, M.J., Everson, C.S., Metelerkamp, B.R., 2009. Bowen ratio evaporation measurement in a remote Montane grassland: Data integrity and fluxes. J. Hydrol. 376, 249−260.

Savage, M.J., Everson, C.S., Odhiambo, G.O., Mengistu, M.G., Jarmain, C., 2004. Theory and practice of evaporation measurement, with spatial focus on SLS as an operational tool for the estimation of spatially-averaged evaporation. Water Research Commission Report No. 1335/1/04, ISBN 1−77005−247−X. Pretoria, South Africa. 204 pp.

Savage, M.J., Heilman, J.L., 2009. Infrared calibration of net radiometers and infrared thermometers. Agric. For. Meteorol. 149, 501–517.

Savage, M.J., McInnes, K.J. Heilman, J.L., 1995. Placement hieght of eddy correlation sensors above s hort turfgrass surface. Agric. For. Meteorol. 74, 195–204.

Savelyev, S.A., Taylor, P.A., 2005. Internal boundary layers: 1. Height formulae for neutral and diabatic flows. Boundary-Layer Meteorol. 115, 1–25.

Schmid, H.P., 2002. Footprint modelling for vegetation atmosphere exchange studies: a review and perspective. Agric. For. Meteorol. 113, 159−183.

Sellers, P.J., Mintz, Y., Sud, Y.C., Dalcher, A., 1986. A simple biosphere model (SiB) for use within general circulation models. J. Atmos. Sci., 43, 505−531.

Shinichi, H., Kazuhikon, O., Atsushi, M., Yoshitaka, K., Shinji, K., Masato, I., 2004. Evapotranspiration characteristics of a field with sugarcane planted in summer in Miyako Island, Okinawa Prefecture. J. Japan. Trop. Agric. 48, 94−100.

Simmons, L.J., Wang, J. Sammis, T.W., Miller, D.R., 2007. An evaluation of two inexpensive energy-balance techniques for measuring water use in flood-irrigated pecans. Agric. Water Manage. 88, 181−191.

Snyder, R.L., Spano, D., Duce, P., Paw U, K.T., 1997. Surface renewal estimates of evapotranspiration. Theory. Acta Hort. 449, 49−55.

Snyder, R.L., Spano, D., Paw U, K.T., 1996. Surface renewal analysis for sensible heat and latent heat flux density. Boundary-Layer Meteorol. 77, 249−266.

South African National Water Act, 1998. Republic of South Africa governonment. Gazette, 26th August 1998, Act 36, No. 19182. Available at (www.info.gov.za/view/DownloadFileAction?id=70693). Accessed, 19th March, 2010.

Spano, D., Duce, P., Snyder, R.L., Paw U, K.T., 1997a. Surface renewal estimates of evapotranspiration: tall canopies. Acta Hort. 449, 63−68.

Spano, D., Snyder, R.L., Duce, P., Paw U, K.T., 1997b. Surface renewal analysis for sensible heat flux density using structure functions. Agric. For. Meteorol. 86, 259−271.

Spano, D., Snyder, R.L., Duce, P., Paw U, K.T., 2000. Estimating sensible and latent heat flux densities from grape vine canopies using surface renewal. Agric. For. Meteorol. 104, 171−183.

Spano, D., Synder, R.L., Duce, P., Paw U, K.T., Falk, M., 2002. Surface renewal determination of scalar fluxes over and old-growth forest. In: 25th Conf. on Agric. For. Meteorol., 19 25 May, Norfolk, Virginia, USA.

Stull, R.B., 1988. An Introduction to Boundary Layer Meteorology. Kluwer Academic Publishers, Dordrecht. 666 pp.

Sugita, M., Kawakubo, N., 2003. Surface and mixed-layer variance methods to estimate regional sensible heat flux at the surface. Boundary-Layer Meteorol. 106, 117-145.

Sun, X.M., Zhu, Z.L. Wen, X.F, Yuan,G.F, Yu, G.R., 2006. The impact of averaging period on eddy fluxes observed at ChinaFLUX sites Agric. For. Meteorol. 137, 188−193.

Swinbank, W.C., 1951. The measurement of vertical transfer of heat and water vapor by eddies in the lower atmosphere. J. Meteorol. 8, 135–145.

Tanner, C.B., 1960. Energy balance approach to evaporation from crops. Soil Sci. Soc. Proc. Amer. 24, 1−9.

Taylor, G.I., 1938. The spectrum of turbulence. Proc Roy. Soc London, Ser A 164, 476–490.

Thom, A.S., 1975. Momentum, mass and heat exchange in plant communities. In: Monteith, J.L. (Ed.), Vegetation and the Atmosphere. Principles. Volume 1. Academic Press. London, UK., pp. 57−109.

Tillman, J.E., 1972. The indirect determination of stability, heat and momentum fluxes in the atmospheric boundary layer from simple scalar variable during dry unstable conditions. J. Appl. Meteorol. 11, 783−792.

van Atta, C.W., 1977. Effect of coherent structures on structure functions of temperature in the atmospheric boundary layer. Arch. Mech. 29, 161−171.

van Dijk, A.I.J.M., Bruijnzeel, L.A., Schellekens, J., 2004. Micrometeorology and water use of mixed crops in upland, West Java, Indonesia. Agric. For. Meteorol. 124, 31−49.

Watanabe, K.,Yamamoto, T., Yamada, T., Sakuratani, T., Nawata, E., Noishana, C., Sributta, A., Higuchi, H., 2004. Changes in seasonal evapotranspiration, soil water content, and crop coefficients in sugarcane, cassava, and maize fields in Northeast Thailand. Agric. Water Manage. 67, 133−143.

Weaver, H.L., 1990. Temperature and humidity flux-variance relations determined by one-dimensional eddy correlation. Boundary-Layer Meteorol. 53, 77−91.

Weber, R.O., 1999. Remarks on the definition and estimation of friction velocity. Boundary-Layer Meteorol. 93, 197−209.

Weiss, A.I., 2002. Determination of thermal stratification and turbulence of the atmospheric surface layer over various types of terrain by optical scintillometry. PhD dissertation, Institute for Atmospheric and Climate Sciences, Eth Zurich, Switzerland.

Wesely, M.L., 1988. Use of variance techniques to measure dry air–surface exchange rates. Boundary-Layer Meteorol. 44, 13–31.

Wesson, K.H., Katul, G., Lai, C.-T., 2001. Sensible heat flux estimation by flux variance and half-order time derivative methods. Water Resour. Res. 37, 2333−2343.

Wever, L.A., Flanagan, L.B., Carlson, P.J., 2002. Seasonal and inteannual variation in evapotranspiration, energy balance and surface conductance in a northern temperate grassland. Agric. For. Meteorol. 12, 31−49.

Wiles, L.W., 2006. Total evaporation estimation from sugarcane using the scintillation technique. M.Sc. thesis, University of KwaZulu-Natal, Pietermaritzburg, South Africa. 126 pp.

Wilson, K.B., Baldocchi, D.D., 2000. Seasonal and interannual variability of energy fluxes over a broadleaved temperate deciduous forest in North America. Agric. For. Meteorol. 100, 1−18.

Wyngaard, J.C., 1973. On surface-layer turbulence. In: Haugen, D.A. (Ed). Workshop on Meteorology. Amer. Meteorol. Soc. Boston, Massachusetts, USA. 101–149.

Wyngaard, J.C., Cote, O.R., Izumi, Y., 1971. Local free convection, similarity and the budgets of shear stress and heat flux. J. Atmos. Sci. 28, 1171−1182.

Zapata, N., Martínez-Cob, A., 2001. Estimation of sensible and latent heat flux from natural sparse vegetation surface using surface renewal. J. Hydrol. 254, 215−228.

Zapata, N., Martínez-Cob, A., 2002. Evaluation of the surface renewal method to estimate wheat evapotranspiration. Agric. Water Manage. 55, 141−157.